



SAPIENZA
UNIVERSITÀ DI ROMA

Dottorato di ricerca:
**Scienze Applicate per la Protezione
dell'Ambiente e dei Beni Culturali**
Dipartimento di Scienze della Terra

Coordinatore: Adriana MARAS

**Tutore/i: Silvano MIGNARDI
Lorenzo NIGRO**

Revisori:

**Germana BARONE
Yiannis PONTIKES**

Docenti Esaminatori:

**Paolo BALLIRANO
Gianluigi DE GENNARO
Marco GIAMELLO**

**Multi-analytical study
of ceramic materials
from the archaeological
site of
Khirbet al-Batrawy
(Jordan)**

**Studio archeometrico
multianalitico del materiale
ceramico proveniente dal sito
archeologico di
Khirbet al-Batrawy (Giordania)**

Laura MEDEGHINI

XXVI Ciclo

Riassunto

Nel presente lavoro sono riportati i risultati di uno studio multianalitico finalizzato alla caratterizzazione archeometrica di frammenti ceramici del sito archeologico di Khirbet al-Batrawy, Giordania, datati tra il 3000 e il 2000 a.C. con lo scopo di definirne la provenienza, le tecnologie di produzione e la relativa evoluzione tecnologica nel tempo.

L'obiettivo principale è stato quello di identificare e caratterizzare dal punto di vista mineralogico-petrografico e composizionale i manufatti ceramici rinvenuti ed i materiali utilizzati nella loro produzione. Tali informazioni risultano indispensabili per uno studio approfondito sull'insieme di influenze e contatti che le popolazioni del Levante possono aver subito nel corso dei secoli. Ci si è proposto, inoltre, di contribuire a definire con maggior dettaglio il livello tecnologico raggiunto: eventuali azioni di selezio-

ne della materia prima e tipologia di rivestimento, massima temperatura e controllo delle condizioni redox durante la cottura.

A questo scopo sono stati analizzati i frammenti provenienti da quattro differenti contesti stratigrafici datati tra il 3000 e il 2000 a.C. e rappresentativi delle diverse produzioni ceramiche rinvenute nel sito: ceramica comune, ceramica dipinta, ceramica lucidata, ceramica da trasposto, ceramica da cucina, la cosiddetta ceramica metallica ed una produzione specializzata caratteristica del Levante definita Khirbet Kerak Ware. I campioni ceramici sono stati caratterizzati mediante analisi macroscopiche, micro-Raman e Spettroscopia Infrarossa (FTIR) per identificare gli inclusi, le decorazioni superficiali dei frammenti e per caratterizzare la matrice. I campioni ceramici sono stati successivamente analizzati mediante microscopia ottica in sezione sottile per definire gruppi petrografici omogenei in termini di microstruttura, massa di fondo e composizione degli inclusi. Analisi micromorfologiche sono state effettuate mediante SEM-EDS per definire la struttura della pasta di fondo, la natura degli inclusi e il grado di vetrificazione della matrice. Parte dei campioni è stata analizzata mediante XRD per definire la composizione mineralogica ed identificare la possibile presenza di fasi di neoformazione originatesi in seguito alla cottura.

La composizione chimica delle ceramiche è stata determinata mediante ICP-MS e i risultati sono stati elaborati applicando l'analisi statistica multivariata con lo scopo di distinguere se le ceramiche fossero prodotte localmente o se vi fossero elementi che potessero permettere di ipotizzare un'importazione su scala regionale.

Sulla base dei risultati dell'analisi minero-petrografica è stato possibile identificare dodici *fabrics* caratterizzate da inclusi di dimensione grossolana disposti nella matrice secondo una distribuzione unimodale; ciò suggerisce la mancanza di qualsiasi intervento o processo di purificazione della materia prima durante le fasi di preparazione dell'impasto ceramico. I risultati delle indagini minero-petrografiche supportano l'ipotesi di un approvvigionamento locale delle materie prime. In particolare, la presenza di inclusi di feldspato alcalino, zircone, apatite e barite è da correlare al contributo delle rocce ignee e metamorfiche del basamento cristallino Pre-Cambriano. La presenza di frammenti di rocce basaltiche è da ascrivere agli estesi affioramenti di tali rocce in prossimità del sito archeologico. Pertanto, questi risultati suggeriscono che le ceramiche di Batrawy probabilmente furono prodotte localmente. Le medesime conclusioni possono essere dedotte anche per i frammenti di Khirbet Kerak Ware, un gruppo ceramico tipologicamente differente dalle altre produzioni del sito di Khirbet al-Batrawy caratterizzato da una superficie di rivestimento lucida di colore rosso/nero. Le analisi chimiche, e in particolare il trattamento statistico dei dati, mostrano che i frammenti ceramici appartengono ad un unico *cluster*, suggerendo l'impiego di materie prime composizionalmente simili, probabilmente estratte nelle medesime aree.

La presenza di calcite primaria, illite, gehlenite e diopside permette di ipotizzare che il materiale di partenza fosse un mix composto prevalentemente da illite e carbonati, cotto a temperature inferiori a 950°C. Un leggero incremento nella temperatura di cottura è stato osservato nelle ultime fasi della storia di Khirbet al-Batrawy, suggerendo una possibile evoluzione delle conoscenze del processo di cottura del materiale ceramico. Per quanto concerne l'evoluzione della produzione ceramica, non sono stati osservati significativi cambiamenti durante la lunga storia della città di Batrawy. Questi risultati supportano l'ipotesi che durante i mille anni di vita della città il background tecnologico di queste popolazioni non abbia subito variazioni significative. Tuttavia, la variabilità osservata nelle *fabrics* petrografiche suggerisce una certa evoluzione tecnologica nel corso del tempo. La correlazione tra *fabrics* e tipologia ceramica osservata nel primo periodo storico è indice della fase di *start-up* della produzione ceramica a Batrawy. La presenza di numerose *fabrics* petrografiche non direttamente correlabili ad una specifica tipologia ceramica nel secondo periodo testimonia una diffusa sperimentazione nella scelta dei materiali di partenza e delle procedure di lavorazione. Nelle ultime fasi storiche si osserva una sorta di standardizzazione degli impasti, testimoniata dal minor numero di *fabrics* identificate e dalla evidente correlazione tra *fabrics* e tipologia ceramica, ed un miglior controllo della fase di cottura. Questi segnali di lento miglioramento starebbero ad indicare anche una maggiore attenzione rivolta alla specializzazione di particolari classi ceramiche.

Ai miei genitori

*“Credo di poter affermare che nella ricerca scientifica né il grado di intelligenza né la capacità di eseguire
e portare a termine il compito intrapreso siano fattori essenziali
per la riuscita e per la soddisfazione personale.
Nell'uno e nell'altro contano maggiormente
la totale dedizione e il chiudere gli occhi davanti alle difficoltà:
in tal modo possiamo affrontare i problemi che altri, più critici e più acuti, non affronterebbero.”*

Rita Levi-Montalcini

TABLE OF CONTENTS

Acknowledgements	v
INTRODUCTION	1
STATE OF THE ART	3
References	7
1. KHIRBET AL-BATRAWY: GEOGRAPHICAL, GEOLOGICAL AND ARCHAEOLOGICAL SETTING	15
1.1 Geographical setting	15
1.2 Historical and Archaeological setting	16
1.2.1 Khirbet al-Batrawy: The Discovery	16
1.2.2 The Excavations	18
1.2.3 The Archaeological remains.....	18
1.2.4 The History of Khirbet al-Batrawy.....	18
1.3 Geological setting	211
1.3.1 Jordan geology	21
1.3.2 Geology and structure of the Amman-Zarqa Basin and Zarqa River	26
1.3.3 Geology of Khirbet al-Batrawy archeological site	28
References	28
2. MATERIALS AND METHODS	31
2.1 Archaeological Samples	31
2.1.1 EB II Samples (3000-2700 B.C.)	32
2.1.2 EB IIIA Samples (2700-2500 B.C.)	33
2.1.3 EB IIIB Samples (2500-2300 B.C.)	33
2.1.4 EB IV Samples (2300-2000 B.C.).....	3434
2.2 Geological Samples	34
2.3 Analytical methods	35
2.3.1 Micro-Raman spectroscopy.....	35
2.3.2 Fourier Transform Infrared Spectroscopy (FTIR).....	35
2.3.3 Optical Microscopy (OM)	36
2.3.4 Scanning Electron Microscopy coupled with Energy Dispersive Spectroscopy (SEM-EDS)	37
2.3.5 X-Ray Diffraction (XRD).....	39
2.3.6 Chemical analysis.....	40
References	42
3. STATISTICAL TREATMENTS	45

3.1 Statistical analysis of FTIR data	47
3.2 Statistical analysis of chemical data.....	50
References	51
4 RESULTS	53
4.1 Macroscopic Analysis.....	53
4.1.1 EB II	53
4.1.2 EB IIIA	53
4.1.3 EB IIIB	53
4.1.4 EB IV.....	53
4.2 Optical Microscopy analysis in thin section (OM).....	65
4.2.1 EB II	66
4.2.2 EB IIIA	68
4.2.3 EB IIIB	71
4.2.4 EB IV.....	74
4.3 Micro-Raman Spectroscopy analysis.....	82
4.3.1 EB II	82
4.3.2 EB IIIA	85
4.3.3 EB IIIB	89
4.3.4 EB IV.....	90
4.4 FTIR analysis.....	93
4.4.1 EB II	93
4.4.2 EB IIIA	95
4.4.3 EB IIIB	97
4.4.4 EB IV.....	97
4.4.5 Statistical Analysis	98
4.5 Scanning Electron Microscopy coupled with Energy Dispersive Spectroscopy (SEM-EDS).....	104
4.5.1 EB II	104
4.5.1.1 Minerals	104
4.5.1.2 Matrix.....	105
4.5.1.3 Vitrification stage analysis.....	106
4.5.2 EB IIIA	106
4.5.2.1 Minerals	106
4.5.2.2 Matrix.....	107
4.5.2.3 Vitrification stage analysis.....	107
4.5.3 EB IIIB	108
4.5.3.1 Minerals	108
4.5.3.2 Matrix.....	110

4.5.3.3 Vitrification stage analysis.....	111
4.5.4 EB IV.....	111
4.5.4.1 Minerals.....	111
4.5.4.2 Matrix.....	112
4.5.4.3 Vitrification stage analysis.....	113
4.5.5 Coarse-sized inclusions.....	114
4.6 X-Ray Diffraction analysis (XRD).....	116
4.6.1 EB II.....	116
4.6.2 EB IIIA.....	117
4.6.3 EB IIIB.....	119
4.6.4 EB IV.....	120
4.6.5 Geological samples.....	122
4.6.6 Firing experiments.....	123
4.7 Chemical analysis.....	129
4.7.1 Statistical analysis of data.....	136
References.....	143
5 DISCUSSION.....	147
5.1 Technological level of production.....	148
5.1.1 Mineralogical phases and petrographic composition.....	148
5.1.2 Firing.....	155
5.1.2.1 Maximum firing temperatures.....	156
5.1.2.2 Firing atmosphere.....	164
5.1.3 Decorations and superficial treatments.....	167
5.1.4 Burial conditions.....	168
5.2 Provenance.....	169
References.....	171
6 ADVANTAGES AND DRAWBACKS OF ANALYTICAL METHODOLOGIES USED: THE CASE OF KHIRBET AL-BATRAWY.....	177
6.1 Technological level of production.....	178
6.1.1 Mineralogical composition.....	178
6.1.2 Firing.....	181
6.1.2.1 Maximum firing temperatures.....	181
6.1.2.2 Firing atmosphere.....	182
6.1.3 Decorations and superficial treatments.....	182
6.2 Provenance.....	183
Conclusions.....	184
7 CONCLUSIONS.....	185
APPENDIX A.....	187

APPENDIX B.....	199
APPENDIX C.....	205
APPENDIX D.....	223

Acknowledgements

I would like to express my gratitude to all the people who supported me during my doctoral studies.

I would thank Prof. Lorenzo Nigro and his research group for the possibility to contribute in the study of Levantine culture providing archaeological ceramics without which I could not develop my project. Maura Sala, in particular, was a huge help in suggesting different archaeological problematics to be faced and solved. She also helped me to interpret some of the data from the archaeological point of view, always supporting me during the writing of the thesis.

I could not forget the physics group of Parma to thank. Prof. Pier Paolo Lottici who always believes in me and who is continuously present to discuss about all my doubts. Danilo Bersani, who taught me the basics of Raman spectroscopy growing my interest in the application of this methodology and for the possibility to attend the school of Raman in Milan. I also would like to thank and acknowledge the hard work of the many undergrads that I had the pleasure of working with in my time here. In particular, Elena Bacchini, Mariangela Turetta and Jennifer Costantini who helped me in the acquisition of Raman results.

I would be remiss if I didn't mention the help and availability of Prof. Paolo Ballirano who give me the possibility to work with particular instrumentations that could open new paths in the study of archaeological ceramic.

Prof. Patrick Quinn was a huge help with learning the petrographic features of archaeological ceramic and their interpretation. I consider the school at UCL in London as the most important experience in my PhD education.

I would also thank Stefano Stellino for the laboratory assistances with XRD, and Marco Albano to teach me the use and the secrets of SEM-EDS instrumentation.

I owe a lot Prof. Adriana Maras for her constant advice through the years of my PhD. Finally last, but by far not least, I have to thank Caterina De Vito who has an inspirational passion for the research. Her support, advices and her motivation to do always the best have made unforgettable my PhD experience.

A particular thank to my reviewers Prof. Germana Barone and Yiannis Pontikes who helped me in the revision of my work. Their comments and suggestions gave and important contribution to improve my thesis.

My special thanks to my guide, my light at the end of the tunnel, Silvano Mignardi who was an inspiration to me. He supported me and also stood me never losing his patience and his self-control. I owe all of the success of this project to them.

Sitting in front of my pc, thinking about my PhD experience I reminded all of the people who have made it possible: my family and my friends who have supported me through this three long years, working hard beside me and helping me. Here I would like to take the opportunity to thank all of these people.

First of all, I have to thank my parents, for their encouragement, love, and faith in me. My Dad, for teaching me the joy to be passionate in something and the hope to realize a dream and my Mom for the passion in maths and science and to inspiring me every day, teaching me the sweet part of the life. I have my brother to thank too, his support and the possibility to confide to him is one of the guarantees in my life.

There is also the rest of all the people who were very supportive and a constant encouragement for me. In particular, I have to thank my colleague and friend Sara who has been my half in this beautiful experience showing me always the funny side of the problems.

Finally, a great thank to my love who is always at my side, sharing with me the happy moments and supporting me in all troubles, who listened to all my ppt presentations and who had been so patient in these intense years.

A great thank to all the people who crossed my path in these three years, in the lab, in the “corridor room”, or who had the bad luck to live with me; who spent with me a day, an afternoon or also only few minutes; who offered me a smile, a consolation word, who stayed with me with facts or simple words...thank you because without knowing it you made me to arrive here.

INTRODUCTION

The present PhD thesis reports the results of a multi-analytical study focused on the archaeometric characterization of Early Bronze Age pottery from the archaeological site of Khirbet al-Batrawy (Northern Jordan), dated back between 3000 to 2000 B.C..

This research is part of the *Archaeological Expedition to Palestine & Jordan* project coordinated by Sapienza-University of Rome and directed by Prof. Lorenzo Nigro, with the cooperation of the Department of Antiquities, the Hashemite Kingdom of Jordan and with the support of the Italian Ministry of Foreign Affairs.

This project, studying the material culture of near East, provides information about the development of the technological aspects of pottery production in the Bronze Age considering that evidences of furnaces or kilns has not yet been found by the archaeologists.

This work stands out for different reasons. First of all the pottery from Khirbet al-Batrawy has never been studied applying an archaeometric approach. Therefore, the results here reported are an *unicum*. Secondly, the city's strategic location has enabled it to arise as a major Early Bronze Age center, controlling the area of the Upper Wadi az-Zarqua. Finally, the history of Khirbet is restricted to a limited period of about 1000 years that permitted the good preservation of the remains and avoided later contaminations. In this view, the study of ceramic material from Khirbet al-Batrawy gives the possibility to obtain information in the reconstruction of trades in this region in a limited period of time. Moreover, the archaeometric analysis of the pottery can supply important information allowing the identification of cases of importation and/or local imitation of pottery as the case of the so-called Khirbet Kerak Ware.

The aim of the study is to determine the mineralogical, petrographic and chemical composition of the Batrawy pottery, to explore the technological processes involved in their production, and to define the nature of the raw materials. This study therefore deals with the characterization of this pottery in order to determine potential differences in composition or technology and their correlation with various time periods and its evolution over time.

To achieve these objectives, 101 potsherds from four different stratigraphic contexts dated between 3000 to 2000 B.C. have been analyzed and compared to geological materials collected from the surroundings of Khirbet al-Batrawy. The investigated samples represent a very diversified inventory of pottery productions such as Simple and Simple Painted Ware (SW-SPW), Storage Ware (StW), Kitchen Ware (KW), Khirbet Kerak Ware (KKW) a specialized pottery production characteristic of southern Levant

and Metallic Ware (MW). Two other productions are distinguished on the basis of the related superficial treatments, i.e., Red Burnished Ware (RBW) and Red Polished Ware (RPW).

All the samples have been investigated using both destructive and non-destructive analytical methods. Macroscopic observations, micro-Raman and Infrared spectroscopies were employed to identify the inclusions of the paste and the composition of decorations.

Firstly, pottery samples have been analyzed by optical microscopy (OM) in thin-section under polarizing microscopy to define homogeneous petrographic groups in terms of microstructure, groundmass, composition of inclusions and textural features. Micro-morphological analysis has been carried out by Scanning Electron Microscopy coupled with Energy Dispersive Spectroscopy (SEM-EDAX) to define the groundmass microstructure, inclusions and the degree of vitrification. Part of each potsherd has been analyzed by X-ray diffraction (XRD) to identify the mineralogical assemblage and in particular the newly formed mineralogical phases. The chemical composition has been determined by Inductively coupled plasma mass spectrometry (ICP-MS) analysis and the results have been developed by a multivariate analysis with the aim to distinguish locally-produced or imported potteries from other settlement in Jordan and to define the different technological background of productions adopted over time.

The results obtained by the application of different analytical techniques are reported and discussed in separate sections to highlight their advantages and drawbacks in the characterization of archaeological pottery.

STATE OF THE ART

Background information

Ancient ceramic artifacts attracted the attention of scientists as being a chronological indicator within archaeological contexts that preserve information regarding their provenance, production process, use and conservation conditions through which they survived until nowadays. Such information are precious in terms of knowledge of the material culture of a people, the evolution of its technological background, provenance of the raw materials and the reconstruction of relationships and commercial trades among populations.

Pottery was the first material created by humans as expression of their cultural background (Rice, 1987). The word "ceramic" is derived from the Greek *keramos* that describes a "burned material" or "burned earth". It is formed primarily of clays with impurities or additives such as sand, carbonates (mollusk shells or crushed limestones), lithic fragments, grog (i.e., crushed ceramics), organic materials and volcanic ash. After mixing with water, the starting paste is processed under firing to produce a harder and permanent object. Indeed, from a petrographic point of view, potsherds are assimilated to artificial "metamorphic rocks" in which the protolith is the original raw material and the activation energy of metamorphism is represented by the firing process (Maritan, 2004).

The oldest pottery artifacts appeared in Neolithic times. Since then, pottery was widely used to the extent of being almost an ubiquitous material in most archaeological sites from early chronologies. Its diffusion is connected to different causes. First of all for the easy availability of raw materials, the simple production methodologies that do not require specialized manufacture and finally its resistance to degradation and alteration. In this view, pottery can be used as a tracer to define the routes of trade and the evolution in the technological aspects of the pottery production.

In the past, archaeological ceramic material was studied only on the basis of the traditional method called "observation with the naked eye" considering shape, style, decorations, superficial treatments, etc. Nowadays, a rigorous scientific approach is applied to reconstruct the production methodologies and technological background of ancient communities (Barone *et al.*, 2012).

According to Maggetti (1982) (Fig. 1) the ceramic sherds went through their life in five steps: (1) the origin, represented by the extraction of the clay material, (2) the manufacture of the ceramic object, (3) the use and the breakdown, (4) the burial and finally (5) the archaeometric study that permits to reconstruct wholly or in part the life cycle of the pottery.

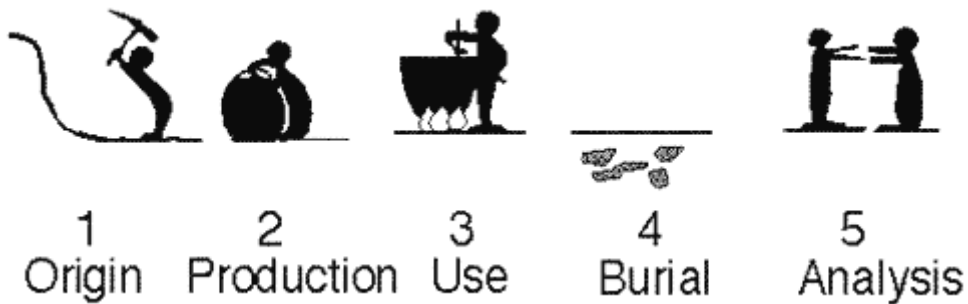


Figure 1: The five steps of pottery life (from Maggetti, 1982).

Methodologies applied in the study of pottery

Ceramic material conserves inside information about its history: the starting raw material, the way of modeling and production, the use and its burial. The analytical methodologies used in the archaeometric characterization of ancient pottery are usually the same adopted by the Earth Sciences (Rice, 1987; Maggetti, 1990; Cuomo di Caprio, 2007).

The characterization of such ancient artifacts is a complicated task due to the mineralogical and chemical heterogeneity of raw materials and the resulting changes in shape, mineralogy, microstructure, driven by heating process it has undergone. A combination of both physical analytical and chemical methods has to be applied for the complete reconstruction of the factors involved in the pottery history. This multi-analytical approach can provide information about the nature and provenance of raw materials, allows to explore the technological aspects of pottery production and to define the firing conditions (i.e., temperature and redox state of the firing atmosphere). Moreover, post-burial processes involving the ceramic can also be investigated (Cultrone *et al.*, 2001; Barone *et al.*, 2002; Sherriff *et al.*, 2002a; Maritan, 2004; Rathossi *et al.*, 2004; Iordanis *et al.*, 2009; Tschegg, 2009; Velraj *et al.*, 2009; Belfiore *et al.*, 2010).

The mineralogical-petrographic characterization of pottery plays a main role in the study of archaeological ceramic. It is aimed at the qualitative and quantitative description of the mineral components of the paste or fabric. In this view, the mineralogical components of pottery can be distinguished in: a) primary phases, naturally present in the raw material or voluntarily added by potters as tempers, b) firing phases, newly formed through complex reactions during the heating process, and c) secondary phases, originated using the vessels or in the burial environments (Heimann and Maggetti 1981; Maggetti, 1981; Buxeda i Garrigós, 1999; Freestone, 2001; De Benedetto *et al.*,

2002; Maritan and Mazzoli 2004; Schwedt *et al.*, 2004, 2006; Buxeda i Garrigós *et al.*, 2005; Secco *et al.*, 2011).

Numerous methodologies have been extensively applied in the definition of the mineralogical composition of ancient pottery: optical microscopy (OM) (Brisbane, 1981; Amadori *et al.*, 1995; Barone *et al.*, 2004; Riederer, 2004; Cuomo di Caprio, 2007; Quinn and Day, 2007; Quinn *et al.*, 2010), X-ray diffraction (XRD) (Tang *et al.*, 2001; Barone, 2002; Iordanis *et al.*, 2009; Andaloro *et al.*, 2011; Kramar, 2012;), time-of-flight neutron diffraction analysis (Botti *et al.*, 2006; Siouris and Walter, 2006; Barilaro *et al.*, 2007; Bersani *et al.*, 2010; Barone *et al.*, 2011a), Mössbauer spectroscopy to define the oxidation state of iron (Sherriff *et al.*, 2002b; Stievano *et al.*, 2003, 2004; Ricciardi *et al.*, 2008); X-ray absorbance spectroscopy (XAS) to identify the oxidation states and local environments of iron and copper oxides (Bardelli *et al.*, 2011, 2012) and scanning electron microscopy (SEM) (Tite and Maniatis, 1975; Froh, 2004; Rathossi *et al.*, 2004). Moreover, SEM equipped by energy dispersive system (SEM-EDS) can be used in provenance studies by the observation of fine-scale microstructures connected to the original clay and by the identification of single minerals in the matrix (see for example, Gliozzo and Turbanti Memmi, 2001).

Spectroscopic analysis, such as μ -Raman spectroscopy and Fourier transform infrared (FTIR) spectroscopy, has also been applied in pottery characterization (Edwards *et al.*, 1999; Barone *et al.*, 2002; De Benedetto *et al.*, 2002; Lofrumento *et al.*, 2004; Barilaro *et al.*, 2005, 2008; Striova *et al.*, 2006; Akyuz *et al.*, 2008; Mangone *et al.*, 2009). In particular, μ -Raman spectroscopy is considered an efficient solution in the investigations of the pigments used in the decorations and superficial treatments (Sabbatini *et al.*, 2000; Middleton *et al.*, 2005; Ospitali *et al.*, 2005; Sendova *et al.*, 2005; Ferrer *et al.*, 2012).

The presence of particular mineral assemblages could be a marker to identify the possible origin of raw material; moreover, the presence or absence of high temperature mineral phases allows to establish the range of firing temperature. This kind of approach is supported by the results of experimental studies on the transformations of different raw materials during firing at different atmosphere redox conditions, temperature ranges and residence time (Duminuco *et al.*, 1996, 1998; Fabbri *et al.*, 1997; Riccardi *et al.*, 1999; Trindade *et al.*, 2009; Tschegg *et al.*, 2009). In the definition of the maximum firing temperature, the potentiality of small angle neutron scattering (SANS), linking the mesoscopic structure of ceramic samples, i.e. the mean size and the surface characteristics of grains, to the development of heating process, was proved (Botti *et al.*, 2006; Barone *et al.*, 2011c;).

Studies on provenance of ceramic objects and sources supplying raw materials are fundamental for the distribution of ancient pottery. To address these purposes, the

mineralogical and chemical composition of the unknown object has been compared with those of known pottery or raw materials. In particular, two main methodologies were applied: optical microscopy and chemical analysis (Turbanti Memmi, 2004).

Optical microscopy in thin section is applied for the mineralogical-petrographic analysis that is aimed at defining the nature of the original clay (Maggetti, 1982). The tempers detected should reflect the geology of the place of the production and, consequently, the comparison of the mineralogical-petrographic composition of the tempers with the geological setting of the area of discovery of the ancient ceramics makes possible to define their local or imported origin. Although, a local production of the ceramic using imported tempers could be supposed, ethnological data supporting this hypothesis are not yet reported in the literature (Maggetti, 1982).

Chemical analysis provides compositional fingerprints of pottery identifying specific elements whose occurrence in the ceramic can be related to the mineralogical-petrographic characteristics of the rocks outcropping in the area of production. In this view, the application of chemical methodologies provides data that can be useful for the differentiation between local or imported potteries. The main chemical analysis methodologies adopted includes inductively coupled plasma atomic emission spectroscopy (ICP-AES) (Bruno *et al.*, 2000; Tiequan *et al.*, 2010), inductively coupled plasma mass spectrometry (ICP-MS) (Mallory-Greenough *et al.*, 1998; Aldrabee and Wriekat, 2011; Vaughn *et al.*, 2011), inductively coupled plasma optical emission spectrometry (ICP-OES) (Barone *et al.*, 2004; Kramar *et al.*, 2012), X-ray fluorescence (XRF) (Barone, 2002, 2011b, 2012; Maritan, 2004; Aquilia *et al.*, 2013), instrumental neutron activation analysis (INAA) (Vaughn *et al.*, 2006; Nyarko *et al.*, 2007; Li *et al.*, 2013), particle induced X-ray emission (PIXE) (Ruvalcaba-Sil *et al.*, 1999; Agha-Aligol *et al.*, 2009; Wu *et al.*, 2013), atomic absorption spectroscopy (AAS) (Mangone *et al.*, 2008), transmission electron microscopy (TEM) (Viti *et al.*, 2003; Botti *et al.*, 2006) and electron microprobe analysis (EMPA) (Ionescu *et al.*, 2011).

Clay minerals can be characterized by a series of analytical methods basing on the thermal behavior that is different and characteristic for each clay mineral under heating process. However, these methods, which include, for example, differential thermal analysis (DTA) and thermo-gravimetric analysis (TGA), are considered difficult to apply to complex mixtures such as natural clays and pottery, but can be used in the characterization of low-fired potteries (Moropoulou *et al.*, 1995; Bertolino and Fabra, 2003; Mohsen and El-maghraby, 2010; Fiori *et al.*, 2011; Barone *et al.*, 2012).

This overview further highlights that the study of pottery is a complicated task due to its complex composition that requires the application of a multi-analytical approach. Indeed, to obtain a whole characterization and to answer to the numerous open ques-

tions regarding archaeological ceramic a numerous methodologies have been applied. In this view, the present study stands as an example of multi-analytical investigation using both destructive and non-destructive analytical methods. Macroscopic observations, micro-Raman and Infrared spectroscopies, OM in thin-section, SEM-EDAX, XRD and chemical analysis have been carried out to identify the mineralogical and chemical composition and to reconstruct the ancient technology and provenance of archaeological pottery.

References

- Agha-Aligol D., Oliayi P., Mohsenian M., Lamahi-Rachti M., Shokouhi F. (2009): Provenance study of ancient Iranian luster pottery using PIXE multivariate statistical analysis. *Journal of Cultural Heritage*, **10**, 487-492.
- Aldrabee A., Wriekat A.K. (2011): Archaeometric characterization of ancient glazed pottery sherds from Khirbet Faris, Jordan by inductively coupled plasma mass spectrometry (ICP-MS). *Microchemical Journal*, **99**, 289-295.
- Amadori M.L., Di Pillo M., Fratini F., Levi S.T., Pecchioni E. (1995): The bronze age pottery of Coppa Nevigata (FG-Italy): raw materials and production. European Meeting of Ancient Ceramics, Barcellona.
- Andaloro E., Belfiore C.M., De Francesco A.M., Jacobsen J.K., Mittica G.P. (2011): A preliminary archaeometric study of pottery remains from the archaeological site of Timpone della Motta, in the Sibaritide area (Calabria - southern Italy). *Applied Clay Science*, **53**, 445-453.
- Aquila E., Barbera G., Barone G., Crupi V., Longo F., Majolino D., Mazzoleni P., Venuti V. (2013): Combined XRF-SEM analysis of varnished pottery: the case of Syracuse and Adrano (Sicily) archaeological finds. *X-Ray Spectrometry*, **42**, 38-44.
- Akyuz S., Akyuz T., Basarn S., Bolcal C., Gulec A. (2008): Analysis of ancient potteries using FT-IR, micro-Raman and EDXRF spectrometry. *Vibrational Spectroscopy*, **48**, 276-280.
- Bardelli F., Barone G., Crupi V., Longo F., Maisano G., Majolino D., Mazzoleni P., Venuti V. (2012): Iron speciation in ancient Attic pottery pigments: a non-destructive SR-XAS investigation. *Journal of Synchrotron Radiation*, **19**, 782-788.
- Bardelli F., Barone G., Crupi V., Longo F., Majolino D., Mazzoleni P., Venuti V. (2011): Combined non-destructive XRF and SR-XAS study of archaeological artefacts. *Analytical and bioanalytical chemistry*, **399**, 3147-3153.
- Barilaro D., Barone G., Crupi V., Donato M.G., Majolino D., Messina G., Ponterio R. (2005): Spectroscopic techniques applied to the characterization of decorated potteries from Caltagirone (Sicily, Italy). *Journal of Molecular Structure*, **744-747**, 827-831.
- Barilaro D., Barone G., Crupi V., Majolino D., Mazzoleni P., Tigano G., Venuti V. (2008): FT-IR absorbance spectroscopy to study Sicilian "proto-majolica" pottery. *Vibrational Spectroscopy*, **48**, 269-275.
- Barilaro D., Crupi V., Majolino D., Venuti V., Barone G., Kockelmann W. (2007): Neutrons as a probe of large volume specimens: the case of archaeological pottery findings. *Journal of Archaeological Science*, **34**, 1148-1152.
- Barone G. (2002) Preliminary archaeometric analysis on amphorae used for transport in VI and V centuries B.C., from excavation at Gela (Sicily). *Periodico di Mineralogia*, **71**, 273 -287.
- Barone G., Bartoli L., Belfiore C. M., Crupi V., Longo F., Majolino D., Mazzoleni P., Venuti V. (2011a): Comparison between TOF-ND and XRD quantitative phase analysis of ancient potteries. *Journal of Analytical Atomic Spectrometry*, **26**, 1060-1067.

- Barone G., Crupi V., Galli S., Longo F., Majolino D., Mazzoleni P., Spagnolo G. (2004): Archaeometric analyses on 'Corinthian B' transport amphorae found at Gela (Sicily, Italy). *Archaeometry*, **4**, 553-568.
- Barone G., Crupi V., Longo F., Majolino D., Mazzoleni P., Venuti V., Aquilia E. (2011b): Potentiality of non destructive XRF analysis for the determination of Corinthian B amphorae provenance. *X-Ray Spectrometry*, **40**, 333-337.
- Barone G., Crupi V., Majolino D., Mazzoleni P., Teixeira J., Venuti V., Scandurra A. (2011c): Small angle neutron scattering as fingerprinting of ancient potteries from Sicily (Southern Italy). *Applied Clay Science*, **54**, 40-46.
- Barone G., Ioppolo S., Majolino D., Migliardo P., Tigano G. (2002): A multidisciplinary investigation on archaeological excavation in Messina (Sicily). Part I: A comparison of pottery findings in 'The Strait of Messina area'. *Journal of Cultural Heritage*, **3**, 145-153.
- Barone G., Mazzoleni P., Spagnolo G., Aquilia E. (2012): The transport amphorae of Gela: a multidisciplinary study on provenance and technological aspects, *Journal of Archaeological Science*, **39**, 11-22.
- Belfiore C.M., di Bella M., Triscari M., Viccaro M. (2010): Production technology and provenance study of archaeological ceramics from relevant sites in the Alcantara River Valley (North-eastern Sicily). *Materials Characterization*, **61**, 440-451.
- Bersani D., Lottici P.P., Virgenti S., Sodo A., Malvestut, G., Botti A., Salvioli-Mariani E., Tribaudino M., Ospitali F., Catarsi M. (2010): Multi-technique investigation of archaeological pottery from Parma (Italy). *Journal of Raman Spectroscopy*, **41**, 1266-1271.
- Bertolino S.R., Fabra M. (2003): Provenance and ceramic technology of pot sherds from ancient Andean cultures at the Ambato valley, Argentina. *Applied Clay Science*, **24**, 21-34.
- Botti A., Ricci M.A., De Rossi G., Kockelmann W., Sodo A. (2006): Methodological aspects of SANS and TOF neutron diffraction measurements on pottery: the case of Miseno and Cuma. *Journal of Archaeological Science*, **33**, 307-319.
- Bruno P., Caselli M., Curri M.L., Genga A., Striccoli R., Traini A. (2000): Chemical characterisation of ancient pottery from south of Italy by Inductively Coupled Plasma Atomic Emission Spectroscopy (ICP-AES): Statistical multivariate analysis of data. *Analytica Chimica Acta*, **410**, 193-202.
- Buxeda i Garrigós J. (1999): Alteration and contamination of archaeological ceramics: the perturbation problem. *Journal of Archaeological Science*, **26**, 295-313.
- Buxeda i Garrigós J., Cau Ontiveros M. A., Madrid i Fernández M., Toniolo A. (2005): Roman amphorae from the *Iulia Felix* shipwreck: alteration and provenance. in "Proceedings of the 33rd International Symposium on Archaeometry", H. Hars and E. Burke, eds., Vrije Universiteit, Amsterdam, 149-51.
- Cultrone G., Rodriguez-Navarro C., Sebastian E., Cazalla O., De La Torre M.J. (2001): Carbonate and silicate phase reactions during ceramic firing. *European Journal of Mineralogy*, **13**, 621-634.
- Cuomo di Caprio N. (2007): *Ceramica Antiche tecniche di lavorazione e moderni metodi di indagine 2*, Roma.
- De Benedetto G.E., Laviano R., Sabbatini L., Zambonin P.G. (2002): Infrared spectroscopy in the mineralogical characterization of ancient pottery. *Journal of Cultural Heritage*, **3**, 177-186.
- Duminuco P., Messiga B., Riccardi, M.P. (1998): Firing process of natural clays. Some microtextures and related phase compositions. *Thermochimica Acta*, **321**, 185-190.

- Duminuco P., Riccardi, M.P., Messiga B., Setti M. (1996): Modificazioni tessiturali e mineralogiche come indicatori della dinamica del processo di cottura di manufatti ceramici. *Ceramurgia*, **5**, 281-288.
- Edwards H.G.M, Drummond L., Russ J. (1999): Fourier transform Raman spectroscopic study of prehistoric rock paintings from the Big Bend Region, Texas. *Journal of Raman Spectroscopy*, **30**, 421-428.
- Fabbri B., Gualtieri S., Santoro S. (1997): L'alternativa chamotte/calcite nella ceramica grezza: prove tecniche. in "Il contributo delle analisi archeometriche allo studio delle ceramiche grezze e comuni. Il rapporto forma/funzione/impasto. Atti della 1° Giornata di archeometria della ceramica (Bologna, 28 febbraio 1997)", Bologna, 183-191.
- Ferrer P., Ruiz-Moreno S., López-Gil A., Chillón M.C., Sandalinas C. (2012): New results in the characterization by Raman spectroscopy of yellow pigments used in ceramic artworks of the 16th and 17th centuries. *Journal of Raman Spectroscopy*, **43**, 1805-1810.
- Fiori C., Vitali D., Camurri E., Fabbri B., Gualtieri S. (2011): Archaeometrical study of Celtic ceramics from Monte Bibele (Bologna, Italy). *Applied Clay Science*, **53**, 454-465.
- Freestone I. C. (2001): Post-depositional changes in archaeological ceramics and glasses. in "Handbook of archaeological sciences", D. R. Brothwell and A. M. Pollard, eds., John Wiley & Sons, Inc., Hoboken, NJ, 615-25.
- Froh J. (2004): Archaeological ceramics studied by scanning electron microscopy. *Hyperfine Interaction*, **154**, 159-176.
- Gliozzo E., Turbanti Memmi I. (2001): Archaeometric study of the pottery manufactory of Marcianella-Chiusi (Siena, Italy). Proceedings of the 32nd International Symposium Archaeometry, Mexico City.
- Heimann R.B., Maggetti M. (1981): Experiments on simulated burial of calcareous terra sigillata (mineralogical change), Preliminary results, British Museum Occasional Paper, **19**, 163-177.
- Ionescu C., Hoeck, V., Ghergari, L. (2011): Electron microprobe analysis of ancient ceramics: A case study from Romania. *Applied Clay Science*, **53**, 466-475.
- Iordanidis A., Garcia-Guinea J., Karamitrou-Mentessidi G. (2009): Analytical study of ancient pottery from the archaeological site of Ariani, northern Greece. *Materials Characterization*, **60**, 292-302.
- Kramar S., Lux J., Mladenović A., Pristacz H., Mirtič B., Sagadin M., Rogan-Šmuc N. (2012): Mineralogical and geochemical characteristics of Roman pottery from an archaeological site near Mošnje (Slovenia). *Applied Clay Science*, **57**, 39-48.
- Li L., Xie G., Feng G., Feng X., Yan L., Zhu J., Li Y. (2013): Provenance research by INAA on ancient Chinese white porcelain excavated from the Maojiawan site of Beijing. *Journal of Archaeological Science*, **40**, 1449-1453.
- Lofrumento C., Zoppi A., Castellucci E.M. (2004): Micro-Raman spectroscopy of ancient ceramics: a study of French sigillata wares. *Journal of Raman Spectroscopy*, **35**, 650-655.
- Maggetti M. (1981): Composition of Roman pottery from Lousonna (Switzerland), British Museum Occasional Paper, **19**, 33-49.
- Maggetti M. (1982): Phase analysis and its significance for technology and origin. In "Archaeological ceramics", J.S. Olin and A.D. Franklin, ed., Smithsonian Institution Press, Washington, 121-133.
- Maggetti M. (1990): Il contributo delle analisi chimiche alla conoscenza delle ceramiche antiche. In "Scienze in Archeologia" Mannoni T., Molinari A., Firenze 1990, 65-88.

- Mallory-Greenough L.M., Greenough J.D., Owen J.V. (1998): New Data For Old Pots: Trace-Element Characterization of Ancient Egyptian Pottery Using ICP-MS. *Journal of Archaeological Science*, **1**, 85-97.
- Mangone A., Giannossa L.C., Ciancio A., Laviano R., Traini A. (2008) Technological features of apulian red figured pottery. *Journal of Archaeological Science*, **35**, 1533-1541.
- Mangone A., Giannossa L.C., Colafemmina G., Laviano R., Traini A. (2009): Use of various spectroscopy techniques to investigate raw materials and define processes in the overpainting of Apulian red figured pottery (4th century BC) from southern Italy. *Microchemical Journal*, **92**, 97-102.
- Maritan L. (2004): Archaeometry study of Etruscan-Padan type pottery from the Veneto region: petrographic, mineralogical and geochemical-physical characterization. *European Journal of Mineralogy*, **16**, 297-307.
- Maritan L., Mazzoli C. (2004): Phosphates in archaeological finds: implications for environmental conditions of burial. *Archaeometry*, **46**, 673-683.
- Middleton A.P., Edwards H.G.M., Middleton P.S, Ambers J. (2005): Identification of anatase in archaeological materials by Raman spectroscopy: implications and interpretation, *Journal of Raman Spectroscopy*, **36**, 984-987.
- Mohsen Q., El-maghraby A. (2010): Characterization and assessment of Saudi clays raw material at different area, *Arabian Journal of Chemistry*, **3**, 271-277.
- Moropoulou A., Bakolas A., Bisbikou K. (1995): Thermal analysis as a method of characterizing ancient ceramic technologies. *Thermochemica Acta*, **269-270**, 743-753.
- Nyarko B.J.B., Bredwa-Mensah Y., Serfor-Armah Y., Dampare S.B., Akaho E.H.K., Osae S., Perbi A., Chatt A. (2007): Investigation of trace elements in ancient pottery from Jenini, Brong Ahafo region, Ghana by INAA and Compton suppression spectrometry. *Nuclear Instruments and Methods in Physics Research Section B: Beam Interactions with Materials and Atoms*, **263**, 196-203.
- Ospitali F., Sabetta T., Tullini F., Nannetti M.C., Di Lonardo G. (2005): The role of Raman microspectroscopy in the study of black gloss coatings on Roman pottery. *Journal of Raman Spectroscopy*, **36**, 18-23.
- Quinn P.S., Day P.M. (2007): Calcareous microfossils in Bronze Age Aegean Ceramics: Illuminating Technology and Provenance. *Archaeometry*, **49**, 775-793.
- Quinn P.S., Day P.M., Kilikoglou V. (2010): Keeping an eye on your pots: The provenance of Neolithic ceramics from Cyclops Cave on the Island of Youra, Greece. *Journal of Archaeological Science*, **37**, 1042-1052.
- Rathossi C., Tsolis-Katagas P., Katagas C. (2004): Technology and composition of Roman pottery in northwestern Peloponnese, Greece. *Applied Clay Science*, **24**, 313-326.
- Riederer J. (2004): Thin section microscopy applied to the study of archaeological ceramics. *Hyperfine Interaction*, **154**, 143-158.
- Riccardi M.P., Messiga B., Duminuco P. (1999): An approach to the dynamics of clay firing. *Applied Clay Science*, **15**, 393-409.
- Ricciardi P., Nodari L., Gualtieri S., De Simone D., Fabbri B., Russo U. (2008): Firing techniques of black slipped pottery from Nepal (12th-3rd century B.C.): The role of Mössbauer spectroscopy. *Journal of Cultural Heritage*, **9**, 261-268.
- Rice M. (1987): Pottery Analysis. A Sourcebook. Chicago, pp. 485.
- Ruvalcaba-Sil J.L., Ontalba Salamanca M.A., Manzanilla L., Miranda J., Cañetas Ortega J., López C. (1999): Characterization of pre-Hispanic pottery from Teotihuacan, Mexico, by a combined PIXE-RBS and XRD analysis. *Nuclear Instruments and Methods in Physics Research Section B: Beam Interactions with Materials and Atoms*, **150**, 591-596.

- Sabbatini L., Tarantino M. G., Zambonin P. G., De Benedetto G. E. (2000): Analytical characterization of paintings on pre-Roman pottery by means of spectroscopic techniques. Part II: Red, brown and black colored shards. *Fresenius Journal of Analytical Chemistry*, **366**, 116-124.
- Schwedt A., Mommsen H., Zacharias N. (2004): Post-depositional elemental alterations in pottery: neutron activation analyses of surface and core samples. *Archaeometry*, **46**, 85-101.
- Schwedt A., Mommsen H., Zacharias N., Buxeda i Garrigós J. (2006): Analcime crystallization and compositional profile-comparing approaches to detect post-depositional alteration in archaeological pottery. *Archaeometry*, **48**, 237-51.
- Secco M., Maritan L., Mazzoli C., Lampronti G.I., Zorzi F., Nodari L., Russo U., Mattioli S.P. (2011): Alteration processes of pottery in lagoon-like environments. *Archaeometry*, **53** (4), 809-829.
- Sendova M., Zhelyaskov V., Scalera M., Ramsey M. (2005): Micro-Raman spectroscopic study of pottery fragments from the Lapatsa Tomb, Cyprus, ca 2500 BC. *Journal of Raman Spectroscopy*, **36**, 829-833.
- Sherriff B.L., Court P., Johnston S., Stirling L. (2002a): The source of raw materials for Roman pottery from Leptiminus, Tunisia. *Geoarchaeology: An International Journal*, **17**, 835-861.
- Sherriff B.L., McCammon C., Stirling L. (2002b): A Mössbauer study of the color of Roman pottery from the Leptiminus archaeological site, Tunisia. *Geoarchaeology*, **17**, 63-874.
- Siouris I.M., Walter J. (2006): A neutron diffraction study of ancient Greek ceramics. *Physica B: Condensed Matter*, **385-386**, 225-227.
- Stievano L., Bertelle M., Calogero S. (2003): Application of ^{57}Fe Mössbauer spectroscopy for the characterisation of materials of archaeological interest: The work performed in Italy. *Hyperfine Interactions*, **150**, 13-31.
- Stievano L., Bertelle M., Calogero S., Wagner F.E. (2004): The application of ^{119}Sn Mössbauer spectroscopy to the investigation of glass coatings: Evolution of the tin species in lead-rich white glazes. *Hyperfine Interactions*, **154**, 83-94.
- Striova J., Lofrumento C., Zoppi A., Castellucci E. M. (2006): Prehistoric Anasazi ceramics studied by micro-Raman Spectroscopy. *Journal of Raman Spectroscopy*, **37**, 1139-1145.
- Tang C.C., MacLean E.J., Roberts M.A., Clarke D.T., Pantos E., Prag A.J.N.W. (2001): The study of Attic Black Gloss sherds using synchrotron X-ray diffraction. *Journal of Archaeological Science*, **28**, 1015-1024.
- Tiequan Z., Changsui W., Hongmin W., Zhenwei M. (2010): The preliminary study on kiln identification of Chinese ancient Qingbai wares by ICP-AES. *Journal of Cultural Heritage*, **11**, 482-486.
- Tite M.S., Maniatis Y. (1975): Examination of ancient pottery using the scanning electron microscope. *Nature*, **257**, 122-123.
- Trindade M.J., Dias M.I., Coroado J., Rocha F. (2009): Mineralogical transformations of calcareous rich clays with firing: a comparative study between calcite and dolomite rich clays from Algarve, Portugal. *Applied Clay Science*, **42**, 345-355.
- Tschegg C. (2009): Post-depositional surface whitening of ceramic artifacts: alteration mechanisms and consequences. *Journal of Archaeological Science*, **36**, 2155-2161.
- Tschegg C., Ntaflou T., Hein I. (2009): Thermally triggered two-stage reaction of carbonates and clay during ceramic firing - A case study on Bronze Age Cypriot ceramics. *Applied Clay Science*, **43**, 69-78.

- Turbanti Memmi I. (2004): Pottery production and distribution: the contribution of mineralogical and petrographical methodologies in Italy. State of the art and future developments. *Periodico di mineralogia*, **73**, 239-257.
- Vaughn K.J., Conlee C.A., Neff H., Schreiber K. (2006): Ceramic production in ancient Nasca: provenance analysis of pottery from the Early Nasca and Tiza cultures through INAA. *Journal of Archaeological Science*, **33**, 681-689.
- Vaughn K.J., Dussubieux L., Williams P.R. (2011): A pilot compositional analysis of Nasca ceramics from the Kroeber collection, *Journal of Archaeological Science*, **38**, 3560-3567.
- Velraj G., Janaki K., Musthafa A.M., Palanivel R. (2009): Spectroscopic and porosimetry studies to estimate the firing temperature of some archaeological pottery sherds from India. *Applied Clay Science*, **43**, 303-307.
- Viti C., Borgia I., Brunetti B., Sgamellotti A., Mellini M. (2003): Microtexture and microchemistry of glaze and pigments in Italian Renaissance pottery from Gubbio and Deruta. *Journal of Cultural Heritage*, **4**, 199-210.
- Wu Q.Q., Zhu J.J., Liu M.T., Zhou Z., An Z., Huang W., He Y.H., Zhao D.Y. (2013): PIXE-RBS analysis on potteries unearthed from Lijiaba Site. *Nuclear Instruments and Methods in Physics Research Section B: Beam Interactions with Materials and Atoms*, **296**, 1-6.

POTTERY ANALYSIS

PROVENANCE



OM

identification of tempers

CHEMICAL
(ICP-AES, ICP-MS, ICP-OES, XRF, INAA, PIXE, AAS)

identification of chemical elements

TECHNOLOGICAL ASPECTS

Nature, firing condition, modeling, decorations

OM

microstructure, groundmass and composition of inclusions → DEFINITION OF FABRIC

XRD, FTIR
Time-of-flight neutron diffraction

of mineralogical phases and new firing minerals

μ-Raman spectroscopy
TEM

inclusions of the paste decorations and superficial treatments

Mössbauer spectroscopy,
XAS

oxidation state of iron

SEM-EDS

micro-morphological analysis allows to define the groundmass microstructure, inclusions, pores and the degree of vitrification

EMPA

compositional zoning and reaction rims developed during firing

DTA e TGA

Analysis of behavior under firing

SANS

Analysis of porosity and definition of firing temperature

1.KHIRBET AL-BATRAWY: GEOGRAPHICAL, GEOLOGICAL AND ARCHAEOLOGICAL SETTING

1.1 Geographical setting

The archaeological site of Khirbet al-Batrawy is located in the periphery of the modern city of Zarqa in the north-central sector of Jordan (Figs. 1a and 1b).

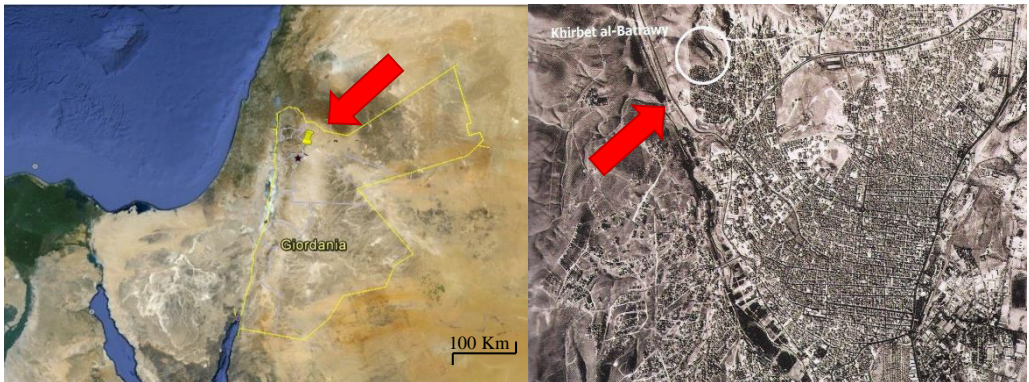


Figure 1: a) Geographical location of Khirbet al-Batrawy in Jordan (from *Google Earth*; changed). b) Image of the modern city of Zarqa with the white circle indicating the cliff of Khirbet al-Batrawy (from *Nigro, 2010*).

The site occupies the top of a limestone cliff, from where it dominates a large part of the Upper Wadi az-Zarqa ($32^{\circ} 5' N$ latitude and $36^{\circ} 4' E$ longitude) at about 660 m above mean sea level; in particular it raises from the surrounding landscape about 100 m in the north-eastern part and more than 150 m in the south-western part (Fig. 2). The cliff is surrounded to the south and the east by the houses of the northern periphery of Zarqa, while to the west, a steep cliff overlooked the river. A huge stone quarry, which had removed the front hill and part of the slopes of Batrawy itself, was located to the north, the only side from which the site could be quite easily approached. The city plateau is characterized by steep irregular slope broken into steps-like features, in most of its directions and sides. The intersecting of the nearly horizontal bedding planes of the limestone formation with the perpendicular vertical joint system at slopes surface resulted in rough slopes interrupted with vertical cuts that break the slope into several ridges forming steps-like landscape surface. These geomorphological elements, which have not only stabilized the plateau slopes but also made the plateau slope, served as an ascending natural defense in climbing into the site (Khrisat, 2006).



Figure 2: Photograph of Khirbet al-Batrawy on the top of a limestone cliff (courtesy of Rome “La Sapienza” Expedition to Palestine & Jordan).

1.2 Historical and Archaeological setting

1.2.1 Khirbet al-Batrawy: The Discovery

In the last decades of the XXth century a great number of territorial and settlement studies in Near East were developed.

In the 1960s numerous surveys were carried out with the aim to locate ancient settlements or basins suitable for the development of human communities in this region. These first researches revealed to the archaeological community the potentiality of the Jordan region and gave the start to a series of regional surveys with a multidisciplinary approach typical of New Archaeology in 1980s and 1990s.

At the end of the 1980s Sapienza-University of Rome also took part in the explorations in Jordanian region. Prof. Gaetano Palumbo, director of the expedition, in cooperation with the American Center of Oriental Research in Amman produced the Jordan Antiques Database and Information System (JADIS), a detailed catalogue of the archaeological heritage in Jordan.

The involvement of Sapienza-University in the archaeological exploration of Jordan stopped in the late 1990s to restart in 2004 when prof. Lorenzo Nigro, in cooperation with two PhD students (Andrea Porcaro and Maura Sala), decided to return in Jordan to study the origins of the Middle East cities and the evolution of the socio-economic aspects of human society in this region during Bronze Age.

Most suitable basins for human occupation in Bronze Age were identified on the basis of the results of a detailed analysis of satellite maps of Jordan. The exploration of the region, carried out in cooperation with prof. Zeidan Kafafi (University of Yarmouk,

Irbid), led to the discovery of Khirbet al-Batrawy, a previously unknown archaeological site, which proved to be a walled town of the Early Bronze Age (Nigro, 2010, 2011).



Figure 3: Topographical plan of Khirbet al-Batrawy, with the indications of excavated areas (courtesy of Rome “La Sapienza” Expedition to Palestine & Jordan).

1.2.2 The Excavations

The aim of the *Archaeological Expedition to Palestine & Jordan* of Sapienza-University is the study of the birth of the cities in Southern Levant during the Bronze Age with the purpose to investigate the development of “Syro-Palestinian culture” (Nigro, 2010, 2011).

The archaeological excavations started in 2005 and are going on till today.

On the basis of the results of the archeological excavations carried out so far, the Khirbet al-Batrawy site was subdivided in six areas (Fig. 3).

- Area A (A-east and A-west): where the acropolis was built and the remains of the small Early Bronze Age IVB (2200-2000 B.C.) village were set;
- Area B: in the northern spur of the cliff where the main Early Bronze II-III city-wall, the city-gate, a round bastion and a further projecting wall were discovered; in the south part a Bronze Age III public building, the so called “Palace of copper axes”, and remains of rural village Bronze Age IVB were brought to light;
- Area C: including the north-western Tower in the north-western spur;
- Area D: in the south-western spur where a big tower was located to control the Wadi az-Zarqa;
- Area E: inside the southern fortification line a secondary entrance was discovered, with a stairway connected to the city;
- Area F: at the center of the easternmost terrace of the site, where the Bronze Age II-III temple of the city was located (Nigro, 2006, 2008, 2012).

1.2.3 The Archaeological remains

The archaeological excavations of Khirbet al-Batrawy site uncovered a very complex inventory of remains.

In addition to pottery sherds, animal bones, Cananean blades, a flint blades and débit-ages, limestone pestle, potter wheel and flint blades have also been found. In the so called “Palace of copper axes” have been unearthed a series of bone tools, including a knife. The most important finds were four copper axes, probably with a symbolic value, discovered in a small hole (Nigro, 2006, 2008, 2012).

1.2.4 The History of Khirbet al-Batrawy

The history of Batrawy spans over a period of about a millennium and crosses the four major historical periods of the Early Bronze Age Levant that are summarized in Table 1.

Khirbet al-Batrawy arose as a major Early Bronze Age centre controlling the area of the Upper Wadi az-Zarqa, which offered a series of geo-ecological niches extremely

favorable to human occupation and stable agriculture since the beginning of the Early Bronze Age.

Archaeological excavations and stratigraphic records allowed defining the history of Batrawy, from the IV millennium B.C. to the development of a fortified city.

The first processes of sedentarization started in the last centuries of IV millennium B.C. when a group of semi-nomadic herders and farmers settled along the Zarqa River and began to practice agricultural activities.



Figure 4: Detail of the destruction layer inside the “Palace of the copper axes” EBIII (courtesy of Rome “La Sapienza” Expedition to Palestine & Jordan).

At the beginning of the III millennium B.C., the rural communities in the Upper Wadi az-Zarqa decided to move from the river banks and to concentrate agricultural products, exchanged goods (also linked to the intensifying copper trade), labor, power and religious places in a protected site leading to the foundation of the fortified city of Batrawy, around 3000 B.C.


Stratigraphic data and structural changes allowed dividing the Batrawy history in four periods from 3000 B.C. to 2000 B.C., when this site was completely abandoned. During the first phase, called Early Bronze II (EB II), dating back between 3000 and 2700 B.C., the city-wall was built all around the hill and the monumental temple and other buildings have been erected on the Acropolis. In 2700 B.C. a violent earthquake stopped the growth of the city causing the destruction of the city-wall, the city-gate and the façade of the temple. During the other two phases, called Early Bronze IIIA (EB IIIA) (2700- 2500 B.C.) and Early Bronze IIIB (EB IIIB) (2500-2300 B.C.), the city of Batrawy was reconstructed and grew up in a more monumental way. In EB IIIA the city-wall was erected again and the temple was rebuilt. Trade activities developed extensively, giving a diffuse wealth in Batrawy until the enemy raids around 2500 B.C. that set on fire the city.

During EB IIIB Batrawy was rebuilt with a strong defensive system including towers and bastions. In this period a big palatine complex (Fig. 4), center of administrative and productive function and collection of luxury goods, was erected. The final de-

struction of the city took place at the end of XXIVth century B.C., when the whole city was set on fire. From this destruction Batrawy did not recover.

The hill was abandoned between 2300 and 2200 B.C. (Bronze Age IV A) and used as a burial area. It was resettled around 2200 B.C. (Bronze Age IV B) by a rural village, but it had a short life and around 2000 B.C. the site was completely abandoned and forgotten (Nigro, 2006, 2008, 2010, 2012).

Table 1: Summary of the main development phases of Khirbet al-Batrawy (courtesy of Rome “La Sapienza” Expedition to Palestine & Jordan).

EARLY BRONZE AGE II	
<p>The building of the town wall. This period ends when the town was destroyed by a violent earthquake.</p>	
EARLY BRONZE AGE IIIA	
<p>Batrawy grew up and was provided with a massive fortification system preserved till today and a religious temple.</p>	

EARLY BRONZE AGE IIIB

During this phase a luxurious palace was rebuilt and at the end of the Early Bronze IIIB the city was completely destroyed and set on fire.

**EARLY BRONZE AGE IV**

A new rural village arose on the hill over the raised ruins of the previous city.



1.3 Geological setting

1.3.1 Jordan geology

Stratigraphic studies describe Jordan as a region characterized by a succession of sandstones and limestones lying on a Pre-Cambrian basement as summarized in Table 2 (Burdon, 1959).

The Pre-Cambrian basement consists of metamorphic rocks of the Aqaba Granite Complex, and molasses-type conglomerates of the Saramuj Series.

The Aqaba Granite Complex extends from Saudi Arabia. The rocks of the complex may be described as a succession passing from the oldest metamorphic rocks to gray granite (granodiorites), red granites, basic intrusive rocks to the youngest acid intrusive rocks. In particular, the rocks of this succession include:

- Garnetiferous biotite-schists and quartzites, some with biotite; gneiss and mica-schists are also present.
- Gray granites with abundant biotite; the orthoclase and oligoclase occur in equal amounts and are altered in sericite and chlorite;
- Red granites containing microcline and perthite and lesser amounts of oligoclase; biotite is present in small amounts;
- Dolerites with granular augite and some large crystals of labradorite in a holocrystalline base of feldspar with magnetite and some calcite;
- Acid intrusive rocks with phenocrystals of orthoclase, plagioclase and hornblende in a microcrystalline base.

The Saramuj Series in Wadi Saramuj extends near the south-east corner of the Dead Sea. The rocks of this series include the older succession of Saramuj Conglomerates and the younger intrusive rocks.

- Saramuj conglomerates consist of well-rounded igneous pebbles and boulders set in strongly consolidated arkosic cement; these beds are separated by well-defined bands of cemented sandstone. The pebbles and boulders derived from the rocks of the Aqaba Granite Complex; the cement and sandstone consist of feldspar and quartz derived from Aqaba Granite Complex;
- Intrusive rocks are augite-nepheline-syenites, diabase-porphyrites and appinites.

In Eastern Jordan the Cambrian consists of the terrestrial sandstones of the Quweira Series, dated by intercalated fossiliferous Middle Cambrian limestone. Outcrops of this series occur in the south-east of the Dead Sea and extend to the south along the rift and eastwards around Aqaba granites. The series consists of a lower and upper sandstone of terrestrial origin and Nubian facies, locally separated by fossiliferous marine beds. The Quweira Series includes the oldest Lower Quweira sandstone, the Burj limestone group (dated low Middle Cambrian), the Upper Quweira sandstone and the youngest intrusive rocks.

- Lower Quweira sandstone outcrops are capped by a series of grits, conglomerates, quartzites and current-bedded sandstone of a predominately dark red colour, which rest on the tilted planed erosion surface.
- Burj Limestone Group consists in a limestone rich in fossils. King (1923) described fossils as *Siphonotreta* sp., *Michometra alata*, *Hyolithus* and *Anomocare cambelli*; Picard (1942) re-examined the fossils and reported other species as for example the *Protolenus orientalis*.
- Upper Quweira Sandstone includes sandstones all of Nubian Facies.
- Intrusive rocks group composed by a diorite dyke that cuts the Qweira sandstone.

Ram sandstone (Palaeozoic) is an entirely terrestrial and non fossiliferous deposit of Nubian facies. It consists in a coarse but even-grained loosely cemented yellowish

sandstone, outcropping extensively in the south of Jordan, where it is clearly distinguished from the Quweira Sandstones and Um Sahn Sandstone.

The Um Sahn Sandstone, and marine beds of Middle Triassic and Middle Jurassic age (Zarqa Group), are also terrestrial in the south, but contain marine beds in the Dead Sea and in the Wadi Zarqa.

Outcrops consist in sandstone well-bedded, pink, red or mauve in color. Proceeding to the north, shales and marls appear, interbedded with the terrestrial estuarine sandstones. On passing further to the north, terrestrial sandstone of Nubian facies become less important and marine and estuarine fossiliferous beds become more common.

The Triassic formation of the Zarqa group shows a series of red sandstones, shales and marls, below which gypsum beds and grey marly limestones are seen with underlying clay beds (Blake and Ionides, 1939).

Jurassic rocks are represented by the Kurnub Sandstone which covers the time-interval from the Upper Jurassic to the Lower Cretaceous; these desert sandstones are composed mainly of Nubian sandstones poorly consolidated with an extensive outcrop north from Mudawwara and along the Rift. In the south-east of Quweira this formation consists of a lower part which lies on the Um Sahn Sandstone composed by shales, hard, spotted, glauconitic sandstones and some quartzites; the upper part is composed by consolidated sandstones, pink, mauve, red and white in color. Northwards the shales are absent and only the multicolored sandstones occur.

During the Turonian the sea spreads and marine beds, mainly limestones and dolomites with marl (rarely shales, sandstone and chinks), were deposited. All these beds have been grouped into the Ajlun Series (Naur, Fuheis, Hummar, Shuayb, and Wadi As Sir formations) with a large outcrop in the north near Amman. In the south, their outcrops tend to be confined to the escarpment of the Jordan Valley. Ajlun series can be subdivided into Cenomanian and Turonian:

- Cenomanian overlies the Kurnub Sandstone and is overlain by the Turonian. In the northern part the outcrops consist of bedded limestones separated by marls; it is highly fossiliferous.
- Turonian is essentially represented by mud shales and sandstones.

At the beginning of the Senonian, limestones and dolomites were replaced by chinks, flint and marls, sometimes bituminous. The marine sedimentation continued into the Eocene, but these limestones are very different from the general chalk-flint-marl sequence. These marine rocks of Eastern Jordan have been grouped into the Belqa Series, comprising all sediments deposited in Eastern Jordan from the end of Turonian to the final emergence in the Oligocene.

The dominant lithotypes are chalks and marls with varying amounts of flint-chert; bituminous cement occurs as well as phosphatic rocks. Sedimentation continued for longer in the north than in the south.

- Coniacian-Santonian: Bituminous marl with rare black flints and some large calcareous concretions.
- Campanian and Lower Maestrichtian: In some places the formation is thick and composed of hard chalk with thin chert beds; in other places, the formation is thinner and includes bedded limestone and thick chert.
- Maestrichtian: Overlying the chert series, beds of pink chalk occur and sometimes are associated with limestone. Above these, phosphate beds (dated as Maestrichtian by the fossiliferous content) usually associated with gypsum occur.
- Danian: The chalk which overlies the phosphate beds is dated as Danian (but no fossils confirms that hypothesis). Green and red marbles are also included.
- Cretaceous-Eocene Transition: The thick series of soft chalk with flints and the succeeding soft grey marls are assigned to this transition phase.
- Eocene: In the north of Eastern Jordan it is represented by flinty limestone, while in the southern part there are many outcrops of nummulitic limestones.

In Eastern Jordan during Upper Oligocene and the Lower Miocene erosion produced peneplain. The plateau basalts were erupted from the Middle Miocene to Historical.

All the sedimentary deposits formed in lakes or land since erosion commenced after the rejuvenation of the Oligocene peneplain by the Middle Miocene uplift and tectonics are attributed to the Neogene Undifferentiated. The beds consist mainly of coarse lacustrine-deltaic sediments, derived by erosion. In the north, fresh-water melanopsis limestones overlie cemented conglomerates and outcrops are confined to terraces at varying heights on the sides of the rift. In the south, outcrops are extensive.

The Lisan Series consists of thin-bedded almost varved, clay and gypsum marls with coarser lateral facies. They were formed throughout most of the Pleistocene in a saline lake, expanding in size. The gypsum layer represents chemical precipitation in the dry season, while the clays and silts represent mechanical sedimentation during the wet season.

Recent sediments are all terrestrial and have been formed or deposited by water and wind, more are residual after the action of other agents of erosion. In the north and centre of Eastern Jordan they consist of sands and gravels of the Jordan Valley and muds and sands in areas of closed drainage and in wadi-bottoms. No igneous activity is known in Eastern Jordan until the eruption of the plateau basalts in the Middle Miocene. These basaltic eruptions have continued down to Historical times and are clearly associated with the formation of the rift Valley.

GEOLOGICAL SCALE			REPRESENTATIVES IN EAST JORDAN		SUMMARISED DESCRIPTION BY SHEETS								
ERA	PERIOD	EPOCH	SERIES	STAGE or FORMATION	SHEET 1, Amman	SHEET 2, Karak	SHEET 3, Ma'an						
CAINOZOIC	QUATERNARY (or Diluvium)	RECENT	11. RECENT	Superficial	12. PLATEAU BASALTS	Gravel, Sands, Talus.	Gravel, Sands, Talus.	Gravel, Sands, Talus.					
		PLEISTOCENE	10. LISAN SERIES	Lacustrine		Marl, Gypsum, Gravels.	Marl, Gypsum, Gravels.	NOT EXPOSED					
	TERTIARY	PLIOCENE	9. NEOGENE UNDIFFERENTIATED	8. BELQA SERIES	Terrestrial and Lacustrine	Freshwater Limestone, Marine Beds, Conglomerates.	Conglomerates, Sands, Shales (+400 m.).	Conglomerates, Sands, Gravels, No Marine Beds.					
		MIOCENE											
		OLIGOCENE							EMERGENCE AND PLANATION				
MESOZOIC	CRETACEOUS	Eocene	7. AJLUN SERIES	8 f. Eocene 8 e. Palaeocene 8 d. Danian 8 c. Maestrichtian 8 b. Campanian+Lr. Macstrich. 8 a. Coniacian-Santonian	7 b. Marine Turonian 7 a. Marine Cenomanian	f. Flinty Limestone e. Marl over Chalk-Flint d. Chalk (Limestone) c. Phosphates and Bitum. b. Puckered Flint in L'ste a. Marl (Bituminous). TOTAL = +400 m.	f. Chalk, Limestone e. Marl over Chalk-Flint d. Chalk and Marble c. Phosphates b. Hard Chalk-Chert a. 60 m. Chalk TOTAL = +400 m.	f. Chalk, Numm. Limestone e. Marl over Chalk-Flint d. Chalk with Flint c. Phosphates (+Bitum.) b. Thick Cherty Chalk — TOTAL = +400 m.					
		PALAEOCENE											
		DANIAN											
		MAESTRICHTIAN											
		CAMPANIAN											
	JURASSIC	Turonian	6. KURNUB SANDSTONE	7 b. Marine Turonian 7 a. Marine Cenomanian	Soft multi-coloured Sandstones of Nubian facies. Slump readily and conceal underlying formations. Shale facies ABSENT. (~ 200 m.)	Limestones, Dolomites, Marls (~ 450 m.).	Multi-coloured Sandstones so poorly consolidated as to be almost sands. Shale facies ABSENT. (~ 150 m.)	Limestone, Dolomite, Gypsum, Sandstone. 7 a. absent (125 m.).					
		Cenomanian											
		Albian											
	TRIASSIC	Aptian	5. UM SAHM SANDSTONE	5 c. Marine Middle Jurassic	ZARQA GROUP Marine Jurassic only in Wadi Zarqa and south along escarpment. Marine Triassic poorly exposed at bottom of W. Zarqa.	No Marine Jurassic so far south. Nubian Sandstones with some Shales and Marls. Marine Triassic in Wadi Zarqa Ma'in.	UPPER. Pink, purple, red and white, poorly consolidated Sandstones (~ 110 m.). LOWER. Hard Shales, Glaucconitic Sandstones and some Quartzite (~ 40 m.).						
		Barremanian											
Hauterivian													
Valanginian													
Portlandian													
PRE-CAMBRIAN PALAEOZOIC	LIPALIAN INTERVAL	PLANATION	2. SARAMUJ SERIES	2 b. Basic Intrusives 2 a. Arkose Conglomerates	NOT EXPOSED	Jointed grey-white to pink Nubian Sandstone. Typical exposures at mouths of Wadi Mujib and Zarqa Ma'in (~ 250 m.)							
							CAMBRIAN	3. QUWEIRA SERIES	3 d. Intrusives 3 c. Upper Quweira Sandstone 3 b. Burj Limestone Group 3 a. Lower Quweira Sandstone	NOT EXPOSED	c. 200 m. of Nubian Sandstone. b. 60 m. of Marine Beds a. 210 m. (Sandstones Conglomerates)	300 m. Current-bedded Sandstones, Quartzites and Shales. Marine Beds die away to south. One late basic dyke.	
													Upper Cambrian
													Middle Cambrian
													Lower Cambrian
EROSION, EXPOSING GRANITES	1. AQABA GRANITE COMPLEX	1 e. Acid Intrusives 1 d. Basic Intrusives 1 c. Red Granite 1 b. Grey Granodiorite 1 a. Metamorphic Schists	NOT EXPOSED	Small outcrops near Feinan. Granites with basic dykes and large porphyry intrusions.	In S.E. corner of Dead Sea; Arkose, Quartzite, Conglomerate; Dykes.	Jebel Harun, Arkose, Conglomerates; some Pyroclastics.							
							Archaean						

The Plateau Basalts consist of labradorite, olivine, augite, magnetite-ilmenite, with glass and apatite as well as hornblende. Secondary minerals are iddingsite after olivine and calcite (Burdon, 1959).

1.3.2 Geology and structure of the Amman-Zarqa Basin and Zarqa River

In this area rocks with age ranging from Triassic to Recent outcrop, being Cretaceous sedimentary lithotypes those more common. On the basis of the geological setting, the outcrops can be divided in: basalts in the north-east, limestones in the centre/centre-north, limestones and marls in the west/north-west with Kurnub sandstone and two different outcrops in the south of marls and sandstones.

The geological formations in the Amman Zarqa Basin are summarized in Table 3 and represented graphically in Fig. 5.

The Lower Cretaceous Kurnub Group is usually found at depth, except in outcrops at the western part of the basin and is mainly composed of sandstone with iron and manganese oxides.

In the north-western part of the basin, formations of Cenomanian age such as Hummar, Fuheis and Na'ur are exposed; outcrops of Kurnub Group (Early Cretaceous), Azab Group (Jurassic) and Ramtha Group (Triassic) have been also observed. Hummar Formation is composed of limestone and dolomitic limestone, Fuheis Formation of marl and limestone and the Na'ur Formation of limestone, dolomite, marl and limestone.

The Amman Formation of Upper Cretaceous age is composed of limestone, chert, chalky and phosphorite. The Wadi Umm Ghundran Formation of Coniacian age is concentrated in the area between the modern cities of Amman and Zarqa. It is composed by chalky-marl and marl. The Shuayb Formation of Turonian age (Ajlun Group) consists of different type of limestones, phosphorite marl and chert. The phosphorite horizon is friable or slightly cemented with calcite. It consist of sand-size phosphate particles, pellets, intraclasts, bones and coprolite (Abdel *et al.* 1996, 2008). The materials associated with phosphate particles are mainly marl and clay.

Limestone in the centre/centre-north is represented by different formations. The Wadi As Sir Formation of Cretaceous age, diffusely exposed in the north-eastern area which consists mainly of hard crystalline dolomitic limestone, chalky limestone with occasional chert bands and nodules. The thickness of this formation reaches up to 80-100 m and forms a part of the upper aquifer in the Amman-Zarqa Basin (Bender, 1974).

Vesicular basalt of Holocene age is exposed in the eastern part of the studied area.

The basin is characterized by the presence of the Zarqa river which is connected to the formation of Jordan Rift Valley. The exposed formations in the area are marine sedi-

ments; along the Zarqa river crystalline limestone alternating with shale, gypsum layer, argillaceous marly lime, shales and iron-rich stone and sandstone.

Table 3: Simplified classification of the rock units in the Amman Zarqa Basin (from Margane *et al.*, 2002 Table 2)

System	Epoch	Group	Formation	Symbol	Lithology	Thickness (m)	
Quaternary	Holocene	Jordan valley (JV)	Alluvium	Basalt	Qal	Clastics	
	Pleistocene		Lisan		JV3	Marl. clay, evaporites	>300
Tertiary	Pliocene	Belqa (B)	Samra		JV1-2	Conglomerate with silicious cement sand, gravel	100–350
	Miocene		Neogene				
	Oligocene		Wadi Shallala		B5	Chalk and marly limestone with	0–555
	Eocene		Umm Rijam		B4	Glauconite, Limestone, chalk, chert	0–311
	Paleocene						
Upper cretaceous	Maastrichtian	Ajlun (A)	Muwaqqar		B3	Chalky marl, marl, limestone, chert	80–320
	Santonian		Amman-Al Hasa		B2	Limestone, chert, chalky, phosphorite	20–140
	Coniacian		W. Umm Ghudran		B1	Chalky marl, marl	
	Turonian		Wadi As Sir		A7	Limestone, dolomitic limestone	20–90
			Shuayb		A5-6	Marl, limestone	60–340
			Hummar		A4	Limestone, dolomitic limestone	40–120
	Cenomanian		Fuheis		A3	Marl, limestone	30–100
Naur			A1-2	Limestone, dolomite, Marl, limestone	30–90		
Lower cretaceous	Kumub (K)	Subeihi		K2	Sandstone, shale	90–220	
		Aarda		K1	Sandstone, shale	120–350	
Jurassic	Zarqa (Z)	Azab		Z2	Siltstone, sandstone, shale	0 ≥ 600	
Triassic		Ramtha		Z1	Siltstone, sandstone, shale, limestone limestone, anhydrite, halite	0 ≥ 1250	

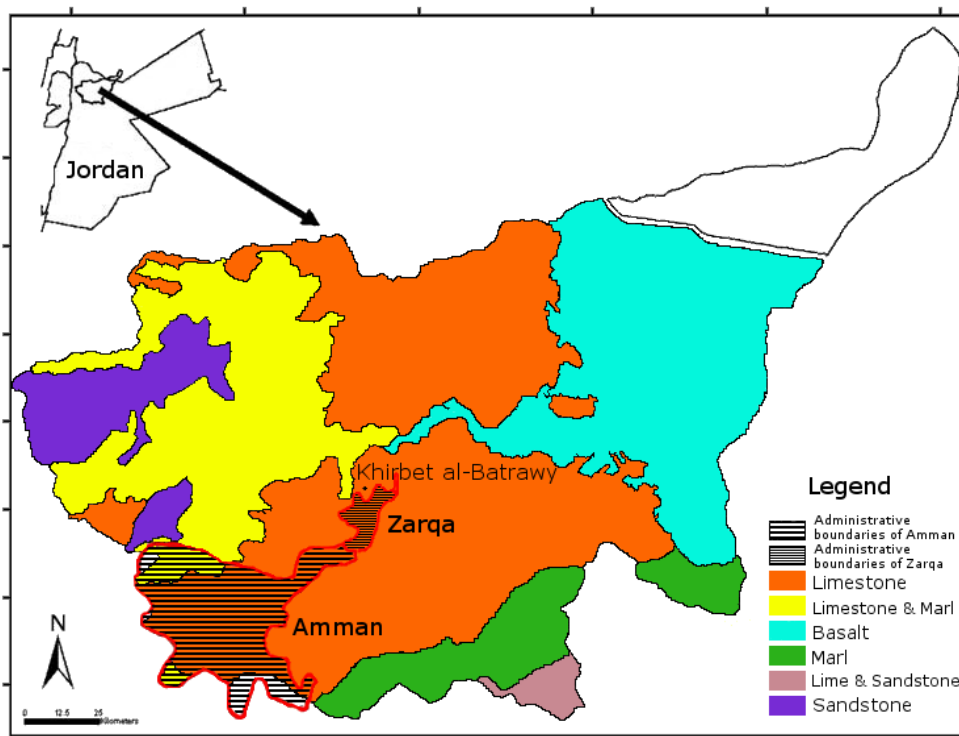


Figure 5: Schematic geological map of Jordan (modified from Shaqour *et al.*, 2008 Fig. 1).

1.3.3 Geology of Khirbet al-Batrawy archeological site

The main physiographical units of the limestone plateau where the archaeological site of Khirbet al-Batrawy is located include: the moderate and high rocky and desert hills, adjacent to the Wadi az-Zarqa, and the up-throw of the geologic Amman-Hallabat Fault Zone.

The formation exposed in the north eastern part of the plateau consists of limestone, ranging from few centimeters to massive clay layers, in the middle and lower part of the formation, interbedded with chert veins and fossiliferous beds (Margane et al., 2002). Even if the limestone belongs to different formations (the Hummar, Shua'yb and Wadi As Sir formations) the limestone forms a unique geomorphological unit with steep slopes of grey-weathering colors batches intercalated with marl. The marlstone, typical of the Khirbet al-Batrawy area, outcropping in the slopes of the wadi beds, is usually intercalated within the limestone and appears as a hardened rock composed by clay, mud, sand and abundant calcareous material (shells) and outcrops along the slopes and in the wadi beds.

The natural clays which are found in the vicinity of the site show some amount of chert micro flakes and broken fossils, which are the product of the local limestone weathering (Fig. 6; Khrisat, 2006).

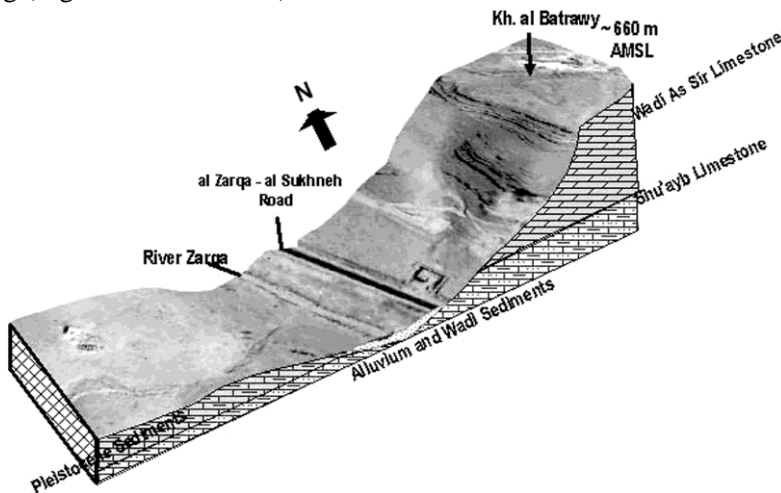


Figure 6: Schematic geological section of the Khirbet al-Batrawy area, (modified from Khrisat, 2006 Fig. 4).

References

- Abed A., Fakhouri K. (1996): On the chemical variability of phosphatic particles from Jordanian phosphorite deposits. *Chemical Geology*, **131**, 1-13.
- Abed A., Sadaqah R., Al Kuisi M. (2008): Uranium and potentially toxic metals during the mining, beneficiation, and processing of phosphorite and their effects on ground water in Jordan. *Mine Water and the Environment*, **27**, 171-182.

- Bender F. (1974): *Geology of Jordan*. Borntraeeger, Berlin, pp. 196.
- Blake G.S., Ionides M.G. (1939): Report on the Water Resources of Transjordan and their Development. Incorporating a Report on Geology, Soils and Minerals and Hydro-geological Correlation. London (Crown Agents for the Colonies).
- Burdon D.J. (1959): Government of the Hashemite Kingdom of Jordan, pp. 82.
- King W.B.R. (1923): Cambrian fossils from the Dead Sea. *Geological Magazine*, **51**, 507-514.
- Khrisat B.R. (2006): Geoarchaeological investigations at Khirbet al-Batrawy. in "Khirbet al-Batrawy. An Early Bronze Age Fortified Town in North-Central Jordan. Preliminary report of the First Seasons of Excavations (2005)", L. Nigro, ed., Rome «La Sapienza» Studies on the Archaeology of Palestine & Transjordan, 3, Rome, 251-261.
- Margane, A., Hobler, M., Al-Momani, M. & Subah, A. (2002): Contributions to the hydrogeology of Northern and Central Jordan. *Geologisches Jahrbuch C 68*, ed., Hannover, pp. 52.
- Nigro L. (2006): Khirbet al-Batrawy. An Early Bronze Age Fortified Town in North-Central Jordan. Preliminary report of the First Seasons of Excavations (2005). L. Nigro, ed., Rome «La Sapienza» Studies on the Archaeology of Palestine & Transjordan, 3, Rome, pp. 280.
- Nigro L. (2008): Khirbet al-Batrawy II. The EB II city-gate, the EB II-III fortifications, the EB II-III temple. Preliminary report of the second (2006) and third (2007) seasons of Excavations. L. Nigro, ed., Rome «La Sapienza» Studies on the Archaeology of Palestine & Transjordan, 6, Rome, pp. 412.
- Nigro L. (2010): In the Palace of the Copper Axes/Nel Palazzo delle Asce di Rame. Khirbet al-Batrawy: the discovery of a forgotten city of the III millennium B.C. in Jordan/Khirbet al-Batrawy: la scoperta di una città dimenticata del III millennio a.C. in Giordania. L. Nigro, ed., Rome «La Sapienza» Studies on the Archaeology of Palestine & Transjordan, Colour Monographs I, Rome, pp. 144.
- Nigro L. (2011): Dominating the River: Khirbet al-Batrawy, an EB II-III City in North-Central Jordan. *Syria*, **88**, 59-74.
- Nigro L. (2012): Khirbet al-Batrawy III. The EB II-III triple fortification line and the EBIIIB quarter inside the city. Preliminary report of the fourth (2008) and fifth (2009) seasons of Excavations. L. Nigro, ed., Rome «La Sapienza» Studies on the Archaeology of Palestine & Transjordan, 8, Rome, pp. 438.
- Picard L. (1942): New Cambrian fossils and Paleozoic problematica from the Dead Sea and Arabia. *Bulletin of the Geology Department*, Hebrew University, Jerusalem, **4**, 1-18.
- Shaqour F.M., Jarrar G., Hencher S., Kuisi M. (2008): Geotechnical and mineralogical characteristics of marl deposits in Jordan. *Environmental Geology*, **55**, 1777-1783.

2. MATERIALS AND ANALYTICAL METHODS

2.1 Archaeological Samples

Archaeological excavations in Khirbet al-Batrawy unearthed a very diversified inventory of pottery productions (Fig. 1):

- Simple and Simple Painted Ware (SW-SPW), mainly represented by bowls, jugs and small and medium size jars;
- Storage Ware (StW), including jars, hole-mouth jars and *pithoi*;
- Kitchen Ware (KW), represented by hole-mouth cooking pots;
- Metallic Ware (MW), that takes the name from the distinctive metallic sound when it is struck and that includes almost exclusively jars.

Two other productions are distinguished on the basis of the related superficial treatments:

- Red Burnished Ware (RBW), including platters, bowls and small and medium size jars;
- Red Polished Ware (RPW), represented almost exclusively by jugs.



Figure 1: Early Bronze IV B pottery vessels (courtesy of Rome “La Sapienza” Expedition to Palestine & Jordan).

Small and medium size jars of SW represent the highest percentage of the assemblage and exhibit ovoid body, flaring neck, everted rim and often a couple of ledge handles. Open shapes of the same group include mainly bowls with curved or straight walls and plain or inturned rim. Most of the pottery appears still coil-built, but open vessels are frequently refined on the slow wheel, and necks and rims of jugs and jars are always manufactured on the wheel, testifying to the technological achievements of the

pottery production. The use of slip to refine the inner or outer surface of vessels was common, especially in the EB IIIA and EB IIIB phases, along with burnishing and polishing.

A large group of samples is represented by the StW and includes both medium size jars and hole-mouth jars for temporary storage and transportation. Also big storage jars and *pithoi*, with coil-built body, and neck and rim manufactured on the slow wheel are present. Medium size jars show flaring neck and everted rim, whereas hole-mouth jars exhibit rounded, flattened or recessed rims and *pithoi* present squared, outer folded or everted rim of triangular section. The use of outer surface treatments such as washing, smoothing or combing is evident in the samples.

Hole-mouth pots, coil-built and characterized by rounded, recessed or inner ridged rims, mainly compose the KW inventory. No evidence of external treatments has been found. Finally, the shapes of MW include almost exclusively medium-large size jars with vertical handles, simple everted rim and flat base, usually showing a combed decoration (Nigro, 2006, 2008, 2012).

The investigated samples, dated between 3000 and 2000 B.C., were divided in different groups on the basis of visual aspect, morphological and stylistic features; in addition their location and stratigraphic data have been considered.

In Appendix A pottery sherds are listed divided in the four periods with the indication of pottery type, class and the place of findings.

2.1.1 EB II Samples (3000-2700 B.C.)

The EB II layer is still under excavations and therefore it was possible to study only eight pottery samples (Appendix A, Fig. 2). The limited number of samples is due to the antiquity of EB II phase and to the fact that it has been under investigations only in a small area of the archaeological site. Pottery sherds consist of jar fragments (SW, StW, RPW), platter fragments (RBW) and bowl fragments (RBW). The use of slip (usually red in color) to refine the inner surface of open vessels was employed in this phase and associated to a horizontal burnishing. These samples were found in the areas B (near the main Early



Figure 2: Representative pottery fragments belonging to Early Bronze Age II (KB.06.E.702/10 top, KB.06.E.703/6 bottom).

Bronze II-III city-wall and the city gate) and E (southern fortification line with the secondary entrance) during the survey in 2006.

2.1.2 EB IIIA Samples (2700-2500 B.C.)

Thirty-six pottery samples of the EB IIIA phase have been investigated (Appendix A, Fig. 3). The potsherds consist of medium and small size jar fragments (StW, SW, RPW), bowl fragments (SW), *pithos* fragments (StW) and platter fragments (RBW, RPW). Inner and outer slip is present on the surface of the vessels, as well as polishing, burnishing and smoothing. Among them, six samples exhibit a surface decoration consisting of simple red



Figure 3: Representative pottery fragments belonging to Early Bronze Age IIIA (KB.05.B.136/5 left, KB.05.B.146/3 right).

strips. A sub-group of nine pottery sherds, showing a highly polished coating, has

been distinguished by the archaeologists and referred to as Khirbet Kerak Ware (hence KKW), an EB IIIA specialized pottery production characteristic of southern Levant. It is distinguished by a major standardization of shapes, fabrics and functions of pottery productions; it appeared in the EB IIIA and it does not seem to be attested afterwards. The KKW fragments consist of bowls and fragmentary medium and small size jars.

Samples have been found in the areas A (Acropolis), B (near the city wall and public building) and E (southern fortification line) during the seasons from 2005 to 2009.

2.1.3 EB IIIB Samples (2500-2300 B.C.)



Figure 4: Photographs of representative pottery fragments belonging to Early Bronze Age IIIB (KB.05.A.204/2 left, KB.05.A.224/2 right).

The phase EB IIIB is represented by thirty-four samples (Appendix A, Fig. 4), fragments of medium and small size jars (SW, StW, RBW, MW), hole-mouth jars (SW, StW), hole-mouth pots (KW) and *pithoi*

(StW). Outer applied rope decorations appear in these vessels. Samples have been found in the areas A (Acropolis) and B (Palace) during the seasons 2005, 2010 and 2011.

2.1.4 EB IV Samples (2300-2000 B.C.)

The sherds analyzed for the EB IV phase include twenty-three samples (Appendix A, Fig. 5), mainly jars (SW, StW, KW, MW), hole-mouth jars (StW) and hole-mouth pots (KW) characterized by outer band combed or incised decoration, while polishing and burnishing are not attested to in this phase. Samples have been found in the areas A (rural village) and B (the remains of the palace) during the seasons 2005-2006.



Figure 5: Photographs of representative pottery fragments belonging to Early Bronze Age IV (KB.05.5/D200 left, KB.05.A.6b/1 right).

2.2 Geological Samples

Generally, it is assumed that the sources of clay used in pottery production were close to the production center and the distance most frequently traveled for both clays and tempers was less than 1 km from the settlement (e.g., Rice, 1987). In the evaluation of supply areas different factors that can influence the distance have to be considered (Rice, 1987). Arnold (1980) revealed that in the past, the 85% of the cases presented the supply areas at a distance lower than 7 km from the production site, suggesting this range as the resource area for procuring their primary clay. Concerning tempers, the analysis of Arnold (1980, 1981) suggests possible areas of supply in a range of several tens of kilometers from the production center.

Unfortunately, political and social issues did not allow the systematic sampling of raw materials in the area for this study and during the season 2012 only two sample of marl outcropping nearby the archaeological site have been collected. Moreover, a sample of brick used in the Batrawy fortification has also been sampled to be com-

pared to the ceramic materials used and to define if its raw material could be the same used in the pottery production.

2.3 Analytical methods

2.3.1 Micro-Raman spectroscopy

About thirty micro-Raman spectra have been collected for each sample in selected spots on the external and internal surface of the sherds as well as in the cross cuts to underline the different composition of the pottery. In particular, in this step Raman spectra have been also collected on thin section that allows the analysis in the cross section. However, the high fluorescence of the ceramic matrix prevented to obtain interpretable Raman spectra; therefore, Raman study was necessarily focused on minerals contained as inclusions in the matrix.

Micro-Raman spectra were collected at room temperature in nearly backscattered geometry using a Jobin-Yvon Horiba Labram apparatus at the Department of Physics and Earth Sciences of the University of Parma (focal distance of 30 cm, 1800 groove/mm grating, 100 μm slit width, $\sim 1.5\text{ cm}^{-1}$ spectral resolution). Radiation at 632.8 nm line of a He-Ne laser was used as excitation and the laser power was set lower than 1 mW on the sample by means of neutral density filter to avoid undesired heating effects. An Olympus microscope with 10x (0.25), 50x (0.75), ULWD 50x (0.55) and 100x (0.90) objectives (with their numerical aperture) and motorized x-y stage was used to focus on the samples with maximum spatial resolution of $\sim 2\ \mu\text{m}$. The system was calibrated using the silicon Raman line at 520.6 cm^{-1} before each experimental session. Collection times were between 30 and 100 s, with 1-3 accumulations. Spectra were baseline corrected and filtered as needed with LabSpec[®] software in order to remove background fluorescence and noise and were analyzed using existing databases as Burgio and Clark (2001), Bouchard and Smith (2003) and the Parma University database (<http://www.fis.unipr.it/phevix/ramandb.php>, accessed July 15, 2012).

2.3.2 Fourier Transform Infrared Spectroscopy (FTIR)

After the removal of the most external layer of ceramic, in order to avoid the direct sampling of possible extraneous substances, a small quantity (a few milligrams) of each potsherd has been finely ground by hand in an agate mortar and prepared for infrared analysis using the KBr pellet method. The mixture was pressed to form a pellet of 0.8 cm in diameter and 1 mm in thickness.

FT-IR analysis was performed using a JASCO FT-IR 6100 Spectrometer at the Department of Physics and Earth Sciences of the University of Parma. The spectra were obtained covering the $4000\text{-}400\text{ cm}^{-1}$ range and recorded with a spectral resolution of

2 cm⁻¹ and signal/noise ratio 42000:1. About 200 scans were added before Fourier transform. Origin[®] software has been used to smooth the data and correct the baseline, and analyzed by Spectra Manager Software[™], by comparison to De Benedetto *et al.* (2002) and by an on line database (rruff.info/).

2.3.3 Optical Microscopy (OM)

Thin sections of the different pottery samples have been made for their analysis in polarizing optical microscopy (ZEISS D-7082 Oberkochen) at the Department of Earth Sciences of Sapienza-University of Rome, following the Whitbread criteria (Whitbread, 1986, 1995).

The most diffuse method to analyze pottery in archaeometric investigations is petrographic analysis. Petrographic techniques are borrowed from geology which used them to describe and classify rocks (Rice, 1987). This method can be applied considering ceramic materials as sedimentary rocks where the fabric consists mainly of clastic grains in a clay matrix, partially altered during firing (Williams, 1983).

The idea of *fabric* is defined by the classification method introduced by Whitbread and it is usually adopted to perform petrographic studies of ancient pottery. This comes from the description of soils and it is related to the “arrangements, size, shape, frequency and composition of components of the ceramic material” (Whitbread, 1986, 1995). This method is based on the description of the three main components of ceramics: clay matrix, inclusions and voids.

The matrix is the most abundant component of ceramics. As first step, sherds are divided on the basis of the presence or absence of fine micritic calcite (calcareous and non-calcareous matrix). After that, it is useful to observe the homo/heterogeneity of the matrix due to differences in color and textural inhomogeneity such as swirls, streaks and other textural features (TFs). The color of the matrix and its color variations have been described according to Munsell soil color chart classification (Munsell, 1975) that allows to hypothesize the composition and atmosphere of firing. The observation of the optical state of clay minerals in cross-polarized light illumination also allows inferring the range of firing temperature (Reedy, 2008). The analysis is based on the evaluation of the change (activity) or invariability (inactivity) of matrix color during the rotation of the stage. The change of matrix color, visible by a collective change in the intensity of the matrix, can be related to a pottery fired at low temperature. Indeed, when ceramics are fired, the vitrification of the clay matrix causes a reduction in the “optical activity” of the matrix producing a matrix unchangeable in color during the rotation of the stage.

Identifying temper is crucial to ceramic petrography. Indeed, natural or added inclusions can be used to characterize the ceramics of specific sites of the regions as, link-

ing inclusions to their probable geological sources, it is possible to infer the provenance of ceramics. The study of the inclusions is based on the description of their frequency (predominant, dominant, frequent, common, few, very few, rare, very rare), grain size (maximum size in mm) and distribution, shape (elongate or equant), angularity or roundness (from very angular to well rounded), spacing (close/single/open spaced), orientation and their relationship to each other. For each type of inclusion, the nature, shape, roundness, modal size and color are also described. Plastic inclusions such as clay pallets are usually included in the description of the inclusions, being they referred to as “textural features” (TFs) and the nature, the boundaries, their concordance with the matrix are described.

The term voids includes interstitial spaces or pores that can occur naturally or as a result of the pottery manufacturing process or thin section preparation. They are classified on the basis of their shape (planar, channels, vughs and vesicles), frequency, size (mega, macro, meso and micro) and alignment. The percentage of voids is defined porosity, which is the factor that imparts specific properties on the finished vessel.

The microscopic analysis also includes the so called “grouping”. Ceramic sherds are grouped and separated into classes with similar composition based upon the nature, abundance and appearance of inclusions, clay matrix and voids. In particular, the features that most contribute in this separation are: size, color, texture and abundance of large inclusions and abundance and nature of large voids.

These groups (or petrographic groups) represent the concept of *fabric*. Ceramic in thin section can also be grouped more objectively using quantitative data on relative abundance of different inclusions and their size. Data can be collected by using comparative charts (Mathew *et al.*, 1991), “point/line/ribbon counting” using mechanical stage and counter (Middleton *et al.*, 1985), or camera and image analysis software (Reedy, 2006; Puglisi *et al.*, 2013). This approach is useful when compositional differences are not obvious to naked eye. Usually, the percentages of inclusions and voids are estimated and then the percentage of matrix is obtained subtracting the total percentage of inclusions/voids from 100.

2.3.4 Scanning Electron Microscopy coupled with Energy Dispersive Spectroscopy (SEM-EDS)

SEM-EDS analysis has been carried out to define the groundmass microstructure, inclusions and the degree of vitrification using a Scanning Electron Microscope FEI-Quanta 400 coupled with an Energy Dispersive X-ray Spectroscopy working at 20 kV at the Department of Earth Sciences of Sapienza-University of Rome. An automatic calibration using AlK and CuK lines of a piece of copper grid on an aluminum stub has been performed.

Data obtained by SEM-EDS analysis give information about the mineralogical composition of the inclusions and a preliminary chemical composition of the matrix. Moreover, the morphological analysis obtained by SEM observations can also provide useful information to estimate the maximum firing temperature following the indications proposed by Tite and Maniatis (Tite and Maniatis, 1975; Tite *et al.*, 1982) that are based on the sinterization grade of the matrix. In particular, SEM examinations can give information about the internal morphology developed during firing, the extent of the vitrification and glassy phases and pore structure. According to the results of the experimental work of these authors, the development of vitrification in pottery samples is divided into:

- non vitrification stage (NV), with temperature ranging from 0 to 850 °C, in which no vitrified phases appear, only crystals of phyllosilicates are evident;
- intermediate stage (NV+) that shows an earlier stage of vitrification in which there are not areas of glass but some slight buckling and rounding of the edges of the clay minerals occur;
- first stage of vitrification (IV) characterized by the appearance of isolated smooth surfaced areas and rare filament of glass. This stage develops in the temperature range 800-850 °C in oxidizing atmosphere and it is similar in both calcareous and non-calcareous clays. The development of vitrification structures depends on the nature of the clay, the atmosphere and an inverse relationship exists between the concentration of high temperature crystalline phases and the development of the glass phase.
- stage of vitrification (V), it starts in oxidizing atmosphere at 850 °C, showing a cellular structure and the amount of glass increases forming high temperature crystalline phases up to 1050 °C. The development of the glass phase in this stage is strictly connected to the amount of CaO: with percentages between 5 and 10% the network of glass tends to be coarser, whereas smooth-surfaced areas of glass are observed when Ca oxide is present in major amounts (>15 wt%).
- diffuse vitrification stage (V+), in the temperature range of 1050-1150 °C, in which the cellular structure begins to be coarser and larger areas of glass are present.
- total vitrification stage (TV), with temperature >1150 °C, showing a completely glassy phase when the cellular structure has almost disappeared and has been replaced by continuous vitrified areas containing isolated pores.

The redox state of the atmosphere during the firing influences the above temperature ranges defined for the different vitrification stages, as the temperature values are higher in oxidizing conditions at about 50 °C than in the reducing ones.

2.3.5 X-Ray Diffraction (XRD)

The potsherds have been finely ground by hand in agate mortar to be analyzed by XRD using a Seifert MZIV automatic powder diffractometer at the Department of Earth Sciences of Sapienza-University of Rome. The instrument was equipped with a graphite monochromator using Cu K α radiation, operating at 40 kV and 20 mA. XRD data were collected from 5° to 60° 2 θ with a step-size of 0.02° and counting time of 8 s. Origin[®] software was used to smooth the data and correct the baseline; X'Pert Highscore Plus[®] software was used to identify the mineralogical assemblage.

One sample for each historical period and one sample of the supposed raw material have been re-fired in an electrically heated kiln equipped with a heating programmer which enable to set, temperature and temperature gradient. Samples were re-fired up to maximum temperature of 950 °C. A heating gradient of 120°C per h was used, the maximum temperature reached (950°C) was maintained in the kiln for 16 h, after that cooling was allowed and it was slowed down to 120°C per h. After re-firing, samples were analyzed by XRD to define in detail the products of reactions that take place during heating process. According to Tite and Maniatis (1975) who indicate 800 °C as the start point of melting in carbonate rich clays, due to the fluxes acting of Ca and Mg (Segnit and Anderson, 1972), samples have been fired at temperature well above that temperature to analyzed the newly formed minerals after the decomposition of carbonate minerals. The X-ray powder diffraction (XRPD) analysis of potsherd was carried out on a parallel-beam Bruker AXS D8 Advance, operating in transmission in θ - θ geometry. The instrument is fitted with an incident-beam Göbel mirror, a position-sensitive detector (PSD) VANTEC-1 set to a 6° 2 θ aperture. The optical system includes a 0.8 mm divergence slit, 3.7° Soller slits on the incident beam, and a radial Soller system along the diffracted beam placed just before the PSD.

A fragment of each potsherd was gently hand ground in an agate mortar under ethanol. The powders were loaded in 0.7 mm diameter borosilicate-glass capillaries that were aligned onto a standard goniometer head. XRPD data were collected on this apparatus in step-scan mode in the 3–145° 2 θ angular range (CuK α), using a step size of 0.0219° 2 θ and a counting time of 10 s. A further series of patterns were collected ex-situ on powdered fragments of the same samples fired at 950 °C. Data analysis was performed by the Rietveld method using Topas 4.2.3. This program implements the Fundamental Parameters Approach FPA.31 FPA is a convolution approach in which the peak-shape is synthesised from a priori known features of the diffractometer (i.e. the emission profile of the source, the width of the slits, the angle of divergence of the incident beam) and the microstructural features of the specimen. Peak shape was modelled through FPA with the peak broadening that was assumed to follow a Lorentzian (size) and a Gaussian (strain) behaviour. Peaks position was corrected for sample displace-

ment from the focusing circle. The background was fitted with a Chebyshev polynomial of the first kind. Refined parameters included: absorption correction, scale factors, cell parameters, and peak shape for all minerals.

2.3.6 Chemical analysis

Chemical composition of pottery can give information about the provenance of raw material allowing to describe the source areas and the possible route of trades.

Chemical analysis has been applied in the study of ceramic material since XIX century (Brongniart, 1844), in order to find appropriate raw material for modern ceramic industries (Le Châtelier, 1907; Verneuil, 1911). Chemical analysis as part of archaeometric investigations started to be applied since 1930 (Levi, 1931), but the spread of its application started with the introduction of spectroscopic techniques that allow a more simple and faster acquisition of data set.

Chemical results in the study of pottery have to be discussed considering that the chemical composition of vessels does not always correspond to chemical composition of clay, as the additions of tempers can change chemistry (Neff *et al.*, 1988; Kilioglou *et al.*, 1988, Grifa *et al.*, 2009) and also the post-burial processes can produce secondary phases (Maggetti, 1982; Freestone, 2001; Maritan and Mazzoli 2004; Schwedt *et al.*, 2004). In this view chemical analysis has to be compared to the petrographic results.

Usually, the chemical composition of sherds has to be compared to those of the scrap firing, that are remains of sure local provenance. However, the scrap firing remains are difficult to be found, and the definition of provenance has to be based on the comparison to the clay collected nearby the site by statistical approach.

The chemical elements analyzed depend on the techniques applied. Djingova *et al.* (1990) and then Kuleff and Djingova (1996) proposed the use of twenty-three elements in the definition of provenance: Al, Ca, Ce, Co, Cs, Cr, Cu, Fe, Hf, La, Mg, Mn, Na, Ni, Rb, Sc, Si, Sm, Sr, Ti, Th, V, Zr.

In the present work, a combination of Lithium Metaborate/Tetraborate fusion ICP whole rock and trace element ICP/MS have been carried out by ActLabs Laboratory. Fused sample is diluted and analyzed by Perkin Elmer Sciex ELAN 9000 ICP/MS. Three blanks and five controls (three before sample group and two after) are analyzed per group of samples.

Samples are prepared and analyzed in a batch system. Each batch contains a method reagent blank, certified reference material and 17% replicates. Samples are mixed with a flux of lithium metaborate and lithium tetraborate and fused in an induction furnace. The molten melt is immediately poured into a solution of 5% nitric acid containing an internal standard, and mixed continuously until completely dissolved (about 30

minutes). The samples are run for major oxides and selected trace elements on a combination simultaneous/sequential Varian Vista 735 ICP. Calibration is performed using 7 prepared USGS and CANMET certified reference materials. One of the 7 standards is used during the analysis for every group of ten samples. Totals should be between 98.5% and 101%. If results come out lower, samples are scanned for base metals. Low reported totals may indicate sulfate being present or other elements like Li which won't normally be scanned for. Samples with low totals however are automatically re-fused and reanalyzed.

For accurate levels of the base metals Cu, Pb, Zn, Ni and Ag, a 0.25 g sample is digested with four acids beginning with hydrofluoric, followed by a mixture of nitric and perchloric acids, heated using precise programmer controlled heating in several ramping and holding cycles which take the samples to dryness. After dryness is attained, samples are brought back into solution using hydrochloric acid. With this digestion certain phases may be only partially solubilized. These phases include zircon, monazite, sphene, gahnite, chromite, cassiterite, rutile and barite. Ag greater than 100 ppm and Pb greater than 5.000 ppm should be analyzed as high levels may not be solubilized. Only sulfide sulfur will be solubilized.

Fusion ICP

Oxide	Detection Limit (%)
SiO ₂	0.01
Al ₂ O ₃	0.01
Fe ₂ O ₃	0.01
MgO	0.01
MnO	0.001
CaO	0.01
TiO ₂	0.001
Na ₂ O	0.01
K ₂ O	0.01
P ₂ O ₅	0.01
Loss on Ignition	0.01

Trace Elements and Detection Limits (ppm)

Element	Detection Limit	Upper Limit	Reported By	Element	Detection Limit	Upper Limit	Reported By
Ag	0.5	100	ICP/MS	Cu	1	10,000	ICP/MS
As	5	2,000	ICP/MS	Dy	0.1	1,000	ICP/MS
Ba	3	500,000	ICP	Er	0.1	1,000	ICP/MS
Be	1	-	ICP	Eu	0.05	1,000	ICP/MS
Bi	0.4	2,000	ICP/MS	Ga	1	500	ICP/MS

Ce	0.1	3,000	ICP/MS	Gd	0.1	1,000	ICP/MS
Cd	0.5	5,000	ICP/MS	Ge	1	500	ICP/MS
Co	1	1,000	ICP/MS	Hf	0.2	1,000	ICP/MS
Cr	20	10,000	ICP/MS	Ho	0.1	1,000	ICP/MS
Cs	0.5	1,000	ICP/MS	In	0.2	200	ICP/MS
Element	Detection Limit	Upper Limit	Reported By	Element	Detection Limit	Upper Limit	Reported By
La	0.1	2,000	ICP/MS	Sr	2	10,000	ICP
Lu	0.04	1,000	ICP/MS	Ta	0.1	500	ICP/MS
Mo	2	100	ICP/MS	Tb	0.1	1,000	ICP/MS
Nb	1	1,000	ICP/MS	Th	0.1	2,000	ICP/MS
Nd	0.1	2,000	ICP/MS	Tl	0.1	1,000	ICP/MS
Ni	1	10,000	ICP/MS	Tm	0.05	1,000	ICP/MS
Pb	5	10,000	ICP/MS	U	0.1	1,000	ICP/MS
Pr	0.05	1,000	ICP/MS	V	5	10,000	ICP
Rb	2	1,000	ICP/MS	W	1	5,000	ICP/MS
S	0.001%	20%	ICP/MS	Y	2	10,000	ICP
Sb	0.5	200	ICP/MS	Yb	0.1	1,000	ICP/MS
Sc	1	-	ICP	Zn	1	10,000	ICP/MS
Sm	0.1	1,000	ICP/MS	Zr	4	10,000	ICP
Sn	1	1,000	ICP/MS				

References

- Arnold D.E. (1980): Localized Exchange: An Ethnoarchaeological Perspective. In “Models and Methods in Regional Exchange” Fry R.E. ed., SAA Papers 1, Washington D.C., Society for American Archaeology, 147-150.
- Arnold D.E. (1981): A Model for the Identification of Non-Local Ceramic Distribution: A View from the Present. In “Production and Distribution: A Ceramic View point British Archaeologica Reports (International Series)” Howard H., Morris E.L. eds., BAR, Oxford, 31-44.
- Bouchard M., Smith D.C. (2003): Catalogue of 45 reference Raman spectra of minerals concerning research in art history or archaeology, especially on corroded metals and coloured glass. *Spectrochimica Acta A*, **59**, 2247-2266.
- Brongniart A. (1844): *Traité des arts céramiques, ou des poteries considérées dans leur histoire, leur pratique et leur théorie*. Béchét jeune, Paris, vol. 2., pp.708.
- Burgio L., Clark R.J.H. (2001): Library of FT-Raman spectra of pigments, minerals, pigment media and varnishes, and supplement to existing library of Raman spectra of pigments with visible excitation. *Spectrochimica Acta A*, **57**, 1491-1521.
- De Benedetto G.E., Laviano R., Sabbatini L., Zambonin P.G. (2002): Infrared spectroscopy in the mineralogical characterization of ancient pottery. *Journal of Cultural Heritage*, **3**, 177-186.
- Djingova R., Kuleff I., Penev I. (1990): Instrumental neutron activation analysis of reference materials for archaeometric investigations of pottery. *Journal of radioanalytical and nuclear chemistry*, **144**, 397-406.

- Freestone I. C. (2001): Post-depositional changes in archaeological ceramics and glasses. in "Handbook of archaeological sciences", D. R. Brothwell and A. M. Pollard, eds., John Wiley & Sons, Inc., Hoboken, NJ, 615-25.
- Grifa C., Cultrone G., Langella A., Mercurio M., De Bonis A., Sebastian E., Morra V. (2009): Ceramic replicas of archaeological artefacts in Benevento area (Italy): Petrophysical changes induced by different proportions of clays and temper. *Applied Clay Science*, **46**, 231-240.
- Kilikoglou V., Maniatis Y., Grimanis A.P. (1988): The effect of purification and firing of clays on trace element provenance studies. *Archaeometry*, **30**, 37-46.
- Kuleff I., Djingova R. (1996): Provenance study of pottery: choice of elements to be determined. *Revue d'archéométrie*, **20**, 57-67.
- Le Châtelier H. (1907): Archaeological-keramische Untersuchungen. *Zeitschrift für Angewandte Chemie*, **13**, 517-523.
- Levi A. (1931): L'Analyse Chimique des Terres Cuites Anciennes et leur provenance. *Museion*, **15**, 64-66.
- Maggetti M. (1982): Phase analysis and its significance for technology and origin. In "Archaeological ceramics", J.S. Olin and A.D. Franklin, ed., Smithsonian Institution Press, Washington, 121-133.
- Maritan L., Mazzoli C. (2004): Phosphates in archaeological finds: implications for environmental conditions of burial. *Archaeometry*, **46**, 673-683.
- Mathew A.J., Woods A.J., Oliver C. (1991): Spots before the eyes: New comparison charts for visual percentage estimation in archaeological material. In "Recent Developments in Ceramic Petrology", Middleton A. and Freestone I., British Museum, Occasional Paper **81**, London, pp. 211-263.
- Middleton A., Freestone I.C., Leese M.N. (1985): Textural Analysis of Ceramic Thin Sections: Evaluation of Grain Sampling Procedures. *Archaeometry*, **27**, 64-74.
- Munsell (1975): Munsell Soil Color Charts. Color Munsell ed., Macbeth Division of Kallmorgen Corporation, Baltimore.
- Neff H., Bishop R.L., Sayre E.V. (1988): A simulation approach to the problem of tempering in compositional studies of archaeological ceramics. *Journal of Archaeological Science*, **15**, 159-172.
- Nigro L. (2006): Khirbet al-Batrawy. An Early Bronze Age Fortified Town in North-Central Jordan. Preliminary report of the First Seasons of Excavations (2005). L. Nigro, ed., Rome «La Sapienza» Studies on the Archaeology of Palestine & Transjordan, 3, Rome, pp. 280.
- Nigro L. (2008): Khirbet al-Batrawy II. The EB II city-gate, the EB II-III fortifications, the EB II-III temple. Preliminary report of the second (2006) and third (2007) seasons of Excavations. L. Nigro, ed., Rome «La Sapienza» Studies on the Archaeology of Palestine & Transjordan, 6, Rome, pp. 412.
- Nigro L. (2012): Khirbet al-Batrawy III. The EB II-III triple fortification line and the EBIIIB quarter inside the city. Preliminary report of the fourth (2008) and fifth (2009) seasons of Excavations. L. Nigro, ed., Rome «La Sapienza» Studies on the Archaeology of Palestine & Transjordan, 8, Rome, pp. 438.
- Puglisi G., Stanco F., Barone G., Mazzoleni (2013): P. Automatic Petrographic Feature Extraction from Pottery of Archaeological Interest. Interest, 8th International Symposium on Image and Signal Processing and Analysis (ISPA 2013) September 4-6, 2013, Trieste, Italy.
- Reedy C.L. (2006): Review of Digital Image Analysis of Petrographic Thin Sections in Conservation Research. *Journal of the American Institute for Conservation*, **45**, 127-146.
- Reedy C.L. (2008): Thin-Section Petrography of Stone and Ceramic Cultural Materials, Archaetype Publications, London, pp. 288.

- Rice M. (1987): Pottery Analysis. A Sourcebook. Chicago, pp. 485.
- Schwedt A., Mommsen H., Zacharias N. (2004): Post-depositional elemental alterations in pottery: neutron activation analyses of surface and core samples. *Archaeometry*, **46**, 85-101.
- Segnit E.R., Anderson C.A. (1972): Scanning electron microscopy of fired illite. *Transactions and Journal of the British Ceramics Society*, 71, 85-88.
- Tite M.S., Freestone I.C., Meeks N.D., Bimson M. (1982): The use of scanning electron microscopy in the technological examination of ancient ceramics. In "Archaeological Ceramics", ed. Olin J.S., Franklin A.D., Smithsonian Institution Press, Washington DC, 109-120.
- Tite M.S., Maniatis Y. (1975): Examination of ancient pottery using the scanning electron microscope. *Nature*, **257**, 122-123.
- Verneuil M.A. (1911): Sur la préparation de l'Email Noir, ou Lustre des Poteries Italogrecques. *Comptes Rendus Hebdomadaires des Seances de l'Academie des Sciences*, **152**, pp. 380.
- Whitbread I.K. (1986): The characterization of Argillaceous Inclusions in Ceramic Thin Sections. *Archaeometry*, 28, 79-88.
- Whitbread I.K. (1995): Greek transport amphorae: a petrological and archaeological study. British School at Athens, Fitch Laboratory Occasional Paper 4, Athens, pp. 453.
- Williams D.F. (1983): Petrology of ceramics. In "The petrology of archaeological artefacts", Kempe, D.R.C., Harvey A.P. eds., Clarendon press, Oxford, pp. 301-323.

3. STATISTICAL TREATMENTS OF DATA

Recently, the application of statistical procedures in the elaboration of results concerning cultural heritage artifacts has been greatly appreciated as they permit to correlate a large number of variables (Baxter and Buck, 2000; and see for example, Aruga *et al.*, 1993; Cotrim *et al.*, 1999; De Benedetto *et al.*, 2005; Papachristodoulou *et al.*, 2006; Nel *et al.*, 2010).

Statistical approaches to analytical data are a complementary tool useful to the discussion of the results providing information about the relationships among and between the analyzed samples.

Multivariate statistical techniques are the most diffused methodologies used to identify groupings among the samples on the basis of multivariate measurements, which can be clearly differentiated from each other, in order to find an archaeological classification (Hart and Adams 1983; Aruga *et al.*, 1993; Bruno *et al.*, 1994; Mirti *et al.*, 1995, 1998). Moreover, statistical data handling can be useful to assign pottery to a specific group of objects with similar features.

In this work, analytical data have been processed applying two different statistical multivariate methods: the cluster analysis (CA) (Baxter, 1999), and the principal component analysis (PCA) (Baxter and Buck, 2000) using XLSTAT[®] software.

Both methods belong to the “*unsupervised learning*” methods that established that no groups have been created *a priori* (Baxter, 2006).

The Hierarchical cluster analysis is a statistical method that allows to create, in a set of data, a series of coherent groups. This method permits to separate statistic units that present differences from the others groups and for this reason are isolated (*outlier*) (Baxter, 1999). The method is based on the measure of dissimilarity between cases in a data matrix. Considering k the number of variables (wavelength of FTIR spectrum or chemical elements) and n the observations (samples), after log transformation, Euclidean distance is chosen as the measure of dissimilarity between cases.

The method applied is the hierarchical agglomerative which grouped samples on the basis of inter-object distances in high dimensional space defined by an agglomerative algorithm. In the first stage, each object forms a cluster, then two objects closest together are joined. In the next step, either a third object joins the first two or two other objects join together in a different cluster. Each step results in one lesser cluster than the step before, until, at the end, all objects are in one cluster. The metric distance and linkage determine how the distance between two clusters is calculated. In this view, in each cluster similar cases are found, but significantly different from the cases put in other cluster (Baxter, 2006).

Differences between samples have been processed graphically in a dendrogram in which each sample is located in different branches and the level of union between samples is proportional to the dissimilarity.

Dendrograms can be created by different methods: *Average–Linkage Cluster Analysis*; *Single Linkage (Nearest Neighbour)*; *Complete Linkage (Furthest Neighbour)*; *Centroid Method*; *Median Method*; *Ward’s Method*.

In this work the Ward’s method has been applied. It is based on the calculation of deviance connected to the groups evaluating the distance between *cluster* through *their variance*.

In the Ward’s method the variability within the j th cluster is defined as

$$S_j = \sum_{i=1}^{n_j} \sum_k (y_{ik} - \bar{y}_k)^2$$

Where n_j is the number of cases in cluster j and \bar{y}_k is the mean of the k th variable in the cluster.

Groups have been defined as a set of samples with minimum deviance, whereas the distance between two groups has been calculated as subtraction between total deviance and the sum of the two groups’ deviance. Moreover, the Ward’s method is considered efficient in the description of samples distributions avoiding the creation of excessive number of groups (Mommson *et al.*, 1988).

PCA is a statistical method based on the variance of variables that reduces the number of the variables considering only those that maximize the difference between samples (Johnson, 1998). This method allows to define the anomalous behavior of samples (outlier) respect to the others (Baxter, 1999) and to define how variables, in this case how chemical elements, influence the differences between samples. It calculates orthogonal linear combinations of the auto-scaled variables, by using the correlation matrix, based on the maximum variance criterion. Such linear combinations are called *principal components scores* and *loadings* the coefficients of the linear combinations.

The PCA considers an X data matrix with n rows (samples) and p columns (wave-number of FTIR spectrum or chemical elements, in our case) in order to create new variables in a lower number respect to the untreated data that preserves most of the total variance. From X data matrix the principal components are calculated according to the maximum variance criterion, i.e. each successive component is an orthogonal combination of the original variables such that it covers the maximum of the variance not accounted for by the previous components. Each of principal components can describe a percentage of variance in the system. Usually, if there is a strictly correlation between variables, the first two or three principal components are able to describe the majority of the variance of the system (Baxter, 1999). The projection of plots of objects onto the first two or three principal components axes is a linear projection of ob-

jects onto the two- or three-dimensional subspace that maintains most of the total variance (*score plot*). The coefficients by which the original variables must be multiplied to give the new parameters, are referred to as *loadings*. The numerical value of the loading of each variable on a given principal component shows how much the variable has in common with that component. Therefore, the *loading plot* of the variables onto the two-dimensional subspace, defined by the first two principal components, displays the correlation between the old variables (wavenumber of FTIR spectrum or chemical elements) and these PCs.

In the score plot, the samples are represented by points and the outliers are located at the extreme of the plot, as results of the maximization of variance along the new axes since the distance between samples is inversely proportional between each other. The outlier influences the results, so it is usually deleted and the statistical analysis is carried out again on the new set of data (Baxter, 1999; Papageorgiou *et al.*, 2001).

3.1 Statistical analysis of FTIR data

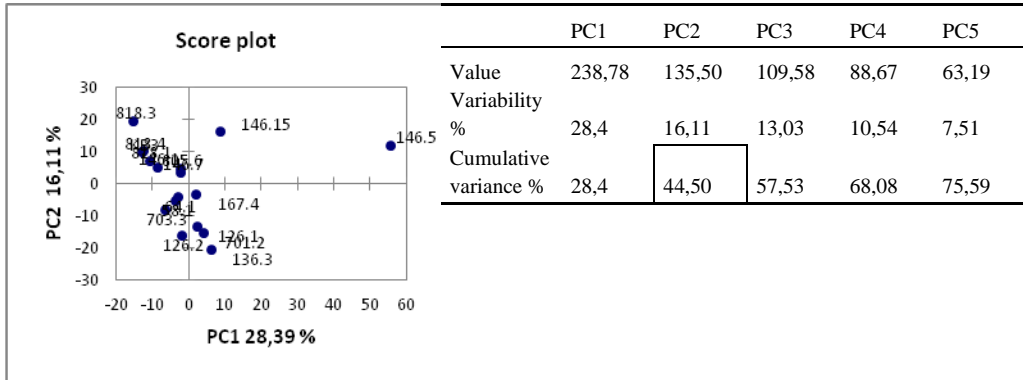
The interpretation of FTIR spectra, based on the attribution of all the spectra transition is not straightforward. Recently, the application of statistical methods to IR data, with the purpose to check if similarities in the spectra can create a grouping among samples, drew the interest of the whole scientific community (Forina *et al.*, 1993; De Maesschalck *et al.*, 1999; Ruiz-Jiménez *et al.*, 2004). Biotechnological, agricultural, chemical and medical studies (Wood *et al.*, 1996; Goncalves *et al.*, 1998, 2005; Coimbra *et al.*, 1999; Cotrim *et al.*, 1999; Goncalves and Ruzene, 2001; Miranda *et al.*, 2001; Zagonel *et al.*, 2004; Yu, 2005) have been focused on the use of multivariate analysis technique of FTIR data. The most common statistical technique applied to identify the major features useful in the definition of “pattern recognition” in FTIR spectra is the PCA method (Cotrim *et al.*, 1999; De Benedetto *et al.*, 2005; Nel *et al.*, 2010; Sarmiento *et al.*, 2011).

The infrared spectrum is composed by measurements of absorbance at different X wavelengths. If N is the number of spectra (i.e., of samples), these data can be arranged in a matrix (N,X). For FTIR spectra, the pre-treatment methods of data and the choice of spectral region vary depending on the object to be analyzed; in particular, the spectral region has been chosen on the basis of the vibrations on which the works are focused on. Whereas, pre-treatment of data usually consists in the baseline correction or the second derivative, the normalization of data and the smoothing, but the order and the kind of treatment to be applied vary from case to case (Cotrim *et al.*, 1999; De Benedetto *et al.*, 2005; Nel *et al.*, 2010; Sarmiento *et al.*, 2011).

In this work, prior to elaborate a statistical analysis, it was needed to choose the pre-treatment of data. In order to improve the PCA model, the complete FTIR spectra

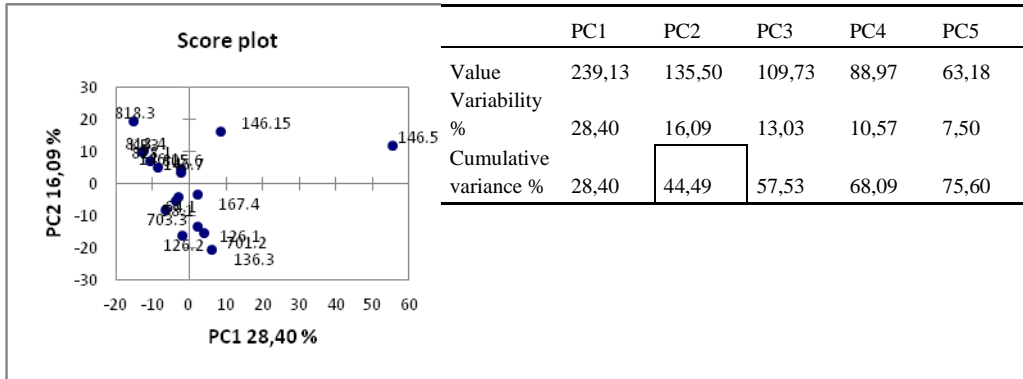
(range 400-4000 cm⁻¹), the spectra between 400 and 1600 cm⁻¹ and the spectra reduced in the range 400-1200 cm⁻¹ have been pretreated following five different models proposed in literature in order to select the most suitable. Data were pretreated using ORIGIN PRO® software, and the five models were applied only for a limited number of spectra of samples belonging to the EB IIIA phase.

Model 1) the spectra were normalized between 0 and 1 and then the baseline correction has been applied (De Benedetto *et al.*, 2005).



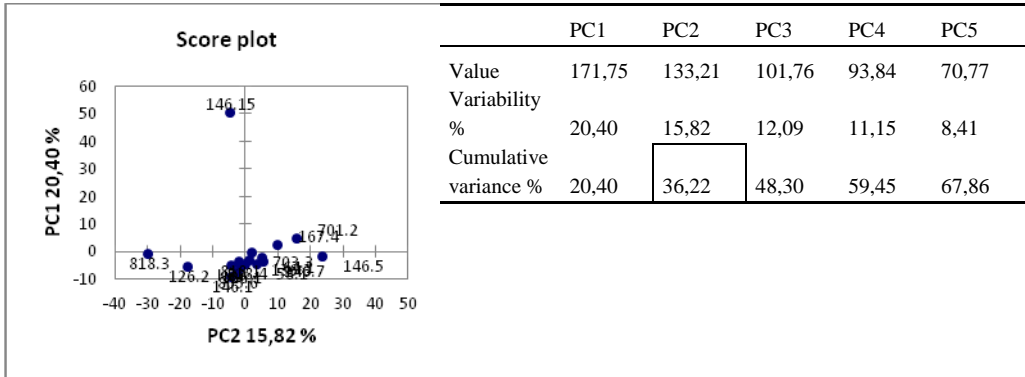
Model 1a) the spectra were normalized between 0 and 1, the baseline correction has been applied and finally the data were smoothed using Savitzky-Golay method with nine-point and third order polynomial filter (Nel *et al.*, 2010).

MODEL 1a



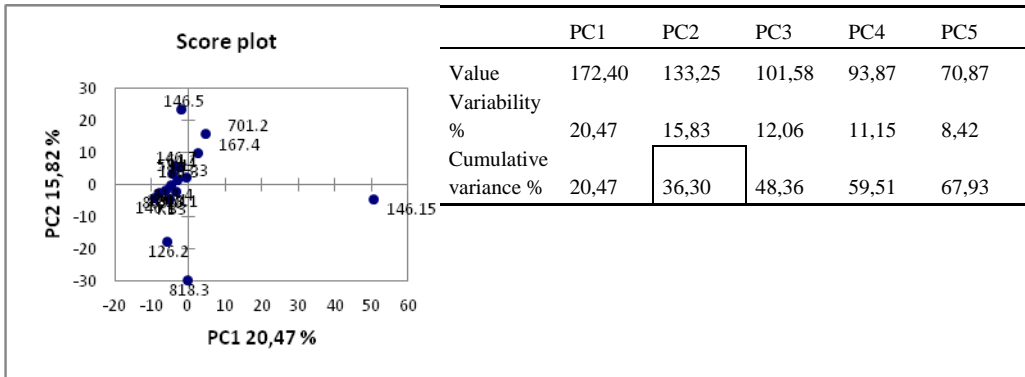
Model 2) the spectra were normalized between 0 and 1, the second derivative was calculated and finally the data were smoothed using Savitzky-Golay method with nine-point and third order polynomial filter (De Benedetto *et al.*, 2005).

MODEL 2



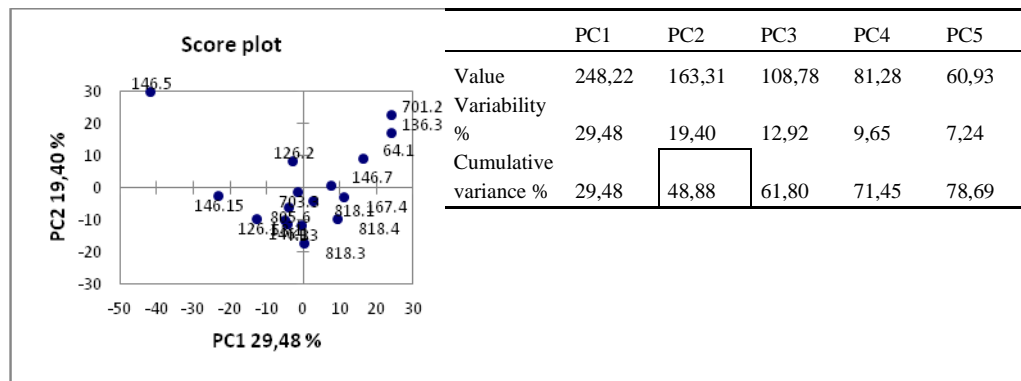
Model 2a) the spectra were normalized between 0 and 1, data were smoothed using Savitzky-Golay method with nine-point and third order polynomial filter and finally the second derivative was calculated.

MODEL 2a



Model 3) firstly, the baseline correction has been applied and then data were normalized between 0 and 1 (Cotrim *et al.*, 1999; Sarmiento *et al.*, 2011).

MODEL 3



The selection of the spectral regions was necessary to identify the areas where all the compounds of interest had characteristic absorptions bands. The most favorable area to carry out this study was the spectral region between 400 and 1600 cm^{-1} which takes into account the contribution of the fingerprint of inorganic compounds, below 1000 cm^{-1} , and the carbonate absorption band at about 1400 cm^{-1} .

In the applied pre-treatment models, mathematical treatments baseline correction resulted to be affected by excessive modification due to the operator that influenced and modified the PCA results. For this reason, the second derivative of the spectra was considered to be the best choice as involving a correction in the baseline and increasing the small differences among the spectra highlighting small shoulders and peaks only through the applying of mathematical operations.

Therefore, among the five proposed, model 2 has been chosen to be applied in this work in the spectral range between 400 and 1600 cm^{-1} .

The ASCII data were elaborated with ORIGIN PRO[®] software and imported into statistical software (XLSTAT[®]) which runs as additional component of Microsoft Excel[®].

3.2 Statistical analysis of chemical data

Chemical data have been processed by two different statistical multivariate methods: the cluster analysis (CA) (Baxter, 1999), and the principal component analysis (PCA) (Baxter and Buck, 2000). In this work, the compositional data of bulk material of pottery samples have been studied using XLSTAT[®] software which runs as additional component of Microsoft Excel[®].

Statistical analysis was performed on concentration matrix of the twenty-three elements proposed by Djingova *et al.* (1990) and Kuleff and Djingova (1996) with the addition of Ga, Nb, Y, K and Zn of seventeen ceramic samples, two samples of clay

material and one sample collected from a brick. In particular, the starting data set was deprived of some chemical components, in particular P_2O_5 and Ba, as they could have been affected by post burial contamination processes (Maggetti, 2001). Afterwards, data were log₁₀ transformed in order to avoid deleterious effects of scale effects of clustering results (e.g., V-shaped chemical data; Aruga *et al.*, 1993).

References

- Aruga R., Mirti P., Casoli A. (1993): Application of multivariate chemometric techniques to the study of Roman pottery (terra sigillata). *Analytical Chimical Acta*, **276**, 197-204.
- Baxter M.J. (1999): Detecting multivariate outliers in artefact compositional data. *Archaeometry*, **41**, 321-338.
- Baxter M.J. (2006): A review of supervised and unsupervised pattern recognition in archaeometry. *Archaeometry*, **48**, 671-694.
- Baxter M.J., Buck C.E. (2000): Data handling and statistical analysis. in: "Modern analytical methods in art and archaeology", Ciliberto and Spoto eds., John Willey, New York, 681-746.
- Bruno P., Caselli M., Curri M.L., Favia P., Laganara C., Lamendola R., Mangone A., Traini A. (1994): XPS, ICP and DPASV analysis of medieval pottery- Statistical multivariate treatment of data. *Fresenius Journal of Analytical Chemistry*, **350**, 168-177.
- Coimbra M.A., Barros A., Rutledge D.N., Delgadillo I. (1999): FTIR spectroscopy as a tool for the analysis of olive pulp cell-wall polysaccharide extracts. *Carbohydrate Research*, **317**, 145-154.
- Cotrim A.R., Ferraz A., Gonçaves A.R., Silva F.T., Bruns R.E. (1999): Identifying the origin of lignins and monitoring their structural changes by means of FTIR-PCA and -SIMCA. *Bio-resource Technology*, **68**, 29-34.
- De Benedetto G.E., Fabbri B., Gualtieri S., Sabbatini L., Zambonin P.G. (2005): FTIR-chemometric tools as aids for data reduction and classification of pre-Roman ceramics. *Journal of Cultural Heritage*, **6**, 205-211.
- De Maesschalck R., Candolfi A., Massart D. L., Heuerding S. (1999): Decision criteria for soft independent modelling of class analogy applied to near infrared data. *Chemometrics and Intelligent Laboratory Systems*, **47**, 65-77.
- Djingova R., Kuleff I., Penev I. (1990): Instrumental neutron activation analysis of reference materials for archaeometric investigations of pottery. *Journal of radioanalytical and nuclear chemistry*, **144**, 397-406.
- Forina M., Drava G., Contarini G. (1993): Feature selection and validation of SIMCA models: a case study with a typical Italian cheese. *Analisis*, **21**, 133-147.
- Gonçaves A.R., Benar P., Costa S.M., Ruzene D.S., Moriya R.Y., Luz S.M., Ferretti L.P. (2005): Integrated processes for use of pulps and lignins obtained from sugarcane bagasse and straw. *Applied biochemistry and biotechnology*, **123**, 821-826.
- Gonçaves A.R., Esposito E., Benar P. (1998): Evaluation of *Panus tigrinus* in the delignification of sugarcane bagasse by FTIR-PCA and pulp properties. *Journal of biotechnology*, **66**, 177-185.
- Gonçaves A.R., Ruzene D. S. (2001): Bleachability and characterization by Fourier Transform Infrared principal component analysis of acetosolv pulps obtained from sugarcane bagasse. *Applied biochemistry and biotechnology*, **91**, 63-70.
- Hart F.A., Adams S.J. (1983): The chemical analysis of romano-british pottery from the Alice holt forest, Hampshire, by means of Inductively-Coupled Plasma Emission Spectrometry. *Archaeometry*, **25**, 179-185.

- Johnson D.E. (1998): Applied multivariate methods for data analysts, Duxbury Press, pp. 567.
- Kuleff I., Djingova R. (1996): Provenance study of pottery: choice of elements to be determined. *Revue d'archéométrie*, **20**, 57-67.
- Maggetti M. (2001): Chemical analyses of ancient ceramics: What for?. *CHIMIA International Journal for Chemistry*, **55**, 923-930.
- Miranda T.M.R., Gonçalves A.R., Amorim, M.T.P. (2001): Ultraviolet-induced crosslinking of poly (vinyl alcohol) evaluated by principal component analysis of FTIR spectra. *Polymer international*, **50**, 1068-1072.
- Mirti P., Aceto M., Preacco Ancona M.C. (1998): Campanian pottery from ancient Bruttium (Southern Italy): scientific analysis of local and imported products. *Archaeometry*, **40**, 311-329.
- Mirti P., Casoli A., Barra Bagnasco M., Preacco Ancona M.C. (1995): Fine ware from Locri Epizephiri: a provenance study by Inductively Coupled Plasma Emission Spectroscopy. *Archaeometry*, **37**, 41-51.
- Mommsen H., Kreuser A., Eweber, J. (1988): A method for grouping pottery by chemical composition. *Archaeometry*, **30**, 47-57.
- Nel P., Lonetti C., Lau D., Tam K., Sagona A., Sloggett R.S (2010): Analysis of adhesives used on the Melbourne University Cypriot pottery collection using a portable FTIR-ATR analyzer. *Vibrational Spectroscopy*, **53**, 64-70.
- Papachristodoulou C., Oikonomou A., Ioannides K., Gravani K. (2006): A study of ancient pottery by means of X-ray fluorescence spectroscopy, multivariate statistics and mineralogical analysis. *Analytica chimica acta*, **573**, 347-353.
- Papageorgiou I., Baxter M.J., Cau M.A (2001): Model-based cluster analysis of artefact compositional data. *Archaeometry*, **43**, 571-588.
- Ruiz-Jiménez J., Priego-Capote F., García-Olmo J., Castro M.D. (2004): Luque de, Use of chemometrics and mid infrared spectroscopy for the selection of extraction alternatives to reference analytical methods for total fat isolation. *Analytica Chimica Acta*, **525**, 159-169.
- Sarmiento A., Pérez-Alonso M., Olivares M., Castro K., Martínez-Arkarazo I., Fernández L.A., Madariaga J.M. (2011): Classification and identification of organic binding media in artworks by means of Fourier transform infrared spectroscopy and principal component analysis. *Analytical and Bioanalytical Chemistry*, **399**, 3601-3611.
- Wood B.R., Quinn M.A., Burden F.R., McNaughton D. (1996): An investigation into FTIR spectroscopy as a biodiagnostic tool for cervical cancer. *Biospectroscopy*, **2**, 143-153.
- Yu P. (2005): Applications of hierarchical cluster analysis (CLA) and principal component analysis (PCA) in feed structure and feed molecular chemistry research, using synchrotron-based Fourier transform infrared (FTIR) microspectroscopy. *Journal of agricultural and food chemistry*, **53**, 7115-7127.
- Zagonel G.F., Peralta-Zamora P., Ramos L.P. (2004): Multivariate monitoring of soybean oil ethanolsis by FTIR. *Talanta*, **63**, 1021-1025.

4. RESULTS

4.1 Macroscopic Analysis

Macroscopic analysis of ceramic samples is a preliminary observation necessary to direct the subsequent investigations of the sherds. It is based on the observation on eyes and gives information about homogeneity or inhomogeneity of the artifacts color, differentiation of the color between intern and extern part, the present or absence of decoration and superficial slips. In particular, the color of each samples has been described according to Munsell color system (1975), the most common system used in archaeometric studies of ceramic.

4.1.1 EB II

Macroscopic analysis showed a great variability in the analyzed potsherds. On the basis of the different color matrix three groups of sherds have been recognized: 1) red-pale brown, 2) the so called “black core” and 3) gray color.

Samples KB.06.E.702/10 and KB.06.E.704/6 show a homogeneous red-brown matrix color, ranging from red to light brown. Externally these fragments are characterized by a very thin red superficial slip as showed in the Figure 1.

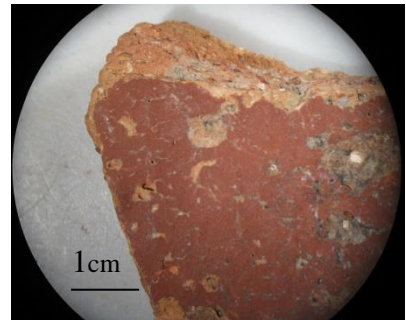


Figure 1: Fragment KB.06.E.702/10 showing a red superficial slip.

Samples KB.06.B.392/8, KB.06.E.703/5, KB.06.E.703/6, and KB.06.E.704/1 show the so-called “black core”, a typical sandwich structure having red margin and black central part. In particular, sample KB.06.E.703/6 shows the inner surface black and not red probably due to a non homogeneous diffusion of oxygen. In this group only sample KB.06.E.704/1 shows an inner slip (2.5YR5/6 red) and inner horizontal burnish.



Figure 2: Example of potter's wheel traces on the surface.

The last group includes samples KB.06.E.706/1 and KB.06.E.706/2 showing a very light gray color, ranging from pale brown to gray. Both samples show an inner and outer red slip.

The results clearly show that there is no correlation between color and type of potteries. The majority of the fragments show trace of

The results clearly show that there is no correlation between color and type of potteries.

The majority of the fragments show trace of

handmade manufacturing process (Fig. 2). In particular, samples KB.06.E.706/1 and KB.06.E.706/2 shows a series of parallel tracks on the surface, which are typical in the ceramics made up with a wheel.

The superficial decorations and treatments of these samples are very different. Samples KB.06.B.392/8, KB.06.E.703/5 and KB.06.E.703/6 do not present any kind of superficial decoration or final treatments. On the contrary, samples KB.06.E.702/10, KB.06.E.704/1, KB.06.E.704/6, KB.06.E.706/1 and KB.06.E.706/2 are characterized by a red thin slip, polished with instruments in order to make shiny the surface.

The observation carried out by using the stereomicroscope showed that the size of the inclusions cover a dimensional range from micrometric to millimetric in the same shard. The samples present a seriate granulometric distribution characterized by inclusions belonging to different dimensional granulometric classes. By stereomicroscopy white, dark and red inclusions have been shown and fragments of grog, i.e. pieces of ceramic objects, grounded and reused in the paste have been also identified.

Table 1 shows the morphological and typological characteristics of the fragments.

Table 1: Morphological and typological characteristics of the fragments belonging to Early Bronze Age II.

EB II 3000-2700 B.C.				Color			
	Class	Pottery Type	Technique of manufacture	Matrix	Fabric	Decorat-ion	Burnish
KB.06.B.392/8	Storage ware	Jar	-	1FOR GLEY4/N (dark gray)+ 10R5/6 (red)	Black core	-	-
KB.06.E.702/10	Red Polished ware	Jug	-	7.5YR6/2 (red)	Red. Brown	Outer red slip	Outer
KB.06.E.703/5	Simple ware	Jar	Made by hand	1FOR GLEY4/N (dark gray)+ 10R5/6 (red).	Black core	-	-
KB.06.E.703/6	Storage ware	Jar	Made by hand	1FOR GLEY4/N (dark gray)+ 10R5/6 (red)	Black core	-	-
KB.06.E.704/1	Red burnished ware	Platter	Made by hand	1FOR GLEY4/N (dark gray)+ 7.5YR6/2 (red)	Black core	Inner red slip	Inner
KB.06.E.704/6	Red burnished ware	Bowl	Made by hand	7.5YR6/4 (light brown)	Red Brown	Inner red slip	Inner
KB.06.E.706/2	Red burnished ware	Platter	Made by hand, wheel	10YR6/3 (pale brown)	Gray	Inner red slip	Inner
KB.06.E.706/1	Red burnished ware	Platter	Made by hand, wheel	7.5YR5/1 (gray)	Gray	Inner and outer slip	Inner

4.1.2 EB IIIA

The samples of this archaeological layer can be divided in four groups on the basis of the matrix color: 1) red/brown, 2) the so called “black core”, 3) gray and 4) not homogeneous color.

Samples KB.05.A.58/1, KB.05.A.64/1, KB.05.B.136/1, KB.05.B.146/3, KB.05.B.146/5, KB.05.B.146/6, KB.05.B.146/15, KB.05.B.146/20, KB.06.B.376/4, KB.06.B.413/2, KB.06.E.701/2, KB.06.E.703/3, KB.08.B.805/6 and KB.09.B.820/13 show an homogeneous red/brown color matrix ranging from pink, pale red, red, reddish yellow, reddish brown to brown.

Samples KB.05.A.52/8, KB.05.B.136/3, KB.05.B.146/4 and KB.05.B.146/8 show the typical “black core” with red margin and black central part.

Samples KB.05.A.64/13, KB.05.B.126/3, KB.05.B.146/1, KB.05.B.146/7, KB.05.B.146/30, KB.06.B.167/4, KB.06.B.427/1, KB.09.B.820/10, KB.09.B.820/12, KB.08.B.805/32, KB.08.B.805/33 and KB.08.B.805/34 show an homogeneous gray-dark color ranging from gray, bluish gray to dark gray.

Samples KB.05.B.110/15, KB.05.B.126/1, KB.05.B.126/4, KB.05.B.136/5 and KB.05.B.146/24 are characterized by not homogeneous red and gray color.

There is no evident correlation between color and type of pottery. In particular the color of EB IIIA SW potteries ranges from pink, light red, pale red, reddish yellow, red, to very pale brown, while that of StW potteries ranges from red, reddish yellow, gray, to dark gray, and the color KKW potteries ranges from reddish yellow, light reddish brown, gray, to dark gray.

The samples of EB IIIA phase are characterized by superficial slip of different color, variable from pink, red to brown and different final processing as burnish, polished and a particular one defined as “net-burnish” visible on the sample KB.05.B.146/1. The burnishing is a type of final treatment in which the surface of the pottery is polished using an hard instrument as a rock, before firing. The so called “net-burnish” is a burnishing in which the instrument is used to notch the surface with the purpose to create a netting drawing.

EB IIIA samples show different type of decorations: geometrical drawings obtained notching the surface (the so called “combed” in sample KB.05.A.64/13) or painting the surface in the samples KB.05.A.64/1, KB.05.B.126/1, KB.05.B.126/3, KB.05.B.146/3, KB.05.B.146/15. Sample KB.06.B.167/4 shows a particular decoration called “grain wash” obtained coating the pottery before firing with red, orange or brown vertical and parallel bands (Fig. 3).

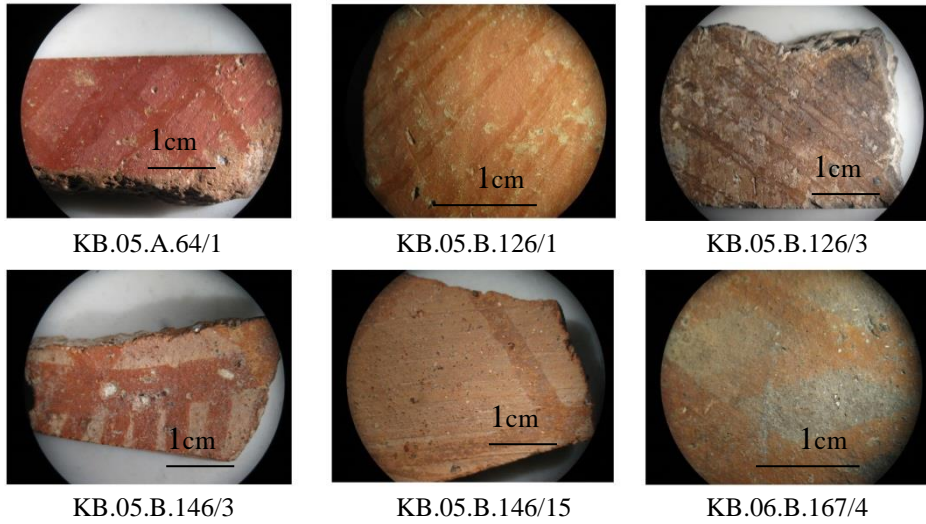
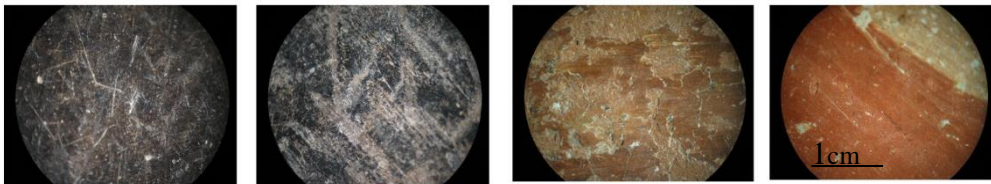


Figure 3: Photographs of EB IIIA fragments showing different superficial treatments.

The wheel process is common in the shards of this period (KB.05.A.64/13, KB.05.B.126/3, KB.05.B.136/3, KB.05.B.146/1, KB.05.B.146/4, KB.05.B.146/7, KB.05.B.146/8, KB.05.B.146/15), as these samples showed parallel traces on the external surface. Sherds belonging to the KKW group are all made by hand and externally they are characterized by a dark slip, shining or burnished (KB.09.B.820/10, KB.09.B.820/12, KB.09.B.820/13), whereas sample KB.08.B.805/6 shows a red shine slip (Fig. 4).



KB.09.B.820/10 KB.09.B.820/12 KB.09.B.820/13 KB.08.B.805/6

Figure 4: Photographs of KKW fragments with different superficial treatments.

The observations by the stereomicroscope showed that the size of the inclusions ranges from micrometric to millimetric in the same shards. The samples present a seriate granulometric distribution characterized by white, dark and red inclusions. Also fragments of grog have been observed. In sample KB.05.B.146/20 fragments of fossils have also been identified.

Tables 2 and 3 shows the morphological and typological characteristics of the fragments of this period.

Table 2: Morphological and typological characteristics of the fragments belonging to Early Bronze Age IIIA.

EB IIIA 2700-2500 B.C.				Color				
	Class	Pottery Type	Technique of manufacture	Matrix	Fabric	Decoration	Burnishing	Polishing
KB.05.A.52/8	Storage Ware	Hole-mouth jar	Wheel	2.5YR 4/8 (red)	Black core	Outer red slip	-	-
KB.05.A.58/1	Red polished ware	Jug	-	2.5YR6/8 (light red)	Red-brown	Outer red slip	-	Outer
KB.05.A.64/1	Red burnished ware	Platter	Wheel	7.5YR5/4 (brown)	Red-brown	Outer red slip and bands decoration	Outer net-burnish	-
KB.05.A.64/13	Storage ware	Jar	Made by hand	1 FOR GLEY5/N (gray)	Gray	Outer combed	-	-
KB.05.B.110/15	Red polished Ware	Jug	-	2.5YR6/8 (light red)	Color variable	Outer red slip	-	Outer
KB.05.B.126/1	Red polished ware	Jug	Made by hand	2.5YR6/2 (pale red)	Color variable	Outer red slip and bands decoration Inner red-dish brown	-	Outer
KB.05.B.126/3	Red burnished ware	Platter	Wheel	2.5YR5/1 (gray)	Gray	slip and bands decoration	Inner	-
KB.05.B.126/4	Simple painted ware	Bowl	Made by hand	2.5YR6/2 (pale red)	Color variable	Inner red slip	Inner	-
KB.05.B.136/1	Simple painted ware	Jar	Made by hand	2.5YR 4/8 (red)	Red-brown	Outer painting with red crossing bands	-	-
KB.05.B.136/3	Simple ware	Jar	Wheel	10R5/8 (red)+10R4/1 (dark reddish gray)	Black core	-	-	-
KB.05.B.136/5	Storage ware	Phitos	Made by hand	7.5YRN/5 (gray)	Color variable	-	-	-
KB.05.B.146/1	Red burnished ware	Platter	Wheel	7.5YR5/1 (gray)	Gray	Outer weak red slip, outer paint with red bands	Outer net-burnish	-
KB.05.B.146/3	Simple painted ware	Jar	Made by hand	2.5YR7/8 (light red)	Red-brown	Outer pink slip, outer red painted	-	-

EB IIIA				Color				
	2700-2500 B.C.	Class	Pottery Type	Technique of manufacture	Matrix	Fabric	Decoration	Burnishing
KB.05.B.146/4	Simple ware	Jar	Wheel	7.5YR7/4 (pink)+2.5Y6/1 (gray)	Black core	Outer red slip	-	-
KB.05.B.146/5	Simple ware	Juglet	Made by hand	2.5YR6/8 (light red)	Red-brown	-	-	-
KB.05.B.146/6	Simple ware	Juglet	Made by hand	7.5YR6/6 (reddish yellow)	Red-brown	-	-	-
KB.05.B.146/7	Red polished ware	Jug	Wheel	1 FOR GLEY5/N (gray)	Gray	Outer reddish brown slip	-	Outer
KB.05.B.146/8	Red burnish ware	Platter	Wheel	2 FOR GLEY5/5PB (bluish gray)	Black core	Inner light red slip	-	Inner
KB.05.B.146/15	Simple painted ware	Bowl	Wheel	10R5/6 (red)	Red-brown	Outer reddish brown painted	-	-
KB.05.B.146/20	Kitchen Ware	Hole-mouth pot	-	10R5/6 (red)	Red-brown	-	-	-
KB.05.B.146/24	Simple ware	Juglet	Made by hand	10YR8/3 (very pale brown)	Color variable	Outer reddish brown slip	-	-
KB.05.B.146/30	Red polished ware	Jug	Made by hand	2 FOR GLEY6/1 (bluish gray)	Gray	Outer reddish brown slip and brown bands decoration	-	Outer
KB.06.B.167/4	Storage (grain wash)	jar	Made by hand	7.5YR4/1 (dark gray)	Gray	Outer washed with red bands	-	-
KB.06.B.376/4	Red polished ware	Jug	Made by hand	2.5YR6/6 (light red)	Red-brown	Outer red slip	-	Outer
KB.06.B.413/2	Kitchen Ware	Hole-mouth pot	-	7.5YR5/4 (brown)	Red-brown	-	-	-
KB.06.E.701/2	Simple painted ware	Jar	Made by hand	2.5YR5/6 (red)	Red-brown	Outer pink slip and outer painted with weak red color	-	-

EB IIIA				Color				
2700-2500 B.C.	Class	Pottery Type	Technique of manufacture	Matrix	Fabric	Decoration	Burnishing	Polishing
KB.06.E.703/3	Simple ware	Juglet	Made by hand	7.5YR7/4 (pink)	Red-brown	Outer smooth	-	-

Table 3: Morphological and typological characteristics of the KKW fragments.

EB IIIA KKW				Color				
2700-2500 B.C.	Class	Pottery Type	Technique of manufacture	Matrix	Fabric	Decoration	Burnished	Polished
KB.06.B.427/1	KKW	Jug	-	2.5YR5/1 (gray)	Gray	-	-	Outer
KB.08.B.805/6	KKW	Jug	Made by hand	7.5YR6/6 (reddish-yellow)	Red-brown	Outer red slip	-	Outer
KB.09.B.820.10	KKW	Bowl	-	2.5YR5/1 (gray)	Color variable	Inner/outer black slip	-	Inner/outer
KB.09.B.820.12	KKW	Bowl	Moulded	10YR4/1 (dark gray)	Gray	Inner/outer black slip	-	Inner/outer
KB.09.B.820/13	KKW	Jug	Made by hand	5YR6/4 (light reddish brown)	Red-brown	Outer black slip	-	Outer
KB.08.B.805/32	KKW	Jug	-	2.5YR5/1 (gray)	Gray	-	-	Outer
KB.08.B.805/33	KKW	Jug	-	2.5YR5/1 (gray)	Gray	-	-	Outer
KB.08.B.805/34	KKW	Jug	-	2.5YR5/1 (gray)	Gray	-	-	Outer
KB.09.B.820/12	KKW	Jug	-	2.5YR5/1 (gray)	Gray	-	-	Outer

4.1.3 EB IIIB

Macroscopic analysis showed a great variability in the analyzed potsherds. As the previous samples, also the fragments of this period can be divided in four groups on the basis of the different matrix color: 1) red, 2) the so called “black core”, 3) gray and 4) not homogeneous color. Outer applied rope decorations are common in these vessels. Samples KB.05.A.46/8, KB.05.A.204/2, KB.05.A.204/3, KB.11.B.1054/12, KB.11.B.1054/13, KB.10.B.1054/24, KB.10.B.1054/62, KB.11.B.1124/1,

KB.11.B.1124/3, KB.11.B.1124/15, KB.11.B.1124/19, KB.11.B.1128/52 and KB.11.B.1128/65 show an homogeneous red/brown color matrix ranging from pink, reddish yellow, red, light brown to brown.

Samples KB.05.A.46/2, KB.05.A.216/4, KB.05.A.220/5, KB.05.A.224/2, KB.06.A.120/6, KB.05.B.111/3, KB.10.B.1040/8, KB.11.B.1054/2, KB.11.B.1124/10, KB.11.B.1124/24, KB.11.B.1124/33, KB.11.B.1124/8, KB.11.B.1128/1, KB.11.B.1128/50 and KB.11.B.1128/51 show the typical “black core” with red margin and black central part.

Samples KB.10.B.1054/6, KB.11.B.1124/22 and KB.11.B.1124/29 show an homogeneous gray-dark color ranging from gray to dark gray.

Samples KB.11.B.1054/21, KB.10.B.1054/22 and KB.11.B.1124/28 are characterized by not homogeneous red and gray color.

Table 4 shows the morphological and typological characteristics of the fragments.

Table 4: Morphological and typological characteristics of the fragments belonging to Early Bronze Age IIIB.

EB IIIB 2500-2300 B.C.				Color		
	Class	Pottery Type	Technique of manufacture	Matrix	Fabric	Decorat-ion
KB.05.A.46/2	Storage Ware	Jar	Made by hand	25YR5/8 (red)	Black core	-
KB.05.A.46/8	Storage Ware	Pithos	Made by hand	5YR6/6 (reddish yellow)	Red-brown	Applied rope decoration
KB.05.A.216/4	Storage Ware	Jar	Made by hand	1FORGLEY5/N (gray) + 2.5YR5/6 (red)	Black core	-
KB.05.A.204/2	Storage Ware	Hole-mouth jar	Made by hand	7.5YR6/4 (light brown)	Red-brown	outer punctuated
KB.05.A.204/3	Kitchen Ware	Hole-mouth pot.	Made by hand	7.5YR5/4 (brown)	Red-brown	-
KB.05.A.220/5	Storage ware	Pithos	Made by hand	10R5/8 (red)+ 7.5YR5/4 (brown)	Black core	Outer applied rope decoration
KB.05.A.224/2	Storage Ware	Pithos	Made by hand	10YR5/2 (grayish brown)+10R5/6 (red).	Black core	Outer applied rope decoration
KB.06.A.120/6	Red Polished Ware	Jug	-	-	Black core	-
KB.05.B.111/3	Simple Ware	Jar.	Made by hand	10R6/2 (pale red)	Black core	-
KB.10.B.1040/8	Storage Ware	Pithos	-	-	Black core	-

EB IIIB 2500-2300 B.C.				Color		
	Class	Pottery Type	Technique of manufacture	Matrix	Fabric	Decorat-ion
KB.11.B.1054/2	-	Pithos	-	-	Black core	-
KB.10.B.1054/6	Simple Ware	Vat	-	-	Gray	-
KB.11.B.1054/12	Simple Ware	Jar	-	-	Red-brown	-
KB.11.B.1054/13	Red burnished Ware	Jar	-	-	Red-brown	-
KB.11.B.1054/21	Metallic Ware	Pattern combed jar	-	7.5YR7/2 (pinkish gray)+ 2.5YR6/4 (light reddish brown)	color variable	-
KB.10.B.1054/22	Red burnished Ware	Jar	-	-	color variable	-
KB.10.B.1054/24	Storage Ware	Pithos	-	2.5YR5/6 (red)	Red-brown	-
KB.10.B.1054/62	Simple Ware	Jar	-	10R5/6 (red)	Red-brown	-
KB.11.B.1124/1	-	Hole mouth Jar	-	-	Red-brown	-
KB.11.B.1124/3	Storage Ware	Hole mouth Jar	-	2.5YR5/6 (red)	Red-brown	-
KB.11.B.1124/10	Storage Ware	Pithos	-	-	Black core	-
KB.11.B.1124/15	Storage Ware	Hole mouth jar	-	2.5YR5/6 (red)	Red-brown	-
KB.11.B.1124/19	-	Spouted vat	-	-	Red-brown	-
KB.11.B.1124/22	Simple Ware	Jar	-	-	Gray	-
KB.11.B.1124/24	Storage Ware	Jar	-	-	Black core	-
KB.11.B.1124/28	-	Pithos	-	-	color variable	-
KB.11.B.1124/29	Storage Ware	Jar	-	7.5YR4/1 (dark gray)	Gray	-
KB.11.B.1124/33	Red burnished Ware	juglet	-	-	Black core	-
KB.11.B.1124/8	Storage Ware	jar	-	-	Black core	-

EB IIIB 2500-2300 B.C.				Color		
	Class	Pottery Type	Technique of manufacture	Matrix	Fabric	Decorat-ion
KB.11.B.1128/1	Storage Ware	jar	-	-	Black core	-
KB.11.B.1128/50	Storage Ware	pithos	-	2.5YR5/6 (red)+ 1FOR GLEY 3/N (very dark gray)	Black core	-
KB.11.B.1128/51	Storage Ware	pithos	-	5YR6/6 (reddish yellow)+ 1 FOR GLEY 3/N (very dark gray)	Black core	-
KB.11.B.1128/52	Storage Ware	Hole-mouth jar	-	-	Red-brown	-
KB.11.B.1128/65	Red burnished ware	juglet	-	7.5YR7/4 (pink)	Red-brown	-

4.1.4 EB IV

The ceramic fragments belonging to this phase only rarely show superficial decorations. For these sherds also the different matrix color allows to recognize four groups: 1) red-brown, 2) pink, 3) the so called “black core” and 4) gray color.

Samples KB.05.5/D200, KB.05.A/6b1, KB.05.A.18/5, KB.05.A.21/27, KB.05.A.31/2, KB.05.A.62/2, KB.05.A.8b/3b, KB.05.A.88/1, KB.05.A.96/1, KB.05.A.98/1, KB.05.A.212/6, KB.05.B.128/3 and KB.06.A.ø/18 show an homogeneous red or brown matrix color, ranging from pink, reddish yellow, yellowish brown, red, light brown to strong brown.

Samples KB.05.A.62/1, KB.05.A.68/2, KB.05.A.82/4, KB.05.A.84/3, KB.05.A.210/2, KB.05.A.216/12, KB.06.A.248/2, and KB.06.A.256/1 show the so called “black core”. In particular, the difference in color between the central part and the margin is clearly evident in sample KB.05.A.68/2, while the core of other samples is gray in color.

Samples KB.05.A.210/4, and KB.06.A.248/2 show a gray matrix color.

There is no correlation between color and type of potteries; in particular, the color of EB IV SW potteries ranges from light yellowish-red to reddish-yellow, while that of StW ranges from pink, light yellowish brown to light-pale brown. All KW potteries were usually reddish-brown or strong brown, while MW are grey.

These fragments show superficial treatments, outer red slip or combed, applied and incised decoration.

Among these fragments, the superficial treatments have not been diffuse, as example Figure 5 shows the sample KB.05.A.18/5 with a combed decoration and sample KB.05.A.204/2 with an incised decoration.

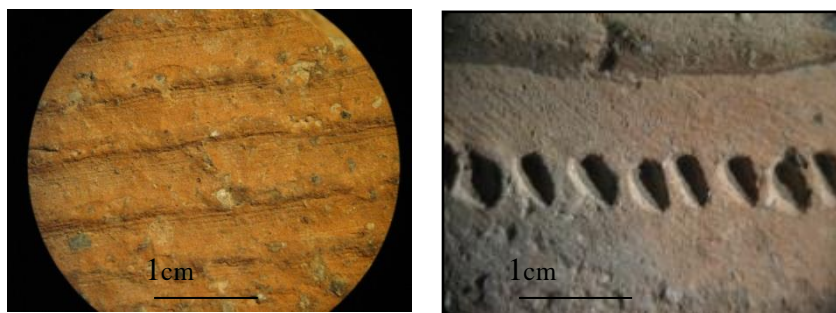


Figure 5: Photographs representing superficial treatments: the sample KB.05.A.18/5 (left) with a combed decoration and the sample KB.05.A.204/2 (right) with an incised decoration.

The majority of the fragments show trace of handmade manufacturing process. Only samples KB.05.A.62/1, KB.05.A.96/1 and KB.06.A.256/1 show a series of parallel tracks on the surface, which are typical in the ceramics made up with a wheel.

The size of the inclusions ranges from micrometric to millimetric in the same shards. A seriate granulometric distribution of the inclusions has been observed also in the sherds of this period. White dark, gray, yellow and red inclusions have been observed and also fragments of grog have been identified.

Table 5 shows the morphological and typological characteristics of the fragments.

Table 5: Morphological and typological characteristics of the fragments belonging to Early Bronze Age IV.

EB IV 2300-2000 B.C.				Color		
	Class	Pottery Type	Technique of manufacture	Matrix	Fabric	Decoration
KB.05.5/D200	Simple Ware	Jar	Made by hand	7.5YR 6/4 (light brown)	Red-brown	applied
KB.05.A.6b/1	Kitchen Ware	Hole-mouth pot	-	2.5YR5/6 (red)	Red-brown	-
KB.05.A.18/5	Simple Ware	Jar	Made by hand	7.5YR 6/4 (light brown)	Red-brown	outer band-combed
KB.05.A.21/27	Storage Ware	Jar	-	2,5 YR 6/8 (light red)	Red-brown	outer band-combed
KB.05.A.34/2	Simple Ware	Jar	-	2.5YR6/2 (pale red)	Red-brown	Outer incised
KB.05.A.62/1	Simple Ware	Jar	Wheel	7.5YR7/6 (reddish yellow) +2.5Y6/1 (gray)	Black core	-
KB.05.A.62/2	Simple Ware	Jar	Made by hand	5YR6/6 (reddish yellow)	Red-brown	Outer incised

EB IV 2300-2000 B.C.				Color		
	Class	Pottery Type	Technique of manufacture	Matrix	Fabric	Decoration
KB.05.A.68/2	Storage Ware	Jar	-	10 YR 5/2 (grayish brown)+ 2.5 Y 2.5/1 (black)	Black core	-
KB.05.A.82/4	Simple Ware	Jar	-	10 YR 6/4 (light yellowish brown) +10 YR 7/4 (very pale brown)	Black core	-
KB.05.A.84/3	Simple Ware	Jar	Made by hand	2.5YR6/8 (light red)+ 2 FOR GLEY5/5PB (bluish gray)	Black core	outer wavy and hand- combed
KB.05.A.8b/3b	Kitchen Ware	Hole-mouth pot	-	2.5YR5/6 (red)	Red-brown	-
KB.05.A.88/1	Storage Ware.	Hole-mouth jar.	Made by hand	10YR6/3 (pale brown)	Red-brown	outer smooth.
KB.05.A.96/1	Simple Ware	Jar	Wheel	7.5YR6/6 (reddish yellow)	Red-brown	-
KB.05.A.98/1	Kitchen Ware.	Hole-mouth pot	Made by hand	7.5YR5/6 (strong brown)	Red-brown	-
KB.05.A.210/2	Simple Ware	Jar	-	1 FOR GLEY 5/N (gray)+ 5 YR 6/6 (reddish yellow)	Black core	-
KB.05.A.210/4	Simple Ware	Jar	-	7.5YR6/0 (gray)	Gray	-
KB.05.A.212/6	Simple Ware	Jar	Made by hand	7.5YR8/3 (pink)	Red-brown	-
KB.05.A.216/12	Storage Ware	Jar	Made by hand	2.5YR5/6 (red)+ 1 FOR GLEY 5/N (gray)	Black core	-
KB.05.B.128/3	Kitchen Ware.	Hole-mouth pot	Made by hand	7.5YR5/6 (strong brown)	Red-brown	-
KB.06.A.248/2	Storage Ware	Jar	Made by hand	5Y5/1 (gray)	Black core	outer combed
KB.06.A.256/1	Storage Ware	Jar	Made by hand, whell	5YR7/6 (reddish yellow)+ 1 FOR GLEY 5/N (gray)	Black core	-
KB.06.A.ø/18	Storage Ware	Jar	Made by hand	10YR6/4 (light yellowish brown)	Red-brown	outer ap- plied.
KB.06.B.383/7	Storage Ware	Jar	Made by hand	7.5YR6/0 (gray)	Gray	-

4.2 Optical Microscopy analysis in thin section (OM)

The study of archaeological pottery in thin sections under the optical microscope is a traditional approach used to describe and to characterize ancient ceramic artifacts. This kind of analysis can give information to define how the pottery was made in the past. In particular, the definition of the mineralogical composition can provide information about the provenance of the pottery; the percentage, grain size and distribution of the inclusions can allow to reconstruct the technique used to produce the pottery; and finally the presence of high temperature minerals, as well as the occurrence or absence of primary calcite and the “optical activity” of the matrix allow to estimate the firing temperature.

Considering the nature of the inclusions, their packing and the mean size, here are distinguished twelve petrographic *fabrics* (following the indication of Whitbread, 1986, 1995) among the analyzed thin sections (Appendix B and Tables 6 and 7).

These groups have almost the same mineralogical composition, however *Fabric A* is characterized by the presence of micritic and sparry calcite as inclusions in a fine calcareous matrix with vesicles as pores. Samples of *Fabric B*, containing clay pallets and fragments of grog, are divided into three subgroups (B1, B2 and B3) on the basis of the different percentage of elongated vughs and on the aspect of the matrix. *Fabric C* is characterized by the presence of diffuse fragments of calcite, clay pallets and iron oxides in a calcareous matrix with mega-vughs; it is possible to divide this *fabric* into C1, having small sized of inclusions of calcite, and C2 with coarse grained calcite inclusions. The main feature of *Fabric D* is the prevalence of calcite crystals in a calcareous matrix with mega-vughs; moreover on the basis of the percentage of porosity *Fabric D* is further divided into D1 and D2. *Fabric E* is mainly represented by the presence of fine inclusions of micritic calcite in a calcareous matrix containing mainly vesicles. *Fabric F*, characterized by the presence of fragments of fossils and sedimentary rocks as inclusions, can further divided into F1 and F2 considering the percentage of inclusions and the nature of the matrix. *Fabric G*, containing inclusions of basaltic rocks and fragments of fossils, is divided into two *fabrics* on the basis of the color of the matrix, whereas *Fabric H* shows the same inclusions associate to large-sized of clay pallets and iron oxides. Large-sized fragments of fossils and in particular fragments of shells, are the main feature of *Fabric I*. *Fabric L* with coarse inclusions of calcite, divided into L1 with high percentage of inclusions and L2 with low percentage, is distinguished by the *Fabric M* which shows crystals of calcite associated to micritic calcite and fragments of sedimentary rocks; on the basis of the shape of pores are identified the subgroups M1 and M2. Finally, *Fabric N* is characterized by diffuse clay pallets and rare inclusions of calcite in calcareous matrix with mega-vughs.

The results of optical microscopy analysis of pottery from Khirbet al-Batrawy have been shown and discussed according to the four periods of Batrawy urbanization and following the division into *fabrics*.

4.2.1 EB II

All the analyzed samples show almost the same petrographic features. However they can be attributed to four different *fabrics* (described above, Appendix B): *Fabric A-calcite, micritic and sparry calcite with vesicles*) KB.06.E.706/1, KB.06.E.706/2 (Fig. 6); *Fabric B-clay pallets and fragments of grog* B1) KB.06.B.703/6 and B2) KB.06.B.392/8, KB.06.E.703/5; *Fabric C-calcite and clay pallets* C1) KB.06.E.702/10 and *Fabric D-crystals of calcite* D1) KB.06.E.704/1, KB.06.E.704/6.

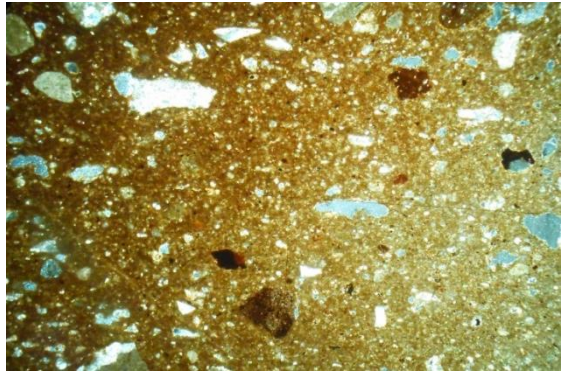


Figure 6: Thin section photomicrographs of KB.06.E.706/1 sample, representative of *Fabric A* (mag 2.5 x and crossed polarizers).

The *Fabric A-calcite, micritic and sparry calcite with vesicles* is characterized by the presence of inclusions essentially consisting of sand-sized particles (< 2mm), equant-elongate, from angular to sub-rounded in a calcareous fine clay matrix. The spatial distribution of inclusions is quite uniform with good sorting and a packing around 20%. The inclusions are represented by micritic calcite (equant and elongated, from angular to well-rounded, with size ranging from 0.5 to 1.3 mm), sparry calcite (equant and elongated, from angular to sub-rounded, with size ranging from 0.5 to 1.3 mm), fragments of chert (elongated, angular, with size ranging from 0.4 to 2.0 mm), ARF (equant, from sub-angular to rounded, with size around 1.2 mm) and quartz (equant, from sub-angular to sub-rounded, whose size ranges from 0.1 to 0.5 mm). Diffuse are the iron oxides nodules. With the terms *iron oxides* or *ferriferous nodules* are described aggregates of iron very common in pastes of archaeological pottery; the authors can referred to them in different way: “aggregates of iron oxides in form of lateritic pisoids” (Laviano and Muntoni, 2003) or “limonitic nodules” (Szakmany and Starnini, 2007). The largely sand inclusions do not show any preferred alignment. The groundmass is generally homogeneous with a light-brown color. The samples contain meso- and micro-vesicles, rare macro-elongated vughs. They do not exhibit a preferred alignment parallel to each other and to the margins of the sections.

Under the optical microscope, the fragments belonging to the *Fabric B-clay pallets and fragments of grog* are texturally homogeneous and display inclusions of similar type, abundance and grain size. The groundmass has a color ranging from red, beige to dark brown and is mostly characterized by an optical active portions of the groundmass. Pores are generally large in size, containing macro- and mega-elongated vughs, less diffuse micro-vesicles. They can exhibit a preferred alignment parallel to each other and to the margins of the sections. Inclusions are generally represented by moderately abundant coarse-sized micritic calcite (equant and elongated, from angular to sub-rounded, with size ranging from 0.3 to 1.5 mm), sparry calcite (equant and elongated, from angular to sub-rounded, with size between 0.5 and 1.5 mm), iron oxides (equant and elongated, from sub-rounded to rounded, with size ranging from 0.3 to 1.0 mm) and fine quartz (equant, from angular to well-rounded, with size ranging from 0.1 to 0.05 mm). All these inclusions do not show any preferred alignment. Dark clay pellets (0.3 to 2.2 mm), grog (equant and elongated, from angular to sub-angular, with size ranging from 0.5 to 1.0 mm) and ARF (equant, from angular to rounded, with size between 0.5 and 2.0 mm) are also present. Clay textural features (TFs) appear to represent lumps of the base clay used to produce these ceramics. The clay TFs generally have neutral optical density and blend into the matrix, but can have a more conspicuous darker, reddish color.

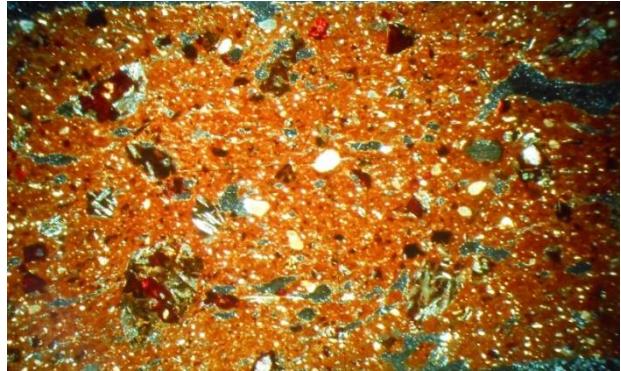
The third group (*Fabric D-crystals of calcite*) is represented by a homogeneous *fabric* characterized by equant-elongate, from sub-angular to sub-rounded, medium sand-sized inclusions in a non-calcareous red-orange colored fine clay matrix, optically active. It shows a packing of about 30% and unimodal grain size distribution. The inclusions are mainly represented by coarse-sized micritic calcite (equant and elongated, from sub-angular to sub-rounded, with size ranging from 0.3 to 1.0 mm), iron oxides, fragments of fossils (equant and elongated, from sub-angular to sub-rounded, with size ranging from 0.5 to 1.0 mm) and quartz (equant, from sub-angular to well-rounded, with size ranging from 0.1 to 0.8 mm). All these inclusions do not show any preferred alignment. The samples contain meso- and macro-elongated vughs that can exhibit a preferred alignment parallel to each other and to the margins of the sections.

Finally, one sample (KB.06.E.702/10) has been considered grouped into the subgroups C2 of *Fabric C-calcite and clay pallets*, with compositional and textural features not found in the other samples. It presents equant and elongate, from angular to sub-rounded medium sand-sized inclusions in percentage around 20%, in an orange-reddish calcareous fine clay matrix. The clasts are calcite (fine: equant, from rounded to well-rounded with size between 0.1 and 0.05 cm and coarse: equant and elongated, from angular to sub-angular, with size ranging from 0.3 to 0.5 mm) and quartz (equant, from rounded to well-rounded, with size ranging from 0.1 to 0,4 mm) as in-

clusions that do not show any preferred alignment. Iron oxides nodules (equant and elongated, sub-rounded, with size ranging from 0.3 to 1.0 mm) have been identified. The samples mainly contain mega- macro-vughs and rare meso-vughs that do not exhibit a preferred alignment.

4.2.2 EB IIIA

The composition of the non-plastic inclusions, the packing and the mean size allow to distinguish six groups (described above, Appendix B) having different petrographic *fabric*s for EB IIIA Khirbet al-Batrawy potteries: *Fabric B-clay pallets and fragments of grog* (B2)



KB.05.B.146/4 and B3) KB.05.B.136/5, KB.05.A.64/13; *Fabric C-calcite and clay pallets* (C2)

Figure 7: Thin section photomicrographs of KB.06.E.701/2 sample representative of *Fabric G1* (mag 2.5 x and crossed polarizers).

KB.05.B.146/7, KB.05.B.146/8; *Fabric E-fine calcite*) KB.05.B.146/6, KB.05.A.58/1, KB.05.B.146/24, KB.05.B.126/1, KB.05.B.136/1, KB.06.E.703/3; *Fabric F-fossils and sedimentary rocks* (F1) KB.05.B.146/30, KB.06.B.427/1, KB.05.B.146/1, KB.05.B.126/3 and (F2) KB.05.A.64/1, KB.06.B.376/4, KB.09.B.820.12; *Fabric G-basaltic rocks and fragments of fossils* (G1) KB.06.E.701/2, KB.05.B.146/3, KB.05.B.146/5, KB.05.B.146/15 (Fig. 7) and (G2) KB.09.B.820/13, KB.08.B.805/6, KB.05.B.110/15, KB.09.B.820.10, KB.05.B.136/3; *Fabric H-clay pallets, calcite and iron oxides*) KB.06.B.167/4, KB.05.A.52/8 and finally, *Fabric I-shells*) KB.06.B.413/2, KB.06.B.146/20.

These groups have almost the same mineralogical composition. However, the petrographic group (*Fabric B-clay pallets and fragments of grog*) present mainly mega-elongated vughs, diffuse clay pallets and fragments of grog. The microscopic observation have shown that the pottery samples are characterized by a unimodal grain size distribution, with around 10-20% of equant-elongate, from very-angular to sub-rounded medium sand-sized inclusions. The calcareous clay matrix shows a variable color between reddish to brown with active optical behaviour. The grain-size is generally coarse, with a maximum size of 2.5 mm and the inclusions are composed by micritic calcite (equant and elongated, from angular to sub-rounded, with size ranging from 0.1 to 2.5 mm), sparry calcite (equant and elongated, from angular to sub-

rounded, with size ranging from 0.5 to 1.5 mm), fragments of marl (equant and elongated, angular, with size ranging from 0.6 to 1.0 mm), iron oxides (equant and elongate, from sub-angular to well-rounded, with size ranging from 0.2 to 1.2 mm), grog (equant, from sub-angular to sub-rounded, with size ranging from 1.0 to 2.0 mm), olivine (equant and elongated, well-rounded, ranging from 0.2 to 0.5 mm), quartz (equant, from sub-angular to sub-rounded around 0.1 mm). Dark clay pellets (sharp to margining boundaries, 0.2-0.8 mm, from rounded to well-rounded, elongated, with included quartz crystals and discordant with the matrix) and ARF (equant, from very-angular to angular, with size ranging from 0.4 to 1.2 mm) are also present. Porosity varies from sample to sample and is mainly represented by macro- and mega-vughs that exhibit a lightly alignment parallel to each other and to the margins of the sections.

The petrographic group (*Fabric C-calcite and clay pellets*) is an homogeneous group with fragments showing similar petrographic features. The inclusions cover the 20% of the total and are mainly represented by calcite (micritic and sparry, equant and elongated, from angular to sub-rounded, ranging from 0.5 to 2.0 mm), diffuse are quartz (equant, sub-rounded, with size around 0.1) and rare olivine (equant, angular around 0.5 mm). Fragments of grog (equant, from sub-angular to sub-rounded, with size ranging from 0.1 to 2.0 mm with sharp boundaries, prolate and equant with discordant features. Light brown to light red, composed of clay with quartz) and iron oxides nodules (equant, rounded, with size around 0.8 mm) have been also identified. The calcareous matrix presents a heterogeneous colour due to strong core/margin color differentiation, from light red to dark (thickness margin is variable from 0.8 to 1.8 mm). The pores consist mainly of macro- and mega-vughs, less diffuse meso-vughs no aligned to the margin of sample.

The *Fabric E-fine calcite* is characterized by fine-grained micritic calcite in a calcareous brown clay matrix optically active. The inclusions are mainly equant, from sub-angular to well-rounded without any preferred alignment; in general the amount of non-plastic inclusions does not exceed 20% of the total volume. Non-plastic inclusions are composed of micritic calcite (equant and elongated, from very angular to sub-rounded, ranging from 0.2 to 0.3 mm), iron oxides (equant and elongate, rounded, ranging from 0.1 to 2.1 mm) and quartz (equant, from angular to sub-rounded, ranging from 0.1 to 0.5 mm). Porosity is low and the shapes of the voids are usually meso-vesicles that do not exhibit an alignment parallel to each other and to the margins of the sections.

The petrographic group (*Fabric F-fossils and sedimentary rocks*) is discriminated on the basis of fragments of fossils and sedimentary rocks as inclusions. It can be considered a homogeneous *fabric* characterized by equant-elongate, from very-angular to

well-rounded medium sand-sized inclusions with maximum size of 2.1 mm in a calcareous reddish-brown colored fine clay matrix.

The abundance of inclusions is about 20%, coarse-sized micritic calcite (equant and elongated, from very angular to well-rounded, ranging from 0.1 to 0.8 mm), sparry calcite (equant and elongated, from very angular to sub-rounded, ranging from 0.2 to 1.2 mm), fragments of fossils (equant and elongated, from very angular to well-rounded, ranging from 0.2 to 2.0 mm), iron oxides (equant and elongate, from sub-angular to rounded, ranging from 0.1 to 2.1 mm), fragments of sedimentary rocks (probably marl and chert, equant and elongated, from angular to rounded, ranging from 0.3-1.3 mm) and piroxene (equant, very angular around 0.2 mm) as inclusions have been identified. The inclusions do not show any preferred alignment. The samples contain mainly meso-vughs and meso-vesicles that do not exhibit an alignment parallel to each other and to the margins of the sections. The clay matrix of the samples is optically active.

The petrographic group (*Fabric G-basaltic rocks and fragments of fossils*) presents fragments showing similar petrographic features with dominant inclusions of basaltic rocks and fragments of fossils divided into two sub-groups. The ceramics are characterized by the presence of coarse sized inclusions with a packing, ranging between 20 and 30%. The inclusions are represented by micritic calcite (equant and elongated, from very-angular to well-rounded, with size between 0.2 and 2.1 mm), fragments of basaltic rocks (equant, from very-angular to sub-angular from 0.2 to 2.5 mm), fragments of fossils (equant and elongated, very-angular to well-rounded, ranging from 0.2 to 0.8 mm), olivine (equant and elongated, well-rounded, ranging from 0.2 to 0.5 mm), fragment of marl (equant and elongated, from angular to rounded, ranging from 0.5 to 2.5 mm) and quartz (equant, from sub-angular to sub-rounded, with size around 0.1 mm). In all the samples ferriferous nodules (equant and elongate, from very-angular to well-rounded, ranging from 0.1 to 3.0 mm) have been often observed in variable quantity and size. Clay pallets appear to represent lumps of the base clay used to produce these ceramics. The clay TFs ranging from 0.6 to 1.2 mm, generally have neutral optical density and blend into the matrix, but can have a more conspicuous darker, reddish color.

Pores are mainly represented by meso-vesicles and meso- and macro-elongated vughs that do not exhibit a preferred alignment parallel to each other and to the margins of the sections.

Finally, the *Fabric I-shells* present 40% of coarse-sized elongated from very-angular to angular fragments of fossils with maximum size of 3.0 mm in a calcareous brown colored fine clay matrix.

4.2.3 EB IIIB

The thin sections of fragments belonging to EB IIIB show similar petrographic features. However they can be subdivided into five different *fabrics* (described above, Appendix B) according to the grain size and the type of the aggregate. *Fabric B-clay pallets and fragments of grog* (B3) KB.05.B.111/3, KB.05.A.204/3, KB.10.B.1040/8,

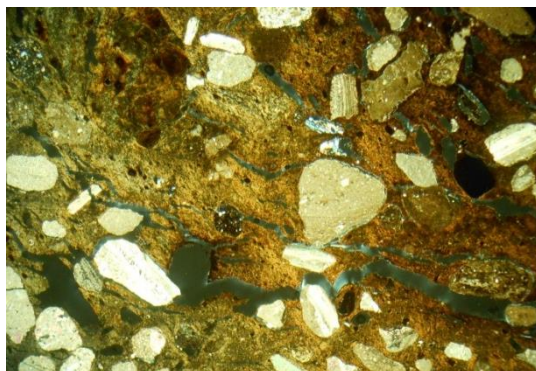


Figure 8: Thin section photomicrographs of KB.10.B.1054/6 sample representative of *Fabric M1* (mag 2.5 x and crossed polarizers).

KB.11.B.1124/24, KB.11.B.1128/76; *Fabric E-fine calcite* KB.10.B.1054/21, KB.10.B.1054/22, KB.11.B.1124/33, KB.11.B.1128/65; *Fabric H-clay pallets, calcite and iron oxides* KB.10.B.1054/24, KB.11.B.1124/8, KB.11.B.1124/10; *Fabric L-calcite and micritic calcite* (L2) KB.05.A.204/2, KB.11.B.1054/12; *Fabric M-micritic, calcite and sedimentary rocks* (M1) KB.05.A.46/8, KB.05.A.216/4, KB.06.A.220.5, KB.05.A.224/2, KB.10.B.1054/6, KB.10.B.1054/62, KB.11.B.1124/29, KB.11.B.1128/50, KB.11.B.1128/1 (Fig. 8) and (M2) KB.11.B.1124/3, KB.11.B.1124/15, KB.11.B.1128/52, KB.11.B.1128/51, KB.11.B.1224/22, KB.06.A.120/6. Furthermore, one sample (KB.11.B.1054/13) can be grouped into the subgroup D2 of *Fabric D-crystals of calcite*.

The subgroup B3 of *Fabric B-clay pallets and fragments of grog* is characterized by fine clay matrix with color ranging from orange, beige to dark brown calcareous containing equant and elongate, from very-angular to sub-rounded medium sand-sized inclusions. The non-plastic inclusions are less diffuse rather than those plastic. Between non-plastic inclusions calcite (equant and elongated, from angular to sub-rounded, with size ranging from 0.1 to 2.0 mm), micritic calcite (equant and elongated, from sub-angular to sub-rounded, ranging from 0.1 to 1.5 mm), sparry calcite (equant and elongated, from sub-angular to sub-rounded, with size ranging from 0.2 to 0.9 mm), fragments of basaltic rocks (equant, sub-angular, with size around 0.5 mm), fragments of sedimentary rocks (equant and elongated, from sub-angular to sub-rounded, ranging from 0.4 to 1.4 mm) and fine quartz (equant, from angular to well-rounded, ranging from 0.1 to 0.3 mm) have been identified. These inclusions do not show any preferred alignment. Plastic inclusions are diffuse in thin sections: dark clay pellets (0.3 to 1.0 mm), grog (equant and elongated, from very-angular to sub-rounded, ranging from 0.1 to 1.1 mm), and ARF (equant and elongated, from angular to sub-rounded, ranging

from 0.5 to 1.8 mm). Clay textural features (TFs) appear to represent lumps of the base clay used to produce these ceramics. The clay TFs generally have neutral optical density and blend into the matrix, but can have a more conspicuous darker, reddish color.

Iron nodules (equant and elongated, from sub-rounded to well-rounded, with size ranging from 0.1 to 0.8 mm) are diffuse in thin section. The samples contain meso- and macro-vughs, less diffuse micro-vesicles. They can exhibit a preferred alignment parallel to each other and to the edges of the sections.

The fine-grained sherds of *Fabric E-fine calcite* contain a low percentage (10-20%) of micritic calcite (equant and elongated, from sub-angular to rounded, ranging from 0.3 to 2.3 mm) and calcite (equant and elongated, from very-angular to angular, with size ranging from 0.2 to 1.9 mm) in a calcareous orange-brown fine clay matrix. Iron oxides (equant and elongated, from rounded to well-rounded, ranging from 0.1 to 1.0 mm), and fine quartz (equant, from angular to sub-angular, ranging from 0.1 to 0.05 mm) have also been identified. Dark clay pellets (0.3 to 1.2 mm, neutral optical density and blend into the matrix, but can have a more conspicuous darker, reddish color), fragments of fossils (equant and elongated, from angular to well-rounded, with size ranging from 0.2 to 1.2 mm) and fragments of sedimentary rocks (equant and elongated, from sub-angular to sub-rounded, ranging from 0.5 to 0.9 mm) are also present.

The sherds belonging to *Fabric H-clay pallets, calcite and iron oxides* are mainly characterized by the presence of fragments of basaltic rocks (equant, from sub-angular to sub-rounded, ranging from 0.2 to 2.0 mm) and fragments of fossils (equant and elongated, from angular to well-rounded, with size ranging from 0.2 to 1.0 mm) in a calcareous fine matrix with color ranging from red, beige to dark brown.. In the matrix, minor amounts of micritic calcite (equant, from sub-angular to rounded, ranging from 0.1 to 1.3 mm), calcite (equant and elongated, from angular to sub-rounded, with size ranging from 0.3 to 1.9 mm), iron oxides (equant and elongated, from sub-angular to well-rounded, ranging from 0.1 to 1.2 mm) and fine quartz (equant, from angular to well-rounded, ranging from 0.1 to 0.05 mm) have also been identified. Dark clay pellets (0.1 to 2.1 mm) and ARF (equant and elongated, from sub-angular to sub-rounded, ranging from 0.5 to 2.0 mm) are also present. The pores exhibit a preferred alignment parallel to each other and to the margins of the sections and are mainly meso- and macro-vughs

The subgroup L2 of *Fabric L-calcite and micritic calcite* includes samples that are characterized by a calcareous brown clayey mass lightly optically active, with micritic and sparry calcite inclusions and pores with the shape of vesicles. Large clasts are diffuse in the samples conferring a coarse-grained paste.

Micritic calcite inclusions (equant and elongated, from sub-angular to sub-rounded, with size ranging from 0.1 to 1.9 mm), are diffuse in thin section; iron oxides (equant and elongated, from rounded to well-rounded, ranging from 0.2 to 0.6 mm) and fine quartz (equant, from angular to sub-angular, with size around 0.1 mm) have been identified in lower amount. Fragments of fossils (equant and elongated, from angular to well-rounded, with size ranging from 0.2 to 1.0 mm), fragments of sedimentary rocks (equant and elongated, from sub-angular to sub-rounded, ranging from 0.8 to 1.1 mm) and fragments of basaltic rocks (equant, sub-angular, with size ranging around 0.6 mm) are also present. Vesicles are irregular, lens-shaped or elongated, mostly between 0.1 and 0.2 mm in size.

The samples with coarse-grained aggregate belonging to *Fabric M-micritic, calcite and sedimentary rocks* are characterized by the presence of poorly sorted coarse calcite grains (micritic calcite, equant and elongated, from angular to sub-rounded, ranging from 0.1 to 2.1 mm; and calcite, equant and elongated, from very-angular to sub-rounded, ranging from 0.1 to 2.0 mm), randomly distributed in a calcareous fine clay matrix with color ranging from beige to brown.

In the matrix, minor amounts of iron oxides (equant and elongated, from sub-angular to well-rounded, with size ranging from 0.1 to 2.0 mm) and fine quartz (equant, from angular to sub-rounded, ranging from 0.1 to 0.5 mm) have been also observed. Dark clay pellets (0.5 to 1.8 mm), grog (equant, from sub-angular to sub-rounded, ranging from 0.4 to 1.0 mm), fragments of fossils (equant and elongated, from angular to well-rounded, with size between 0.1 and 2.0 mm), fragments of sedimentary rocks (equant and elongated, from angular to rounded, ranging from 0.5 to 2.1 mm) and fragments of basaltic rocks (equant, from sub-angular to sub-rounded, ranging from 0.5 to 1.2 mm) are also present.

Porosity is represented by macro- and meso-elongated vughs that exhibit a preferred alignment parallel to the margins of the sections.

Finally, one sample (KB.11.B.1054/13) has been grouped into the subgroup D2 of *Fabric D-crystals of calcite*, having different compositional and textural features respect to the others. It presents equant and elongate, from angular to sub-rounded medium sand-sized inclusions in percentage of 20%, in a calcareous fine clay matrix with color red-brown. The clasts are represented by calcite (equant and elongated, from angular to sub-rounded, ranging from 0.5 to 1.1 mm) and quartz (equant, from sub-angular to sub-rounded, ranging from 0.1 to 2.0 mm) as inclusions that do not show any preferred alignment. Fragments of fossils (elongated, from angular to well-rounded, with size between 0.3 and 2.0 mm) and fragments of sedimentary rocks (equant and elongated, from angular to sub-rounded, ranging from 0.5 to 1.0 mm) have also been identified.

The samples contain meso- and macro-irregular vughs and meso-vesicles that do not exhibit a preferred alignment parallel.

4.2.4 EB IV

According to optical microscopy results, all investigated pottery samples could be divided into four groups comparable in terms of non-plastic inclusions, packing and means size (described above, Appendix B): *Fabric F-fossils and sedimentary rocks*) KB.05.A.82/4, KB.05.A.96/1, KB.05.5/D200; *Fabric G-basaltic rocks and fragments of fossils*) KB.05.A.18/5 and KB.05.A.34/2; *Fabric H-clay pallets, calcite and iron oxides*) KB.05.A.62/1 and KB.05.B.128/3; *Fabric L-calcite and micritic calcite* L1) KB.05.A.6b/1, KB.05.A.21/27, KB.05.A.8b/3b, KB.05.A.88/1, KB.05.A.98/1, KB.06.ø/18 and L2) KB.05.A.68/2 KB.06.A.248/2; *Fabric N-clay pallets and rare calcite*) KB.05.A.84/3, KB.05.A.210/2, KB.05.A.210/4, KB.05.A.216/12, KB.06.B.383/7, KB.06.A.256/1 (Fig. 9). Furthermore, one sample (KB.05.A.212/6) can be considered as petrographic ‘loner’, having green matrix and low percentage of inclusions.

The *Fabric F-fossils and sedimentary rocks* is distinguished on the basis of the diffuse presence of fossils fragments as inclusions. The spatial distribution of inclusions is not uniform and the packing has been estimated ranging between 10 and 30% with maximum size of 2.3 mm. They are represented by dominant fragments of fossils (elongated, sub-rounded, ranging from 0.5 to 2.3 mm), micritic calcite (equant and

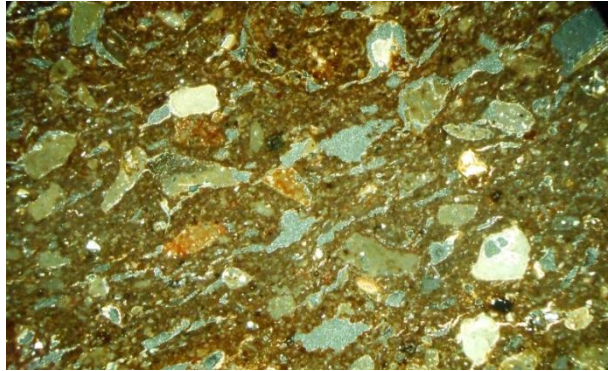


Figure 9: Thin section photomicrographs of KB.05.A.210/4 sample representative of *Fabric N* (mag 2.5 x and crossed polarizers).

elongated, from angular to sub-rounded, with size ranging from 0.2 to 1.5 mm) and calcite (equant and elongated, from angular to sub-rounded, ranging from 0.1 to 2.0 mm). Fine quartz (equant, from angular to rounded, ranging from 0.1 to 0.05 mm) and fragments of basaltic rocks (equant, sub-angular, ranging from 0.5 to 0.9 mm) have also been observed as inclusions, but in minor amounts. Dark clay pellets (0.5 to 2.2 mm), ARF (equant and elongated, from angular to sub-rounded, ranging from 0.5 to 2.0 mm) and ferriiferous nodules (equant and elongated, from sub-rounded to rounded, ranging from 0.2 to 1.9 mm) have been identified in thin section. The groundmass is optically active with a color ranging from beige to brown-red. The pores are irregular

and mainly represented by meso- and macro-elongated vughs, meso- and micro-vesicles that exhibit a lightly preferred alignment parallel to the margins of the sections.

The *Fabric G-basaltic rocks and fragments of fossils* is characterized by coarse inclusions in a beige-brown calcareous matrix. The inclusions are mainly represented by calcite (micritic and sparry, equant and elongated, from angular to sub-rounded, ranging from 0.2 to 1.5 mm) and diffuse quartz (equant, sub-angular to sub-rounded around 0.3-1.9). Iron oxides nodules (equant, from sub-rounded to rounded, 0.3-1.9 mm) have been also identified. The calcareous matrix presents a heterogeneous colour from beige-reddish to dark-brown with diffuse clay pallets (sharp to margining boundaries, 0.8-1.2 mm, rounded, equant and concordant with the matrix). The pores consist mainly of meso-vesicles, rare meso-vughs, not aligned to margin of sample.

Microscopic analysis indicated that the fragments were homogeneous from a petrographic point of view and therefore they are grouped in the *Fabric H-clay pallets, calcite and iron oxides*. These samples are characterized by homogeneous and optically active groundmass with color ranging from beige to brown. Pores are mainly represented by meso- and macro/mega-elongated vughs, meso-vesicles and rare micro-vesicles that exhibit a preferred alignment parallel to each other or to the margins of the sections.

Inclusions are diffuse in a percentage between 10 and 30%, with maximum size of 2.5 mm. They are composed mainly by fragments of fossils (elongated, sub-rounded, ranging from 0.3 to 1.8 mm) and fragments of basaltic rocks (equant, from angular to sub-angular, ranging from 0.5 to 2.5 mm). Micritic calcite (equant and elongated, from angular to well-rounded, ranging from 0.2 to 2.0 mm), sparry calcite (equant and elongated, from angular to sub-rounded, with size ranging from 0.2 to 1.3 mm), iron oxides (equant, from sub-rounded to well-rounded, ranging from 0.2 to 1.9 mm) and fine quartz (equant, from sub-angular to sub-rounded, ranging from 0.1 to 0.05 mm) have been also identified, in minor amount. Samples contain also argillaceous inclusions as clay pallets (neutral optical density and blend into the matrix, with a more conspicuous darker, reddish color).

The samples that belong to *Fabric L-calcite and micritic calcite* present the same petrographic features, characterized by moderately sorted non-plastic inclusions with the prevailing size falling into the classes of coarse-sand. Calcite (equant and elongated, from angular to sub-rounded, ranging from 0.1 to 2.2 mm) micritic calcite (equant and elongated, from angular to sub-rounded, with size ranging from 0.1 to 2.0 mm), sparry calcite (equant and elongated, from angular to sub-rounded, ranging from 0.1 to 1.5 mm) are definitely the main mineralogical constituent. Iron nodules (equant and elongated, from sub-angular to well-rounded, ranging from 0.1 to 1.0 mm), fine quartz

(equant, from angular to sub-rounded, ranging from 0.1 to 0.05 mm) dark clay pellets (0.1 to 1.0 mm), grog (equant and elongated, from sub-angular to sub-rounded, ranging from 1.0 to 1.1 mm), fragments of fossils (equant and elongated, from angular to sub-rounded, ranging from 0.1 to 2.0 mm) and ARF (equant, from angular to sub-rounded, ranging from 0.5 to 1.0 mm) are also present, but in much smaller quantities. The packing of these sand inclusions generally ranges between 20 and 30% and the groundmass is optically active. Another textural feature characteristic of *Fabric L-calcite and micritic calcite* samples is the presence of pores with irregular shape, consisting mainly of meso- and macro-vesicles and meso- or macro-elongated vughs that do not exhibit a preferred alignment parallel to the margins of the sections.

The petrographic group *Fabric N-clay pallets and rare calcite* includes samples characterized by mega- elongated-vughs and diffuse clay pallets, and fragments of grog. The spatial distribution of inclusions is variable with a packing ranging between 10 and 30%. The inclusions are represented mainly by the plastic ones as dark clay pellets (0.1 to 1.0 mm), grog (equant, from sub-angular to sub-rounded, ranging from 0.5 to 1.0 mm), and ARF (equant and elongated, from angular to sub-rounded, ranging from 0.3 to 1.3 mm). Fragments of fossils (elongated, from angular to sub-angular, with size ranging from 0.5 to 2.0 mm), fragments of basaltic rocks (equant, from angular to sub-angular, ranging from 0.2 to 1.0 mm), fragments of sedimentary rocks (equant and elongated, from sub-angular to sub-rounded, ranging from 1.0 to 2.0 mm) are also present but in small amounts. Calcite (equant and elongated, from angular to sub-rounded, ranging from 0.7 to 2.0 mm), micritic calcite (equant and elongated, from angular to rounded, ranging from 0.2 to 2.2 mm), sparry calcite (equant and elongated, from angular to sub-rounded, with size ranging from 0.2 to 0.9 mm), iron oxides (equant, from sub-rounded to well-rounded, ranging from 0.2 to 1.2 mm) and fine quartz (equant, from angular to sub-rounded, ranging from 0.1 to 0.05 mm) have been observed in accessory quantities. The groundmass is generally heterogeneous with a variable color ranging from red to beige-grayish. Fragments present a high porosity mainly represented by large-sized vughs (meso- and macro-) and rare meso-vesicles showing a preferred alignment parallel to each other or to the margins of the sections.

Finally, one sample (KB.05.A.212/6) has been considered as petrographic 'loner' not showing similar features respect the other samples. It shows equant and elongate, from angular to sub-rounded medium sand-sized inclusions in low percentage (5%), in a calcareous fine clay matrix with beige-green color. There is a medium abundance of coarse-sized micritic calcite (elongated, from sub-angular to sub-rounded, ranging from 0.6 to 1.8 mm), iron oxides (equant and elongated, from sub-rounded to well-rounded, ranging from 0.1 to 1.0 mm) and fine quartz (equant, from angular to sub-

angular, ranging from 0.1 to 0.05 mm) as inclusions that do not show any preferred alignment. Fragments of grog (equant and elongated, from angular to sub-rounded, with size ranging from 1.0 to 1.5 mm) are also present.

The samples contain macro-vughs that exhibit a lightly preferred alignment parallel to each other or to the margins of the sections. The clay matrix of the samples is not optically active.

Table 6: Summary describing the features of different petrographic groups.

SAMPLES		MICROSTRUCTURE	GROUNDMASS	INCLUSIONS	aplastic	plastic
<i>Fabric A</i>	KB.06.E.706/1 KB.06.E.706/2	diffuse meso- and micro-vesicles, rare macro-elongated vughs.	fine calcareous matrix light-brown color	20% sand-sized (< 2mm) equant-elongate from angular to sub-rounded	dominant micritic calcite, sparry calcite, common fragments of chert and fine quartz	iron oxides nodules
<i>Fabric B</i>	B1 (KB.06.B.703/6) B2 (KB.06.B.392/8,KB.06.E.703/5, KB.05.B.146/4) B3 (KB.05.B.136/5,KB.05.A.64/13, KB.05.B.111/3, KB.05.A.204/3, KB.10.B.1040.8, KB.11.B.1124/24, KB.11.B.1128/76)	diffuse macro- and mega-elongated vughs rare micro-vesicles	calcareous matrix from orange-beige to dark brown	10-20% coarse-sized (<2.5 mm) equant-elongate from very-angular to sub-rounded	dominant calcite, micritic calcite, sparry calcite, diffuse fragments of sedimentary rocks, fragments of basaltic rock, common fine quartz, very rare olivine	dominant grog clay pellets diffuse iron oxides nodules
<i>Fabric C</i>	C1 (KB.06.E.702/10) C2 (KB.05.B.146/7,KB.05.B.146/8)	mainly macro- and mega-vughs, rare meso-vughs	calcareous fine matrix from light red to dark gray	20% medium sand-sized inclusions equant and elongate, from angular to sub-rounded	dominant micritic calcite, sparry calcite rare fine quartz, very rare olivine	dominant clay pellets, diffuse iron oxides nodules, grog
<i>Fabric D</i>	D1 (KB.06.E.704/1,KB.06.E.704/6) D2 (KB.11.B.1054/13)	meso- and macro-elongated vughs and meso-vesicles	fine calcareous matrix from orange to brown	20-30% medium sand-sized inclusions equant-elongate, from sub-angular to sub-rounded	dominant crystals of calcite, diffuse micritic calcite, less common fragments of fossils and fragments of sedimentary rocks, rare fine quartz	diffuse iron oxides nodules
<i>Fabric E</i>	KB.05.B.146/6,KB.05.A.58/1,KB.05.B.146/24 KB.05.B.126/1,KB.05.B.136/1,KB.06.E.703/3 KB.10.B.1054/21,KB.10.B.1054/22, KB.11.B.1124/33,KB.11.B.1126/65	low-porosity is low with meso-vesicles	calcareous fine matrix orange-brown	10-20% fine-grained equant, from sub-angular to well-rounded	dominant micritic calcite, calcite, less common fragments of fossils, fragments of sedimentary rocks, rare fine quartz	common iron oxides and clay pellets
<i>Fabric F</i>	F1 (KB.05.B.146/30,KB.06.B.427/1,KB.05.B.146/1 KB.05.B.126/3) F2 (KB.05.A.64/1,KB.06.B.376/4,KB.09.B.820/12 KB.05.A.82/4,KB.05.5/D200,KB.05.A.96/1)	meso- and macro-vughs and meso- and micro-vesicles	calcareous fine matrix from beige to brown-red	10-30% coarse-sized (<2.3 mm) equant-elongate, from very-angular to well-rounded	dominant fragments of fossils, sedimentary rock, diffuse micritic calcite, sparry calcite, rare fine quartz, very rare pyroxene, fragments of basaltic rocks	common iron oxides nodules and clay pellets

<i>Fabric G</i>	G1 (KB.06.E.701/2,KB.05.B.146/3,KB.05.B.146/5a KB.05.B.146/15,KB.05.B.126/4) G2 (KB.09.B.820/13,KB.08.B.805/6,KB.05.B.110/15 KB.09.B.820/10,KB.05.B.136/3,KB.05.A.34/2 KB.05.A.18/5)	meso-vesicles and meso- and rare macro-elongated vughs	calcareous matrix from red to beige-brown	20-30% coarse sized inclusions equant-elongate, from very-angular to well-rounded	dominant inclusions of basaltic rocks and fragments of fossils, common fragment of marl, micritic calcite, sparry calcite, rare olivine, fine quartz	diffuse iron oxides nodules and clay pallets
<i>Fabric H</i>	KB.06.B.167/4,KB.05.A.52/8,KB.10.B.1054/24 KB.11.B.1124/8,KB.11.B.1124/10,KB.05.A.62/1 KB.05.B.128/3	mainly meso- and macro-vughs by meso- and macro/mega-elongated vughs, meso-vesicles and rare micro-vesicles	calcareous fine matrix with color ranging from red, beige to dark brown.. color ranging from beige to brown	10 and 30%, with maximum size of 2.5 mm.	fragments of basaltic rocks fragments of fossils minor amounts of micritic calcite calcite fine quartz	iron oxides dark clay pellets
<i>Fabric I</i>	KB.06.B.413/2, KB.06.B.146/20	mainly meso- and mega-vughs	calcareous fine matrix red	40% coarse-sized (<3.0 mm) elongated from very-angular to angular	fragments of fossils	
<i>Fabric L</i>	L1 (KB.05.A.204/2,KB.11.B.1054/12,KB.05.A.68/2 KB.06.A.248/2) L2 (KB.05.A.6b/1,KB.05.A.21/27,KB.05.A.8b/3b KB.05.A.88/1,KB.05.A.98/1, KB.06.ø/18	meso- and macro-vesicles	calcareous matrix from orange to dark	20-30% coarse-grained inclusions	dominant calcite and micritic calcite, less common fragments of sedimentary rocks, fragments of basaltic rocks, fragments of fossils and fine quartz	less diffuse iron oxides and clay pellets
<i>Fabric M</i>	M1 (KB.05.A.46/8,KB.05.A.216,KB.06.A.220/5 KB.05.A.224/2,KB.10.B.1054/6,KB.10.B.1054/62 KB.11.B.1128/1,KB.11.B.1124/29,KB.11.B.1128/50) M2 (KB.11.B.1124/15,KB.06.A.120/6,KB.11.B.1124/3 KB.11.B.1128/52,KB.11.B.1128/51,KB.11.B.1224/22)	macro- and meso-elongated vughs	calcareous fine matrix ranging from beige to brown	40% coarse grains equant-elongate, from very-angular to well-rounded	dominant calcite, micritic calcite, common fragments of fossils, fragments of sedimentary rocks, rare fragments of basaltic rocks and fine quartz	common iron oxides, clay pellets, grog
<i>Fabric N</i>	N1 (KB.05.A.210/2,KB.05.A.210/4,KB.06.B.383/7 KB.06.A.256/1,KB.05.A.84/3) N2 (KB.05.A.216/12)	mega- elongated-vughs and rare meso-vesicles	calcareous matrix from red to beige-grayish	10-30% equant-elongate, from very-angular to well-rounded	in small amounts fragments of fossils, fragments of basaltic rocks, fragments of sedimentary rocks, accessory quantities calcite, micritic calcite, sparry calcite and rare fine quartz	dominant clay pallets and iron oxides, rare fragments of grog

Table 7: Grouping results divided into the four periods of Batrawy urbanization. The samples are identified by the last part of the acronym, and the pottery productions are indicated by different colors: Simple Ware = blue; Storage Ware = green; Red Burnished and Red Polished Ware = red; Simple Painted Ware = violet; Metallic Ware = orange; Kitchen Ware = gray; Khirbet Kerak Ware = black.

FAB A	FAB B			FAB C		FAB D		FAB E	FAB F		FAB G		FAB H	FAB I	FAB L		FAB M		FAB N	
	B1	B2	B3	C1	C2	D1	D2		F1	F2	G1	G2			L1	L2	M1	M2	N1	N2
EB II																				
706/1 platter	703/6 jar	392/8 jar		702/10 jug		704/1 platter														
706/2 platter		703/5 jar				704/6 bowl														
EB IIIA																				
		146/4 jar	64/13 jar		146/7 jug			58/1 jug	126/3 platter	820.12 bowl	701/2 jar	136/3 jar	167/4 jar	146/20 hole-mouth pot						
			136/5 pithos		146/8 platter			126/1 jug	146/1 platter	64/1 platter	146/3 jar	805/6 jug	52/8 hole-mouth jar	413/2 hole-mouth pot						
								146/6 jug	146/30 jug	376/4 jug	146/5a jug	110/15 jug								
								146/24 jug	427/1 jug		146/15 bowl	820.10 bowl								
								136/1 jar			126/4 bowl	820.13 jug								
								703/3 jug												
EB IIIB																				
			111/3 jar				1054/13 jug	1054/21 jar					1124/10 pithos		204/2 hole-mouth jar		46/8 pithos	1124/3 hole-mouth jar		
			204/3 hole-mouth jar					1054/22 jug					1054/24 pithos		1054/12 jar		216/4 jar	1124/15 hole-mouth jar		
			1040/8 pithos					1124/33 jug					1124/8 jar				1054/6 vat	1124/22 jar		

			1128.76 SW					1128/65 jug							1054/62 jar	1128/1 jar			
FAB A	FAB B			FAB C		FAB D		FAB E	FAB F		FAB G		FAB H	FAB I	FAB L		FAB M		FAB N
			1124/24 jar														224/2 pithos	1128/52 hole- mouth jar	
																	1124/29 jar		
																	1128/50 pithos		
																	1128/51 pithos		
																	220/5 pithos		
EB IV																			
									82/4 jar		34/2 jar	62/1 jar		68/2 jar	6b/1 hole- mouth pot			84/3 jar	216/12 jar
								96/1 jar		18/5 jar	128/3 hole- mouth jar		248/2 jar	21/27 jar				210/2 jar	
								D.200/1 jar						8b/3b hole- mouth pot				210/4 jar	
														88/1 hole- mouth jar				383/7 jar	
														98/1 hole- mouth pot				256/1 jar	
														ø/18 jar					

4.3 Micro-Raman Spectroscopy analysis

Macroscopic samples and thin sections have been analyzed by mean of micro-Raman spectroscopy, a non-destructive technique, with the aim to investigate the mineralogical assemblage of Khirbet al-Batrawy pottery.

Recently, this methodology is becoming increasingly important in cultural heritage studies because the measurement can be performed without damage of the artifacts and gives exhaustive results compared with those obtained by other traditional destructive techniques.

The widespread use of micro-Raman spectroscopy is due to the possibility to identify minerals in a selected spot due to its excellent spatial resolution and, therefore providing information about the presence of different crystalline and amorphous phases, as well as distinguishing between polymorphs on the basis of their vibrational Raman spectra (Bartholomew, 2013).

Furthermore, micro-Raman spectroscopy results can help in the definition of manufacturing processes (i.e. temperature and firing atmosphere) as well as provide information on the provenance of the raw material.

Here are discussed the results of the application of Raman spectroscopy on the inclusions of the Jordan potteries as the matrix has not given information due to its high fluorescence.

4.3.1 EB II

Micro-Raman spectra indicate the diffuse presence of calcite [CaCO_3], quartz [SiO_2], hematite [$\alpha\text{-Fe}_2\text{O}_3$]. Less widespread, apatite [$\text{Ca}_5(\text{PO}_4)_3[\text{F}, \text{OH}, \text{Cl}]$], magnetite [$\alpha\text{-Fe}_3\text{O}_4$], gypsum [$\text{CaSO}_4 \cdot 2\text{H}_2\text{O}$], ilmenite [FeTiO_3], bassanite [$\text{CaSO}_4 \cdot 0.5\text{H}_2\text{O}$], barite [BaSO_4], feldspar [K-feldspar (KAlSi_3O_8)], and two different polymorphs of titanium dioxide (anatase and rutile [TiO_2]) have also been observed in the sherds (Fig. 10). The presence of carbon as tempering is diffuse in the analyzed samples (Table 8).

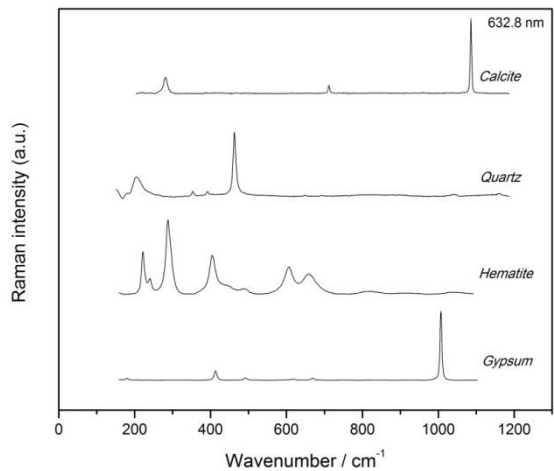


Figure 10: Raman spectra of the main mineralogical components found in the analyzed sherds (a.u. = arbitrary units); calcite (KB.06.B.392/8), quartz (KB.06.E.704/6), hematite (KB.06.E.706/1) and gypsum (KB.06.E.702/10).

CARBONATES

Calcite has been identified in all sample as the most abundant mineral phase. The Raman spectrum is characterized by a strong band at 1086 cm^{-1} connected to the symmetric stretching ν_1 of CO_3 group, by another band at 712 cm^{-1} due to the in-plane bending ν_4 of CO_3^{2-} ions and another weak peak at 281 cm^{-1} and at 155 cm^{-1} due to the lattice vibration modes.

OXIDES and HYDROXIDES

In all the sherds, hematite and magnetite have been identified.

The bands of hematite occurring at 225 cm^{-1} , 290 cm^{-1} , 410 cm^{-1} are due to the O-Fe-O bending vibrations, whereas the peak at 612 cm^{-1} is due to the stretching mode of Fe-O. Magnetite, characterized by a strong band at 660 cm^{-1} as reported in the literature (De Faria *et al.*, 1997), has also been found. This is the only band clearly associated to magnetite in a range between 661 to 671 cm^{-1} and the observed variation could be due to different local temperatures induced in different measurements. Hematite and magnetite are usually coupled in the Raman spectra and a rather strong band at 670 - 680 cm^{-1} has been frequently observed in the hematite spectrum as a result of a common natural phenomenon called martitization, i.e. the transformation of magnetite to hematite (Ramdohr, 1969; De Faria *et al.*, 1997; Baratto *et al.*, 1998; Bersani *et al.*, 1999; Lofrumento *et al.*, 2004).

The structure of magnetite is similar to the inverse spinel structure described by the formula $\text{Y}(\text{XY})\text{O}_4$ ($\text{Fe}^{3+}(\text{Fe}^{2+}\text{Fe}^{3+})\text{O}_4$). Eight Y cations ($\text{Y}=\text{Fe}^{3+}$) occupy eight octahedral sites and eight occupy tetrahedral sites, while X cations ($\text{X}=\text{Fe}^{2+}$) occupy eight octahedral sites.

Magnetite can also contain high percentage of Mg and Mn that replace Fe^{2+} and of Al, Cr, Mn^{3+} , Ti^{4+} that replace Fe^{3+} .

Ilmenite, belonging to the hematite group, is a mineral of Fe^{2+} and Ti^{4+} and in the Raman spectrum is easily differentiated from that of magnetite for a shift of main band at 680 - 690 cm^{-1} .

The two different polymorphs of titanium dioxide rutile and anatase have been easily differentiated on the basis of on their Raman spectra (Fig. 11). Indeed, the high-temperature polymorph, rutile, is characterized by two bands at about 477 and 610 cm^{-1} , whereas the low-temperature anatase form is characterized by a very strong band at

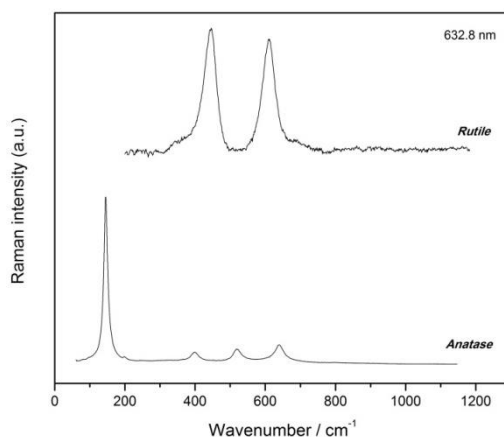


Figure 11: Representative Raman spectra of the polymorphs of titanium dioxide present in the sherds (a.u. = arbitrary units); rutile (KB.06.E.706/1) and anatase (KB.06.E.703/6).

144 cm^{-1} and three other medium intensity bands at 396, 515 and 639 cm^{-1} (Murad, 1997; Bersani *et al.*, 1998; Bersani *et al.*, 2000; Schroeder, 2003; Sendova *et al.*, 2005).

SULFATES

In addition to other minerals, the pottery samples from Khirbet al-Batrawy also contain gypsum, bassanite and barite.

Gypsum is characterized by a strong band at 1008 cm^{-1} due to the symmetric stretching mode of SO_4^{2-} and a medium band at 415 cm^{-1} related to sulfate vibrational mode ν_2 (Edwards *et al.*, 1999).

Bassanite is characterized by the main band shift at 1010-1012 cm^{-1} whereas barite has a spectrum characterized by the main peak at about 987 cm^{-1} .

PHOSPHATES

In some samples, apatite is also found with a band observed at about 961 cm^{-1} due to the phosphate symmetric vibration. The apatite-group includes fluoroapatite, hydroxyapatite and chlorapatite having as dominant ions F^- , OH^- and Cl^- respectively. The Raman spectra of different phosphates could be distinguished on the basis of the lower intensity vibration modes in the ranges 260-400 cm^{-1} and 3510-3650 cm^{-1} (Penel *et al.*, 1997; Wei *et al.*, 2003). However, in the case of pottery from Khirbet al-Batrawy only the peak at 961 cm^{-1} could be detected preventing the possibility to define the type of phosphates.

SILICATES

Quartz is the most diffuse silicate mineral in all samples from EB IIA phase. It can be easily identified by a strong band at 465 cm^{-1} due to the symmetric stretching vibration modes of SiO_4 tetrahedra, a medium band at 207 cm^{-1} due to lattice distortion, and a weak bands at 356 cm^{-1} due to asymmetric bending modes of Si tetrahedra (Sendova *et al.*, 2005).

Only one sample has revealed the presence of feldspar, with a typical two-peaked feature around 500 cm^{-1} . In particular, the spectrum shows the typical K-feldspar strong band at 513-514 cm^{-1} due to the A_g vibrational mode, but fluorescence does not permit to observe other additional peaks useful to identify the different kind of K-feldspar (Mernagh, 1991).

ORGANIC MATERIAL

Carbon occurs as inhomogeneous distributed phase on the surface of the Khirbet al-Batrawy pottery sherds and it has been found in two different forms: amorphous and graphite. The typical amorphous carbon spectrum is characterized by two broad bands at 1370 and 1590 cm^{-1} (Fig. 12), whereas the graphite spectrum presents sharp peaks at 1331 and 1581 cm^{-1} (Pimenta *et al.*, 2007).

The bands at 1370 cm^{-1} and 1590 cm^{-1} are called respectively “G band”, due to the stretching vibrations of the well-ordered polyaromatic rings in the planar graphite structure, and the “D band” due to the in-plane defects and the presence of heteroatoms. The intensity of G band is the only feature visible in well-crystalline mineral graphite and it is connected with the crystalline order of mineral. Instead, the D band grows as the particle size of the carbonaceous material decreases and as the degree of disordered increases (Smith, 2004). The spectra collected show the presence of amorphous carbon, only in rare case a little bit more ordered.

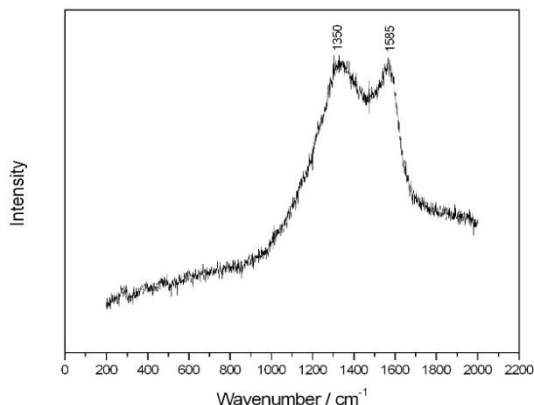


Figure 12: Representative Raman spectra of amorphous carbon detected in the KB.06.B.392/8 sample.

Table 8: Mineralogical phases detected by micro-Raman spectroscopy in macroscopic samples (c) and in thin section (s) of EB II samples.

EB II (3000-2700 B.C.)	Carbonates		Oxides and Hydroxides				Sulfates			Phosphates	Silicates		
	CALCITE	HEMATITE	MAGNETITE	ILMENITE	ANATASE	RUTILE	GYPSUM	BASSANITE	BARITE	APATITE	QUARTZ	K-FELDSPAR	CARBON
KB.06.B.392/8	c s	c s								c			c s
KB.06.E.703/6	s	s			c s		c		s		c		c s
KB.06.E.703/5	c s	s		c	s					c	c	c	c s
KB.06.E.702/10	c s	c s	s	c s	c s		c s			c	c s		c s
KB.06.E.704/1	c s	c s	c					s			c s		c s
KB.06.E.704/6	c s	c s	s							s	c		c
KB.06.E.706/2	c s	c					c	s			c s		c
KB.06.E.706/1	c s	s				c			c		c		c s

4.3.2 EB IIIA

Micro-Raman spectra show diffuse presence of calcite, quartz, hematite and magnetite. Less widespread goethite [FeO(OH)], ilmenite, anatase, rutile, corundum [Al₂O₃], gypsum, barite, apatite, K-feldspar, diopside [CaMgSi₂O₆]/hedenbergite (CaFeSi₂O₆),

forsterite $[\text{Mg}_2\text{SiO}_4]$, albite $[\text{NaAlSi}_3\text{O}_8]$, anorthite $[\text{CaAl}_2\text{Si}_2\text{O}_8]$, zircon and lazurite have also been observed in the sherds. The presence of carbon as tempering is diffuse in the analyzed samples (Table 9 and Table 10).

OXIDES and HYDROXIDES

Goethite has been found only in one sample (KB.09.B.820/12, Fig. 13), whereas the aluminum oxide corundum in other three samples (KB.05.B.146/8, KB.05.B.146/24, KB.06.E.703/3).

According to De Faria and Lopes (2007), goethite is identified by the strong Raman bands at 385 and 299 cm^{-1} and weak bands at 243, 479 and 550 cm^{-1} which may be related to the presence of OH groups in the crystal structure (Thierry *et al.*, 1988). Goethite, the most stable and common iron oxy-hydroxide, is formed in oxidizing conditions as a product of the alteration process of iron rich minerals.

The Raman spectrum of corundum has been discussed by Porto and Krishnan (1967) being characterized by seven Raman active phonon modes at frequencies 378, 416, 432, 451, 580 and 644 cm^{-1} .

SILICATES

Some samples have revealed the presence of plagioclases with the strong band between 500 and 510 cm^{-1} due to the characteristic A_g vibrational mode, and a second intense band in the range 478-488 cm^{-1} (Mernagh, 1991). In particular, albite has been detected by the occurrence of the strong main peak at about 507 cm^{-1} at low temperature and 510 cm^{-1} at high temperature. Anorthite has been also detected with the main peak at 504.9 cm^{-1} .

Pyroxenes have been identified by the peaks at 1008 e 662 cm^{-1} (Fig. 14). The latest peak has been assigned in different ways. According to Omori (1971), it represents the

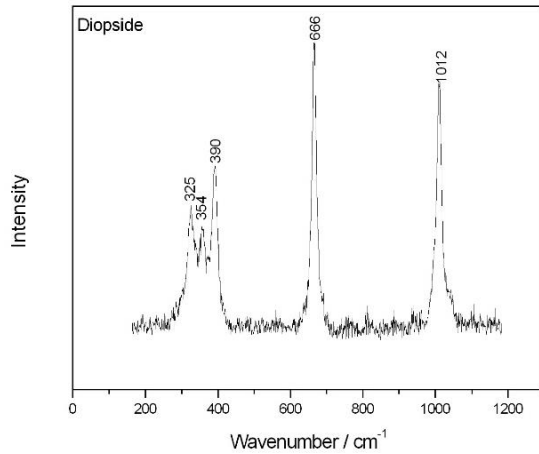


Figure 13: Representative Raman spectra of the iron oxy-hydroxide goethite present in the KB.09.B.820/12 sample.

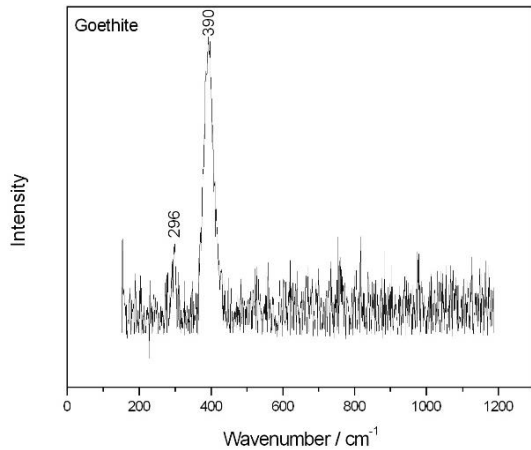


Figure 14: Representative Raman spectra of the diopside identified in the KB.05.A.64/1 sample.

Si-O-Si bending mode due to non-bridging oxygen, whereas according to Tomisaka and Iishi (1980) and Furukara *et al.* (1981) it would represent a mixed stretching bending mode of the Si-O-Si bridging bond. The triple peak at 321, 352 e 385 cm^{-1} which involves Ca-O or Mg-O stretching (Richet *et al.*, 1998) has been also detected.

Databases used recognized the spectrum as an intermediate augite term intermediate between diopside and hedenbergite. Indeed, it is difficult to discriminate augite and diopside as their frequencies are very close.

Minerals belonging to the group of olivine have been identified only in few samples. The lattice modes between 330 and 435 cm^{-1} in forsterite is assigned to SiO_4 rotations. The modes from 300 to 390 cm^{-1} that showed the greatest variation with composition or showed signs of two-mode behavior in the olivine are assigned as M2 translations. The SiO_4 internal stretching and bending modes were assigned to the highest frequencies; they vary little from forsterite to fayalite and appear to depend more on cation mass than volume. In particular, fayalite is characterized by peaks at 813 e 843 cm^{-1} , whereas forsterite shows peak at higher frequencies at 823 and 857 cm^{-1} (Chopelas, 1991).

The bands at 975 and 1008 cm^{-1} , due to Si-O stretching, those at 269 and 439 cm^{-1} due to Si-O bending and others modes at 393, 355, 225, 214 and 202 cm^{-1} identifies zircon (Zhang *et al.*, 2000).

Lazurite has also been identified, the spectrum is characterized by a strong peak at 548 cm^{-1} due to the stretching symmetric mode of the ion S_3^- (Catalano *et al.*, 2007).

Table 9: Mineralogical phases detected by micro-Raman spectroscopy in macroscopic samples (c) and in thin section (s) of EB IIIA samples.

EB IIIA (2700-2500 B.C.)	Carbonates		Oxides and Hydroxides					Sulfates		Phosphates	Silicates								
	CALCITE	HEMATITE	MAGNETITE	ILMENITE	ANATASE	RUTILE	CORUNDUM	GYPSUM	BARITE	APATITE	QUARTZ	DIOPSIDE	FORSTERITE	ALBITE	ANORTHITE	K FELDSPAR	ZIRCON	LAZURITE	CARBON
KB.05.A.52/8	c s	c s	c s	s				c		c	c	c s	c	c s	c	c			
KB.05.A.58/1	s	c s	c		c s						c								
KB.05.A.64/13	c	c	c		c			c		c	c			c					c
KB.05.A.64/1	c s	c s		s		c				c	c	c s	c			c			
KB.05.B.110/15	c s	c s	s	c							c s	c		c		c			
KB.05.B.126/1	c s	s	s								c								c
KB.05.B.126/3	c	c								c	c								c
KB.05.B.126/4	s	s	c s							s	c	c s		s	s				c

	CALCITE	HEMATITE	MAGNETITE	ILMENITE	ANATASE	RUTILE	CORUNDUM	GYPSUM	BARITE	APATITE	QUARTZ	DIOPSIDE	FORSTERITE	ALBITE	ANORTHITE	K FELDSPAR	ZIRCON	LAZURITE	CARBON
KB.05.B.136/1	c	c									c								
KB.05.B.136/3	c s	c s	s	c								c		c		c			c
KB.05.B.136/5	c s	c s						c	c		c					c			c
KB.05.B.146/1	c s	s									c								c s
KB.05.B.146/3	c	c s	c s								c								
KB.05.B.146/4	c s	s																	
KB.05.B.146/5	s	c s	c	s		c		c	c		c	c		c				c	c
KB.05.B.146/6		c s			c						c s							c	
KB.05.B.146/7	s	c s	s																c
KB.05.B.146/8	c	c			c		c				c								c
KB.05.B.146/15	c	c	c					c		c						c			
KB.05.B.146/20	c s	c s																	c
KB.05.B.146/24	c	c						c	c		c					c	c		
KB.05.B.146/30	c s	c s	c s	c							c								s
KB.06.B.167/4		c	c									c		c		c			
KB.06.B.376/4		c s	s					c		s	s								
KB.06.B.413/2	c	c						c											c
KB.06.E.701/2	c s	c s									c								
KB.06.E.703/3		s	c				c				c								

Table 10: Mineralogical phases detected by micro-Raman spectroscopy in macroscopic samples (c) and in thin section (s) of KKW samples.

EB IIIA WAVE	Carbonates	Oxides and Hydroxides					Sulfates		Silicates						
	CALCITE	GOETHITE	HEMATITE	MAGNETITE	ILMENITE	GYPSUM	BARITE	QUARTZ	DIOPSIDE	ALBITE	K FELDSPAR	CARBON			
KB.06.B.427/1	c							c		c				c	
KB.08.B.805/6	c		c							c					c
KB.09.B.820/10	c		c s								c				c s
KB.09.B.820/12	c	c									c				c
KB.09.B.820/13	c s		s	s	s		c				s	s	s		c s
KB.08.B.805/32	c														c
KB.08.B.805/34	c														c

4.3.3 EB IIIB

The occurrence of calcite, quartz, hematite, magnetite and ilmenite has been shown by micro-Raman spectra. Less frequently, anatase, rutile, corundum, gypsum, apatite, K-feldspar, diopside/augite, fayalite/forsterite and zircon have also been detected in the sherds. Also carbon as tempering is frequently found in the analyzed samples (Table 11).

Table 11: Mineralogical phases detected by micro-Raman spectroscopy in macroscopic samples (c) and in thin section (s) of EB IIIB samples.

EBIIIB	Carbonates	Oxides and Hydroxides						Sulfates		Phosphates	Silicates					
	CALCITE	HEMATITE	MAGNETITE	ILMENITE	ANATASE	RUTILE	CORUNDUM	GYPSUM	BARITE	APATITE	QUARTZ	AUGITE DIOPSIDE	FORSTERITE OLIVINA	K-FELDSPAR	ZIRCON	CARBON
KB.05.A.46/2	c	c	c									c				c
KB.05.A.46/8	c	c	c							c	c					c
KB.05.A.204/2	c s		s								c s					c s
KB.05.A.204/3	c					c						c				c
KB.05.A.216/4	c	c						c	c		c					c
KB.05.A.220/5	c	c														c
KB.05.A.224/2	c	c														c
KB.06.A.120/6	c s	c s									s					s
KB.05.B.111/3	s	c s	s	S			c s									c
KB.10.B.1040/8	c	c	c								c				c	c
KB.11.B.1054/2	c	c	c					c	c			c				c
KB.10.B.1054/6	c	c	c								c					c
KB.11.B.1054/12	c	c	c					c	c		c					c
KB.11.B.1054/13	c	c									c		c			c
KB.10.B.1054/21	c s	c s	c		c						c			c		c s
KB.10.B.1054/22	c	c	c													c
KB.10.B.1054/24	c s	c s	s	S							c					s
KB.10.B.1054/62	c s	c s	s					c			c					
KB.11.B.1124/1	c	c	c				c				c	c				c
KB.11.B.1124/3	c s	s	s	S	c s						c s					s
KB.11.B.1124/10	c	c	c			c		c				c		c		c
KB.11.B.1124/15	c s	s				c					c	s				c s
KB.11.B.1124/19	c	c														c

EBIII B	Carbonates		Oxides and Hydroxides					Sulfates		Phosphates	Silicates					
	CALCITE	HEMATITE	MAGNETITE	ILMENITE	ANATASE	RUTILE	CORUNDUM	GYPHUM	BARITE	APATITE	QUARTZ	AUGITE DIOPSIDE	FORSTERITE OLIVINA	K-FELDSPAR	ZIRCON	CARBON
KB.11.B.1124/22	c															c
KB.11.B.1124/24	c	c									c					c
KB.11.B.1124/28	c	c	c		c			c	c		c					c
KB.11.B.1124/29	c s	c														c s
KB.11.B.1124/33	c s															c s
KB.11.B.1124/8	c s	c s	s	S	c											s
KB.11.B.1128/76	c	c									c					c
KB.11.B.1128/1	c	c	c			c		c	c		c					c
KB.11.B.1128/50	c s	s		S	s			c	c		c s					c s
KB.11.B.1128/51	c s	c						c s	c		s					c s
KB.11.B.1128/52	c	c	c					c	c	c	c					c
KB.11.B.1128/65	c s	c s			c	s		c			c s					

4.3.4 EB IV

Micro-Raman spectra indicate diffuse presence of calcite, quartz, hematite, magnetite and ilmenite. Less frequently, anatase, rutile, corundum, lepidocrocite [γ -FeO(OH)], gypsum, apatite, K-feldspar, diopside/augite, fayalite/fosterite, aegirine [$\text{NaFe}^{3+}\text{Si}_2\text{O}_6$], zircon have been also observed in the sherds. The presence of carbon as tempering is diffuse in the majority of the analyzed samples (Table 12).

OXIDES and HYDROXIDES

Sample KB.05.A.62/2 is characterized by the occurrence of lepidocrocite, a polymorph of goethite, with the Raman peaks at 252, 379 and 530 cm^{-1} according to Bouchard and Smith (2003). The Raman bands of lepidocrocite are well established in literature, even if some differences have been observed. For example: 1303, 650, 522, 493, 373, 245 cm^{-1} (De Faria *et al.* 1997); 393, 257 cm^{-1} (Johnston, 1990); 380, 252 cm^{-1} (Thibeau *et al.*, 1978); 376, 250 cm^{-1} (Williams *et al.*, 1996).

SILICATES

Five samples show the occurrence of aegirine, a pyroxene characterized by the main peaks at 216, 348, 386, 546, 973 and 1043 cm^{-1} . The bands are classified into four regions: the bands between 800-1200 cm^{-1} are assigned to Si-O stretching vibrations re-

lated to the non-bridged Si–O bonds in the SiO₄ tetrahedra; the bands in the range 650–800 cm⁻¹ are mainly attributed to the vibrations related to the bridged Si–O–Si vibrations within the Si₂O₆ chains (McMillan, 1984; Mysen, 1990); the Si–O bending bands of SiO₄ tetrahedra are mainly located between 425–650 cm⁻¹ (Redhammer and Roth, 2002); the bands in the range 50–425 cm⁻¹ are mainly due to lattice vibration bands (Zhang et al., 2002).

Table 12: Mineralogical phases detected by micro-Raman spectroscopy in macroscopic samples (c) and in thin section (s) of EB IV samples.

EB IV	Carbonates		Oxides and Hydroxides							Phosphates		Silicates					
	CALCITE	HEMATITE	MAGNETITE	ILMENITE	ANATASE	RUTILE	CORUNDUM	LEPIDOCROCITE	GYPSUM	APATITE	QUARTZ	AUGITE DIOPSIDE	AEGIRINE	FOSTERITELIVINA	K-FELDSPAR	ZIRCON	CARBON
KB.05.A/D200	s c	s c	s c	s					c		s c						s c
KB.05.A.18/5	s c	c	c	c	s						s c		c			c	s c
KB.05.A.6b/1	s c	s c	s	c							s c				s		s c
KB.05.A.21/27	s c	s c								s c	s c	s c	c		c		s c
KB.05.A.34/2	s c	s c	s	c					c	s c	s c	s c		c			c
KB.05.A.62/1	s c	s c	s c	c					s c			s c					c
KB.05.A.62/2	c		c					c			c						
KB.05.A.68/2	s c	c	c								c						s c
KB.05.A.82/4	s c	s	s c	c			S		c	c			c				c
KB.05.A.84/3	s c	s c	s c	s c					c	s	c						s c
KB.05.A.8b/3b	s c	s									s						
KB.05.A.88/1a	s c	s c	s	C	c				c		c	c	c	s c			c
KB.05.A.88/1b	s c	s c	s	s c	c				c		c		c		c		s c
KB.05.A.96/1	s c	c				s	c				s c				c		s c
KB.05.A.98/1	s c	c	c	S							c						s c
KB.05.A.210/2	s	s c									c						s
KB.05.A.210/4	c	s c	c	S			s c										
KB.05.A.212/6	s c	s c					s c										s
KB.05.A.216/12	s c	s c	c														s c
KB.05.B.128/3	s c	s c										c					c
KB.06.A.248/2	c	c					c				c						c
KB.06.A.256/1	c	c									c						c
KB.06.A.ø18	s c	s c	c	S							c						c
KB.06.B.383/7	c	s c	s	C			s c		c		s c	s c		c			c

The results of this section are reported in the article:

Medeghini L., Mignardi S., De Vito C., Bersani D., Lottici P.P., Turetta M., Costantini J., Bacchini E., Sala M., Nigro L. (2013): The key role of micro-Raman spectroscopy in the study of ancient pottery: the case of pre-classical Jordanian ceramics from the archaeological site of Khirbet al-Batrawy. *European Journal of Mineralogy*, 25, 881-893.

4.4 FTIR analysis

FTIR analysis has been carried out to characterize the mineralogical composition of both the inclusions and the components of the matrix of the pottery.

The main advantages of FTIR absorbance measurements is the high sensibility that permits the detection of many components, also when they are present in low amounts in the ceramic sample. However, the bulk matrix strongly contributes to the absorbance spectral profile making it difficult to identify pigments (Barilaro *et al.*, 2005).

FTIR spectra show the bands usually attributed to minerals, and for their identifications the range $<2000\text{ cm}^{-1}$ is usually considered, whereas the presence or absence of organic components is investigated by the study of the range $>2000\text{ cm}^{-1}$. The assignment of the bands has been made on the basis of the characteristic IR wavenumbers of the minerals (Gadsen, 1975; De Benedetto *et al.*, 2002; Barilaro *et al.*, 2005; De Benedetto *et al.*, 2005), following in particular the work of De Benedetto *et al.* (2002) who reported the results of IR spectroscopic analysis of ancient potteries.

4.4.1 EB II

FTIR spectra show diffuse occurrence of carbonates and silicates in all the analyzed sherds. The relative amounts are extremely variable in the different samples as shown by the intensity of the peak due to Si-O stretching at about 1060 cm^{-1} and the band at about 1430 cm^{-1} due to CO_3^{2-} vibration frequencies.

Figure 15 shows the difference in silicates and carbonates amount observed, for example, in the FT-IR spectra of the archaeological samples KB.06.E.704/1 and KB.06.E.706/1.

The mineralogical phases of the ceramic body are mainly represented by quartz, calcite and minor amounts of illite. K-feldspar, hematite, magnetite gypsum and albite have also been identified only in some samples. Table 13 lists the mineralogical phases identified in the samples and their abundances estimated on the basis of the peaks intensity.

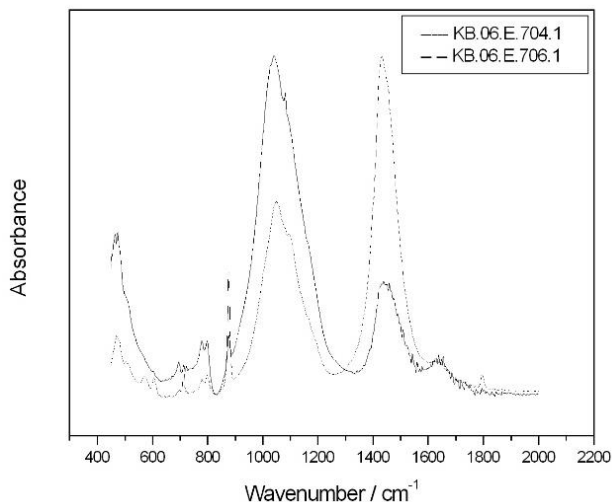


Figure 15: FTIR spectra of the samples KB.06.E.704/1 and KB.06.E.706/1 showing the difference in silicates and carbonates content.

The absorption peaks at 1425, 877 and 714 cm^{-1} are attributed to calcite. The presence of quartz in all investigated samples is marked by the main Si-O stretching band at 1080 cm^{-1} , the peaks at 695 and 512 cm^{-1} and the distinctive doublet at 797 cm^{-1} due to Si-O bending and at 778 cm^{-1} due to Si-O-Si stretching (Farmer, 1974; Legodi and de Waal, 2007). Illite was identified by peaks at 1032 and 989 cm^{-1} and by the characteristic main modes at 460 and 430 cm^{-1} that discriminate it from muscovite (Fig. 16).

The absorption bands in the region 1100-900 cm^{-1} are due mostly to bond stretching vibrations of the SiO_2 belonging to K-feldspar (absorption peaks at about 1120, 1000, 580, 530 and 460 cm^{-1}). Hematite is identified by the absorption band at 540 cm^{-1} due to one of the two E_u modes that involves the oxygen atoms whose displacement is axial with respect to a tetrahedron of Fe ions. A second peak at 470 cm^{-1} is present and can be ascribed mainly to an E_u mode displacement (Sabbatini *et al.*, 2000). Gypsum (1147, 1005 and 607 cm^{-1}), magnetite (578 cm^{-1}) and albite (1096, 723 cm^{-1}) have also been identified in the studied pottery.

The bands located over 2000 cm^{-1} are due to the organic components in the archaeological samples. The two peaks at 2852 and 2922 cm^{-1} belong to the C-H stretching vibrations, indicating the presence of organic material.

A broad band at 3440 cm^{-1} due to O-H stretching (Legodi and de Waal, 2007) and bands at about 1630 cm^{-1} due to H-O-H bending are assigned to water, most probably originating from hydration of oxides in the ceramic body during the burial period. The presence of clay minerals contributes to the intensity of the hydroxyl stretching band at 3440 cm^{-1} , but it is difficult to distinguish the contribution of water and of clay minerals.

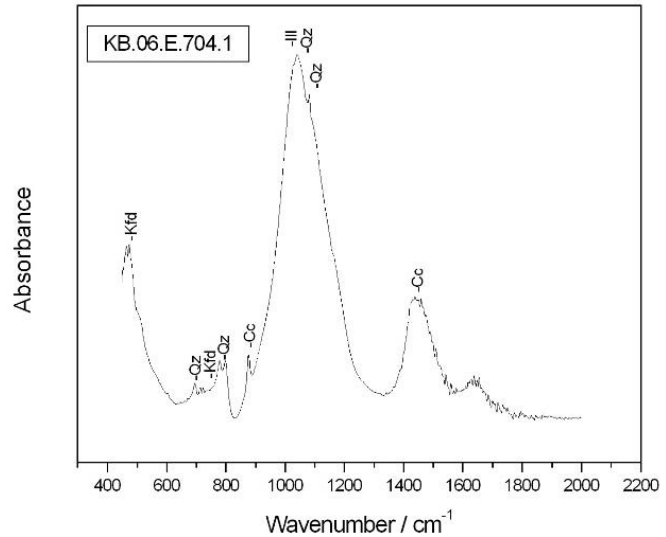


Figure 16: FTIR spectra of the sample KB.06.E.704/1 containing Ill (illite), Qz (quartz), Cc (calcite) and Kfd (K-feldspar).

Table 13: Mineralogical phases detected by FTIR spectroscopy of EB II samples.

	Calcite	Quartz	K-Feldspar	Albite	Gypsum	Hematite	Magnetite	Illite	Anorthite	Diopside
KB.06.B.392 /8	+++	++	tr	-	-	tr	tr	tr	-	-
KB.06.E.702/10	+	+++	tr	-	-	-	tr	tr	-	-
KB.06.E.703/5	++	+++	-	tr	-	-	tr	tr	-	-
KB.06.E.703/6	+++	++	tr	tr	++	-	tr	tr	-	-
KB.06.E.704/1	+	+++	tr	-	-	-	-	tr	-	-
KB.06.E.704/6	++	+++	tr	-	-	-	tr	tr	-	-
KB.06.E.706/2	+++	++	+	-	+	tr	tr	tr	-	-
KB.06.E.706/1	+++	++	tr	-	tr	-	tr	tr	-	-

4.4.2 EB IIIA

FTIR spectra collected from the analyzed sherds belonging to EB IIIA show similar feature (except for the sample KB.05.B.146/5) with a greater amount of silicates than carbonates (Fig. 17). On the contrary, the subgroup KKW presents fragments showing spectra with a greater amounts of carbonates than silicates.

FTIR spectra show mainly the presence of quartz and traces of illite. Only in a few samples gypsum, magnetite, K-feldspar, hematite, magnetite, anorthite (1095, 948, 760, 733, 669, 571, 482 cm^{-1}), albite and pyroxene diopside (1074, 962, 920, 870, 669, 630, 508, 471 cm^{-1}), have also been identified. Table 14 reports the mineralogical composition of the analyzed samples with the relative abundances of the mineral phases estimated on the basis of the position and intensity of the peaks.

Sample KB.05.B.146/5 shows a different mineralogical composition compared to the other pottery fragments. Indeed, it is characterized by a very high content of gypsum.

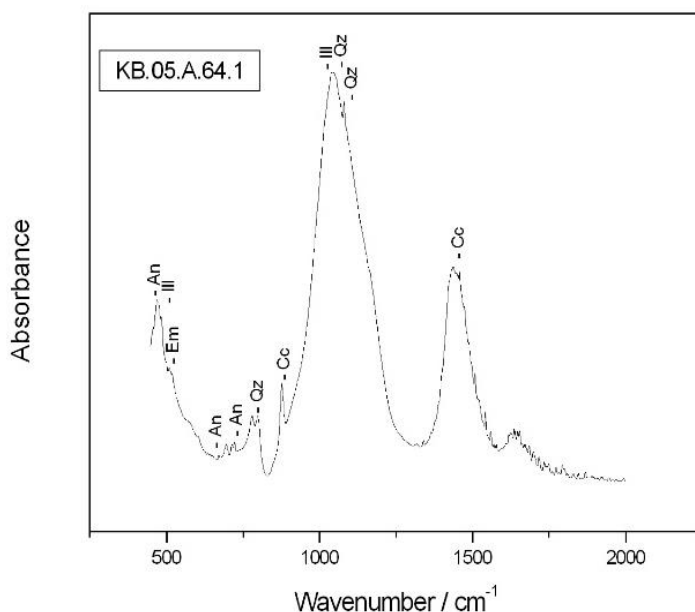
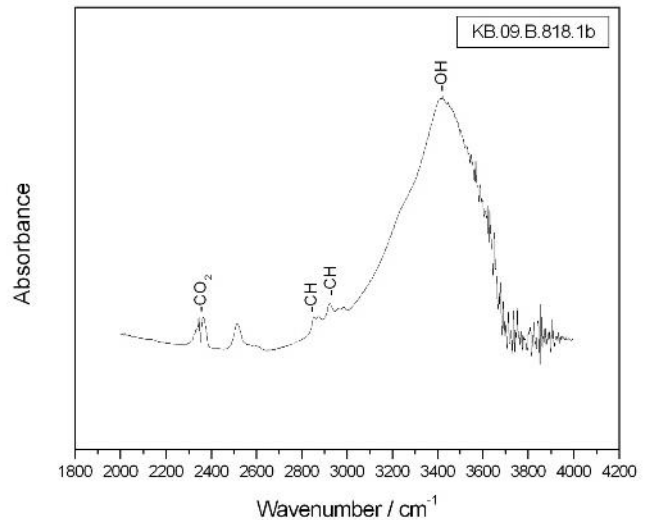


Figure 17: FTIR spectra of the sample KB.05.A.64/1 containing Ill (illite), Qz (quartz), Cc (calcite), An (Anorthite) and Em (Hematite).

Table 14: Mineralogical phases detected by FTIR spectroscopy of EB IIIA samples.

	Calcite	Quartz	K-Feldspar	Albite	Gypsum	Hematite	Illite	Anorthite	Diopside
KB.05.A.58/1	+	+++	-	-	-	-	-	+	+
KB.05.A.64/1	++	+++	-	-	-	tr	+	tr	-
KB.05.B.126/1	+++	++	tr	-	Tr	-	tr	-	-
KB.05.B.126/3	+++	++	tr	-	Tr	-	tr	-	-
KB.05.B.136/3	++	+++	tr	-	-	-	tr	tr	tr
KB.05.B.146/1	+++	++	tr	-	Tr	-	tr	-	-
KB.05.B.146/5	+	+	-	+	+++	-	-	-	+
KB.05.B.146/7	+++	++	-	+	-	-	-	+	+
KB.05.B.146/15	++	++	+	+++	-	-	tr	+++	++
KB.05.B.146/24	+++	+	-	tr	-	-	-	+	+
KB.06.B.167/4	+	+++	-	+	-	-	tr	tr	+
KB.06.B.413/2	+++	++	-	-	tr	-	tr	-	-
KB.06.E.701/2	+	+++	-	tr	-	-	tr	tr	tr
KB.06.E.703/3	+	+++	tr	-	tr	-	tr	-	-
KB.08.B.805/6	+++	++	-	-	tr	tr	-	-	-
KB.09.B.820/10	+++	++	tr	-	-	-	tr	-	tr
KB.09.B.820/12	+++	++	tr	tr	-	-	tr	-	-
KB.09.B.820/13	+++	++	tr	-	-	-	tr	-	-
KB.08.B.805/34	+++	++	-	-	-	-	tr	-	-

This result can be probably due to the sampling that had mainly collected the superficial area of the ceramic fragment. The black superficial layer in the samples belonging to KKW has also been investigated by FTIR analysis. The results obtained for sample KB.09.B.820/10 have been here reported as an example (Fig. 18). The region between 4000 to 2500 cm^{-1} is the range of X-H stretching where is evident the band at about 3400

**Figure 18:** FTIR spectra of the sample KB.09.B.820/10 showing C-H stretching vibrations, CO₂ and -OH bands.

cm^{-1} due to hydroxyl group connected to the presence of water. The bands at about 2920 cm^{-1} and 2850 cm^{-1} are related to C-H stretching vibrations indicating the presence of organic components (methylene group). Other weak peaks at about 2987 cm^{-1} and 2877 cm^{-1} have also been attributed to C-H stretching (methyl group). However, the weak intensity of the peaks prevents some identification of this kind of organic material. Finally, in the range $2500\text{-}2000 \text{ cm}^{-1}$ is well evident the doublet of CO_2 .

4.4.3 EB IIIB

The absorption bands of quartz and calcite have been recognized in all the samples of EB IIIB phase. Numerous FTIR spectra show the presence of illite in traces by the characteristic main modes at 460 and 430 cm^{-1} that discriminate it from muscovite. In addition, minor amounts of hematite, magnetite, plagioclase, K-feldspar and diopside have been identified.

A summary of the mineralogical phases, identified by FTIR analysis is reported in Table 15. The relative abundances of each phases, estimated on the basis of the intensity of peaks in the FT-IR patterns, are also given.

Table 15: Mineralogical phases detected by FTIR spectroscopy of EB IIIB samples.

	Calcite	Quartz	K-Feldspar	Albite	Hematite	Illite	Anorthite	Diopside
KB.05.A.204/2	+++	+++	-	-	-	-	++	-
KB.05.A.204/3	+++	+++	-	++	+	-	++	tr
KB.06.A.120.6	++	+++	+	+	+	+	+	-
KB.05.B.111/3	+++	+++	-	++	+	+	++	-
KB.11.B.1054/21	+++	++	+	+	+	+	+	tr
KB.11.B.1054/24	++	+++	+	+	+	+	+	-
KB.11.B.1054/62	++	+++	+	+	++	+	+	-
KB.11.B.1124/3	+++	++	+	+	+	+	++	-
KB.11.B.1124/8	+++	+++	+	+	+	+	+	-
KB.11.B.1124/15	+++	+++	+	+	+	+	+	tr
KB.11.B.1124/29	++	+++	+	++	+	+	+	-
KB.11.B.1124/33	++	+++	+	+	+	+	+	-
KB.11.B.1128/50	++	+++	+	+	+	+	+	-
KB.11.B.1128/51	++	+++	+	+	+	+	++	-
KB.11.B.1128/65	+++	+++	+	+	+	+	+	-

4.4.4 EB IV

Comparing the frequencies identified in FTIR spectra of Khirbet al-Batrawy samples with those available in the literature, the different types of inclusions were identified

(Table 16). Quartz and calcite are the main mineralogical phase identified in the samples of this period. Diffuse is the presence of feldspar, K-feldspar or plagioclases and illite, hematite and diopside have also been detected.

Table 16: Mineralogical phases detected by FTIR spectroscopy of EB IV samples.

	Calcite	Quartz	K-Feldspar	Albite	Hematite	Illite	Anorthite	Diopside
KB.05.A/D200	++	+++	-	++	+	+	++	-
KB.05.A.18/5	++	+++	++	-	+	-	-	+
KB.05.A.6b/1	+++	+++	-	++	-	+	-	-
KB.05.A.21/27	+++	++	-	++	-	-	++	tr
KB.05.A.34/2	+++	++	-	++	+	+	++	-
KB.05.A.62/1	+++	+++	-	++	+	+	++	+
KB.05.A.62/2	+++	+++	++	++	-	-	++	+
KB.05.A.68/2	+++	+++	-	++	-	+	-	++
KB.05.A.82/4	+++	+++	-	++	-	+	++	+
KB.05.A.84/3	+++	+++	-	++	-	-	++	+
KB.05.A.8b/3b	+++	+++	++	-	-	-	-	-
KB.05.A.88/1	+++	+++	-	-	-	-	-	tr
KB.05.A.96/1	+++	+++	-	++	-	+	++	-
KB.05.A.98/1	++	+++	-	++	-	+	++	-
KB.05.A.210/2	+++	+++	-	++	-	+	++	tr
KB.05.A.210/4	+++	+++	++	++	-	+	++	-
KB.05.A.212/6	++	+++	-	++	-	-	++	-
KB.05.A.216/12	+++	+++	-	++	-	-	++	-
KB.05.B.128/3	+++	+++	++	++	-	-	-	-
KB.06.A.248/2	+++	+++	++	++	+	+	-	-
KB.06.A.256/1	+++	+++	++	-	-	+	-	-
KB.06.A.C/18	+++	++	-	++	-	+	-	-
KB.06.B.383/7	+++	+++	-	-	+	+	++	-

4.4.5 Statistical Analysis

After the identification of the different mineral phases, the FTIR “reduced” spectra of all the sample listed in Tables 13 - 16, after the pre-treatment as described in chapter 3, were investigated using PCA.

The loading plot provides information about the bands that mainly contribute in the differentiation among the spectra. The first 10 PCs together explain 68,55 % of the total spatial variance (Table 17), where PC1 and PC2 represent 21.79 % and 9.7 % of the total variance, respectively.

Table 18: Results of PCA performed on dataset.

	PC1	PC2	PC3	PC4	PC5	PC6	PC7	PC8	PC9	PC10
Value	237,65	100,95	84,96	69,81	66,97	58,10	54,73	45,25	41,82	37,81
Variability %	19,89	8,45	7,11	5,84	5,60	4,86	4,58	3,79	3,50	3,16
Cumulative variance %	19,89	28,34	35,45	41,29	46,89	51,75	56,33	60,12	63,62	66,78

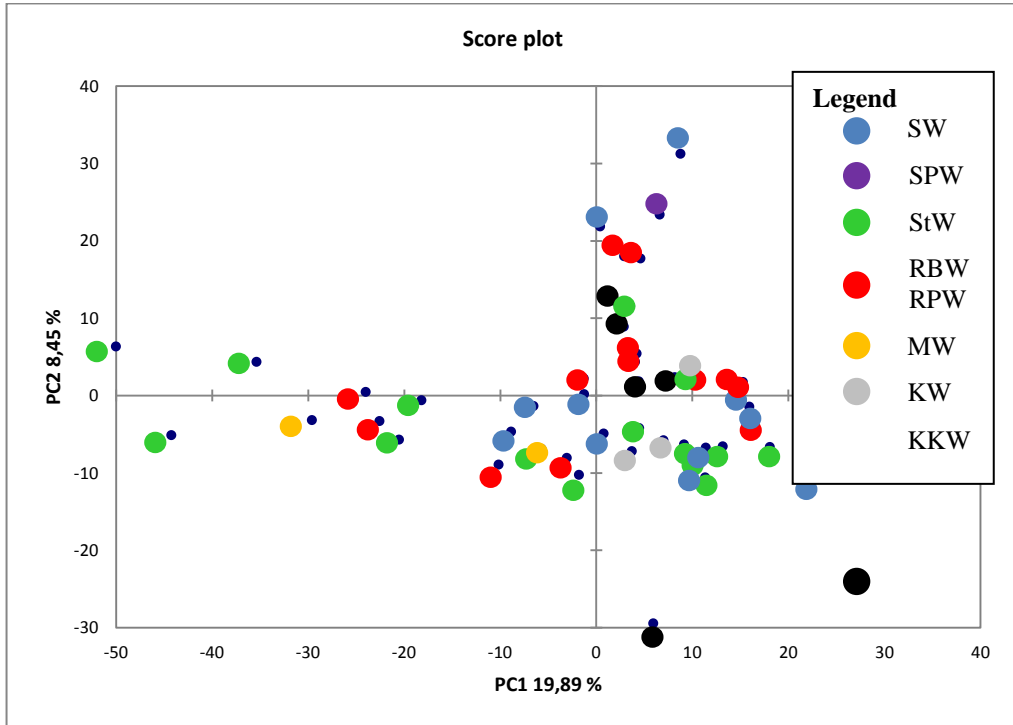


Figure 20: Score plot of PCA model obtained using the FTIR results on pottery sherds divided following their pottery types, excluding the two outlier samples KB.05.B.146/15 and KB.11.B.1128/65. (SW: Simple Ware; SPW: Simple Painted Ware; StW: Storage Ware; RBW: Red Burnished Ware; RPW: Red Polished Ware; MW: Metallic Ware; KW: Kitchen Ware; KKW: Khirbet Kerak Ware).

The score plot of PC1 vs PC2 is presented here in two different form to allow the speculation about relationship among samples belonging to the different phases of Khirbet al-Batrawy urbanization (Fig. 21) and to the different pottery type (Fig. 20). All the samples are very close together and can be grouped into an unique cluster. The first diagram prevent the possibility to identify groups between the different pottery types. The samples are distributed in an homogeneous way, without any preference. The only information we can obtain from this diagram is related to the KKW samples. Indeed, KKW fragments are located in the area occupied by the samples of other pot-

tery type and different historical period. This finding further support the attribution of KKW samples to the local pottery production.

Despite the low variability among the samples, the diagram of Figure 21 clearly shows the samples belonging to different historical periods fall in distinctive area. However, the numerous variables considered (1195) in the statistical analysis prevent the possibility to identify the contributions of each variables into the two PCs.

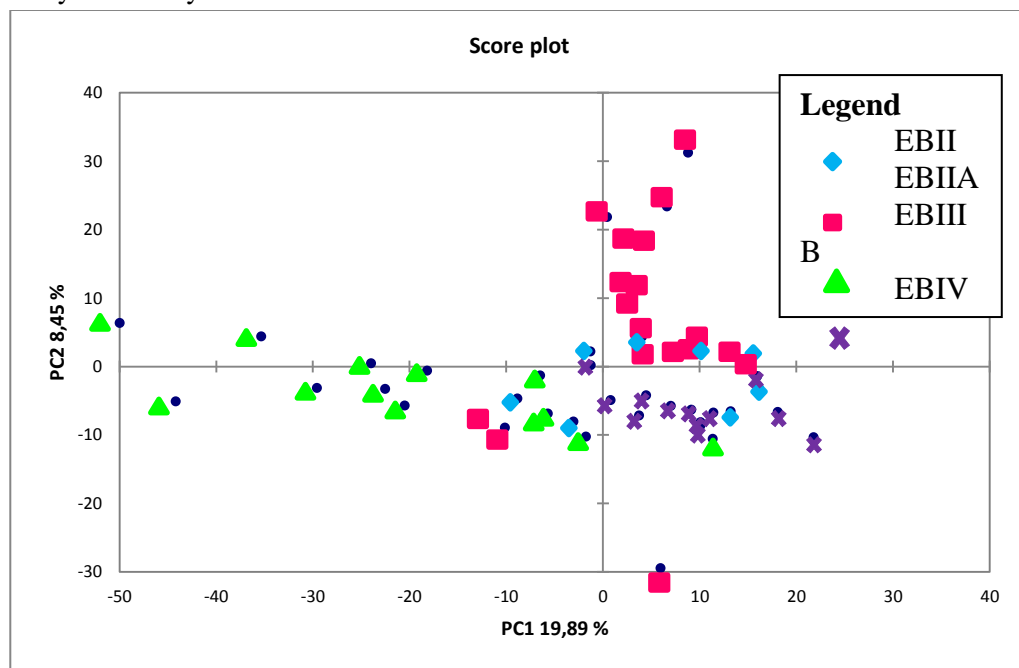


Figure 21: Score plot of PCA model obtained using the FTIR results on pottery sherds divided into the four periods of Batrawy urbanization, excluding the two outlier samples KB.05.B.146/15 and KB.11.B.1128/65.

For this reason, the PCA was performed again considering only the variables that mainly discriminate among samples. Therefore, a series of elaborations with PCA were performed step by step in order to reduce the number of variables:

- 1) For the first elaboration, the variables with a values of variables-PCs correlation in the range $<-0,7$ and $>0,7$ for the PC1 and the range $<-0,6$ and $>0,6$ for the PC2 were considered. Thus, a new plot (Fig. 22) was performed considering 268 variables.

As showed in Figure 22, the separation between samples persists, but the high number of variables creates difficulties in the evaluation of the contribution of each variables to this separation.

- 2) The PCA was performed again on a set of variables with a values of the variables-PCs correlation $<-0,8$ and $>0,8$ for PC1 and $<-0,7$ and $>0,7$ for PC2.

Also in this case, the separation persists, but the number of variables remains too much higher (207) to identify their single contribution.

- 3) Finally, the values of the variables-PCs correlation $<-0,9$ and $>0,9$ for PC1 and $<-0,8$ and $>0,8$ for the PC2 were considered and a new set of 160 variables was used for the PCA.

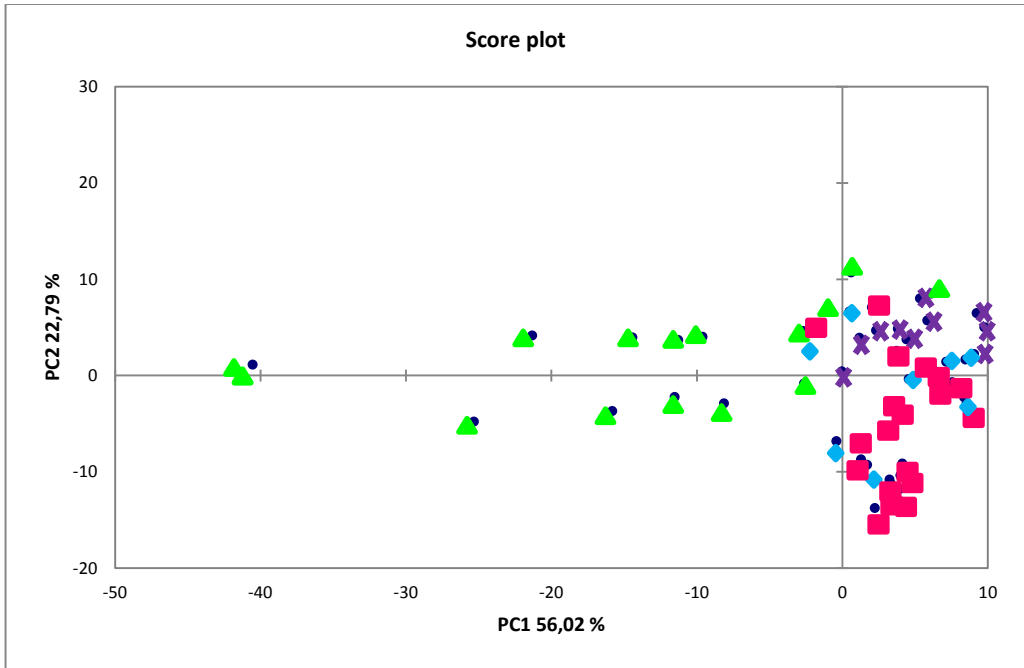


Figure 22: Score plot of PCA model obtained using the FTIR results on pottery sherds, divided into the four periods of Batrawy urbanization, considering only the 268 variables that mainly contribute to the separation of the sherds.

The new plot (Fig. 23) obtained maintains the separation of samples and the lower number of variables allows the analysis of this differentiation.

Considering that the PC1 is mainly affected by the contributions of the wavelengths around $1500-1600\text{ cm}^{-1}$ and the major contribution in the PC2 is due to wavelengths between 700 and 900 cm^{-1} , we can distinguish the spectra on the basis of this information. The major variability observed among the samples is due to PC1 that is influenced by vibrational bands not due to mineralogical compounds, whereas the variability along PC2, referring to minerals bands, is limited. In particular, EB II samples plotting around the centre of the diagram show that the two different PCs do not play a predominant role. EB IIIA are mainly located in the space with positive values of PC1 and PC2, showing a small variability along the two different PCs. EB IIIB samples show a great variability along negative values of PC1 highlighting that data are mainly

affected probably by the signal of organic compounds. Finally, EBIV samples plot in the area with positive values of PC1 and negative of PC2 and show major variability along PC1.

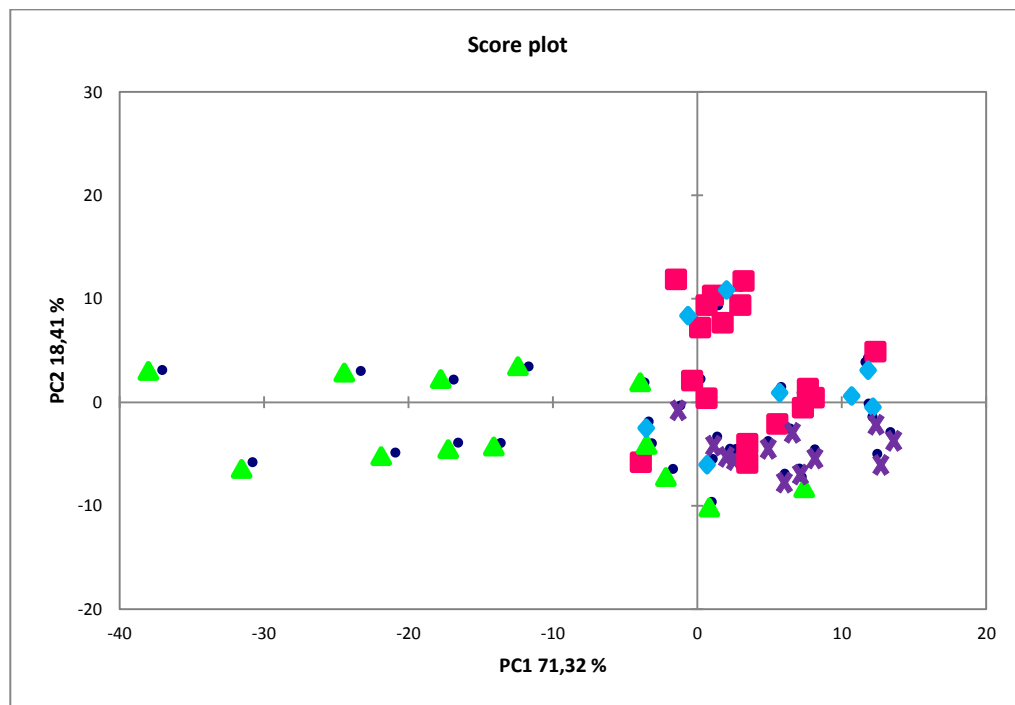


Figure 23: Score plot of PCA model obtained using the FTIR results on pottery sherds, divided into the four periods of Batrawy urbanization, considering only the 160 variables that mainly contribute to the separation of the sherds.

In this particular case, the successive elaborations of data with the aim to decrease the number of variables do not identify the contribution of vibrational bands connected to the occurrence of particular minerals, so preventing the possibility to explain the separation among samples on the basis of their mineralogical composition. However, the model here proposed to process statistical data in presence of high number of variables shows its validity. Indeed, the variability and separations are due to vibrational bands that are not assigned to mineralogical components confirming that the mineralogical composition of the samples do not change during the history of Batrawy.

4.5 Scanning Electron Microscopy coupled with Energy Dispersive Spectroscopy (SEM-EDS)

Scanning electron microscopy (SEM) imaging, using secondary and backscattered electrons, and EDS chemical microanalysis was carried out on polished specimens with the aim to acquire data useful in defining the groundmass microstructure, the characterization of the inclusions and the degree of vitrification of the matrix.

Results are here discussed divided into the four periods of Khirbet al-Batrawy urbanization.

4.5.1 EB II

4.5.1.1 Minerals

According to BSE images and EDS data, the crystalline inclusions are mainly represented by coarse-sized grains of calcium carbonates, quartz, feldspars, Fe, Mn, Ti, Fe-Ti oxides, whereas less widespread are apatite, zircon, barite and fossils (Table 19).

The oxides of metallic elements have been easily identified because they appear with contrasting colors in BSE images. Iron oxides have been identified by the presence of Fe and O; however, as the Fe peaks do not differentiate Fe(II) from Fe(III) this analytical methodology cannot distinguish hematite from magnetite.

Iron-titanium oxides, probably ilmenite, have been identified by the peaks of Ti, Fe and O. In the EDS spectra the peak of Mg is also present as this element is usually present in the ilmenite structure, although in scarce amounts.

BSE images revealed the existence of well-formed crystals of titanium oxides embedded within the matrix. However, EDS spectra do not provide information about the crystal structure of these minerals and therefore it was not possible to discriminate between rutile and anatase.

Apatite has been also identified in the studied pottery. In particular, SEM images have been studied to differentiate mineral apatite from that of bones. Bones in pottery are characterized by high porosity resulting from the bacterial attack with the typical network of small pores (0.1-1.0 μm in diameter) confined to discrete zone (each 10-40 μm across) giving a spongiform appearance to fragments of bones (Turner-Walker and Syversen, 2002). These typical features of apatite of bones have not been recognized in the acquired images. On the basis of this result it seems possible to exclude that bones have been used in the pottery production at Khirbet during the EB II period.

Table 19: Mineralogical phases detected in EB II samples.

EB II	Calcite	Quartz	Feldspars	Mn oxides	Iron oxides	Ilmenite	Apatite	Barite	Zirconone	Fossils	Titanium oxides
KB.06.B.392/8	•	•	•		•	•	•			•	
KB.06.E.704/6	•	•		•	•			•			•
KB.06.E.706/2	•	•			•	•	•	•	•	•	
KB.06.E.706/1	•	•			•		•	•			

4.5.1.2 Matrix

EDS spectra of the matrix revealed a similar chemical composition, made mainly of Si, Al and minor amounts of K, Na, Mg, Ca and Fe. Concerning the chemical composition of sample KB.06.E.704/6, differences have been observed with respect to other sherds as it has a lower Ca content. Pottery fragments with the typical “black core” structure have been carefully examined by analyzing in particular areas of the samples showing different colors. EDS results show the same chemical composition for these points, highlighting that color differences are not connected to different chemical composition.

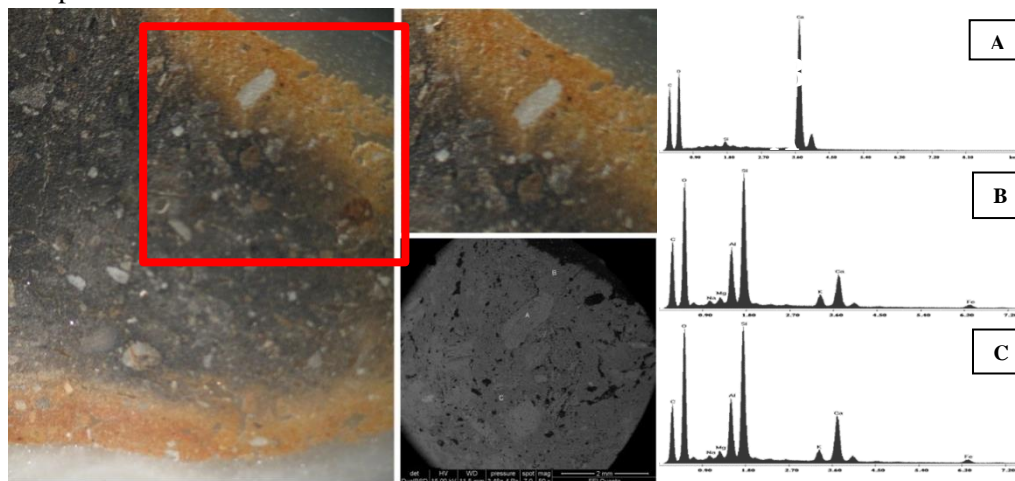


Figure 24: Microphotographs and BSE images of sample KB.06.B.392.8 with EDS spectra of three points : (a) calcite crystal, (b) rim and (c) internal part of sample.

Figure 24, clearly highlights these results as the microphotograph on the left shows the difference in color between the core and the margins of the fragment, whereas the BSE image on the lower right side shows that the internal and external parts have the

same color. EDS spectra of three analyzed points a (calcite crystal (A), rim (B) and internal part (C) of the sample) clearly show that the observed differences in color are not due to different chemical composition, while probably they have been induced by the firing conditions.

4.5.1.3 Vitrification stage analysis

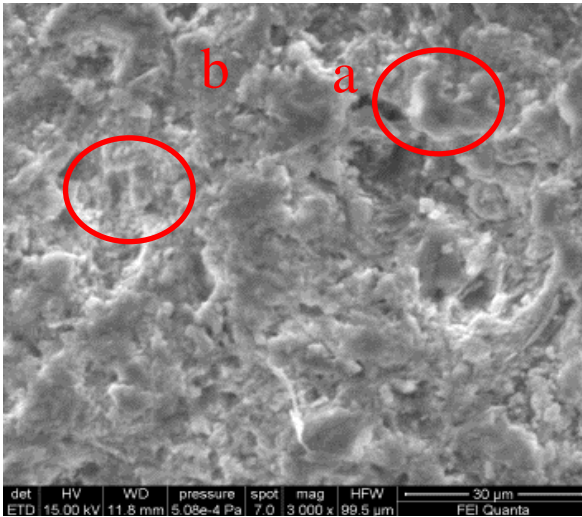


Figure 25: SEM image of sample KB.06.E.704/6 showing (a) plate line grains without contact grain to grain and (b) rounding of edges of the clay pallets.

SEM micro-photographs of the sherds show that pottery contains plate line grains, without contact grain to grain that allow to hypothesize a low fired ceramic. The presence of some slight buckling and rounding of edges of the clay pallets allows to identify the earlier stage in the development of vitrification (Fig. 25). Such stage is known as “no vitrification stage” (NV) or “intermediate stage of vitrification” (NV+) and suggests that the sample was fired below 900° C in oxidizing atmosphere (Tite and Maniatis, 1975; Tite *et al.*, 1982).

4.5.2 EB IIIA

4.5.2.1 Minerals

SEM-EDS results show that EB IIIA sherds are typified by the occurrence of coarse-sized inclusions in the matrix. These are mainly represented by calcite, quartz, feldspars, iron oxides, iron-titanium oxides. Olivine, apatite, barite, pyroxene and fragments of fossils have also been identified in minor amounts (Table 20).

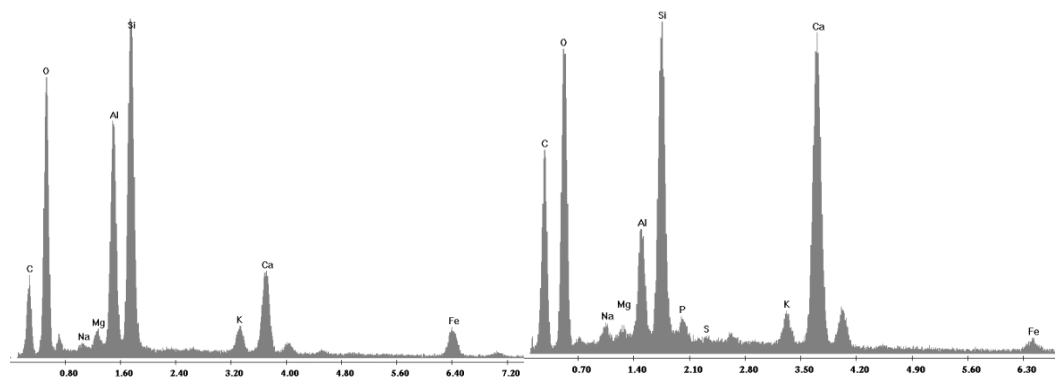
Table 20: Mineralogical phases detected in EB IIIA samples.

EB IIIA	Calcite	Quartz	Feldspars	Pyroxene	Olivine	Iron oxides	Ilmenite	Apatite	Barite	Fossils	Pyroxenes
KB.05.A.52/8	•	•					•				
KB.05.A.64/13	•		•			•	•				
KB.05.B.126/3	•					•		•		•	•
KB.05.B.136/1		•				•					
KB.05.B.146/8	•	•	•		•	•	•	•			

EB IIIA	Calcite	Quartz	Feldspars	Pyroxene	Olivine	Iron oxides	Ilmenite	Apatite	Barite	Fossils	Pyroxenes
KB.05.B.146/15	•		•	•			•		•		•
KB.05.B.146/24	•	•				•					•
KB.06.B.167/4	•		•	•		•	•				•
KB.06.B.413/2a	•	•	•			•				•	
KB.06.B.427/1	•	•		•							
KB.08.B.805/6	•	•	•	•		•	•	•	•		
KB.09.B.820/12	•		•	•		•	•	•			•
KB.09.B.820/13	•		•		•		•	•		•	

4.5.2.2 Matrix

The matrix of the pottery mainly contains Si and Al with minor amounts of Ca, K, Na, Mg and Fe (Fig. 26). The fragments belonging to the EB IIIA phase have similar chemical composition, while those of the KKW subgroup are distinguished by higher contents of Ca.



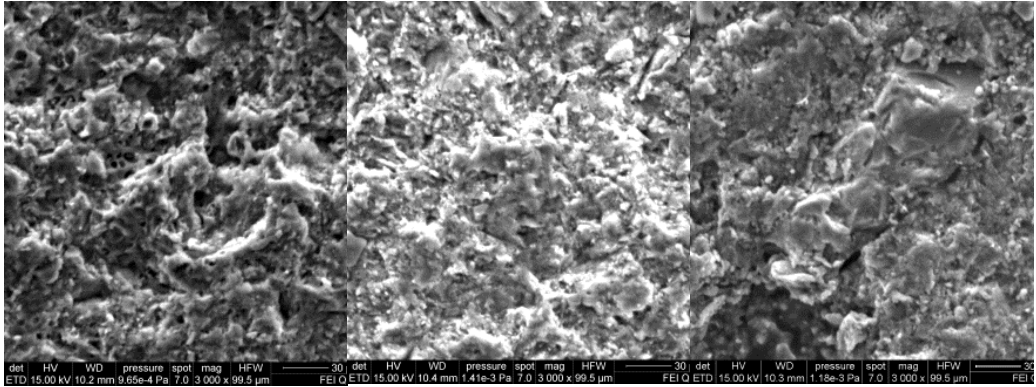
KB.05.B.136/1

KB.08.B.805/6 (KKW)

Figure 262: EDS spectra collected on the internal matrix, showing the different amounts of Ca in KKW samples.

4.5.2.3 Vitrification stage analysis

Samples of EB IIIA phase did not show diffuse vitrification, but only a surface in which is evident the glass developing with rare filaments and isolated smoothed surface (Fig. 27); the pores are present and only in a few points the cellular structure typical of low fired ceramics has been observed. According to Tite and Maniatis (1975) and Tite et al. (1982), the first stage of vitrification (IV) have been identified.



KB.05.A.52/8

KB.05.A.64/13

KB.05.B.126/3

Figure 273: SEM image of samples belonging to EB IIIA showing rare filaments of glass and isolated smoothed surface (for example, see sample KB.05.B.126/3).

4.5.3 EB IIIB

4.5.3.1 Minerals

SEM-EDS results allow to confirm the occurrence of calcite (Fig. 28), quartz, feldspars (Fig. 29), iron oxides (Fig. 28), iron-titanium oxides, apatite (Fig. 28 and Fig. 30) and fragments of fossils, being these latter the main diffuse inclusions in the matrix. Less widespread are barite, zircon, pyroxene and amphiboles (Table 21).

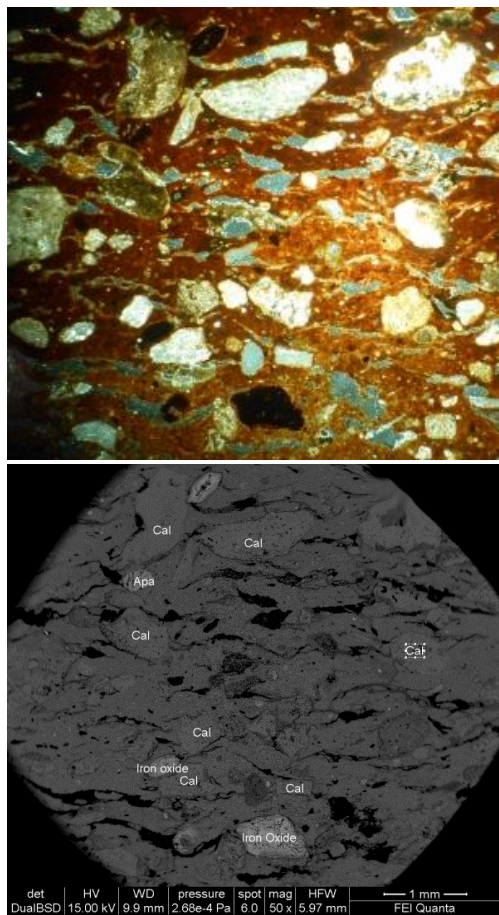


Figure 284: Microphotograph and BSE image of sample KB.11.B.1124/3 showing the presence of calcite (Cal), apatite (Apa) and iron oxides.

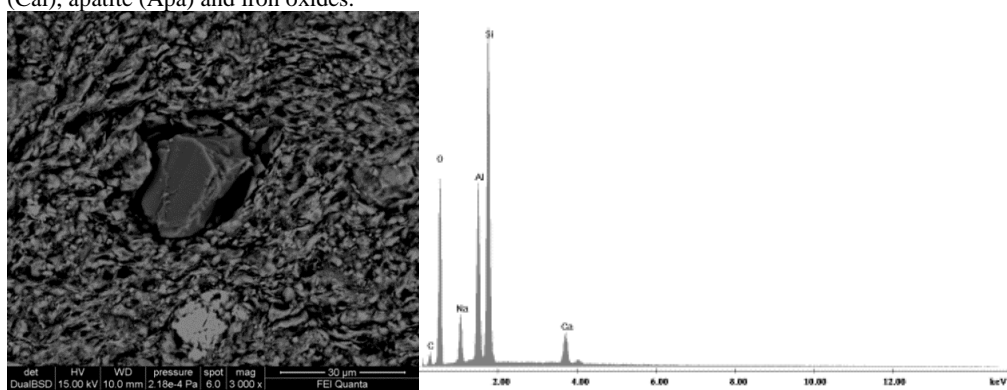


Figure 295: BSE image and EDS spectrum of an inclusion of feldspar in sample KB.06.A.120/6.

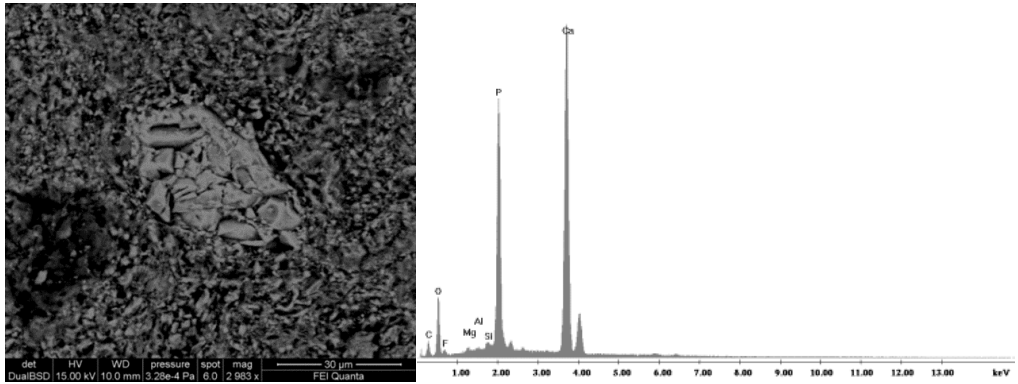


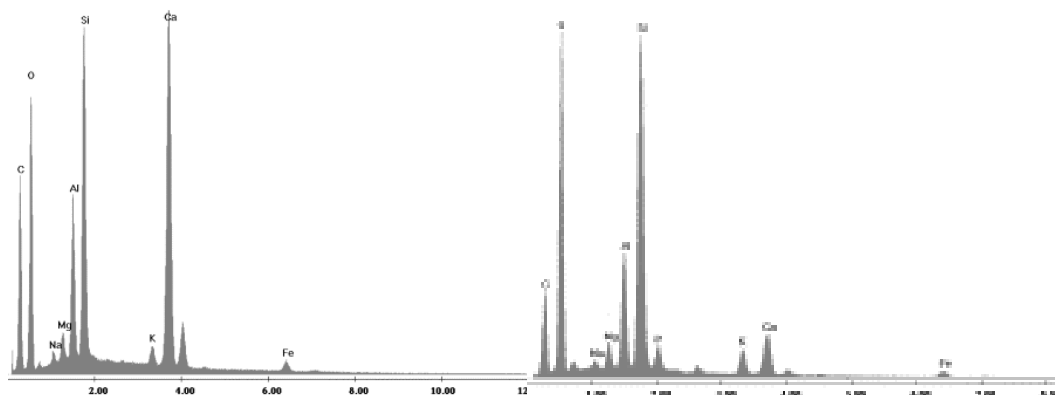
Figure 306: BSE image and EDS spectrum of an inclusion of apatite in sample KB.10.B.1054/24.

Table 212: Mineralogical phases detected in EB IIIB samples.

EB IIIB	Calcite	Quartz	Iron oxides	Ilmenite	Feldspars	Apatite	Barite	Zircon	Pyroxenes	Fossils	Amphibole
KB.06.A.120/6	•		•		•	•				•	
KB.05.A.204/3	•	•	•								
KB.10.B.1054/21	•	•	•	•		•					
KB.10.B.1054/24	•		•	•	•	•			•		
KB.10.B.1054/62	•		•	•	•	•	•		•	•	
KB.11.B.1124/3	•	•	•			•					
KB.11.B.1124/8	•		•	•	•				•	•	
KB.11.B.1124/15	•					•				•	•
KB.11.B.1124/29	•	•	•			•				•	
KB.11.B.1124/33	•	•	•			•	•			•	
KB.11.B.1126/65	•	•	•	•	•			•			

4.5.3.2 Matrix

The chemical composition of major elements of the pottery samples includes Si, Al, Ca, Fe, K, Mg and Na and all the studied fragments have similar composition, with the exception of sample KB.10.B.1054/24 due to its high content of Ca (Fig. 31).



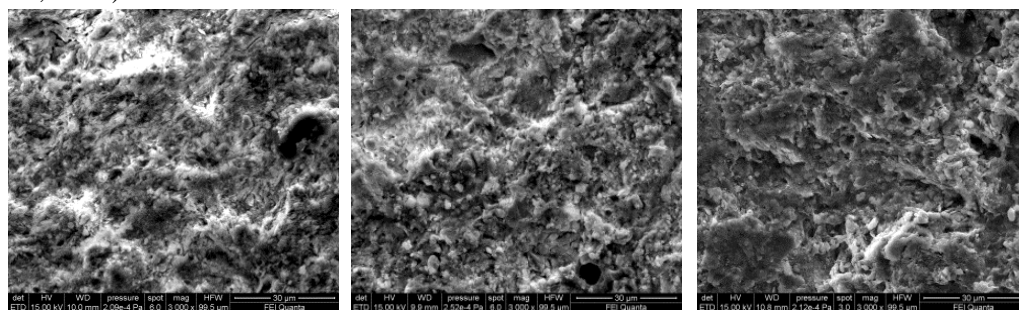
KB.11.B.1054/24

KB.11.B.1054/62

Figure 31: EDS spectra collected on the internal matrix, showing the different amounts of Ca in the sample KB.10.B.1054/24.

4.5.3.3 Vitrification stage analysis

The EB III B samples do not show clear evidence of sintering or partial melting. The preservation of the illite grains with limited glass areas, no-degraded changed carbonate grains may be connected to a low firing temperature (Fig. 32). The absence of diffuse small pores further supports the definition of an initial stage of vitrification that could indicate a firing temperature under 900° C (Tite and Maniatis, 1975; Tite *et al.*, 1982).



KB.06.A.120/6

KB.11.B.1054/24

KB.11.B.1054/62

Figure 327: SEM image of samples belonging to EB III B showing limited areas of glass and isolated smoothed surface.

4.5.4 EB IV

4.5.4.1 Minerals

SEM-EDS results show the occurrence of calcite (Fig. 33), quartz, feldspars, iron oxides, iron-titanium oxides as the main diffuse inclusions. Apatite, barite, olivine and fragments of fossils (Table 22) have been identified, although in minor amounts.

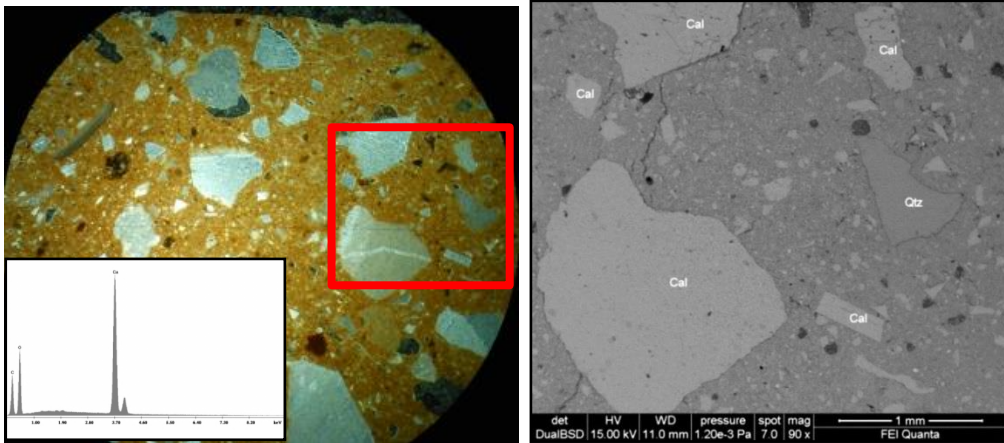


Figure 33: Microphotograph and BSE image of sample KB.06.A.248/2 showing the presence of calcite (Cal) and quartz (Qtz), EDS spectra of calcite crystal has also been reported.

Table 22: Mineralogical phases detected in EB IV samples.

EB IV	Calcite	Quartz	Iron oxides	Ilmenite	Feldspars	Apatite	Barite	Olivine	Fossils
KB.05.A.6b/1	•	•	•	•	•				
KB.05.A.21/27	•	•	•	•	•	•	•		
KB.05.A.68/2	•	•	•	•		•	•		
KB.05.A.84/3	•		•	•	•	•	•		
KB.05.A.88/1	•	•	•	•	•	•		•	
KB.06.A.248/2	•	•	•	•					•
KB.06.A.256/1	•	•	•	•	•				

4.5.4.2 Matrix

EDS analysis points out that the matrix of all the EB IV sherds has a similar chemical composition made of high contents of Si, Ca and Al along with minor amounts of Mg, Na, Fe and K. EDS spectra of internal and marginal areas of the matrix show the same chemical composition (Fig. 34). Moreover, the obtained results highlight the high Ca content of the slip occurring on the surface of the sherds.

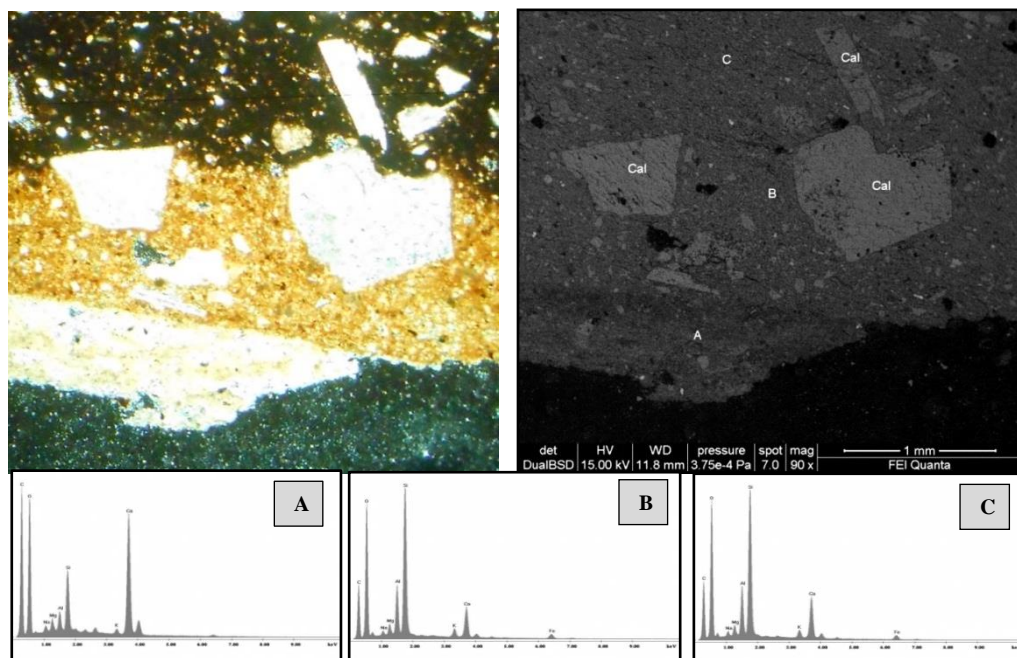


Figure 348: Microphotograph and BSE images of sample KB.05.A.68/2 with EDS spectra of three points : (a) white slip, (b) rim and (c) internal part of sample.

4.5.4.3 Vitrification stage analysis

SEM images show a poor compact micromass, in which unaltered grains of carbonates, indicating a lower firing temperature, occur (Fig. 35). The matrix is characterized by aggregates of flaky clay particles, cracks of small dimensions interrupted by zones with the original structure; however, a cellular structure or small dimension pores, testifying an initial vitrification stage have not been recognized in the studied samples.

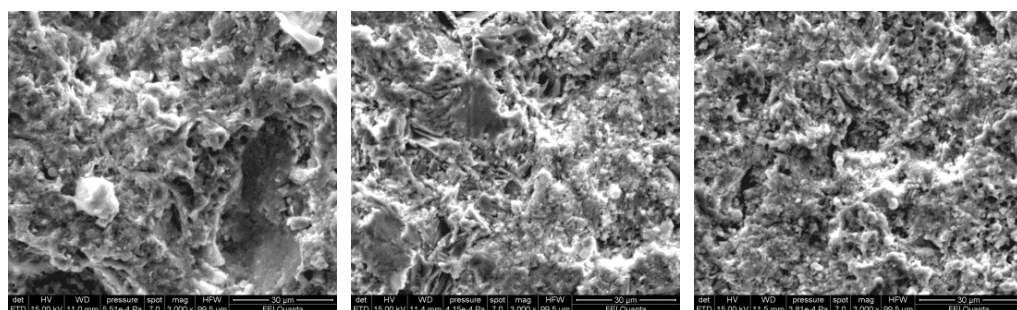


Figure 395: SEM image of samples belonging to EB IV showing limited areas of glass and clay particles.

4.5.5 Coarse-sized inclusions

Coarse-sized inclusions, with shapes from very angular to angular, have been observed in numerous samples belonging to the four different phases of urbanization. On the basis of their optical features (OM) they were identified as fragments of basaltic rocks, and for this reason a detailed characterization of these inclusions has been carried out by SEM-EDS (Figs. 36 and 37).

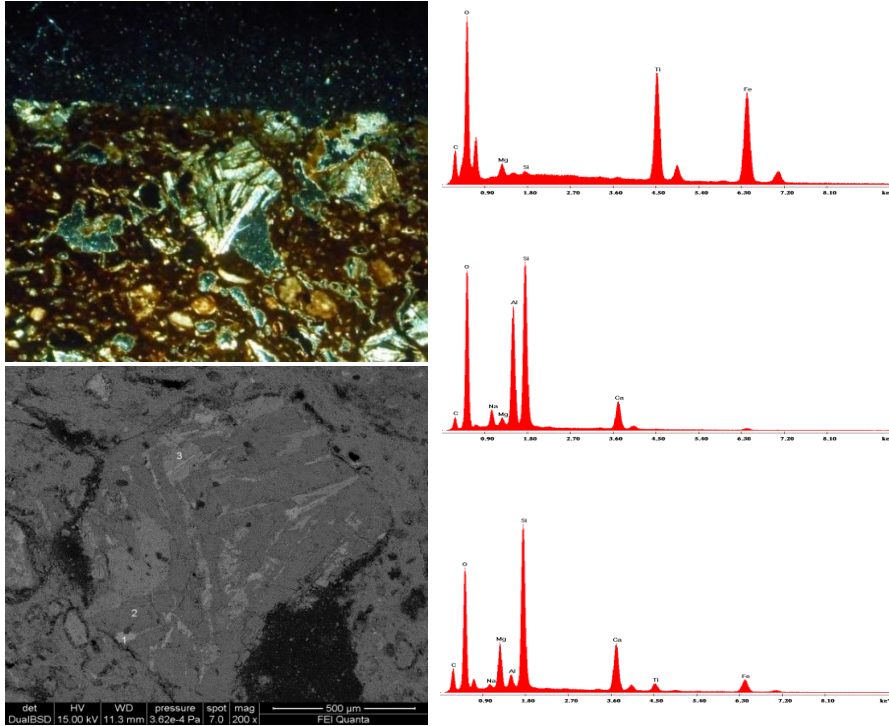


Figure 3610: Microphotograph and BSE image of sample KB.06.B.167/4 with EDS spectra of three points : (1) iron and titanium oxides, (2) plagioclase and (3) pyroxene.

These fragments containing ilmenite, olivine, plagioclase and apatite support the hypothesis that they are inclusions of remains of basaltic rocks. In particular, according to Burdon (1959) it is also possible to infer a local provenance for these rocks fragments as they show a mineralogical composition substantially close to that of the Jordan Plateau Basalt.

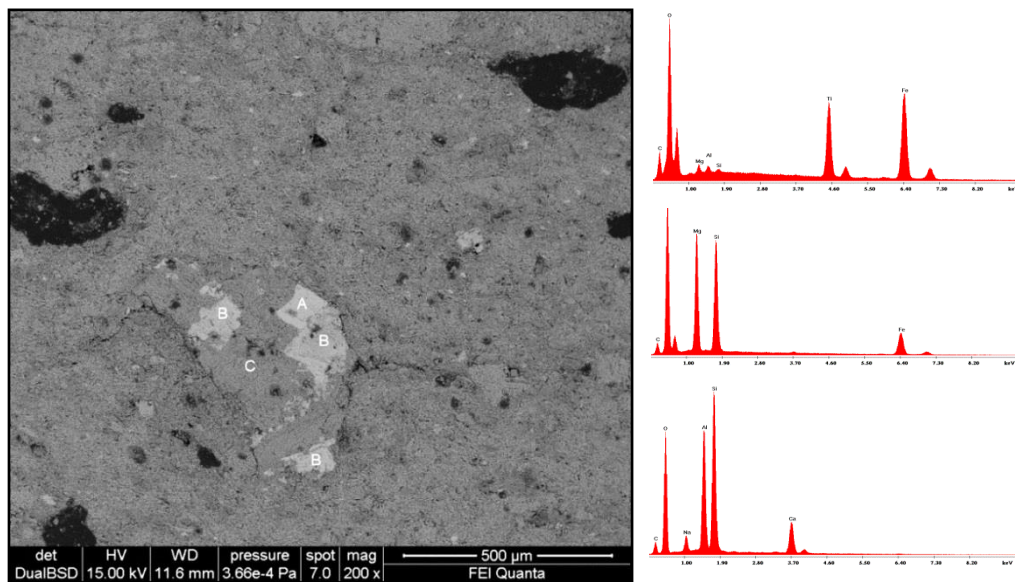


Figure 3711: Microphotograph and BSE image of sample KB.05.A.88/1 with EDS spectra of three points : (A) iron and titanium oxides, (B) olivine and (C) plagioclase.

4.6 X-Ray Diffraction analysis (XRD)

In a pottery the “mineralogical assemblage” refers to the set of mineralogical phases present in the matrix and occurring as inclusions. This assemblage differs from the mineralogical composition of the starting raw material (a mixture of clay and tempers) as it is modified during the firing process through a series of complex pathway of reactions leading to the formation of newly formed minerals and/or to amorphous phases. The mineralogical assemblage of the pottery is strictly affected by the mineralogical composition of the clay used for the ceramic production and the tempers added by the potters. Moreover, it depends also on the firing temperatures, i.e. maximum temperature reached, the time of firing process, the heating and cooling rates and the redox state of the atmosphere developed during heating process. For this reason, the presence or absence of specific mineralogical phases is used to estimate the maximum firing temperature.

A summary of the mineralogical phases detected in each sample and their relative abundances, estimated on the basis of the intensity of the peaks in the XRD patterns, are shown in Tables 23-26, following the four phase of Khirbet al-Batrawy urbanization. The semi-quantitative analysis has been performed by the application of the X’Pert Highscore Plus software®.

4.6.1 EB II

The results of XRD analysis show that quartz and calcite are ubiquitous and the most abundant mineral phases encountered in all samples. Referring on the calcite content with respect to that of quartz, the ceramic samples were divided in different groups. The group with high calcite content includes samples KB.06.B.392/8, KB.06.E.703/6, KB.06.E.703/5,

KB.06.E.706/2 and KB.06.E.706/1; whereas the group having high amounts of quartz is formed by samples KB.06.E.702/10, KB.06.E.704/1 and KB.06.E.704/6 (Fig. 38).

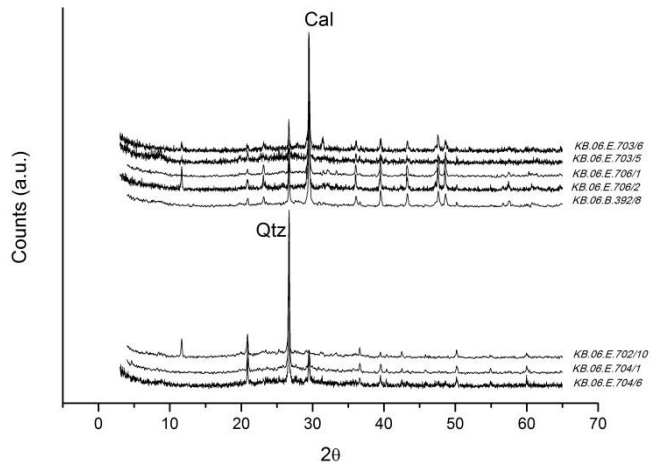


Figure 12: XRD spectra showing (above) the group of EB II samples with high amount of calcite and (below) the group of EB II samples with high amounts of quartz.

The XRD patterns of the analyzed samples, showing a predominance of quartz and calcite content, present high and large peaks which make difficult investigations of other minerals present in minor amounts. However, minor amounts of gypsum, illite, K-feldspar, plagioclase, gehlenite and hematite have been identified (Table 23). Moreover, the high background of spectra suggests some amorphous content.

In addition, the presence or absence of illite and gehlenite permits to discriminate among the following mineralogical assemblages as summarized:

-calcite+quartz±feldspars

-calcite+quartz+gehlenite±feldspars±gypsum

-calcite+quartz+gehlenite+hematite±gypsum

-calcite+quartz+illite+hematite±feldspars±gypsum

Table 233: Mineralogical phases and relative abundances of EB II samples (+++=abundant; ++=present; +=scarce; tr=traces) identified by XRD analysis. Cal: calcite; Qtz: quartz; Gp: gypsum; Ill: illite; Kfs: K-feldspar; Pl: plagioclase; Hem: hematite; Gh: gehlenite.

EBII	Cal	Qtz	Gp	Ill	Kfs	Pl	Hem	Gh
KB.06.B.392/8	+++	++			tr	tr		
KB.06.E.703/6	+++	+	+			tr		+
KB.06.E.703/5	+++	++	Tr	+	tr		tr	
KB.06.E.702/10	tr	+++	+	tr	tr	tr	tr	
KB.06.E.704/1	+	+++			tr			
KB.06.E.704/6	+	+++			tr	tr		
KB.06.E.706/2	+++	+	+				tr	tr
KB.06.E.706/1	+++	++					tr	tr

4.6.2 EB IIIA

The XRD results of EB IIIA samples show the diffuse occurrence of calcite and quartz in all sherds, with extremely variable amounts. On the basis of relative contents of the calcite and quartz, two groups of samples have been recognized.

The high-calcite group includes samples KB.05.A.52/8, KB.05.B.110/15, KB.05.B.126/1, KB.05.B.126/3, KB.05.B.126/4, KB.05.B.136/3, KB.05.B.136/5, KB.05.B.146/1, KB.05.B.146/4, KB.05.B.146/5, KB.05.B.146/20, KB.06.B.167/4 and KB.06.B.413/2; whereas the high-quartz is formed by samples KB.05.A.58/1, KB.05.A.64/1, KB.05.A.64/13, KB.05.B.136/1, KB.05.B.146/3, KB.05.B.146/4, KB.05.B.146/6, KB.05.B.146/7, KB.05.B.146/24, KB.05.B.146/30, KB.06.B.376/4, KB.06.E.701/2 and KB.06.E.703/3. All the sherds of KKW group are characterized by high content of calcite. These samples also contain minor quantities of plagioclase, illite, K-feldspar, diopside, hematite, gehlenite, epidote and gypsum (Table 24 and Fig. 39). Moreover, the high background of spectra suggests some amorphous content.

Furthermore, the XRD analyses have also been performed on the decoration of EB IIIA group, for which to minimize the matrix interference, was directly scraped by the surface. In spite of this procedure, the XRD patterns show a high background and only the peaks of quartz and/or calcite have been identified.

On the basis of the presence or absence of illite, gehlenite and diopside, the mineralogical assemblages found in the samples of EB IIIA phase can be summarized as follows:

- calcite+quartz±feldspars
- calcite+quartz+hematite±feldspars
- calcite+quartz+hematite+diopside±feldspars
- calcite+quartz+gehlenite±feldspars
- calcite+quartz+gehlenite+hematite±feldspars
- calcite+quartz+gehlenite+diopside±feldspars±epidote
- calcite+quartz+gehlenite+diopside+hematite±feldspars
- calcite+quartz+illite±feldspars±epidote
- calcite+quartz+illite+hematite±feldspars
- calcite+quartz+illite+hematite+diopside±feldspars
- calcite+quartz+illite+diopside±feldspars±epidote
- calcite+quartz+illite+gehlenite±feldspars
- calcite+quartz+illite+gehlenite+hematite±feldspars
- calcite+quartz+illite+gehlenite+diopside+hematite±feldspars
- quartz+gehlenite+hematite±feldspars
- quartz+gehlenite+diopside+hematite±feldspars±gypsum

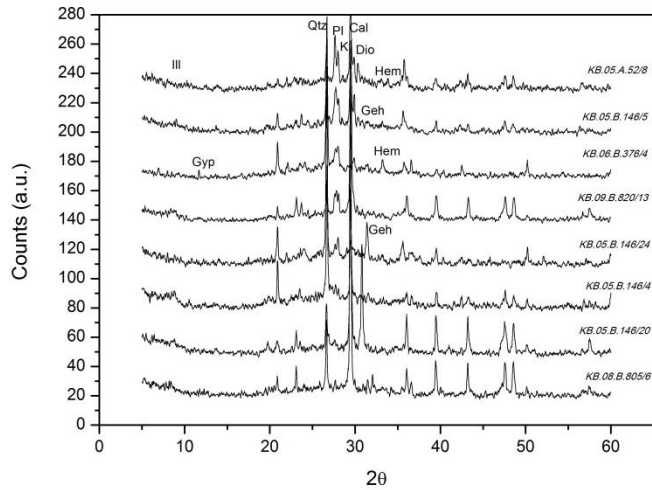


Figure 13: Representative spectra of EB IIIA phase showing the occurrence of quartz (Qtz), illite (Ill), plagioclase (Pl), K-feldspars (K), calcite (Cal), diopside (Dio), hematite (Hem), gehlenite (Geh) and gypsum (Gyp).

Table 244: Mineralogical phases and relative abundances of EB IIIA samples (+++=abundant; ++=present; +=scarce; tr=traces) identified by XRD analysis. Cal: calcite; Qtz:quartz; Gp: gypsum; Ill: illite; Kfs: K-feldspar; Pl: plagioclase; Hem: hematite; Di: diopside; Gh: gehlenite; Ep: epidote.

EB IIIA	Cal	Qtz	Gp	Ill	Kfs	Pl	Hem	Di	Gh	Ep
KB.05.A.52/8	+++	++		Tr	++	++	tr	+		
KB.05.A.58/1	++	+++			tr	Tr	tr			
KB.05.A.64/1	+	+++			+	+				
KB.05.A.64/13	++	+++				++	tr		tr	
KB.05.B.110/15	+++	+			tr	++		+	tr	
KB.05.B.126/1	+++	+							tr	
KB.05.B.126/3	+++	++					tr			
KB.05.B.126/4	+++	++		Tr	++	++	tr	++		
KB.05.B.136/1	++	+++		Tr	tr	tr	tr			
KB.05.B.136/3	+++	++		Tr	++	++		+		
KB.05.B.136/5	+++	+			+	+			tr	
KB.05.B.146/1	+++	+					tr		tr	
KB.05.B.146/3	++	+++			++	+++	tr	+		
KB.05.B.146/4	++	+++		Tr	tr	tr			tr	
KB.05.B.146/5	+++	++		Tr	+	+	tr	+	tr	
KB.05.B.146/6	+	+++		Tr						
KB.05.B.146/7	+	+++			+	+			tr	
KB.05.B.146/15	++	++		Tr	+++	+++		+		+
KB.05.B.146/20	+++	+		Tr	tr					+
KB.05.B.146/24	+	+++			+	+	tr	tr	+	
KB.05.B.146/30	+	+++		Tr	+	+			tr	
KB.06.B.167/4	+++	++			++	++		++	tr	+
KB.06.B.376/4		+++	+		+	+	+	+	tr	
KB.06.B.413/2	+++	+							+	
KB.06.E.701/2	+	+++		Tr	+	+	+	+		
KB.06.E.703/3		+++			tr		tr		tr	
KB.06.B.427/1	+++	++						tr	tr	
KB.08.B.805/6	+++	+		Tr	tr	tr	tr		tr	
KB.09.B.820/10	+++	+			+	+		+	tr	tr
KB.09.B.820/12	+++	+		Tr	tr					++
KB.09.B.820/13	+++	+		Tr	+	+	tr		tr	

4.6.3 EB IIIB

As observed for the samples of EB IIIA phase, the XRD results show the diffuse occurrence of calcite and quartz also in all the sherds of this period, with extremely variable amounts. On the basis of the calcite and quartz relative contents two groups of samples have been recognized.

The group containing high amounts of calcite includes samples KB.05.A.46/8, KB.05.A.216/4, KB.05.A.220/5, KB.05.A.224/2, KB.06.A.120/6, KB.05.A.204/2, KB.05.A.204/3, KB.10.B.1054/21, KB.10.B.1054/62, KB.11.B.1124/8, KB.11.B.1124/3, KB.11.B.1124/15, KB.11.B.1128/50, KB.11.B.1128/51; whereas the group with high amounts of quartz includes samples KB.05.A.46/2, KB.05.B.111/3,

KB.10.B.1040/8, KB.10.B.1054/24, KB.11.B.1124/29 and KB.11.B.1128/65. Illite, K-feldspar, plagioclase, hematite, diopside, gehlenite, epidote and gypsum have been identified in minor amounts (Table 25).

On the basis of the presence or absence of illite, gehlenite and diopside, the mineralogical assemblages found in these samples can be summarized as follows:

-calcite+quartz±feldspars

-calcite+quartz±feldspars±hematite

-calcite+quartz+gehlenite±feldspars

-calcite+quartz+gehlenite+hematite±feldspars±gypsum

-calcite+quartz+gehlenite+diopside+hematite±feldspars

-calcite+quartz+illite±feldspars

-calcite+quartz+illite+hematite

-calcite+quartz+illite+gehlenite±feldspars

-calcite+quartz+illite+gehlenite+hematite±feldspars

Table 25: Mineralogical phases and relative abundances of EB IIIB samples (+++=abundant; +=present; +=scarce; tr=traces) identified by XRD analysis. Cal: calcite; Qtz:quartz; Gp: gypsum; Ill: illite; Kfs: K-feldspar; Pl: plagioclase; Hem: hematite; Di: diopside; Gh: gehlenite.

BA IIIB	Cal	Qtz	Gp	Ill	Kfs	Pl	Hem	Di	Gh
KB.05.A.46/2	++	+++			tr	tr			
KB.05.A.46/8	+++	++			tr	tr			
KB.05.A.216/4	+++	++		tr					
KB.05.A.220/5	+++	++		tr			tr		tr
KB.05.A.224/2	+++	++		tr	tr	tr			
KB.06.A.120/6	+++	++		tr	tr		tr		tr
KB.05.A.204/2	+++	++					tr		tr
KB.05.A.204/3	+++	+			tr	tr			tr
KB.05.B.111/3	++	+++				++	tr	tr	++
KB.10.B.1040/8	+++	++			++	++	tr	+	+
KB.10.B.1054/21	+++	++			tr	tr	tr		tr
KB.10.B.1054/24	tr	+++			+	+	tr		tr
KB.10.B.1054/62	+++	+							
KB.11.B.1124/8	+++	++							+
KB.11.B.1124/3	+++	++			tr				tr
KB.11.B.1124/15	+++	++		tr	tr				
KB.11.B.1124/29	++	+++		tr		+	tr		
KB.11.B.1128/65	++	+++	+			tr	tr		tr
KB.11.B.1128/50	+++	+			tr	tr			tr
KB.11.B.1128/51	+++	+		tr	tr	tr			tr

4.6.4 EB IV

Also in the case of samples of this archaeological period, the XRD results show the diffuse occurrence of calcite and quartz also in all the sherds, with extremely variable

amounts. On the basis of the calcite and quartz relative contents two groups of samples have been recognized: high-calcite (samples KB.05.A.6b/1, KB.05.A.18/5, KB.05.A.21/27, KB.05.A.34/2, KB.05.A.62/1, KB.05.A.68/2, KB.05.A.82/4, KB.05.A.8b/3b, KB.05.A.88/1, KB.05.A.96/1, KB.05.A.98/1, KB.05.A.210/4, KB.05.A.212/6, KB.05.A.216/12, KB.06.A.ø/18) and high-quartz (KB.05.A/D200, KB.05.A.84/3, KB.05.A.210/2, KB.05.B.128/3, KB.06.A.256/1, KB.06.A.248/2 and KB.06.B.383/7). Sample KB.05.A.62/2 is characterized by contents of the two mineral phases almost similar.

Also in this set of samples, the intensity of quartz and calcite peaks makes difficult the identification of other mineralogical phases that appear diffuse in variable amounts in the different samples. However, illite, K-feldspar, plagioclase, hematite, diopside, gehlenite and epidote have been also found, rarely along with gypsum (Table 26 and Fig. 40).

On the basis of the presence or absence of illite, gehlenite and diopside, the mineralogical assemblages found in these samples can be summarized as follows:

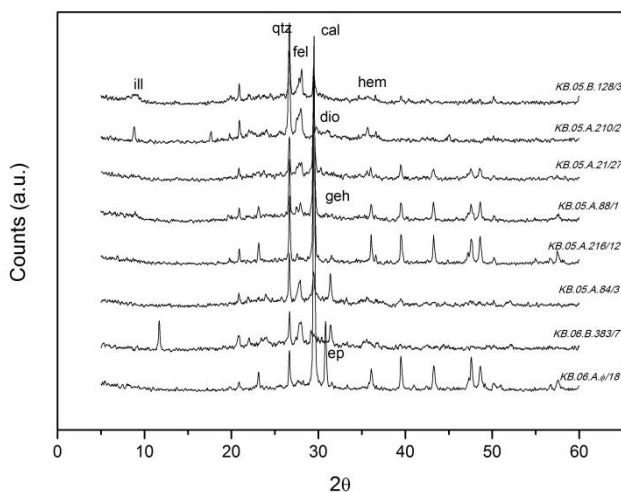


Figure 40: Representative spectra of EB IV phase showing the occurrence of quartz (qtz), illite (ill), feldspar (fel), calcite (cal), diopside (dio), hematite (hem) and gehlenite (geh).

- calcite+quartz±feldspars±epidote
- calcite+quartz+hematite±feldspars
- calcite+quartz+hematite+diopside±feldspars±epidote
- calcite+quartz+hematite+gehlenite+diopside±feldspars
- calcite+quartz+hematite+gehlenite±feldspars±epidote
- calcite+quartz+gehlenite±feldspars±epidote
- calcite+quartz+gehlenite+diopside±feldspars
- calcite+quartz+illite±feldspars
- calcite+quartz+illite+hematite±feldspars
- calcite+quartz+illite+gehlenite
- calcite+quartz+illite+diopside±feldspars
- calcite+quartz+illite+gehlenite+hematite±feldspars±epidote
- quartz+gehlenite+hematite±feldspars±gypsum±epidote

Table 26: Mineralogical phases and relative abundances of EB IV samples (+++=abundant; ++=present; +=scarce; tr=traces) identified by XRD analysis. Cal: calcite; Qtz:quartz; Gp: gypsum; Ill: illite; Kfs: K-feldspar; Pl: plagioclase; Hem: hematite; Di: diopside; Gh: gehlenite; Ep: epidote.

BAIV	Cal	Qtz	Gp	Ill	Kfs	Pl	Hem	Di	Gh	Ep
KB.05.A/D200	++	+++			+	+	tr		+	tr
KB.05.A.6b/1	+++	++		+	+	+				
KB.05.A.18/5	+++	++			tr					
KB.05.A.21/27	+++	++			+	+	tr	+		
KB.05.A.34/2	+++	++			+	+	tr	tr	tr	
KB.05.A.62/1	+++	+			+	+	tr	tr		tr
KB.05.A.62/2	+++	+++				+	+			
KB.05.A.68/2	+++	++			+	+				tr
KB.05.A.82/4	+++	++			+	+		tr	+	
KB.05.A.84/3	++	+++		tr	+	+	tr		+	tr
KB.05.A.8b/3b	+++	++		tr	+			tr		
KB.05.A.88/1	+++	++		tr	+	+				
KB.05.A.96/1	+++	++		tr					tr	
KB.05.A.98/1	+++	++		tr						
KB.05.A.210/2	+	+++		+		++		+		
KB.05.A.210/4	+++	++			+	+		tr	tr	
KB.05.A.212/6	+++	++							tr	
KB.05.A.216/12	+++	++			+				tr	tr
KB.05.B.128/3	++	+++		tr	++	++	tr			
KB.06.A.248/2	++	+++					+			
KB.06.A.256/1	++	+++		tr	tr					
KB.06.A.ø/18	+++	+							tr	++
KB.06.B.383/7		+++	++		++	++	tr		++	+

4.6.5 Geological samples

The results of XRD analysis show that quartz and calcite are the main components of the samples of the supposed raw material collected near the archaeological site. Aragonite [CaCO₃], augite [(Ca,Na)(Mg,Fe,Al,Ti)(Si,Al)₂O₆], apatite and barite are widespread, whereas minor amounts of hematite, illite and gehlenite have been identified (Fig. 41).

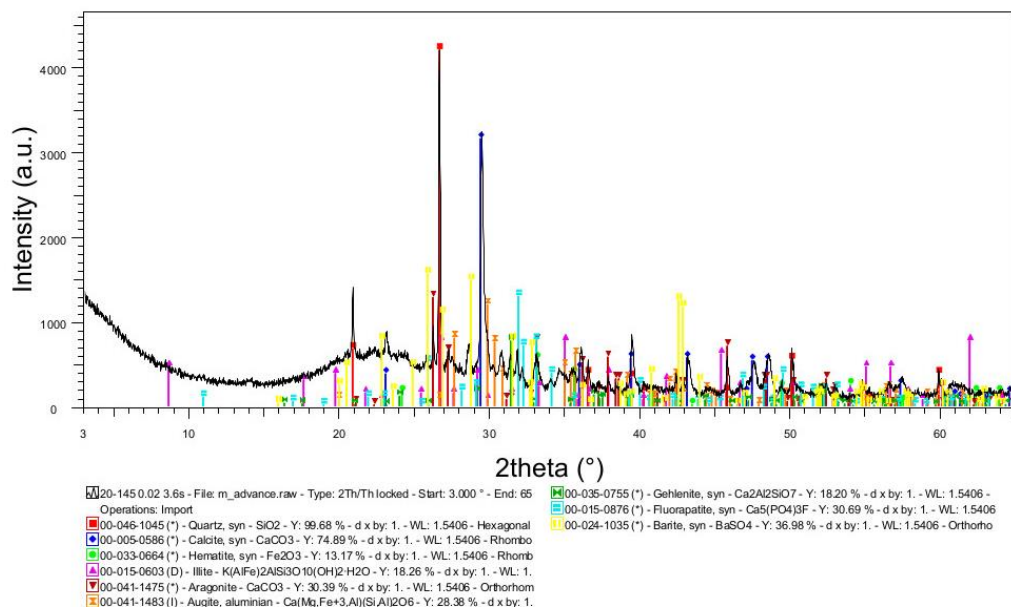


Figure 41: Representative spectra of geological samples showing the occurrence of quartz, calcite, hematite, illite, aragonite, augite, gehlenite, apatite and barite.

4.6.6 Firing experiments

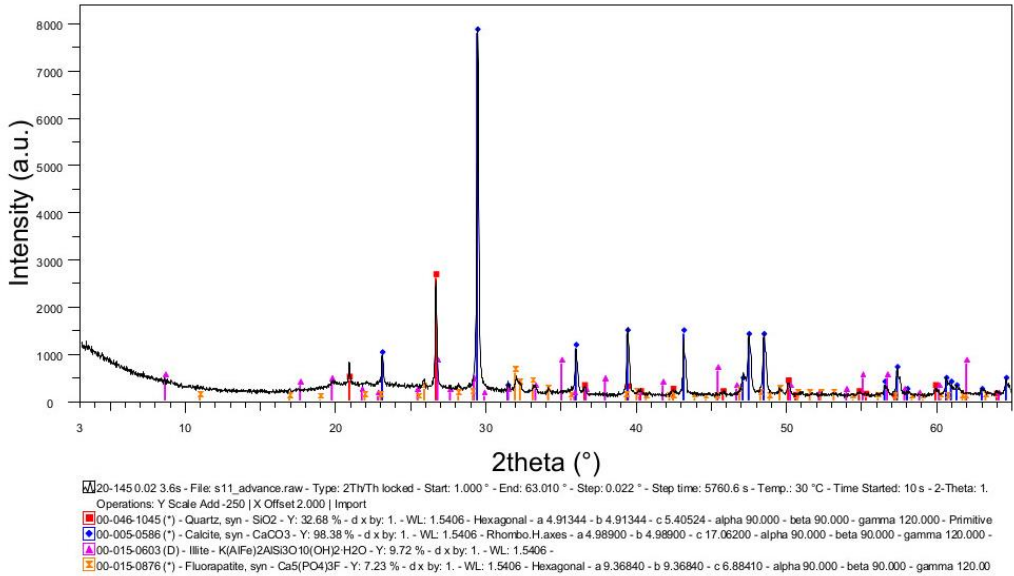
One sample for each historical period and one sample of the supposed raw material have been re-fired at 950 °C for 24 h and analyzed by XRD to define in detail the products of reactions that take place during heating process. A summary of results (Table 27) and XRD spectra, before and after the re-firing, are reported below for each sample (Fig. 42).

In general, it is possible to assert that at 950 °C XRD spectra show that calcite and illite, observed in the pottery samples at room temperature, disappeared and the reactions during firing produced mainly gehlenite, hematite and wollastonite.

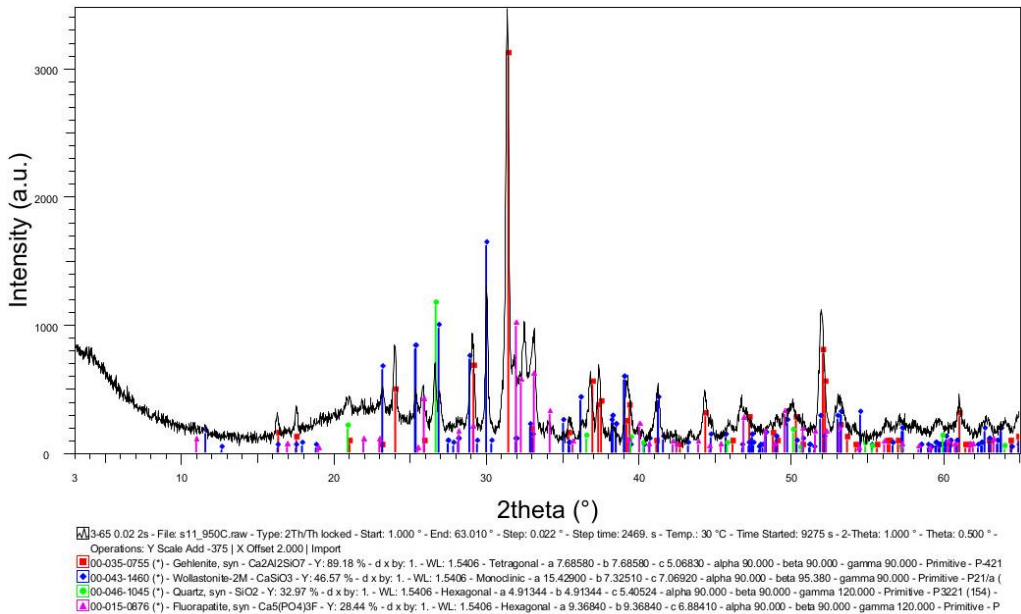
Analyzing in detailed the results, we can also note that apatite, anorthite, gehlenite and augite if detected in samples at room temperature were observed also in samples after re-firing. In sample KB.11.B.1054/12 at 950 °C anorthite appeared probable as the result of the decomposition of gehlenite in presence of wollastonite and high amount of silica (Riccardi *et al.*, 1999).

Figure 42: XRD spectra of representative pottery fragments, before and after the re-firing at 950 °C.

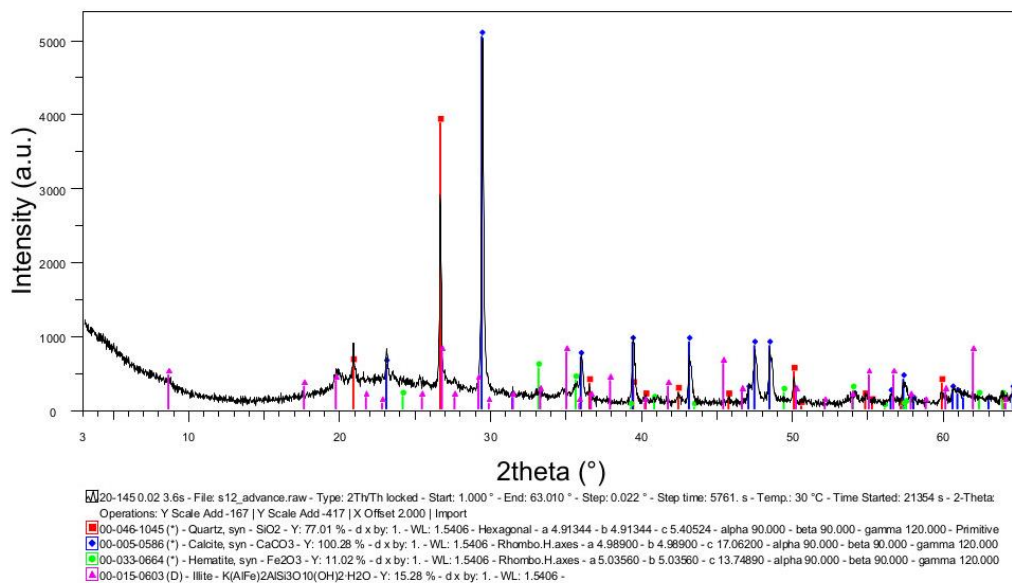
KB.06.E.706/1



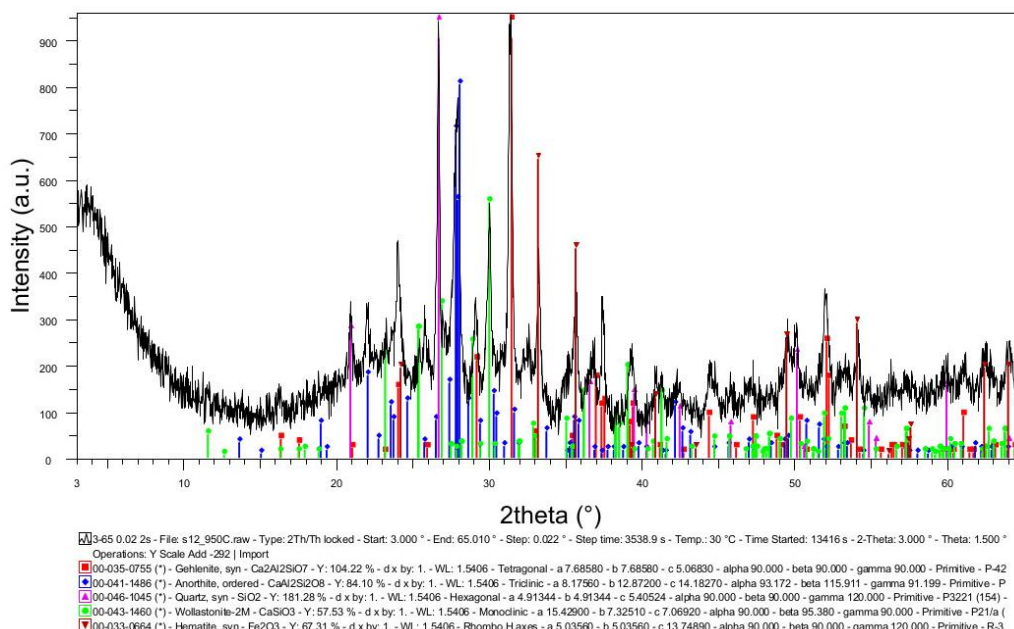
KB.06.E.706/1 950 °C



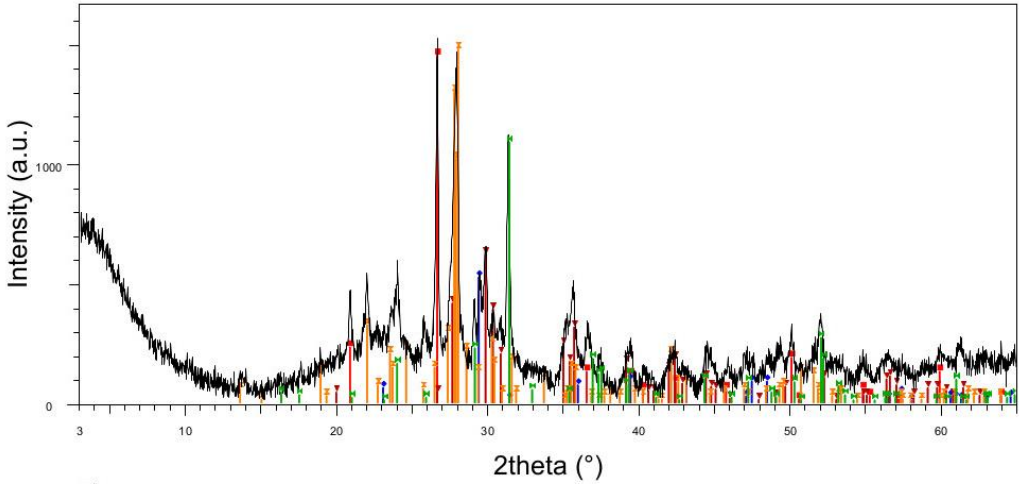
KB.11.B.1054/12



KB.11.B.1054/12 950 °C

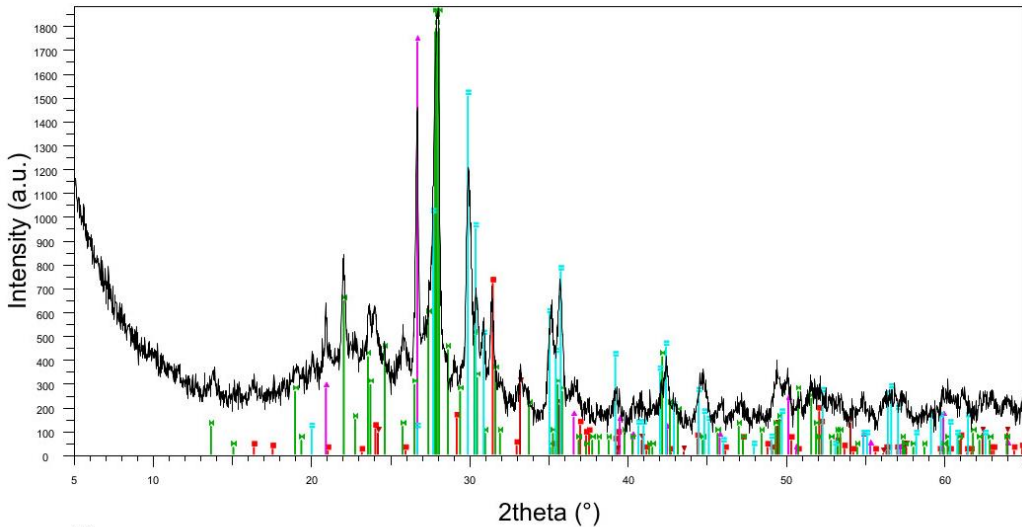


KB.06.B.383/7



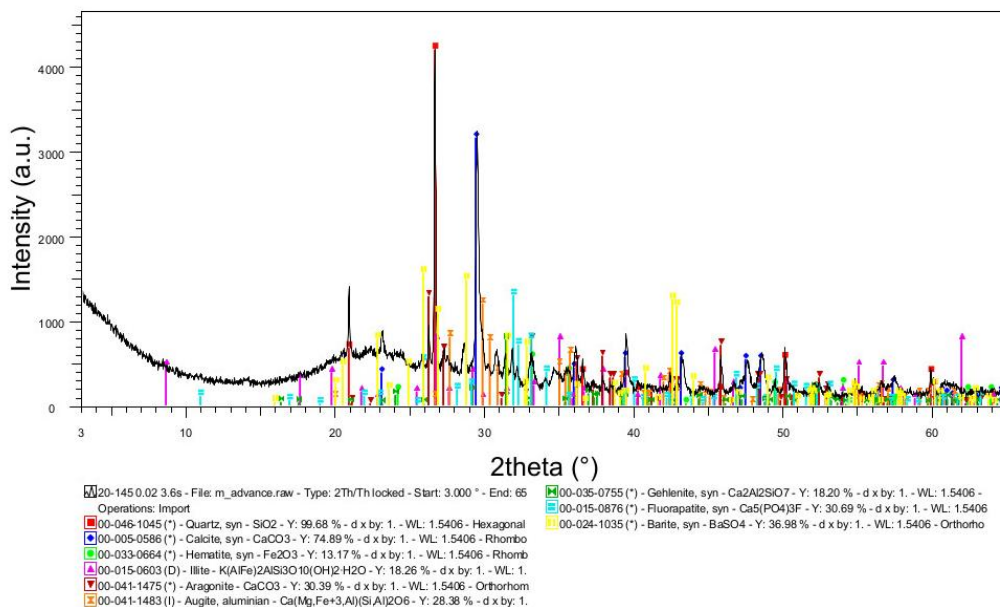
20-145 0.02 3.6s - File: s7_advance.raw - Type: 2Th/Th locked - Start: 1.000 ° - End: 63.010 ° - Step: 0.022 ° - Step time: 5760.6 s - Temp: 30 °C - Time Started: 5 s - 2-Theta: 1.00
 Operations: X Offset(2.000) | Y Scale Add(-500) | Import
 00-046-1045 (*) - Quartz, syn - SiO2 - Y: 95.10 % - d x by: 1. - WL: 1.5406 - Hexagonal - a 4.91344 - b 4.91344 - c 5.40524 - alpha 90.000 - beta 90.000 - gamma 120.000 - Primitive
 00-005-0586 (*) - Calcite, syn - CaCO3 - Y: 34.41 % - d x by: 1. - WL: 1.5406 - Rhombo.H.axes - a 4.98900 - b 4.98900 - c 17.06200 - alpha 90.000 - beta 90.000 - gamma 120.000 - Primitive
 00-041-1483 (I) - Augite, aluminian - Ca(Mg,Fe+3,Al)(Si,Al)2O6 - Y: 40.64 % - d x by: 1. - WL: 1.5406 - Monoclinic - a 9.74280 - b 8.89420 - c 5.27230 - alpha 90.000 - beta 106.111 - gamma 90.000
 00-041-1486 (*) - Anorthite, ordered - CaAl2Si2O8 - Y: 96.91 % - d x by: 1. - WL: 1.5406 - Triclinic - a 8.17560 - b 12.87200 - c 14.18270 - alpha 93.172 - beta 115.911 - gamma 91.199
 00-035-0755 (*) - Gehlenite, syn - Ca2Al2SiO7 - Y: 71.25 % - d x by: 1. - WL: 1.5406 - Tetragonal - a 7.68580 - b 7.68580 - c 5.06830 - alpha 90.000 - beta 90.000 - gamma 90.000

KB.06.B.383/7 950 °C



3-65 0.02 2s - File: s7_950C.raw - Type: 2Th/Th locked - Start: 5.000 ° - End: 65.008 ° - Step: 0.022 ° - Step time: 14813.1 s - Temp: 30 °C - Time Started: 27073 s - 2-Theta: 5.000 ° - Theta: 2.500 °
 Operations: Import
 00-035-0755 (*) - Gehlenite, syn - Ca2Al2SiO7 - Y: 38.25 % - d x by: 1. - WL: 1.5406 - Tetragonal - a 7.68580 - b 7.68580 - c 5.06830 - alpha 90.000 - beta 90.000 - gamma 90.000 - Primitive - P-421
 00-046-1045 (*) - Quartz, syn - SiO2 - Y: 92.35 % - d x by: 1. - WL: 1.5406 - Hexagonal - a 4.91344 - b 4.91344 - c 5.40524 - alpha 90.000 - beta 90.000 - gamma 120.000 - Primitive - P-321 (154)-
 00-033-0664 (*) - Hematite, syn - Fe2O3 - Y: 15.73 % - d x by: 1. - WL: 1.5406 - Rhombo.H.axes - a 5.03560 - b 5.03560 - c 13.74890 - alpha 90.000 - beta 90.000 - gamma 120.000 - Primitive - R-3
 00-041-1486 (*) - Anorthite, ordered - CaAl2Si2O8 - Y: 156.09 % - d x by: 1. - WL: 1.5406 - Triclinic - a 8.17560 - b 12.87200 - c 14.18270 - alpha 93.172 - beta 115.911 - gamma 91.199 - Primitive -
 00-041-1483 (I) - Augite, aluminian - Ca(Mg,Fe+3,Al)(Si,Al)2O6 - Y: 80.20 % - d x by: 1. - WL: 1.5406 - Monoclinic - a 9.74280 - b 8.89420 - c 5.27230 - alpha 90.000 - beta 106.111 - gamma 90.000

Clay sample



Clay sample 950 °C

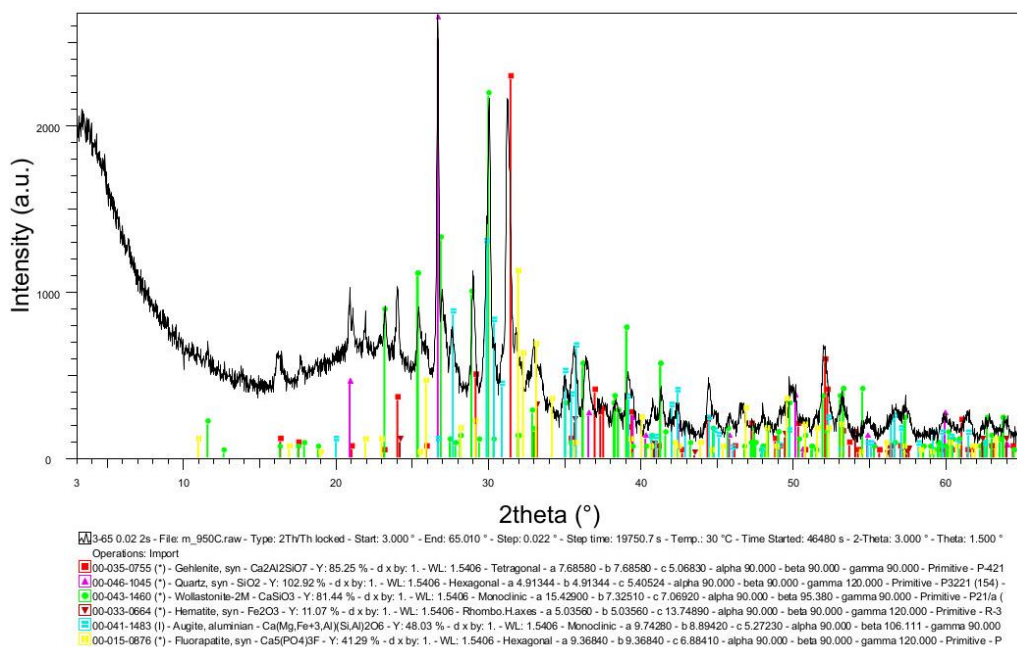


Table 27: Summary of XRD results, before and after the re-firing at 950 °C.

EB II - Sample KB.06.E.706/1	
Non-heated	Calcite + quartz + illite + apatite
Heated	Gehlenite + wollastonite + quartz + apatite
EB IIIB - Sample KB.11.B.1054/12	
Non-heated	Calcite + quartz + illite + hematite
Heated	Quartz + gehlenite + anorthite + hematite + wollastonite
EB IV - Sample KB.06.B.383/7	
Non-heated	Anorthite + quartz + gehlenite + augite + calcite
Heated	Anorthite + quartz + augite + gehlenite + hematite
Geological sample	
Non-heated	Quartz + calcite + barite + apatite + aragonite + augite + gehlenite + illite + hematite
Heated	Quartz + gehlenite + wollastonite + augite + apatite + hematite

4.7 Chemical analysis

Major, minor (in wt.%) and some trace elements (ppm) contents of the analyzed potteries from Khirbet al-Batrawy site are reported in Table 28. The average values and relative standard deviations for each phase of urbanization are also given.

The CaO content, ranging from 11.32 to 32.75% (average 19.56%), is above 6% in all the analyzed samples. This result indicates the calcareous character of Khirbet pottery (Maniatis and Tite, 1981). The contents of fluxes (e.g., K₂O, Fe₂O₃, CaO, MgO and TiO₂) are >9%, allowing the classification of the clays as low refractory clays (Maniatis and Tite, 1981, Musthafa *et al.*, 2010).

The samples show high variability of the contents of SiO₂ as the values range from 23.19 to 55.84%.

The contents of Fe₂O₃ and Al₂O₃ also vary from 2.95% to 8.1% and from 6.08% to 18.41%, respectively. The highest Fe₂O₃ concentrations were measured in sherds KB.05.B.146/24, KB.10.B.1040/8, KB.11.B.1124/24, KB.06.B.383/7, KB.11.B.1054/12, KB.10.B.1054/62 and KB.06.B.167/4. The sherds KB.06.E.703/5, KB.06.B.383/7, KB.05.A.84/3 and KB.05.B.136/5 contain the highest amount of Al₂O₃.

In all analyzed samples a moderate contents of Na₂O (0.31%-1.06%) and high concentrations of K₂O (1.71-4.36%) have been found. The highest values of calcium are detected in samples KB.05.5/D200, KB.06.E.703/5 and KB.10.B.1040/8.

MgO concentrations varies between 0.65% and 4.34%, with the highest values detected in samples KB.06.B.167/4 and KB.09.B.820/12.

MnO content varies between 0.02% and 0.09%, and the concentrations of TiO₂ and P₂O₅ range from 0.56% to 1.3% and from 0.16% to 0.78% respectively. In the analyzed sherds no significant variations of the concentrations of these elements have been observed, with the exception of sample KB.06.E.706/1 whose P₂O₅ content does not fall within the above range.

Table 285: The concentrations of major, minor (in wt.%) and some trace elements (in ppm) contents of the analyzed potteries obtained by chemical analysis.

Analyte Symbol	SiO ₂	Al ₂ O ₃	Fe ₂ O ₃	MnO	MgO	CaO	Na ₂ O	K ₂ O	TiO ₂	P ₂ O ₅	LOI
EB II											
KB.06.E.703/5	40.06	17.14	5.25	0.03	1.30	14.48	0.84	4.17	0.66	0.33	15.93
KB.06.E.703/6	30.84	11.72	4.21	0.04	1.64	28.93	0.83	3.02	0.54	0.52	17.99
KB.06.E.704/6	55.84	13.12	4.69	0.06	2.11	11.32	0.65	3.16	0.66	0.43	8.51
KB.06.E.706/1	23.19	7.53	2.95	0.02	0.65	32.75	0.61	1.71	0.38	3.00	26.26
EB IIIA											
KB.05.B.136/5	43.92	17.50	5.95	0.06	1.57	18.35	0.69	3.68	0.90	0.49	7.55
KB.05.B.146/24	45.03	15.74	6.86	0.06	2.74	14.09	0.57	2.84	1.29	0.78	10.22

Analyte Symbol	SiO ₂	Al ₂ O ₃	Fe ₂ O ₃	MnO	MgO	CaO	Na ₂ O	K ₂ O	TiO ₂	P ₂ O ₅	LOI
EB IIIA											
KB.06.B.167/4	38.99	14.33	8.10	0.08	4.34	19.94	1.02	2.27	1.14	0.36	9.62
KB.06.B.427/1	28.54	6.08	3.19	0.05	1.32	30.27	0.48	2.77	0.48	0.28	26.36
KB.09.B.820.12	25.29	7.94	4.23	0.02	3.65	26.15	0.60	3.18	0.59	0.30	26.64
EB IIIB											
KB.10.B.1040/8	44.49	18.40	6.62	0.06	1.52	14.46	0.57	4.17	0.86	0.28	8.38
KB.11.B.1054/12	35.73	14.15	6.13	0.03	1.49	18.47	0.60	2.89	0.59	0.37	19.13
KB.10.B.1054/62	35.90	14.70	6.19	0.02	1.90	18.54	0.54	2.89	0.56	0.38	18.41
KB.11.B.1124/24	40.14	16.22	6.12	0.05	1.60	15.90	0.98	3.97	0.73	0.22	14.45
EB IV											
KB.05.A.84/3	40.65	17.77	6.20	0.04	1.85	18.02	0.31	2.93	0.75	0.47	11.76
KB.05.A.6b/1	40.38	12.38	5.89	0.09	1.30	17.19	0.59	2.69	0.89	0.16	18.88
KB.05.5/D200	42.27	12.45	4.85	0.07	2.47	17.02	1.06	4.36	0.70	0.40	14.81
KB.06.B.383/7	45.78	18.41	6.36	0.05	2.32	16.71	0.68	2.92	0.93	0.45	5.97
Average	38.65	13.86	5.52	0.05	1.99	19.56	0.68	3.15	0.74	0.54	15.35
SD	8.18	3.84	1.35	0.02	0.91	6.17	0.20	0.71	0.24	0.65	6.75
clay1	37.85	5.28	2.78	0.07	3.68	23.92	1.40	3.20	0.56	2.01	18.83
clay2	38.37	5.32	2.73	0.07	3.63	23.59	1.44	3.25	0.57	1.92	18.73
Brick	11.92	3.56	1.56	0.03	4.36	39.57	0.16	1.20	0.21	0.15	36.83

Analyte Symbol	Sc	Be	V	Cr	Co	Ni	Zn	Cd	S	Cu	Ag	Pb	Ga	Ge	As	Rb	Sr	Y	Zr	Nb	Mo	In	Sn	Sb
KB.06.E.703/5	17.0	2.0	172.0	120.0	13.0	46.0	104.0	0.7	0.2	23.0	0.3	5.0	19.0	1.0	6.0	60.0	200.0	15.0	102.0	10.0	3.0	0.2	2.0	0.5
KB.06.E.703/6	12.0	2.0	135.0	90.0	6.0	23.0	64.0	0.5	0.4	25.0	0.3	5.0	14.0	1.0	16.0	38.0	565.0	14.0	92.0	10.0	2.0	0.2	1.0	0.5
KB.06.E.704/6	14.0	2.0	118.0	90.0	11.0	26.0	59.0	0.5	0.1	12.0	0.5	5.0	15.0	1.0	5.0	62.0	284.0	18.0	123.0	9.0	2.0	0.2	2.0	0.5
KB.06.E.706/1	9.0	1.0	137.0	420.0	2.0	159.0	346.0	3.0	0.3	81.0	0.9	6.0	9.0	1.0	13.0	17.0	632.0	37.0	77.0	7.0	8.0	0.2	1.0	1.2
KB.05.B.136/5	19.0	2.0	141.0	120.0	16.0	46.0	81.0	0.5	0.2	19.0	0.3	8.0	21.0	1.0	14.0	67.0	251.0	20.0	141.0	14.0	2.0	0.2	6.0	0.5
KB.05.B.146/24	15.0	3.0	140.0	130.0	16.0	39.0	41.0	0.5	0.1	15.0	0.8	39.0	24.0	1.0	7.0	39.0	297.0	34.0	462.0	53.0	2.0	0.2	3.0	0.5
KB.06.B.167/4	18.0	2.0	178.0	220.0	29.0	107.0	82.0	0.5	0.1	24.0	0.3	5.0	17.0	2.0	8.0	36.0	335.0	16.0	116.0	13.0	2.0	0.2	1.0	0.5
KB.06.B.427/1	7.0	1.0	63.0	100.0	6.0	45.0	73.0	0.6	0.1	21.0	0.3	5.0	8.0	1.0	5.0	29.0	95.0	16.0	139.0	11.0	2.0	0.2	1.0	0.5
KB.09.B.820.12	7.0	1.0	326.0	50.0	4.0	27.0	80.0	0.5	0.2	14.0	0.3	5.0	10.0	1.0	6.0	44.0	255.0	9.0	102.0	16.0	12.0	0.2	1.0	0.5
KB.10.B.1040/8	18.0	2.0	150.0	120.0	15.0	39.0	78.0	0.5	0.1	11.0	0.3	8.0	20.0	1.0	7.0	69.0	237.0	18.0	136.0	13.0	2.0	0.2	1.0	0.5
KB.11.B.1054/12	12.0	2.0	280.0	90.0	7.0	56.0	119.0	2.4	0.1	33.0	0.3	5.0	14.0	1.0	20.0	36.0	178.0	16.0	121.0	12.0	17.0	0.2	1.0	1.0
KB.10.B.1054/62	11.0	1.0	311.0	80.0	5.0	45.0	90.0	1.1	0.1	32.0	0.3	5.0	15.0	1.0	11.0	35.0	211.0	12.0	98.0	11.0	10.0	0.2	1.0	0.5
KB.11.B.1124/24	16.0	2.0	123.0	110.0	15.0	38.0	80.0	0.5	0.3	10.0	0.3	7.0	19.0	1.0	8.0	47.0	270.0	15.0	118.0	12.0	2.0	0.2	1.0	0.5
KB.05.A.84/3	17.0	2.0	178.0	150.0	15.0	53.0	99.0	0.5	0.1	21.0	0.3	7.0	20.0	1.0	9.0	67.0	395.0	15.0	122.0	11.0	3.0	0.2	2.0	0.5
KB.05.A.6b/1	13.0	2.0	114.0	100.0	16.0	51.0	67.0	0.6	0.1	22.0	0.3	10.0	16.0	1.0	10.0	47.0	239.0	23.0	245.0	18.0	2.0	0.2	2.0	0.5
KB.05.5/D200	13.0	2.0	140.0	90.0	12.0	32.0	45.0	0.5	0.2	10.0	0.3	9.0	15.0	1.0	7.0	65.0	259.0	22.0	150.0	11.0	3.0	0.2	1.0	0.5
KB.06.B.383/7	19.0	2.0	141.0	130.0	15.0	41.0	91.0	0.5	0.2	15.0	0.3	10.0	21.0	2.0	7.0	60.0	330.0	20.0	163.0	16.0	2.0	0.2	2.0	0.5
Average	13.9	1.8	167.5	130.0	11.9	51.4	94.1	0.8	0.2	22.8	0.4	8.5	16.3	1.1	9.4	48.1	296.1	18.8	147.5	14.5	4.5	0.2	1.7	0.6
DS	3.9	0.5	71.6	83.1	6.5	33.4	67.9	0.7	0.1	16.6	0.2	8.1	4.5	0.3	4.2	15.6	132.6	7.2	89.2	10.3	4.5	0.0	1.3	0.2
clay1	6.0	1.0	67.0	90.0	6.0	40.0	178.0	3.6	0.3	42.0	0.3	8.0	7.0	1.0	5.0	17.0	847.0	17.0	42.0	9.0	5.0	0.2	1.0	0.5
clay2	6.0	1.0	64.0	80.0	6.0	38.0	159.0	3.4	0.3	36.0	0.4	5.0	7.0	1.0	5.0	18.0	798.0	18.0	43.0	9.0	5.0	0.2	1.0	0.5
brick	4.0	1.0	58.0	30.0	1.0	13.0	25.0	0.5	0.1	7.0	0.3	5.0	4.0	1.0	5.0	18.0	461.0	6.0	56.0	3.0	2.0	0.2	1.0	0.5

Cs Ba La Ce Pr Nd Sm Eu Gd Tb Dy Ho Er Tm Yb Lu Hf Ta W Tl Bi Th U

6.09 ± 0.88%) and TiO₂ (0.49 ± 0.08 with respect to 0.82 ± 0.21%). Sample KB.05.5/D200 (Group 2) shows the highest contents of K₂O (4.36%) and Na₂O (1.06%) among all the analyzed fragments, while sample KB.06.E.706/1 (Group 1) has the highest P₂O₅ value (3%).

Table 29: Major and minor (in wt.%) elements (in ppm) contents of the analyzed potteries obtained by chemical analysis divided into the two groups identified. Average values and relative standard deviations for group are also given.

Samples	SiO ₂	Al ₂ O ₃	Fe ₂ O ₃	MnO	MgO	CaO	Na ₂ O	K ₂ O	TiO ₂	P ₂ O ₅
Group 1										
KB.06.E.703/6	30.840	11.720	4.210	0.036	1.640	28.930	0.830	3.020	0.538	0.520
KB.06.E.706/1	23.190	7.530	2.950	0.021	0.650	32.750	0.610	1.710	0.379	3.000
KB.06.B.427/1	28.540	6.080	3.190	0.047	1.320	30.270	0.480	2.770	0.480	0.280
KB.09.B.820.12	25.290	7.940	4.230	0.019	3.650	26.150	0.600	3.180	0.585	0.300
Average	26.965	8.318	3.645	0.031	1.815	29.525	0.630	2.670	0.496	1.025
SD	2.939	2.082	0.581	0.011	1.118	2.382	0.126	0.573	0.077	1.144
Clay1	37.850	5.280	2.780	0.071	3.680	23.920	1.400	3.200	0.560	2.010
Clay2	38.370	5.320	2.730	0.070	3.630	23.590	1.440	3.250	0.565	1.920
Group 2										
KB.06.E.703/5	40.060	17.140	5.250	0.025	1.300	14.480	0.840	4.170	0.664	0.330
KB.06.E.704/6	55.840	13.120	4.690	0.062	2.110	11.320	0.650	3.160	0.660	0.430
KB.05.B.136/5	43.920	17.500	5.950	0.060	1.570	18.350	0.690	3.680	0.904	0.490
KB.05.B.146/24	45.030	15.740	6.860	0.055	2.740	14.090	0.570	2.840	1.290	0.780
KB.06.B.167/4	38.990	14.330	8.100	0.082	4.340	19.940	1.020	2.270	1.144	0.360
KB.10.B.1040/8	44.490	18.400	6.620	0.062	1.520	14.460	0.570	4.170	0.861	0.280
KB.10.B.1054/62	35.900	14.700	6.190	0.021	1.900	18.540	0.540	2.890	0.557	0.380
KB.11.B.1054/12	35.730	14.150	6.130	0.029	1.490	18.470	0.600	2.890	0.589	0.370
KB.11.B.1124/24	40.140	16.220	6.120	0.050	1.600	15.900	0.980	3.970	0.725	0.220
KB.05.A.84/3	40.650	17.770	6.200	0.035	1.850	18.020	0.310	2.930	0.749	0.470
KB.05.A.6b/1	40.380	12.380	5.890	0.086	1.300	17.190	0.590	2.690	0.885	0.160
KB.05.5/D200	42.270	12.450	4.850	0.068	2.470	17.020	1.060	4.360	0.702	0.400
KB.06.B.383/7	45.780	18.410	6.360	0.053	2.320	16.710	0.680	2.920	0.931	0.450
Average	42.245	15.562	6.093	0.053	2.039	16.499	0.700	3.303	0.820	0.394
SD	5.176	2.194	0.879	0.021	0.826	2.374	0.217	0.678	0.214	0.151

Concerning trace elements all samples show a quite homogeneous compositions making difficult to distinguish any grouping. However, a variability in the amounts of Zr,

Ni, Cr, Sr e Ba has been observed. In particular, the higher amount of Cr is observed in sample KB.06.E.706/1 (420 ppm) and KB.06.B.167/4 (220 ppm) (the other samples show values ranging from 50 to 150 ppm), the same samples show high values of Ni content (159 and 107 ppm, respectively) (the other samples range from 23 to 56 ppm). KB.06.E.706/1 and KB.06.E.703/6 samples are characterized by high amount of Sr, whereas sample KB.06.B.427/1 shows low content of Sr. High values of Zr are detected in samples KB.05.B.146/24 and KB.05.A.6b/1. Finally, also the amount of Ba shows a strong variability, but it is not considered as being probably affected by post burial contamination processes (Maggetti, 2001).

Considering the chemical data of REE (rare earth elements), the chondrite-normalized REE patterns (Sun and McDonough, 1989) for representative ceramic samples (Fig. 44) show an enrichment in light REE (LREE) respect to the heavy REE (HREE). Moreover, the overall REE patterns of Khirbet al-Batrawy ceramics correspond to the composition of mafic rocks outcropping in the area (Shaw *et al.*, 2003; Mouthfti *et al.*, 2012 and references therein) further supporting the hypothesis of a local supply of the raw material.

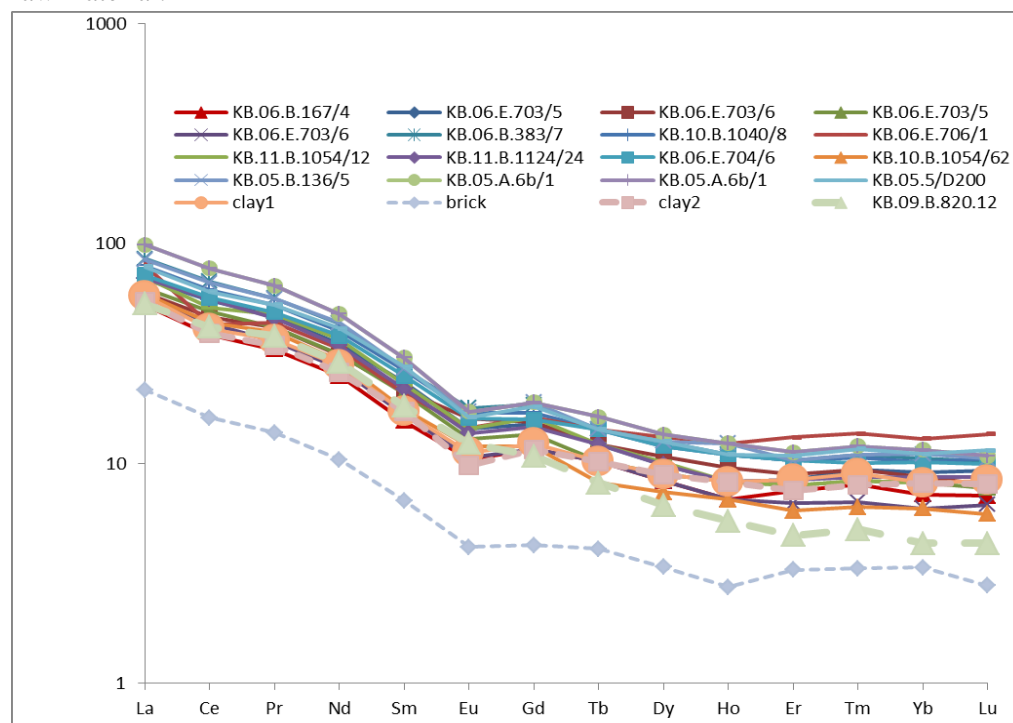


Figure 44: Chondrite-normalized REE patterns for representative ceramic samples from Khirbet al-Batrawy (normalization factor from Sun and McDonough, 1989).

4.7.1 Statistical analysis of data

Multivariate statistical techniques were commonly used to define groups among ceramic sherds with different chemical composition, and to develop a classification on the basis of the historical period or pottery type. Thus providing an additional instrument respect the usual archaeological stylistic classification (e.g., Hart and Adams, 1983; Aruga *et al.*, 1993; Mirti *et al.*, 1995; Mirti *et al.*, 1998). Moreover, the statistical approach can be useful to identify the provenance of pottery sherds comparing their chemical composition to that of the clay material collected near the archaeological site or to previously studied groups (Mirti *et al.*, 1990; Neff, 1992; Mirti *et al.*, 1994; Castellano *et al.*, 1996).

In this study, statistical analysis was performed on chemical composition of matrix of twenty-three elements as proposed by Djingova *et al.* (1990) and Kuleff and Djingova (1996) with the addition of Ga, Nb, Y, K, P and Zn of seventeen ceramic samples, of two samples of clay material and of one sample collected from a brick. In particular, the starting data set was deprived of some chemical components, in particular P_2O_5 and Ba, as they could have been affected by post burial contamination processes (Maggetti, 2001). Afterwards, data were log10 transformed in order to avoid deleterious effects of scale effects of clustering results (e.g., V-shaped chemical data; Aruga, 2003).

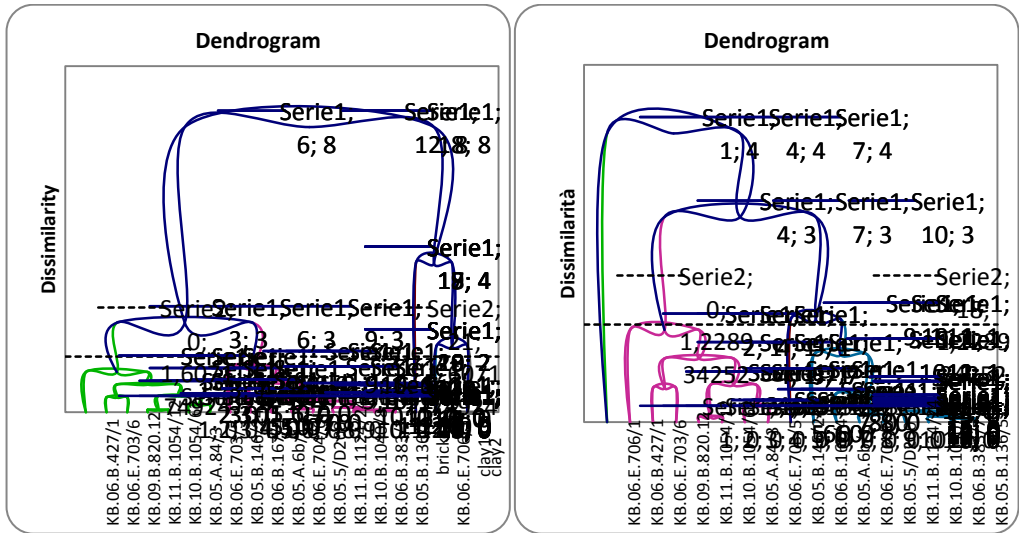
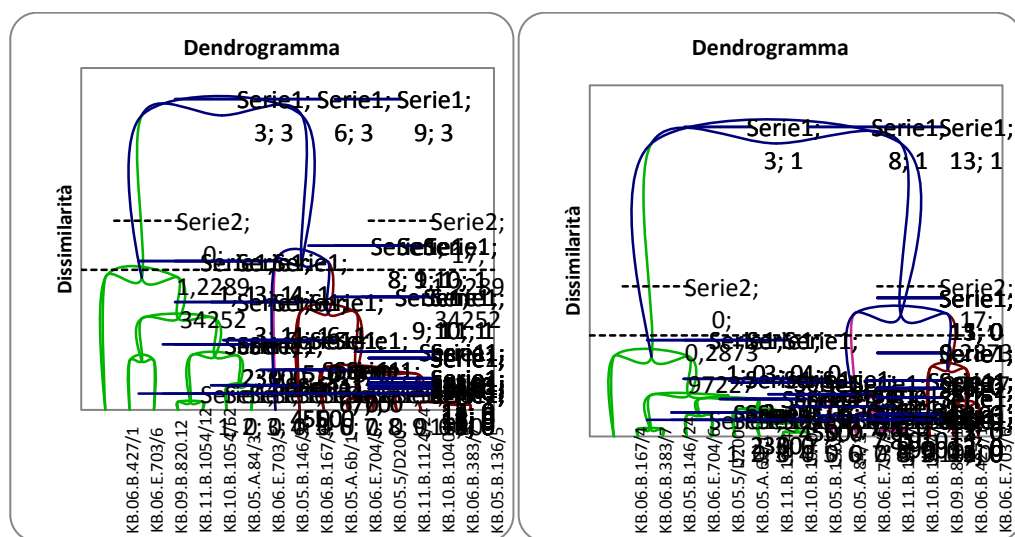


Figure 4514: Hierarchical clustering dendrogram representation (average method, euclidean distance) based on the chemical composition of (a) pottery sherds, clay material and brick samples and (b) only pottery sherds.

The dendrogram of (Fig. 45) resulting from the Hierarchical Clustering Analyses (*average* method, *euclidean* distance) enabled to distinguish four groups clearly related to the four periods of urbanization of Khirbet al-Batrawy.

The analysis performed on the total numbers of samples (Fig. 45a) shows that the composition of the clay materials and the brick is clearly different from that of the ceramic production, suggesting a different source of the raw material for the pottery from Batrawy. In this view, a new dataset, excluding clay samples and brick, was considered for a cluster analysis. Basing on the previous dendrogram that showed sample KB.06.E.706/1 in the same cluster with brick and clay samples, as expected, the resulting dendrogram (Fig. 45b) shows that sample KB.06.E.706/1 has to be considered as an outlier and to be excluded in the statistical analysis (Baxter, 1999). The cluster analysis was performed again considering: a) the contents of major and minor elements (Fig. 46a), b) only the values of major elements (Fig. 46b) and c) only those of trace elements (Fig. 46c).



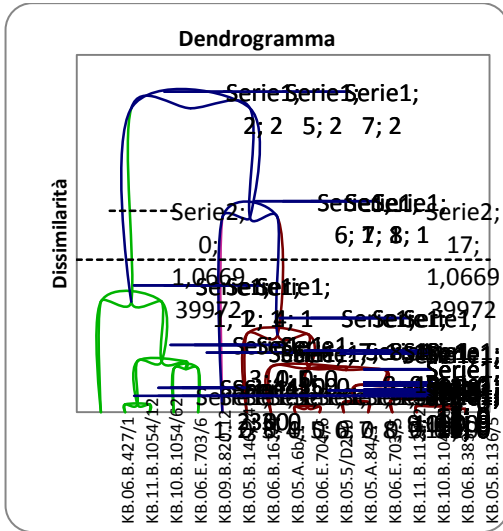


Figure 4615: Hierarchical clustering dendrogram representation (average method, euclidean distance) based on (a) the major and trace element chemical composition (b) only the values of major elements and (c) only the values of trace elements of pottery sherds excluding the outlier sample KB.06.E.706/1.

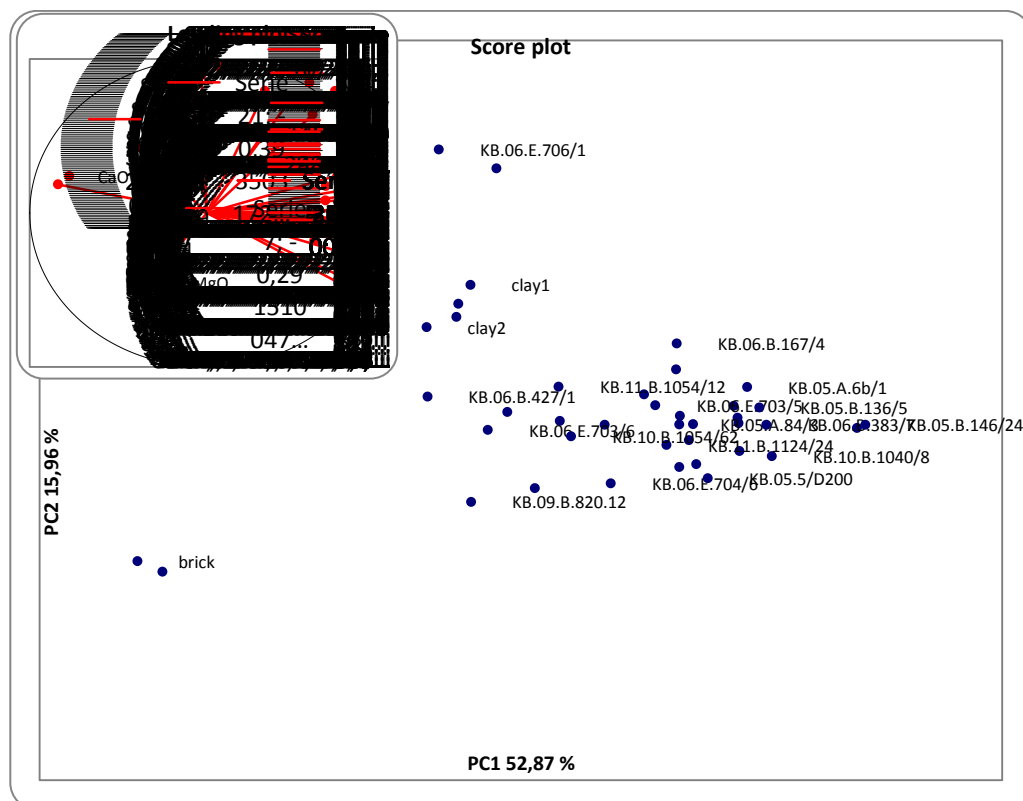
In our case, the clusters identified in the dendrograms do not reflect the historical differences between the sherds or the different pottery type. For this reason the analysis was performed only using the data of the major elements in order to individuate possible chemical groups connected to the pottery type (Fig. 46b). Also in this case, three clusters have been identified; however, differences in the contents of major elements of the ceramics are so little marked by not allowing to distinguish the different ceramic productions. This finding further supports the use of the same, or very similar, raw material for all the workshops. The statistical analysis of trace elements data for these ceramics also did not lead to significantly different clusters and interpretations (Fig. 46c). Therefore, it seems that a calcareous clay raw material has been used by workshops throughout their different operations.

To further simplify statistical procedures, PCA was carried out.

The loading plot provides information about the chemical elements that mainly contribute in the differentiation among samples and, consequently, the correlation existing among the original variables and the samples. The first six PCs together explain 93.43% of the total variance of the system (Table 30), where PC1 and PC2 represent 52.87% and 15.96% of the total variance, respectively.

Table 30: Results of PCA performed on dataset.

	PC1	PC2	PC3	PC4	PC5	PC6
Value	14.80	4.47	2.74	2.03	1.11	1.02
Variability (%)	52.87	15.96	9.77	7.24	3.95	3.64
Cumulative variance (%)	52.87	68.83	78.60	85.84	89.79	93.43

**Figure 4716:** Score and loading plot of PCA model obtained using the results of chemical analysis on pottery sherds, clay material and brick samples.

In Fig. 47 the score plot in PC1 versus PC2, explaining the 68.83% of the total variance, is reported.

With the exception of the outlier KB.06.E.706/1 (Baxter, 1999), the scores plot shows a different chemical composition between the clay, the brick and the pottery samples. In particular, the brick present a high content in MgO and the lowest level of CaO. In order to prove the different provenance, PCA analysis was performed only on trace elements that are the markers of clay materials. As shown in Fig. 48, the results are almost very close to those obtained for major elements. With the exception of the out-

lier, clay material and the brick are located out of the pottery circle, highlighting different chemical composition and different provenance.

In order to analyze in detail the different ceramic samples to identify possible groups, the original data set was deprived of clay and brick data. The new score plot in PC1 versus PC2 (Fig. 48) explains the 63.15% of the total variance.

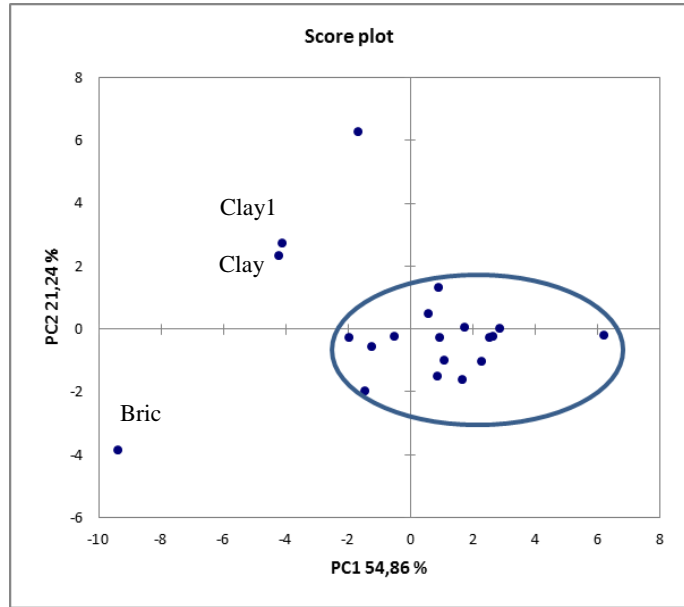


Figure 17: Score plot of PCA model obtained using the trace elements of pottery sherds, clay material and brick samples.

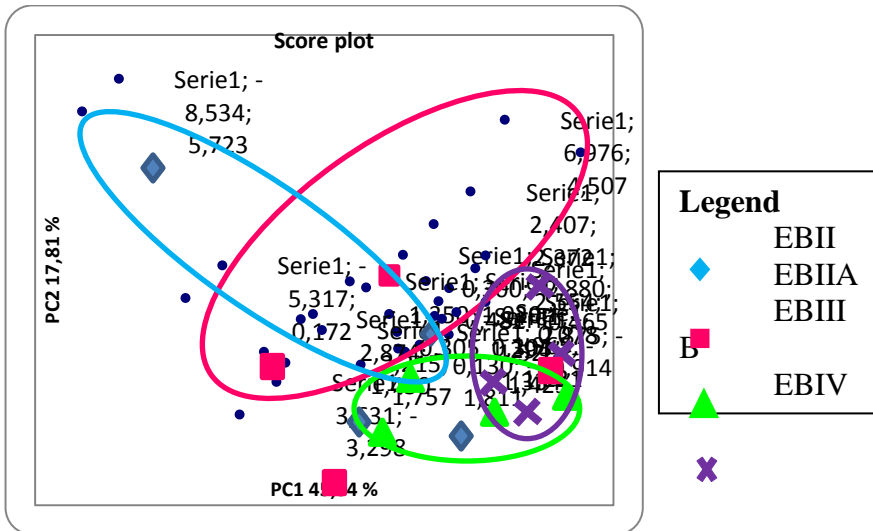


Figure 4918: Score plot of PCA model obtained using the results of chemical analysis on pottery sherds.

As expected, in the plot of Fig. 49 the sample KB.06.E.706/1 is an outlier (Baxter, 1999), and for this reason it has been excluded and the PCA was performed again.

The new PCA plot (Fig. 50) provides information useful to discuss about the relationships between chemical composition, historical phases and destination-type of ceramic.

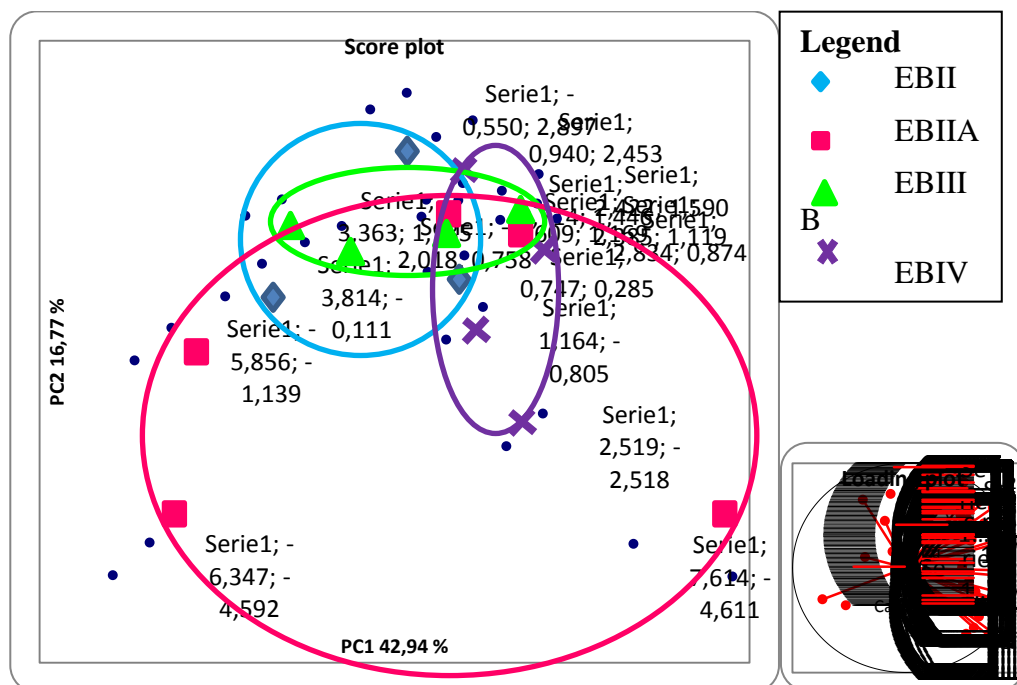


Figure 50: Score and loading plot of PCA model obtained using the results of chemical analysis on pottery sherds divided into the four periods of Batrawy urbanization, excluding the outlier sample KB.06.E.706/1.

The score plot in PC1 versus PC2 (Fig. 50) explains the 59.71% of the total variance of the system. The low values of percentage reflect a low degree of variability in chemical composition among the samples, suggesting the probable use of the same raw material in the pottery production.

The diagram shows the distribution of pottery samples respect to the historical phases they belong to. In particular, the EB IIIA phase is characterized by a major variability in chemical composition respect to the other phases. This result probably is connected to a great experimentation in the pottery production regarding shapes and the choice of materials attested in this phase. Indeed, the need to experiment different procedures and materials in the pottery production is coherent to the development from a small settlement to the city of Batrawy that took place in the EB IIIA. Furthermore, this variability has not been observed in the other phases. In this view, the EB II phase was the moment of the establishment of Batrawy and the need of an improvement in pot-

References

- Aruga R., Mirti P., Casoli A. (1993): Application of multivariate chemometric techniques to the study of Roman pottery (terra sigillata). *Analytica chimica acta*, **276**, 197-204.
- Baratto C., Lottici P.P., Bersani D., Antonioli G., Gnappi G., Montenero A. (1998): Sol-Gel preparation of α -Fe₂O₃ thin films: Structural characterization by XAFS and Raman. *Journal of Sol-Gel Science and Technology*, **13**, 667-671.
- Barilaro D., Barone G., Crupi V., Donato M.G., Majolino D., Messina G., Ponterio R. (2005): Spectroscopic techniques applied to the characterization of decorated potteries from Caltagirone (Sicily, Italy). *Journal of Molecular Structure*, **744-747**, 827-831.
- Bartholomew P.R. (2013): Comparing the success rate of Raman spectroscopy and powder XRD for routine mineral identification. *Geostandards and Geoanalytical Research*, **37**, 353-359.
- Bersani D., Lottici P.P., Lopez T., Ding X. (1998): Raman scattering study of PbTiO₃ and TiO₂ obtained by sol-gel. *Journal of Sol-Gel Science and Technology*, **13**, 849-853.
- Bersani D., Lottici P.P., Montenero A. (1999): Micro-Raman investigation of iron oxide films and powders produced by sol-gel syntheses. *Journal of Raman Spectroscopy*, **30**, 355-360.
- Bersani D., Lottici P.P., Montenero A. (2000): A micro-Raman study of iron-titanium oxides obtained by sol-gel synthesis. *Journal of Material Science*, **35**, 4301-4305.
- Bouchard M., Smith D.C. (2003): Catalogue of 45 reference Raman spectra of minerals concerning research in art history or archaeology, especially on corroded metals and coloured glass. *Spectrochimica Acta Part A: Molecular and Biomolecular Spectroscopy*, **59**, 2247-2266.
- Burdon D.J. (1959): Government of the Hashemite Kingdom of Jordan, pp. 82.
- Castellano A., D'innocenzo A., Pagliara C., Raho F. (1996): Composition and origin of Iapygian pottery from Roca Vecchia, Italy. *Archaeometry*, **38**, 59-65.
- Catalano I.M., Genga A., Laganara C., Laviano R., Mangone A., Marano D., Traini A. (2007): Lapis lazuli usage for blue decoration of polychrome painted glazed pottery: a recurrent technology during the Middle Ages in Apulia (Southern Italy). *Journal of archaeological science*, **34**, 503-511.
- Chopelas A. (1991): Single crystal Raman spectra of forsterite, fayalite, and monticellite. *American Mineralogist*, **76**, 1101-1109.
- De Benedetto G.E., Fabbri B., Gualtieri S., Sabbatini L., Zambonin P.G. (2005): FTIR-chemometric tools as aids for data reduction and classification of pre-Roman ceramics. *Journal of Cultural Heritage*, **6**, 205-211.
- De Benedetto G.E., Laviano R., Sabbatini L., Zambonin P.G. (2002): Infrared spectroscopy in the mineralogical characterization of ancient pottery. *Journal of Cultural Heritage*, **3**, 177-186.
- De Faria D.L.A., Lopes F.N. (2007): Heated goethite and natural hematite: Can Raman spectroscopy be used to differentiate them? *Vibrational Spectroscopy*, **45**, 117-121.
- De Faria D.L.A., Venâncio Silva S., de Oliveira M.T. (1997): Raman microspectroscopy of some iron oxides and oxyhydroxides. *Journal of Raman Spectroscopy*, **28**, 873-878.
- Djingova R., Kuleff I., Penev I. (1990): Instrumental neutron activation analysis of reference materials for archaeometric investigations of pottery. *Journal of radioanalytical and nuclear chemistry*, **144**, 397-406.
- Edwards H.G.M., Drummond L., Russ J. (1999): Fourier transform Raman spectroscopic study of prehistoric rock paintings from the Big Bend Region, Texas. *Journal of Raman Spectroscopy*, **30**, 421-428.

- Han R., Shimamoto T., Hirose T., Ree J.H., Ando J. (2007): Ultralow friction of carbonate faults caused by thermal decomposition. *Science*, **316**, 878-881.
- Hart F. A., Adams S. J. (1983): The chemical analysis of romano-british pottery from the Alice Holt forest, Hampshire, by means of Inductively-Coupled Plasma emission spectrometry. *Archaeometry*, **25**, 179-185.
- Kuleff I., Djingova R. (1996): Provenance study of pottery: choice of elements to be determined. *Revue d'archéométrie*, **20**, 57-67.
- Laviano R., Muntoni I.M (2003): Pulo di Molfetta. Analisi archeometriche. in "Modellare l'argilla. Vasai del Neolitico antico e medio nelle Murge pugliesi". Istituto Italiano di Preistoria e Protostorica, Florence, 143-159.
- Legodi, M.A., de Wall D. (2007): Raman spectroscopic study of ancient South African domestic clay pottery. *Spectrochimica Acta Part A*, **66**, 135-142.
- Lofrumento C., Zoppi A., Castellucci E.M. (2004): Micro-Raman spectroscopy of ancient ceramics: a study of French sigillata wares. *Journal of Raman Spectroscopy*, **35**, 650-655.
- Maggetti M. (2001): Chemical analyses of ancient ceramics: What for?. *CHIMIA International Journal for Chemistry*, **55**, 923-930.
- Maniatis Y., Tite M. S. (1981): Technological examination of Neolithic-Bronze Age pottery from central and southeast Europe and from the Near East. *Journal of Archaeological Science*, **8**, 59-76.
- McMillan P. (1984): Structural studies of silicates glasses and melts – applications and limitations of Raman spectroscopy. *American Mineralogist*, **69**, 622-644.
- Mirti P., Aceto M., Ancona M. P. (1998): Campanian pottery from ancient Bruttium (southern Italy): scientific analysis of local and imported products. *Archaeometry*, **40**, 311-329.
- Mirti P., Aruga R., Appolonia L., Casoli A., Oddone M. (1994): On the role of major, minor and trace elements in provenancing ceramic material. A case study: Roman terra sigillata from Augusta Praetoria. *Fresenius' journal of analytical chemistry*, **348**, 396-401.
- Mirti P., Aruga R., Zelano V., Appolonia L., Aceto M. (1990): Investigation of Roman terra sigillata by atomic absorption and emission spectroscopy and multivariate analysis of data. *Fresenius' journal of analytical chemistry*, **336**, 215-221.
- Mirti P., Casoli A., Barra Bagnasco M., Preacco Ancona M.C. (1995): Fine ware from Locri Epizephiri: a provenance study by inductively coupled plasma emission spectroscopy. *Archaeometry*, **37**, 41-51.
- Moufti M.R., Moghazi A.M., Ali K.A. (2012): Geochemistry and Sr–Nd–Pb isotopic composition of the Harrat Al-Madinah Volcanic Field, Saudi Arabia. *Gondwana Research*, **21**, 670-689.
- Munsell, (1975): Munsel Soil Color Charts. Color Munsell ed., Macbeth Division of Kallmorgen Corporation, Baltimore.
- Murad E. (1997): Identification of minor amounts of anatase in kaolins by Raman spectroscopy. *American Mineralogist*, **82**, 203-206.
- Musthafa A.M., Janaki K., Velraj G. (2010): Microscopy, porosimetry and chemical analysis to estimate the firing temperature of some archaeological pottery shreds from India. *Microchemical Journal*, **95**, 311-314.
- Omori K. (1971): Analysis of the infrared absorption spectrum of diopside. *American Mineralogist*, **56**, 1607-1616.
- Penel G., Leroy G., Rey C., Sombret B., Huvenne J. P., Bres E. (1997): Infrared and Raman microspectrometry study of fluor-fluor-hydroxy and hydroxy-apatite powders. *Journal of Materials Science: Materials in Medicine*, **8**, 271-276.

- Pimenta M.A., Dresselhaus G., Dresselhaus M.S., Cançado L.G., Jorio A., Saito R. (2007): Studying disorder in graphite-based systems by Raman spectroscopy. *Physical Chemistry Chemical Physics*, **9**, 1276-1291.
- Porto S.P.S, Krishnan R.S (1967): Raman Effect of Corundum. *Journal of Chemical Physics*, **47**, 1009-1012.
- Redhammer G.J., Roth G. (2002): Structural variations in the aegirine solid-solution series (Na,Li)FeSi₂O₆ at 298–80. *Zeitschrift für Kristallographie - Crystalline Materials*, **217**, 63-72.
- Richet P., Mysen B.O., Ingrin J. (1998): High-temperature X-ray diffraction and Raman spectroscopy of diopside and pseudowollastonite. *Physics and Chemistry of Minerals*, **25**, 401-414.
- Sabbatini L., Tarantino M.G., Zambonin P.G., De Benedetto G.E. (2000): Analytical characterization of paintings on pre-Roman pottery by means of spectroscopic techniques. Part II: Red, brown and black colored shards. *Fresenius Journal of Analytical Chemistry*, **366**, 116-124.
- Sendova M., Zhelyaskov V., Scalera M., Ramsey M. (2005): Micro-Raman spectroscopic study of pottery fragments from the Lapatsa Tomb, Cyprus, ca 2500 BC. *Journal of Raman Spectroscopy*, **36**, 829-833.
- Shaw J.E., Baker J.A., Menzies M.A., Thirlwall M.F., Ibrahim K.M. (2003): Petrogenesis of the largest intraplate volcanic field on the Arabian Plate (Jordan): a mixed lithosphere-asthenosphere source activated by lithospheric extension. *Journal of Petrology*, **44**, 1657-1679.
- Smith, G.D., Clark R.J.H. (2004): Raman microscopy in archaeological science. *Journal of Archaeological Science*, **31**, 1137-1160.
- Sun S.S., McDonough W. (1989): Chemical and isotopic systematics of oceanic basalts: implications for mantle composition and processes. Geological Society, London, Special Publications, **42**, 313-345.
- Thibeau R.J., Brown C.W., Heidersbach R.H. (1978): Raman Spectra of Possible Corrosion Products of Iron. *Applied Spectroscopy*, **32**, 532-535.
- Thierry D., Persson D., Leygraf C., Delichere D., Joiret S., Pallotta C., Hugot-Le Goff A. (1988): In-Situ Raman Spectroscopy Combined with X-Ray Photoelectron Spectroscopy and Nuclear Microanalysis for Studies of Anodic Corrosion Film Formation on Fe-Cr Single Crystals. *Journal of The Electrochemical Society*, **135**, 305-310.
- Tite M.S., Freestone I.C., Meeks N.D., Bimson M. (1982): The use of scanning electron microscopy in the technological examination of ancient ceramics. In "Archaeological Ceramics", ed. Olin J.S., Franklin A.D., Smithsonian Institution Press, Washington DC, 109-120.
- Tite M.S., Maniatis Y. (1975): Examination of ancient pottery using the scanning electron microscope. *Nature*, **257**, 122-123.
- Tomisaka T., Iishi K. (1980): Some aspects of the lattice dynamics of diopside. *Mineralogical Journal (Japan)*, **10**, 84-96.
- Turner-Walker G., Syversen U. (2002): Quantifying histological changes in archaeological bones using BSE-SEM image analysis. *Archaeometry*, **44**, 461-468.
- Wei M., Evans J. H., Bostrom T., Grøndahl L. (2003): Synthesis and characterization of hydroxyapatite, fluoride-substituted hydroxyapatite and fluorapatite. *Journal of materials science: materials in medicine*, **14**, 311-320.
- Williams K.P.J., Wilcock I.C., Hayward I.P., Whitney A. (1996): Applications of state-of-the-art Raman microscopy an direct Raman imaging, Progr. in corrosion, mineralogy, and materials research. *Spectroscopy (Eugene Oreg.)*, **11**, 45-50.

- Whitbread I.K. (1986): The characterization of Argillaceous Inclusions in Ceramic Thin Sections. *Archaeometry*, 28, 79-88.
- Whitbread I.K. (1995): Greek transport amphorae: a petrological and archaeological study. British School at Athens, Fitch Laboratory Occasional Paper 4, Athens, pp. 453.
- Zhang M., Redhammer G.J., Salje E.K.H., Mookherjee M. (2002): LiFeSi₂O₆ and NaFeSi₂O₆ at low temperatures: an infrared spectroscopic study. *Physics and Chemistry of Minerals*, **29**, 609-616.
- Zhang M., Salje E.K.H., Farnan I., Graeme-Barber A., Daniel P., Ewing R.C., Clark A.M., Leroux H. (2000): Metamictization of zircon: Raman spectroscopic study. *Journal of Physics: Condensed Matter*, 12, 1915-1925.

5. DISCUSSION

Commonly, the investigation of archaeological pottery has been focused on two main aspects: to explore the technological process of pottery production and to provide information about the nature and provenance of raw materials (Cultrone *et al.*, 2001; Barone *et al.*, 2002; Sherriff *et al.*, 2002; Maritan, 2004; Rathossi *et al.*, 2004; Iordanis *et al.*, 2009; Tschegg, 2009; Velraj *et al.*, 2009; Belfiore *et al.*, 2010). For this reason, the discussion chapter has been divided into two paragraphs: “Technological level of production” and “Provenance”.

The investigation of pottery technology gives an overall picture about ancient societies through the use and the level of the pottery production knowledge. Potters engage in a series of action (the choice of a particular material, the collection of clay, forming and firing and finally the decoration of the pottery) that is defined “chaîne opératoire” and reflects the level of material knowledge and broader social identities.

Potters can decide to use unique clay or a mix of different clays on the basis of the properties of the material or the destination of use. They can also add tempers to increase the workability of the raw material or to decrease the firing temperature or in connection to the shape and dimensions of the final product. Also, the choice of particular inclusions rather than others can give information about the level of technology of ancient cultures.

Firing conditions can be analyzed to infer the maximum firing temperature reached during the production at that time and give information about the places where pottery was fired.

The second important aspect in the analysis of archaeological pottery is to distinguish locally manufactured pottery from those imported and to define the provenance of the raw material and in particular the clay used in the production. This aspect of the investigation allows to discriminate pottery produced in different places and different local workshops.

5.1 Technological level of production

The results obtained with different analytical methodologies and reported in the previous chapters are here discussed in order to reconstruct the technological aspects of pottery production.

5.1.1 Mineralogical phases and petrographic composition

According to the results of mineralogical characterization (Appendix C), the ceramic from the archaeological site of Khirbet al-Batrawy seems to have a similar mineralogical, petrographic and chemical composition over the different historical periods and

among the different types of pottery. The potsherds are mainly composed by different amounts of quartz and calcite. The occurrence of such minerals in large amounts may be explained considering them as primary minerals present in the starting raw materials as component of clays and/or as tempers voluntarily added by potters (Maggetti, 1982) to improve the workability preventing cracking of the material or to give a properly features for a distinctive use of the product.

Quartz is a very common constituent of numerous rocks types and, being very resistant to weathering, generally occurs in small amounts in natural clay deposits and in archeological ceramic made from them (Quinn, 2013); therefore, its addition by potters as temper is difficult to be confirmed (Papachristodoulou *et al.*, 2006).

Optical microscopy analysis of Batrawy ceramic allowed to identify different forms of calcite (i.e., crystalline, micritic and sparry calcite); moreover, as constituent of fragments of fossils (shells) and fragments of sedimentary rocks (marl and chert) have also been observed. Probably calcite was present in clays as inclusions, deriving by weathering process of limestones and marls outcropping in the area, as well as tempers added by the potters. In this view, the abundant fragments of fossils observed in thin sections suggest a probable use of marls in the raw material.

Calcite could be preferred as a temper over quartz, especially in the manufacturing of tableware (Papachristodoulou *et al.*, 2006), as calcium carbonate temper generally ensures a thermal shock resistance necessary for objects exposed to repeated heating and cooling cycles during use (Tite *et al.*, 2001; Papachristodoulou *et al.*, 2006). Calcite also plays an important role in the flux decreasing of the refractory nature of clay, allowing the decreasing of firing temperature. In particular, high percentages of calcite inclusions identified in thin section by the optical study have been observed in fragments of Kitchen Ware and Khirbet Kerak Ware suggesting that the pottery from Khirbet al-Batrawy presented high thermal shock resistance and were probably fired at low temperatures.

Alkali feldspar, deriving from igneous and metamorphic rocks outcropping in the Khirbet al-Batrawy area, occurs in the studied pottery as inclusions in the original clays or tempers voluntarily added by ancient potters. However, the low abundance and diffusion of this mineral phase support the hypothesis that K-feldspar crystals were naturally included in the original clays.

The occurrence of hematite in the ceramic matrix was related to the mineralogical composition of the starting clay minerals used (e.g., Hradil *et al.*, 2003), or as the result of reactions that take place during firing in oxidizing atmosphere (Nodari *et al.*, 2007). The diffuse presence of hematite in the studied pottery has been confirmed by the identification in thin sections of diffuse iron nodules. Wieder and Adan-Bayewitz (1999) have reported that such nodules were also added as temper in cases where the

initial material was rich in carbonates, apparently in order to improve the properties of the raw material used in pottery production. The use of hematite iron ore is known from numerous archaeological contexts as inclusions in the coating of pottery for giving color during firing or as a flux for smelting (Higham, 1996). However, iron nodules are commonly natural constituents of clay and are abundant identified in archaeological pottery (Gilead and Goren, 1989; Goren, 1995; Goren, 1996; Goren *et al.*, 2001; Quinn, 2013). Considering the calcareous composition of the sherds, the presence of iron nodules may be connected to both the nature of the original clay material or to a precise choice of potters.

Apatite, barite, gypsum, zircon, ilmenite, rutile, anatase, manganese oxides, corundum, lazurite, olivine, pyroxenes have been identified as rare mineral phases and represent natural aplastic inclusions in clays. Indeed, hydroxides, oxyhydroxides and oxides of iron, aluminum and manganese are the most common accessory minerals found in clays (Brindley and Brown, 1980); in particular the presence of zircon can be considered an important indicator of the provenance of the raw material (Tochilin *et al.*, 2012). Commonly, its occurrence in clay materials could be related to alteration processes of igneous and metamorphic rocks. In this view, the presence of zircon in the studied pottery sherds further supports the hypothesis that sediments of the Pre-Cambrian basement were involved as raw clayey materials in the ceramic production at Khirbet al-Batrawy. Ilmenite is an accessory mineral typical of igneous and metamorphic rocks and its occurrence in the studied pottery could be explained assuming the contribution of the basaltic rocks outcropping nearby the site in the formation of the clays used for the production of the ceramic. Furthermore, the occurrence of rare crystals of olivine could be explained as minerals present in the basaltic rocks of the Jordan area (Burdon, 1959). Barite and gypsum can be considered as accessory minerals of the raw material, being common minerals in sedimentary rocks.

Among the aplastic inclusions identified in thin section, grog (crushed pottery or tiles) and fragments of basaltic rocks also occur in ceramic sherds of the different historical periods.

In the majority of the sherds, minor amounts of illite have been found by means of FTIR and XRD analysis indicating a starting raw material mainly composed by an illitic clay.

Chemical analysis by SEM-EDS pointed out that the chemical composition of the matrix is characterized by high amounts of Si and Al and minor contents of K, Na, Mg, Ca and Fe and it is generally similar in all the analyzed sherds. Minor compositional differences are attributable to the Ca and Fe contents which sometimes differentiate some samples belonging to the same phase of Batrawy development.

The chemical composition of the potsherds is strictly connected to the source of the clays and the other materials used for production. In this view, the amounts of Si, Al, Ca, Mg, Fe and K confirm the presence of aluminosilicates, quartz, iron oxides and feldspars in the raw material.

The mineralogical composition of ceramics was matched to the definition of shapes and size of inclusions. The shape of inclusions was used in the past (Cuomo di Caprio, 2007) with the purpose to define tempers voluntarily added by potter from those naturally present in the clay as a residue from the original rocks from which the clay developed by weathering. In this view, rounded inclusions were associated to natural inclusions of the clay, whereas those with angular shape to tempers added to improve the workability. Nowadays (Cuomo di Caprio, 2007) this distinction has not been used yet because it is difficult to distinguish whether coarse grains have been voluntarily added or were already being part of the clay. In this view, only the presence of grog can be identified as temper voluntarily added to the clay, showing an advanced knowledge that consider the role of grog in the workability of the clay.

In the studied pottery, microscopic analysis shows that the inclusions are usually coarse sized and are distributed in an unimodal grain size suggesting no evidences of purification process or selection of the raw material by the potters. Furthermore, the high variability of manufacturing, supported by the identification of eleven different *fabrics*, suggests that the raw clayey materials used to produce the Batrawy pottery did not undergo any purification before the use. Indeed, the final result of the purification process is a sort of standardized matrix, without coarse inclusions that prevent the possibility to identify the provenance of pottery. The absence of purification in the preparation of the raw material is associate to a low quality of manufacturing. This hypothesis is further supported by the diffuse presence of clay pallets representing lumps of the base clay used to produce these ceramics and not adequately mixed in the phase of forming.

Porosity of the ceramic body is similar between the *fabrics* (a lower percentage of porosity has been observed only in Fabric E-*fine calcite*) and it is probably due to a low time of mixing and modeling which prevented the removal of air from the clay.

The shape of the voids is usually irregular, elongated and parallel to the walls, sometimes rounded in the central part of the section. *Vughs* can exhibit a preferred alignment parallel to each other and to the margins of the sections, which might be related to the phase of drying or forming. The contemporary presence of *vughs* and vesicles and their position in the section, in the external and internal parts respectively, support the hypothesis of mixed technique of hand and potter's wheel. Furthermore, the absence of any orientation of the minerals in thin section confirms that the intensity of shaping the pot on the potters' wheel was low.

The results of the optical microscopy study show that pottery fragments belonging to the four different periods can be grouped in different *fabrics* that occurred during the time (Figs. 1-2). The distinction allow us to speculate on the relationship between shape and pottery type and the *fabric* identified by microscopic analysis.

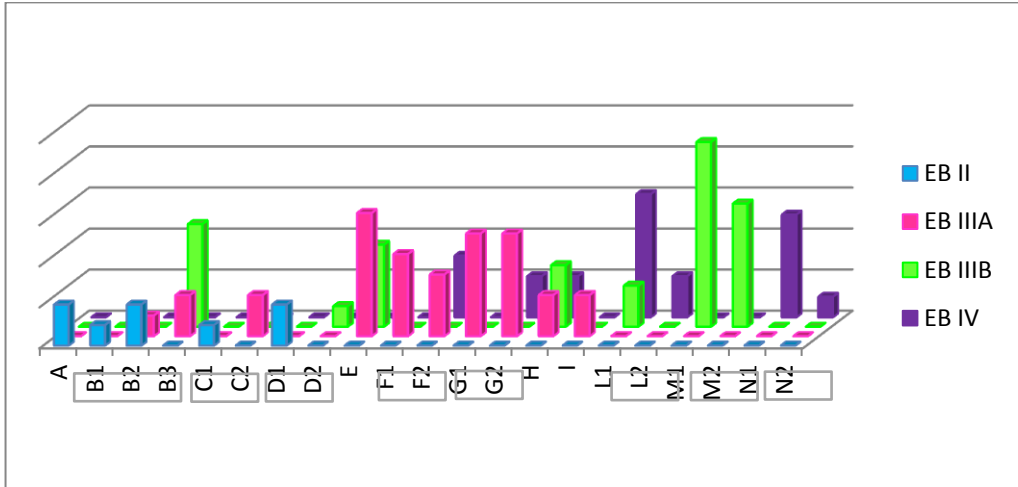


Figure 1: Diagram showing the distribution of the *fabrics* identified by OM in the four phases of Khirbet al-Batrawy urbanization.

The Fabric A-*calcite, micritic and sparry calcite with vesicles* has been identified in EB II phase in the fragments of Red Burnished platters.

Fabric B-*clay pallets and fragments of grog* has been recognized in the pottery of the first three phases of urbanization for jars and *pithoi* belonging to Simple and Storage Ware. Three subgroups (B1, B2 and B3), based on the different percentage of elongated *vughs* and on the aspect of the matrix, have been recognized. A general reduction of *vughs*, in the later phases of urbanization of the city, is due to a better pottery production and a minor content of clayey material in the matrix, suggesting a major control and an increasing of firing temperature in the more recent phases.

Fabric C-*calcite and clay pallets* has been observed in ceramics of EB II and EB IIIA phases. The fragments of this *fabric* are mainly represented by pottery of Red Burnished and Red Polished Ware.

The Fabric D-*crystals of calcite* is observed in EB II and EB IIIB phases in fragments of Red Burnished Ware.

Fabric E-*fine calcite* has been observed only in EB III phases in fragments of jugs and jars. Fabric F-*fossils and sedimentary rocks* has been observed in EB IIIA and EB IV in platters, jugs and jars.

Fabric G-*basaltic rocks and fragments of fossils* has been observed for the EB IIIA and EB IV phases in ceramic fragments belonging to Red Polished Ware, Simple Polished Ware and Khirbet Kerak Ware.

Fabric H-*clay pallets, calcite and iron oxides* has been observed in Simple and Storage jars and *pithoi* of EB IIIA, EB IIIB and EB IV phases.

Fabric I- *shells* is the *fabric* of hole-mouth pot, belonging to the class of Kitchen Ware.

Fabric L-*calcite and micritic calcite* has been observed in EB IIIB and EB IV phases for jars (Storage Ware) and pots (Kitchen Ware).

Particular is Fabric M-*micritic, calcite and sedimentary rocks* that is attested only in the EB IIIB phase.

Finally, Fabric N-*clay pallets and rare calcite* with *mega-vughs* is attested for jars belonging to EB IV phase.

The results of microscopic analysis allow to speculate about the relationship between *fabrics* and the evolution of the pottery production. Indeed, during the first phase EB II a minor variability in the *fabrics* have been observed, suggesting a start-up of the pottery production in Batrawy. In particular, Fabric A-*calcite, micritic and sparry calcite with vesicles*, Fabric C-*calcite and clay pallets* and Fabric D-*crystals of calcite* are observed in the Red Burnished and Polished Ware, whereas Fabric B-*clay pallets and fragments of grog* to Simple and Storage Ware. The major variability in *fabrics* has been observed in EB IIIA that can be explained with the diffuse experimentation of materials and procedures applied in this phase. In this view, the difficulties to correlate Fabric E-*fine calcite*, Fabric F-*fossils and sedimentary rocks* and Fabric G-*basaltic rocks and fragments of fossils* to a specific pottery types can be explained as a diffuse experimentation of material and technology. The Fabric I-*shells*, with its particular features very different respect to the others, is included in this context of experimentation and testing that characterized this period. In the EB IIIB a sort of standardization and selection was observed, as a minor number of *fabrics* have been identified and connected to precise pottery types. Fabric E-*fine calcite*, present in different pottery types in EB IIIA, is associated only to Red Burnished Ware. Fabric H-*clay pallets, calcite and iron oxides*, Fabric L-*calcite and micritic calcite* and in particular Fabric M-*micritic, calcite and sedimentary rocks*, the typical *fabric* of EB IIIB production, are associated to the diffuse production of Simple and Storage Ware shapes. In EB IV phase, no evidence of experimentation has been observed, and the number of *fabrics* decreases maintaining the association between *fabrics* and pottery types occurring in EB IIIB phase.

The distinction of different *fabrics* allows to discriminate the coarser pottery usually used for storage function from the finer pottery typical of small jars, jugs or fine ce-

ramic, suggesting an aware choice due to the final destination. Moreover, Storage Ware fragments present a major chemical variability respect to the Simple Ware fragments, suggesting a minor care in the choice of the used material and proportion between clay and inclusions.

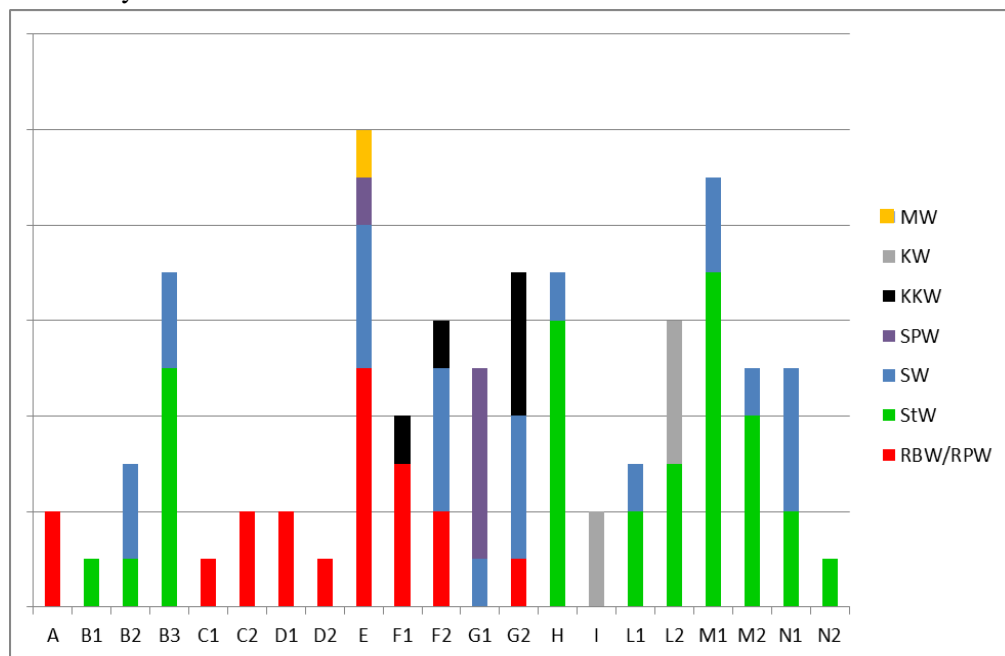


Figure 2: Diagram showing the distribution of the *fabrics* identified by OM respect to the type of pottery.

The low values of the variance percentage, obtained in the statistical treatment of FTIR data, further supports the hypothesis of a very limited variability in the mineralogical composition of sherds belonging to different historical periods. The scores plot (Figs. 20-21, chapter 4), shows that the majority of samples are grouped into an unique cluster, highlighting that samples are characterized by the same composition. The score plot that consider the different pottery type allow to attribute KKW samples to the same local production of the Khirbet al-Batrawy ceramic industry. This finding allows to infer that the technological process and the raw material used in the production of ceramic probably did not change during the phases of Batrawy urbanization. Even if no changes in the supply of raw material and technology have been observed, the high variability of *fabrics* suggest that the raw materials (clay and inclusions) were selected on the basis of the pottery function and destination. However, during the long history of Batrawy only a low increasing in the technology has been observed.

On the basis of the results of the present study it is possible to infer that the raw material used by the potters at Khirbet al-Batrawy was an illitic clay containing quartz, calcite, feldspars and minor amounts of iron oxides and hydroxides. It is noteworthy that the statistical analysis of chemical data highlights that the chemical composition of the bricks used in the walls of the city is clearly different from that of the pottery fragments. This finding indicates a different choice in the raw material used in pottery production from that used in the production of building materials.

The variability of *fabrics* suggests that the raw materials, i.e. clay/inclusions ratio, were selected on the basis of the pottery function, although no changes in the supply of raw material and technology have been observed. The general similarity in the mineralogical composition of pottery, confirmed by the statistical analysis performed on spectroscopic and chemical results, supports the hypothesis that during the history of the city the technological background did not apparently evolve. However, the analysis of *fabrics* allows to draw a whole picture about the evolution of technology in pottery production. The process is characterized by an initial research and study of materials and shape, continuing through a major and diffuse experimentation in the use of materials and procedures of modeling, to finish with a sort of standardization and selection with specific features to satisfy the request and necessity of a particular production.

5.1.2 Firing

In order to define the firing conditions, the evaluation of time of heating, temperature and redox state of the atmosphere are needed.

Commonly, archaeologists discriminate between “kiln firing” to “open firing” (Bonfire or Pit) (Rye, 1981; Tite, 1995; Kingery, 1997). “Kiln firing” includes structures with a firebox and it is assumed a high maximum firing temperature, slow heating rates, long permanence times and variable redox conditions which are usually oxidizing (Maritan *et al*, 2006). The term “open firing” generally indicates every other type of structures. Bonfire is characterized by open firing with vases surrounded by fire, whereas the Pit presents ceramics put into a hole with fuel that surrounds the vases.

The Bonfire procedures present much more difficulties in the maintenance of temperature rather than the Pit (Maggetti *et al*, 2011). Conversely, Pit firing is characterized by low maximum firing temperature, fast heating rates and short duration of firing, usually in reducing conditions (Rye, 1981; Gosselain, 1992). In this view, the “firing methodology” applied is mainly influenced by the structure used and the ceramic products obtained by these two types of “firing” are characterized by different firing features.

5.1.2.1 Maximum firing temperatures

The firing phase deeply modifies the mineral composition of the worked raw material. Indeed, the decomposition of clays involves a series of reactions with the “free compounds”, deriving these latter from the breakdown of tempers or inclusions, to form new mineral phases that depend on the nature of the raw material, the maximum firing temperature and the oxygen fugacity during heating process.

A preliminary information about low or high firing temperatures can be obtained by the results of optical microscopy in thin section and in particular by the analysis of the optical state of clay minerals in cross-polarized light illumination. In the case of Khirbet al-Batrawy pottery, the observation of the change (activity) of matrix color during the rotation of the stage can be an indicator of a pottery fired at temperatures below 850 °C.

Experimental data on thermal transformations during firing have been treated using FTIR by many authors (Russel, 1987; Murad and Wagner, 1998; Venkatachalapathy *et al.*, 2002; Madajova, 2003; Manoharan *et al.*, 2007; Venkatachalapathy *et al.*, 2010). FTIR spectra obtained for the Khirbet al-Batrawy potteries have been compared to the results of the above data treatments to investigate the structure, bonding and chemical properties of clay minerals.

Usually, during firing the expandable layer silicate of clay materials collapses; the band at 915 cm^{-1} , connected to Al(OH) vibrations in the octahedral sheet structure, decreases with the increasing temperature to disappear at about 500 °C (Hlavavy *et al.* 1977; Ramasamy and Kamalakkannan, 1987). The destruction of the clay structure is generally marked by the appearance of a broad symmetric band at 1030 cm^{-1} for the red clay and at 1080 cm^{-1} for white clay (Ghosh, 1978).

In our FTIR spectra no samples showed the absorption band at 915 cm^{-1} , suggesting that probably they have been fired at temperature above 500 °C (Velraj *et al.*, 2009; Venkatachalapathy *et al.*, 2010). According to Mendelovici *et al.* (1979) the absorption band around 3630 cm^{-1} is due to crystalline hydroxyl groups which remain only up to 800 °C. The absence of hydroxyl bands at 3630 cm^{-1} and the presence of a broad symmetric band centered around 1030 cm^{-1} in almost all the FTIR spectra of the studied potteries indicate that the samples have been fired above 800°C and are made up of disordered clay (Venkatachalapathy *et al.*, 2010).

Another method to estimate the maximum firing temperature by FTIR results, proposed by Shoval (1994) and Damjanovi *et al.* (2010), is based on the identification of the position of the broad Si-O stretching bands at about 1000 cm^{-1} due to the contributions from various silicate minerals. Indeed, Si-O vibrations in the distorted SiO_4 tetrahedra in amorphous phases and structural changes, that are produced during firing, can broaden this band. Shoval (1994) found that the maximum of the Si-O band shifts

with the increase of the firing temperature. In particular, at 700 °C a single peak with the maximum at 1042 cm⁻¹ was found, at 800 °C two maxima were observed at 1050 and 1078 cm⁻¹ and at 900 °C a single band appeared at 1082 cm⁻¹. Damjanovi *et al.* (2010) in the analysis of the medieval pottery excavated at Stari (Serbia) confirmed and further improved the results investigating the Si-O stretching shift at different temperatures. At 100 °C the maximum was observed at 1026 cm⁻¹, at 1036 cm⁻¹ at 600 °C and at 1038 cm⁻¹ at 700 °C. A splitting of the band was observed at 800 °C at 1043 cm⁻¹ and 1076 cm⁻¹, whereas a single band was found at 900 °C at 1082 cm⁻¹ and at 1000 °C at 1082 cm⁻¹.

The tentative assignments of FTIR peaks to vibrational band of quartz are shown in Table 1. On the basis of Si-O stretching bands position, the spectra of Khirbet al-Batrawy fragments can be divided into two groups: the first characterized by the typical Si-O stretching band at 1080 cm⁻¹ and the second showing the splitting of the band at 1050 and 1080 cm⁻¹. According to the literature data it is possible to hypothesize a firing temperature above 800 °C for the samples showing the Si-O stretching band at 1080 cm⁻¹; on the contrary, the samples with the band split at 1050 and 1080 cm⁻¹ could be related to a lower firing temperature, estimated at about 800 °C.

Table 1: Assignments of FTIR peaks to vibrational bands of quartz of pottery samples (* standard peaks associated to quartz; sh = shoulder).

Quartz	Si-O stretching						
	1160-1165	1080-1082	1050	797	778	693-695	512
EB II							
KB.06.B.392/8	sh	1080	-	797	779	695	512
KB.06.E.703/5	sh	1080	1052	796	779	694	-
KB.06.E.703/6	1060	1080	-	799	779	696	510
KB.06.E.702/10	1060	1080	1051	798	779	696	-
KB.06.E.704/1	sh	1080	-	797	778	694	-
KB.06.E.704/6	sh	1080	1053	797	777	695	510
KB.06.E.706/2	sh	1080	1050	798	779	695	-
KB.06.E.706/1	sh	1080	1050	797	778	695	-
EB IIIA							
KB.05.A.58/1	1161	1079	1054	796	778	694	516
KB.05.A.64/1	1161	1079	1049	796	778	694	513
KB.05.B.126/1	1163	1079	1050	796	778	694	516
KB.05.B.126/3	1162	1079	1050	796	778	694	516
KB.05.B.136/3	1160	1081	-	796	778	696	-
KB.05.B.146/1	1162	1079	1050	796	778	694	516
KB.05.B.146/5	-	1079	1050	-	-	-	-
KB.05.B.146/7	1160	1080	1054	797	778	696	-
KB.05.B.146/8	1160	1079	1050	-	-	-	511

KB.05.B.146/15	1160	1079	1049	797	781	694	513
KB.05.B.146/24	1160	1079	1052	797	778	694	516
KB.06.B.167/4	1160	1080	1053	797	778	694	516
KB.06.B.413/2	1160	1080	-	797	778	694	-
KB.06.E.701/2	1160	1080	1046	797	778	696	515
KB.06.E.703/3	1160	1080		797	778	696	515
KB.06.B.427/1	1160	-	-	797	779	-	507
Quartz		Si-O stretching					
STD*	1160-1165	1080-1082	1050	797	778	693-695	512
KB.08.B.805/6	1160	1080	1050	797	778	696	516
KB.09.B.820/10	1160	1080	-	797	778	696	512
KB.09.B.820/12	1160	1080	-	797	778	696	514
KB.09.B.820/13	1160	1080	-	797	778	696	510
KB.08.B.805/32	1160	1080	1050	797	778	696	515
KB.08.B.805/34	1160	1080	1048	797	778	696	511
EB III B							
KB.05.A.204/3	1165	1080	1046	798	777	694	511
KB.06.A.120/6	1162	1083	-	799	778	696	506
KB.11.B.1054/21	1162	1080	-	799	778	696	518
KB.10.B.1054/24	1162	1080	-	799	778	696	509
KB.10.B.1054/62	1162	1080	-	799	778	696	500
KB.11.B.1124/3	1162	1080	1049	799	778	696	515
KB.11.B.1124/8	1162	1080	1047	799	778	696	509
KB.11.B.1124/15	1162	1080	1051	799	778	696	510
KB.11.B.1124/29	1162	1079	1047	799	778	696	508
KB.11.B.1124/33	-	1080	1046	799	778	696	510
KB.11.B.1128/50	1162	1080	1047	799	778	696	509
KB.11.B.1128/51	1162	1080	-	799	778	696	509
KB.11.B.1126/65	1162	1080	1046	799	778	696	511
EB IV							
KB.05.A/D200	1166	1080	1050	798	777	694	511
KB.05.A.18/5	1160	1079	1053	798	777	694	512
KB.05.A.6b/1	1164	1080	1046	798	777	694	518
KB.05.A.21/27	-	1080	-	798	777	694	-
KB.05.A.31/2	-	1080	1046	798	777	694	516
KB.05.A.62/1	1162	1080	1055	798	777	694	516
KB.05.A.68/2	1161	1080	1049	798	777	694	511
KB.05.A.82/4	1164	1079	1050	798	777	694	513
KB.05.A.84/3	1168	1080	-	798	777	694	511
KB.05.A.88/1	1162	1080	1047	798	777	694	-
KB.05.A.96/1	1166	1080	1048	798	777	694	513
KB.05.A.98/1	1161	1080	1056	798	777	694	512
KB.06.A.ø/18	1164	1079	-	798	777	694	512

It is also possible to estimate the maximum firing temperature considering the mineralogical assemblages identified in the pottery fragments and comparing the results to those obtained by experimental works (Riccardi *et al.*, 1999; Aras, 2004; Maritan *et al.*, 2005, 2006).

The distinction between primary minerals, newly formed minerals and secondary minerals connected to the burial environment using XRD allowed to recognize the following mineral assemblages in the pottery from Khirbet al-Batrawy (Table 2).

Table 2: Mineralogical assemblages and relative firing temperature estimated taking into account the thermal decomposition of the minerals, divided into the four periods of urbanization of Khirbet al-Batrawy. Temperatures below 900 °C can be inferred for the mineralogical assemblages without hematite, diopside and gehlenite; the occurrence of hematite moves the value of temperature in the range 750-900 °C, in the range 800-900 °C when gehlenite occurs and in the range 850-900 °C when diopside is present.

EBII	
calcite + quartz ± feldspars	<900 °C
calcite + quartz + gehlenite + hematite ± feldspars ± gypsum	800-900 °C
calcite + quartz + illite + hematite ± feldspars ± gypsum	750-900 °C
EBIIIA	
calcite + quartz + illite + gehlenite + diopside + hematite ± feldspars	800-900 °C
calcite + quartz + illite + gehlenite + diopside + hematite ± feldspars ± epidote	850-900 °C
calcite + quartz + illite ± feldspars ± epidote	<900 °C
calcite + quartz + illite + hematite ± feldspars	750-900 °C
quartz + gehlenite + diopside + hematite ± feldspars ± gypsum	900-1050 °C
EBIIIB	
calcite + quartz + illite + hematite ± feldspars	750-900 °C
calcite + quartz + illite + gehlenite + hematite ± feldspars ± gypsum	800-900 °C
calcite + quartz + gehlenite + diopside + hematite ± feldspars	850-900 °C
calcite + quartz + illite ± feldspars	<900 °C
EBIV	
calcite + quartz + illite + hematite ± feldspars	750-900 °C
calcite + quartz + illite + hematite + gehlenite + diopside ± feldspars ± epidote	850-900 °C
calcite + quartz + illite + gehlenite + hematite ± feldspars ± epidote	800-900 °C
calcite + quartz + illite ± feldspars ± epidote	<900 °C
quartz + gehlenite + hematite ± feldspars ± gypsum ± epidote	900-1050 °C

The number of mineralogical phases present in a ceramic material is much higher than those predict by Gibbs' Phase Rule; moreover, a rapid heating (very likely in the ancient ceramic materials) induces significant overstepping in minerals reactions, preventing the formation of stable mineralogical phases and facilitating the formation

of metastable ones. Therefore, the reactions that take place between tempers and clay minerals during firing are not at the equilibrium conditions, but the compositional differences from site to site create “microsites” in which local equilibria produce different mineral assemblages. Considering that at constant values of variables, starting from different compositions, different mineralogical assemblages are formed (Riccardi *et al.*, 1999; Cultrone *et al.*, 2001; Nodari *et al.*, 2007), a preliminary estimation of firing temperature has been proposed interpreting the mineralogical data and comparing them to literature data.

In particular, the presence or absence of specific minerals can be used as indicator to define the maximum firing temperatures. In this work, information about the maximum firing temperatures has been obtained taking into account the presence or absence of primary calcite, hematite, illite, diopside and gehlenite in the studied samples.

The decomposition of calcite follows the reaction (1) for small sized crystals (Shoval, 2003) and, producing free CO₂, determines a loss in weight of about 12%, and in turn the formation of secondary porosity that can be filled, at high temperature, by neo-formed silicates minerals (Duminuco *et al.*, 1998).



In this view, calcite is an important indicator of firing temperature: its thermal decomposition into CaO and CO₂ begins around 650 °C and it is completed at about 900 °C (710-950 °C in O’Gorman and Walker, 1973; 850° C in Duminuco *et al.*, 1998, Maritan *et al.*, 2006, Maritan *et al.*, 2007; 650-800 °C in Trinitade *et al.*, 2009). At the upper limit temperature, at about 850-900 °C (Riccardi *et al.*, 1999; Maritan *et al.*, 2006; Trinitade *et al.*, 2009) the process results in the formation of calcium silicate or calcium aluminum silicates, such as gehlenite and pyroxenes.

The identification of calcite with the typical features of primary phases in the studied samples allows to estimate the firing temperature in a range below the temperature of thermal decomposition of calcite. This results is confirmed by the optical inactivity of clay matrix which suggest a firing temperature lower than 850 °C.

Minor amounts of illite have been found in the sherds from Khirbet al-Batrawy. Clay minerals, such as illite, are dehydrated by the removal of the hydroxyl groups of the silicate lattice at temperature ranging between 459 and 900 °C (Jordàn *et al.*, 1999; Iordanidis *et al.*, 2009).

In the upper temperature range, between 800 and 900 °C, the free CaO reacts with silica and alumina, from the breakdown of clay minerals, to form calcium silicates such as diopside and wollastonite and calcium aluminum silicates such as anorthite and

gehlenite (Duminuco *et al.* 1998; Riccardi *et al.* 1999; Aras, 2004; Rathossi and Pontikes, 2010; Barone *et al.*, 2011; Shoal and Nathan, 2011).

The estimation of firing temperature needs to consider the mineralogical and chemical composition of the original clays. The results of chemical analysis of Khirbet al-Batrawy pottery suggest that the clay material was Ca-enriched thus, the products of the thermal reactions can be identified considering the ACS diagram (quartz-calcite-corundum, Fig. 3).

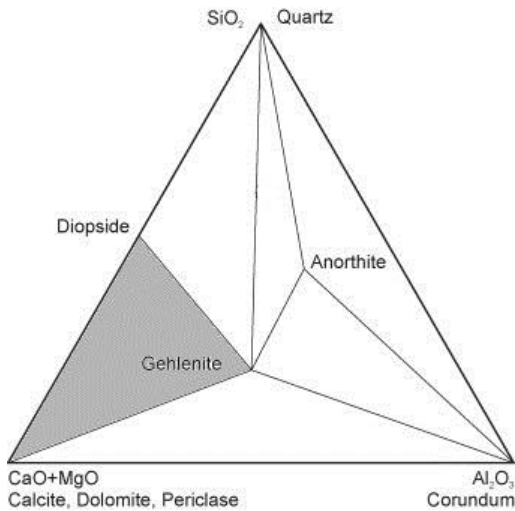


Figure 3: ACS diagram (Al₂O₃ - (CaO + MgO)-SiO₂), from Nodari *et al.*, 2007 Fig. 4 modified.

In the case of the coarse-grained and Ca-enriched pottery of Batrawy, gehlenite has been identified and it formed around the grains of carbonate inclusions (Veniale, 1990), that cannot happen in ceramic with small grain size (Maggetti and Kupfer, 1978).

The formation of gehlenite as shown in Eq. (2) is due to the reaction between CaO (from carbonates), Al₂O₃ and SiO₂ (from clay minerals) (Cultrone *et al.*, 2001) and it takes place between 750 and 850° C (De Benedetto *et al.*, 2002), depending on the SiO₂ concentration in the system.



When the amount of SiO₂ is low, the thermal stability is reached at 850° C while at higher content of SiO₂, the equilibrium temperature reduces to 800° C (Riccardi *et al.*, 1999; Traoré *et al.*, 2000; Rathossi *et al.*, 2004). Moreover, if the clay component is represented mainly by illite, the temperature range increases up to 800-1050 °C (Duminuco *et al.*, 1998).

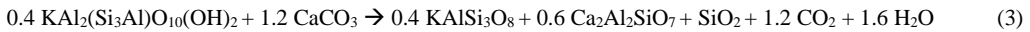
Gehlenite is stable at temperature up to 950° C in presence of wollastonite or decomposes to wollastonite and anorthite in presence of enough silica to react (Riccardi *et al.*, 1999).

Therefore, the occurrence of gehlenite suggests the probable use of clay materials plus calcium carbonates naturally or voluntarily added in the clayey materials (Peters and Iberg, 1978; Perez-Monserrat *et al.*, 2012).

The absence of calcite and the predominance of gehlenite in the experimental re-firing would suggest a firing temperature under 950 °C for Khirbet al-Batrawy samples. However, the duration of firing and the controlled conditions of temperature in modern kilns cannot be compared to the ancient heating process. In this view, the small quantities of gehlenite in the Batrawy samples seems to suggest its initial formation in the temperature range between 800° and 950°C. The probable maximum firing temperature was about 950 °C, but maintained for a very short time that did not allow the complete decomposition of calcite. Conversely, the samples in which gehlenite has not been found, were fired at lower temperature than 800 °C.

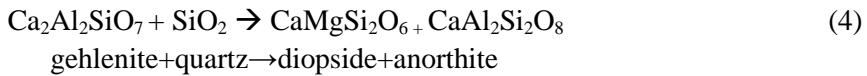
Diopside and anorthite, forming at temperature close to 900° C, result from the reaction between clay minerals, quartz and calcite (Maritan *et al.*, 2006); in particular between quartz and gehlenite being this latter an intermediate mineral that is unstable in presence of SiO₂ (Trindade *et al.*, 2009). The occurrence of diopside in the ceramic samples contributes to estimate the firing temperature as its crystallization starts at temperatures higher than 850 °C as a product of the reaction between clay minerals and calcium carbonate.

Results of experimental works explained that the increasing of feldspars with the temperature (in both pit and kiln firing) is the result of the continuous reaction (3) (Maritan *et al.*, 2006):



(Peters and Iberg, 1978; Dondi *et al.*, 1995; Duminuco *et al.*, 1996, 1998).

The occurrence of illite as rare mineral phase in the studied pottery indicates an incomplete collapse of clay minerals, supported by the scarce occurrence of gehlenite. Moreover, gehlenite would be transformed into plagioclase and diopside reducing the amount of this mineralogical phase in pottery fragments.



During firing, hematite is formed in oxidizing atmosphere conditions for the availability of free iron due to the collapse of the clay minerals (Nodari *et al.*, 2007) and the replacement of aluminum by iron at temperature around 600-750° C (Maniatis and Tite, 1981; Komadel, 2003).

Titanium oxides were used in the past as markers to estimate the firing temperature. Indeed, at low temperature anatase is the most common polymorph of titanium dioxide, stable in the range 600-900 °C; above this temperature threshold it converts into

rutile (Bouzidi *et al.*, 2013). Therefore, the presence of anatase may indicate a firing temperature lower than 900 °C (Gennari and Pasquevich, 1999). Several studies (Hishta *et al.*, 1983; Gennari and Pasquevich, 1999; Sendova *et al.*, 2005; Raškovska *et al.*, 2010; Liou *et al.*, 2011) demonstrated that different origin and environmental conditions could interfere on the temperature transition, making titanium oxides useless as thermometers. Indeed, the presence of rutile can be related not only to the above phase transition, but also to accessory mineral present in the original clays (Gennari and Pasquevich, 1999).

A low firing temperature has been confirmed by electron microscopy results that identified a low degree of vitrification for the Batrawy samples. According to Velray *et al.* (2009), the firing temperature, the atmosphere in the kiln and the chemical composition of the raw material, especially its calcium and iron contents, determine the extent of the vitrification of clays. Basing on the composition of the sherds (calcareous or non-calcareous) and in particular of the vitrification structure developed during firing, it is possible to assign the samples to one of the vitrification stages proposed by Maniatis and Tite (1981) that are associated to the firing temperatures employed in the manufacture of the pottery.

In calcareous clay (CaO>6%), the vitrification is limited by the formation of crystalline phases of high temperature (anorthite, gehlenite, wollastonite and diopside). Samples from Khirbet al-Batrawy did not present a vitrification structure but signs of an initial vitrification stage, according to the definition of Maniatis and Tite (1981). Experimental results (McConville *et al.*, 2000; Rathossi and Pontikes, 2010) pointed out that sintering stage in clay-calcite mixtures starts at around 950° C. In this view the results of this study suggest a firing temperature in the pottery from Batrawy below this temperature, thus testifying a low degree of technology. On the basis of electron microscopy results, we can infer that the low degree of vitrification observed in Batrawy samples indicates low firing temperatures in a range between 800 and 950° C.

Considering the mineralogical assemblage identified in the Khirbet al-Batrawy fragments, the information drawn by the FTIR vibrational assignments (of Al(OH) in the octahedral sheet structure and of the Si-O stretching) and the vitrification stage of the matrix, a firing temperature lower than 900-950 °C can be inferred; in particular, this range can be limited between 850-950 °C in the sherds in which diopside has been detected. In this view, the concurrent presence of diopside, illite and calcite in several ceramic samples suggests a firing temperature range consistent with that of the phase transitions of these mineral phases, from 850 to 950 °C. The samples of EB II phase represent an exception as the absence of any firing mineral, such as diopside, clearly indicates low firing temperature, estimated lower than 850°C.

This finding draws to the hypothesis that during the history of Khirbet al-Batrawy a limited evolution in the control of firing temperature developed. The inferred decrease in the range of temperature of pottery from EB II to EB IV phases suggests a major control of temperature conditions and a major duration of firing process.

5.1.2.2 Firing atmosphere

A preliminary indication of firing atmosphere is provided by the color of ceramic body. The total amount of iron in the raw material and the redox conditions are the main factors that drive the color of ceramic. The color is deeply connected to the atmosphere condition firing so red-orange matrix is usually related to an oxidizing atmosphere, whereas black-gray to reducing firing condition. During firing, clay materials change their color in response to atmosphere conditions which control the presence of the different forms of iron oxides; however, as reported in the literature, the presence of small-sized CaCO_3 crystals could play an important role.

In calcareous clays, CaO formed by the decomposition of CaCO_3 at temperature above $750\text{ }^\circ\text{C}$ reacts with iron oxides and free ions deriving from the collapse of clay minerals. These reactions produce a decrease in the size of iron oxides crystals and consequently the bleaching of the ceramic matrix from red to pink, and cream for temperature above $850\text{ }^\circ\text{C}$ (depending on the percentage of CaCO_3 and iron oxides in the starting raw material) (Nodari *et al.*, 2007). In particular, the pale creamy color is typical of ceramic produced by firing of calcareous clay at low temperature (Papa-christodoulou *et al.*, 2006).

Macroscopic analysis gives preliminary information about firing condition; indeed, color differences of the matrix, analyzed in the cut cross section, might be due to different atmosphere conditions during firing.

Five potsherds color types are distinguished in the pottery from Khirbet al-Batrawy:

- a) red with black core
- b) gray
- c) red-brown
- d) color variable in cross section

Jordan potteries present a great variability in color matrix and it is not possible to distinguish samples of different phases of Khirbet al-Batrawy urbanization or different types of pottery basing on the color matrix.

Macroscopic data highlight that the majority of Jordan potteries show red-brown color that allow to hypothesize a diffuse oxidizing atmosphere during firing.

The occurrence of hematite in the matrix may be related to the forms Fe_3O_4 and $\text{Fe}(\text{OH})_3$ naturally present in the starting clay minerals used (Hradil *et al.*, 2003; Legodi and De Waal, 2007). Illitic clays usually assure a development of metallic ox-

ides during firing, giving much more red colors to the ceramic body (Molera *et al.*, 1998).

In our red samples, along with hematite, Raman spectra showed the presence of magnetite, that in oxidizing atmosphere, converts into hematite. The occurrence of magnetite is probably due to an incomplete transformation process of Fe_3O_4 to Fe_2O_3 in oxidizing atmosphere during firing (Harrel and Russel, 1967; Lofrumento *et al.*, 2004) or to uncontrolled status of the fugacity of oxygen (Lofrumento *et al.*, 2004)..

In addition to the conditions of the atmosphere, also firing temperature can affect the presence of magnetite and hematite in the ceramic. In particular, at about 200°C the transformation from magnetite $\alpha\text{-Fe}_3\text{O}_4$ to maghemite $\gamma\text{-Fe}_2\text{O}_3$ has been observed, and at about 400°C that of maghemite $\gamma\text{-Fe}_2\text{O}_3$ to hematite $\alpha\text{-Fe}_2\text{O}_3$ (Lofrumento *et al.*, 2004).

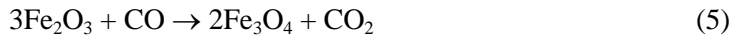
“Black core” structure, the typical sandwich structure characterized by a black-gray reduced core and a reddish oxidizing margin (Nodari *et al.*, 2004), is usually associated to firing in reducing conditions with an oxidizing cooling stage, where the dark core is reduced during firing and at the end, when the fuel is finished, the oxygen comes into the ceramic body and oxidizes the carbonaceous particles in the margin, resulting in the formation of hematite (Maggetti *et al.*, 2011).

The dark-gray color is due to the high value of the ratio $\text{Fe}^{2+}/\text{Fe}^{3+}$, in particular to the presence of magnetite (Fe_3O_4), wustite (FeO) in the paste (Harrel and Russel, 1967), or uncombusted carbon particles (Letsch and Noll, 1983), the red and beige margin color is probable due to hematite ($\alpha\text{-Fe}_2\text{O}_3$) and Fe-Ca silicates, respectively (Kreimeyer, 1987; Molera *et al.*, 1998; Maritan L., 2004). The red and beige color of the margins is due to the occurrence of hematite and Fe-Ca silicates, respectively (Kreimeyer, 1987; Molera *et al.*, 1998; Maritan, 2004); in particular, the pinkish or reddish hues of the margin is probably connected to different proportion of hematite and maghemite which respectively contribute with their red and brown colors. Indeed, during firing the decomposition of Fe-bearing clay minerals probably causes the formation of amorphous phases that reduce the porosity and consequently the permeability of ceramic paste. In this situation, the growth of oxidized mineral phases with expanded octahedral structure is inhibited explaining the high content of Fe(II) in the cores.

Analytical studies revealed that sandwich structure pottery can be associated to different combinations of redox conditions and bulk chemical composition of raw material (Nodari *et al.*, 2004). Moreover, the sandwich structure was experimentally obtained by the firing of clays rich in organic matter under oxidizing atmosphere (Picon, 1973; Rye, 1981; Maritan, 2002) or in kiln having oxidizing atmosphere, a low heating rate and a long residence time (Maritan *et al.*, 2006).

Jordan pottery fragments with the “black core” have been carefully examined in areas of the ceramic body showing different colors. These fragments present magnetite and amorphous carbon in the dark central body and hematite in the margins and EDS analysis revealed that the chemical composition of the cores and margins is very close. This finding suggests that the different colors are probably the result of different redox states of the atmosphere developed during firing, further supporting the results of previous studies.

Samples with gray color matrix, containing abundant carbon and magnetite, are associated to reducing conditions that are typical of pit firing with low maximum firing temperature, fast heating rates and short duration of firing (Maritan *et al.*, 2006). In this conditions hematite in reducing atmosphere reacts with CO resulting in the formation of magnetite according to the following equation:



Gray or dark color matrix is not very diffuse in pottery samples from Batrawy, but it is mainly present in the KKW samples highlighting probably a particular procedure technique of these specialized pottery.

Some of the studied samples present a variability of the color in thin section. Frequently the variation in color is associated to a particular shape, in handles rims or bases. For example, sample KB.06.E.703/5 (a handle of a jar) has light red color in the core and dark red in the margins. The light red color in the core is typical of ceramic produced firing calcareous clay at low temperatures with reducing conditions in the final phase of the firing or during cooling (Iordanidis *et al.*, 2009). It is possible that the fragment was the product of calcareous clay with low content of organic material, fired in a partial oxidizing atmosphere with an oxidizing cooling phase that promoted the development of a color much more reddish in the margin. Moreover, in section the sample shows a small dark area in the junction between the handle and the body, where probably oxygen did not penetrate in the body, preventing the complete combustion of the organic material.

Organic material has been identified in the studied pottery samples in addition to mineralogical phases. Raman spectra revealed the presence of amorphous carbon showing an elevated disorder (Fig. 4) without the peak at about $\sim 971 \text{ cm}^{-1}$ due to phosphate ion present in bones and ivory (Van der Weerd *et al.*, 2004). The presence of carbon in the studied ceramic may be due to the use of organic material as fuel that during firing, probably in reducing atmosphere, did not completely decompose.

Jordan pottery presents a great variability in the color of matrix, suggesting different atmosphere conditions in the different cases. However, no evident relationship has been recognized between the redox state of the atmosphere and phases of Batrawy urbanization or between the different types of pottery. Moreover, the extreme variability of the color in the same sample in thin section suggests that they were incompletely oxidized probably due to a short firing duration, or reduced and rapidly cooled in air. The heterogeneous results indicate uncontrolled firing conditions, which were frequent in open kiln, where the control of temperature and the diffusion of oxygen were difficult to monitor and keep constant.

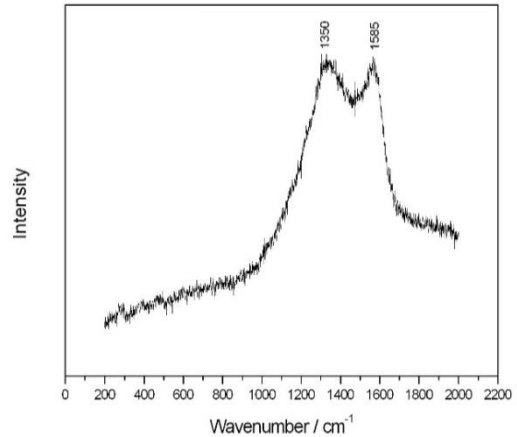


Figure 4: Representative Raman spectra of amorphous carbon.

5.1.3 Decorations and superficial treatments

Decorations and superficial treatments of the studied Jordan ceramics show an evolution during the long history of Batrawy. In particular, the EB II Red Burnished and Red Polished Ware were attested. The results of the analysis of the red color showed that hematite is the main coloring substance. The red slip having clayey nature did not undergo vitrification, due to the low firing temperature developed, resulting, therefore, porous and permeable to the fluids. It was usually obtained diluting non-calcareous clay with high amount of iron oxides in water to obtain a homogeneous suspension that was applied by immersion or by brush.

The EB IIIA phase shows a diffuse experimentation in the decorations of the pottery: burnishing, polishing and painting are largely attested in this phase. Concerning the superficial decorations of Jordan pottery, micro-Raman spectroscopy allowed to identify the pigment used on the surface; hematite has been found in the red areas, whereas black pigment was due to amorphous carbon. The superficial decorations have also been investigated by XRD; however, the thin thickness of the coating and the limited quantities found in the potsherds generally affected negatively the analytical characterization of the materials used in surface decorations. The abundance of quartz and calcite in the layer below the decoration hides in XRD patterns the features of the mineralogical phases used as pigments. Indeed, the identification of the pigments in the pottery decorations of the EB IIIA group by XRD analysis failed due to the high

background of XRD patterns, although only the powder of the decorations scrapped by the surface of the samples was analyzed in order to minimize the matrix interference.

The red or brown slips occurring on the surface of some samples of EB IIIA phase, the so called Khirbet Kerak Ware, have been analyzed by SEM. The results did not show traces of gloss layer or thin layer with different chemical composition and texture; this finding confirms the use of burnishing or polishing as superficial treatments. This procedure does not involve the use of a selected fine clay added on the surface or a particular firing process, but it is connected to mechanic hand-burnishing that allows the alignment of particles parallel to the surface, giving a lustrous aspect. The last two phase (EB IIIB and EB IV) developed a new kind of decoration mainly based on combed, applied and punctuate decoration.

5.1.4 Burial conditions

In the studied pottery post-burial processes resulted in the formation of secondary mineral phases such as gypsum, bassanite, calcite, lepidocrocite and goethite. They are probably the result of mineralogical changes due to the interaction between the ceramic and aqueous solutions circulating in the burial environment (Heimann and Maggetti 1981; Maggetti, 1982; Buxeda i Garrigós, 1999; Freestone, 2001; De Benedetto *et al.*, 2002; Maritan and Mazzoli 2004; Schwedt *et al.*, 2004, 2006; Buxeda i Garrigós *et al.*, 2005; Secco *et al.*, 2011). In this view, groundwater plays a principal role in the dissolution and precipitation of mineral phases, connected to chemical and mineralogical transformations of pottery (Schwedt *et al.*, 2004, 2006; Secco *et al.*, 2011).

In our samples, gypsum has been identified both on the surface as gray incrustations and in the matrix as scattered crystals along rare bassanite. Commonly, calcium sulfates are the most abundant sulfate minerals occurring in evaporitic sequences and calcareous sedimentary deposits (Freyer and Voigt, 2003). Numerous studies at atmospheric pressure have been focused on the temperature stability, phase transitions, and formation of the sulfate phases (e.g., O’Gorman and Walker, 1973; Freyer and Voigt, 2003; Mirwald, 2008). In isothermal conditions the transformation gypsum-bassanite starts at about 120 °C (393 K), whereas the transition bassanite-anhydrite is completed at about 135 °C (408 K) (Ballirano and Melis, 2009a, 2009b). The thermal decomposition of anhydrite starts at 780 °C in reducing conditions, whereas in neutral and oxidizing conditions this decomposition does not take place below 1000 °C (O’Gorman and Walker, 1973). On the basis of these experimental results we can make two assumptions for the studied pottery: the raw materials contained gypsum that during heating cycle was transformed via dehydration into anhydrite, which re-

mained stable up to 1000 °C. Conversely, the raw material contained anhydrite which remained unaffected during the heating process. In post-heating processes anhydrite was rehydrated via bassanite into gypsum. On the contrary, the occurrence of gypsum as crusts on the surface of the fragments has to be related to the interaction of the sherds with sulfate-rich fluids in the burial environment.

The presence of goethite and lepidocrocite may be explained as a result of hydration of hematite during burial or as residual original minerals which were already present in the original clay and, then transformed in hematite during firing. Dehydration at 230-280 °C of goethite results in the formation of disordered hematite and well-crystallized hematite gradually develops at temperature close to 900 °C at oxidizing conditions (Brindley and Brown, 1980; Trinidad *et al.*, 2009). The γ -forms of the oxyhydroxides (lepidocrocite) are transformed by heating to the corresponding γ -form of the oxides at 230-280 °C and this latter is transformed to normal hematite at 400-500°C (Majzlan *et al.*, 2003). The goethite-hematite and lepidocrocite-hematite transformations occur at temperature lower than the estimated firing temperature according to the mineral assemblage. In this view, the occurrence of iron oxyhydroxides, that cannot be explained after an heating process, can be ascribable to the interaction with fluids in the burial environment. However, the desertic environment and the dry climate of the Jordan region probably prevented the diffuse formation of goethite and lepidocrocite, which have been identified only in a few samples.

5.2 Provenance

Mineralogical composition of pottery can provide important information to define the provenance of the raw material. The main components of the studied pottery, quartz and calcite, cannot give a significant contribution in this purpose, being commonly found in clay deposits and in limestones and marls (Papachristodoulou *et al.*, 2006). Fragments of fossils, identified as diffuse in thin section, suggest a probable use of marls in the raw material. In this view, the occurrence of microfossils in the local geological formations (Burdon, 1959) further supports the hypothesis of a local supply of the raw material used for the pottery production.

The presence of fragments of basaltic rocks, widespread diffuse in this region, provide information useful to localize the sourcing area of the raw material. Therefore, optical microscopy and chemical analysis further support the hypothesis of a local provenance of these fragments. In particular, EDS analysis showed that these fragments contain ilmenite, olivine, plagioclase and apatite. According to Burdon (1959) it is also possible infer a local provenance for these basaltic fragments as their mineralogical composition is very close to that of Jordan Plateau Basalt.

K-feldspar crystals could be crystals deriving from igneous or metamorphic rocks outcropping in the area. Moreover, hydroxides, oxyhydroxides and oxides of iron, aluminum and manganese, are the commonest accessory minerals in clays (Brindley and Brown, 1980). Zircon may occur in clay (Tochilin *et al.*, 2012), and in the case of pottery from Khirbet al-Batrawy, may due to alteration processes of igneous and metamorphic rocks of the Pre-Cambrian basement.

The results of chemical analyses suggest that the composition of the clay materials used in the pottery production from Batrawy is calcareous and low refractory type, according to Maniatis and Tite (1981). The silica content of the studied ceramics is related to the presence of quartz and feldspar in the samples.

The large variability in Fe_2O_3 contents reflects the presence of hematite/magnetite in the clayey material, while the high contents of clay minerals and K-feldspar is testified by the contents of Al_2O_3 and K_2O .

The Hierarchical Clustering Analyses and Principal Component Analysis performed on pottery fragments, clay materials and brick samples highlight that the local clay sediments have a different chemical composition, suggesting a different source of supply of raw material. Furthermore, the different chemical composition of the brick suggests a different choice in the raw material used in pottery production from those used in the production of building material. The low percentage of the total variance in PCA carried out only on the pottery samples, highlights that do not exist marked chemical differences either within their class or among the different historical phases of urbanization. The results suggest that the same raw material was probably used during the long history of Batrawy. However, in the different phases of Batrawy urbanization, a low variability has been observed. The historical variability in chemical composition of the pottery can be explained considering the period of development and experimentation of EB IIIA and the standardized phase taking place in the latter phases EB IIIB and EB IV. Regarding the different pottery type no evident differences have been identified, suggesting a low variability in chemical composition. In particular, Storage Ware and Simple Ware fragments present a major variability in the chemical composition with respect to the other fragments, probably due to the lack of need to select refined material and to a not-cure in the proportion between clay and inclusions for these types. Moreover, the KKW fragments are characterized by higher percentage of CaO and lower values of SiO_2 .

The results of chemical analysis further contribute to the definition of pottery provenance. In particular, statistical treatment of experimental data showed a different source of supply of raw material between bricks and pottery fragments, suggesting a conscious different choice of the raw material used in pottery production from those used in the production of building material.

Different contents of trace elements have been recognized also between pottery fragments and the samples of clay materials analyzed, highlighting a different source of raw material from those collected and analyzed. The low percentage of the total variance in PCA highlights that do not exist marked chemical differences either within their class or among the historical phases of urbanization.

These considerations allow to hypothesize that the same raw material was probable used since the birth of Batrawy as previously quoted.

References

- Aras A. (2004): The change of phase composition in kaolinite and illite-rich clay-based ceramic bodies. *Applied Clay Science*, **24**, 257-269.
- Ballirano P., Melis E. (2009a): Thermal behaviour and kinetics of dehydration in air of bassanite, calcium sulphate hemihydrate ($\text{CaSO}_4 \cdot 0.5\text{H}_2\text{O}$), from X-ray powder diffraction. *European Journal of Mineralogy*, **5**, 985-993.
- Ballirano P., Melis E. (2009b): Thermal behaviour and kinetics of the hydration of gypsum in air from in situ real-time laboratory parallel-beam X-ray powder diffraction. *Physics and Chemistry of Minerals*, **36**, 391-402.
- Barone G., Crupi V., Longo F., Majolino D., Mazzoleni P., Tanasi D., Venuti V. (2011): FT-IR spectroscopic analysis to study the firing processes of prehistoric ceramics. *Journal of Molecular Structure*, **993**, 147-150.
- Barone G., Ioppolo S., Majolino D., Migliardo P., Tigano G. (2002): A multidisciplinary investigation on archaeological excavation in Messina (Sicily). Part I: A comparison of pottery findings in 'The Strait of Messina area'. *Journal of Cultural Heritage*, **3**, 145-153.
- Belfiore C.M., di Bella M., Triscari M., Viccaro M. (2010): Production technology and provenance study of archaeological ceramics from relevant sites in the Alcantara River Valley (North-eastern Sicily). *Materials Characterization*, **61**, 440-451.
- Bouzidi N., Bouzidi A., Gaudon P., Merabet D., Blanchart P. (2013): Porcelain containing anatase and rutile nanocrystals. *Ceramics International*, **39**, 489-495.
- Brindley G.W., Brown G. (1980): Crystal Structures of Clay Minerals and their X-ray Identification. Mineralogical Society, London, pp. 495.
- Burdon D.J. (1959): Government of the Hashemite Kingdom of Jordan, pp. 82.
- Buxeda i Garrigós J. (1999): Alteration and contamination of archaeological ceramics: the perturbation problem. *Journal of Archaeological Science*, **26**, 295-313.
- Buxeda i Garrigós J., Cau Ontiveros M. A., Madrid i Fernández M., Toniolo A. (2005): Roman amphorae from the *Iulia Felix* shipwreck: alteration and provenance. in "Proceedings of the 33rd International Symposium on Archaeometry", H. Hars and E. Burke, eds., Vrije Universiteit, Amsterdam, 149-51.
- Cultrone G., Rodriguez-Navarro C., Sebastian E., Cazalla O., De La Torre M. J. (2001): Carbonate and silicate phase reactions during ceramic firing. *European Journal of Mineralogy*, **13**, 621-634.
- Cuomo di Caprio N., 2007. Ceramica Antiche tecniche di lavorazione e moderni metodi di indagine in Archeologia 2, Roma.
- Damjanovi L., Holclajtner-Antunovi I., Mio U.B., Biki V., Milovanovi D., Evans I.R. (2010): Archaeometric study of medieval pottery excavated at Stari (Old) Ras, Serbia. *Journal of Archaeological Science*, **37**, 1-11.

- De Benedetto G.E., Laviano R., Sabbatini L., Zambonin P.G. (2002): Infrared spectroscopy in the mineralogical characterization of ancient pottery. *Journal of Cultural Heritage*, **3**, 177-186.
- Dondi M., Ercolani G., Guarini G., Marsigli M., Venturi I. (1995): Evoluzione Della Microstruttura Durante La Cottura Rapida Di Impasti Per Piastrelle Porose. *Ceramurgia*, **25**, 301-314.
- Duminuco P., Messiga B., Riccardi M.P. (1998): Firing process of natural clays. Some microtextures and related phase composition. *Thermochimica Acta*, **321**, 185-190.
- Duminuco P., Riccardi M.P., Messiga B., Setti M. (1996): Modificazioni tessiturali e mineralogiche come indicatori della dinamica del processo di cottura di manufatti ceramici. *Ceramurgia*, **26**, 281-288.
- Freestone I. C. (2001): Post-depositional changes in archaeological ceramics and glasses. in "Handbook of archaeological sciences", D. R. Brothwell and A. M. Pollard, eds., John Wiley & Sons, Inc., Hoboken, NJ, 615-25.
- Freyer D., Voigt, W. (2003): Crystallization and phase stability of CaSO₄ and CaSO₄-based salts. *Monatshefte für Chemie*, **134**, 693-719.
- Gennari F.C., Pasquevich D.M. (1999): Enhancing Effect of Iron Chlorides on the Anatase-Rutile Transition in Titanium Dioxide. *Journal of the American Ceramic Society*, **82**, 1915-21.
- Gilead I., Goren Y. (1989): Petrographic analyses of fourth millennium BC pottery and stone vessels from the Northern Negev, Israel. *Bulletin of the American Schools of Oriental Research*, 5-14.
- Ghosh S.N. (1978): Infra-red spectra of some selected minerals, rocks and products. *Journal of Materials Science*, **13**, 1877-1866.
- Goren Y. (1995): Shrines and ceramics in Chalcolithic Israel: The view through the petrographic microscope. *Archaeometry*, **37**, 287-305.
- Goren Y. (1996). The southern Levant in the early Bronze Age IV: the petrographic perspective. *Bulletin of the American Schools of Oriental Research*, 33-72.
- Goren Y., Goring-Morris A. N., Segal I. (2001): The technology of skull modelling in the Pre-Pottery Neolithic B (PPNB): Regional variability, the relation of technology and iconography and their archaeological implications. *Journal of Archaeological Science*, **28**, 671-690.
- Gosselain O.P. (1992): Bonfire of the enquiries: pottery firing temperatures in archaeology: what for? *Journal of Archaeological Science*, **19**, 243-259.
- Harrel G.O., Russel R.R. (1967): Influence of ambient atmosphere in maturation of structural clay products. *Engineering Experiment Station Bulletin*. Ohio State University, Columbus, pp. 204.
- Heimann R.B., Maggetti M. (1981): Experiments on simulated burial of calcareous terra sigillata (mineralogical change), Preliminary results, *British Museum Occasional Paper*, **19**, 163-177.
- Higham C. F. (1996): A review of archaeology in mainland Southeast Asia. *Journal of Archaeological Research*, **4**, 3-49.
- Hishita S., Mutoh I., Koumoto K., Yanagida H. (1983): Inhibition mechanism of the anatase-rutile phase transformation by rare earth oxides. *Ceramics International*, **9**, 61-67.
- Hlavavy J., Jonas K., Elek S., Inczedy J. (1977): Characterisation of the particle size and the crystallinity of certain minerals by infrared spectrometry and other instrumental methods I. Investigation on clay minerals. *Clays and Clay Minerals*, **25**, 451-456.
- Hradil D., Grygar T., Hradilova J., Bezdicka P. (2003): Clay and iron oxide pigments in the history of painting. *Applied Clay Science*, **22**, 223-236.

- Iordanidis A., Garcia-Guinea J., Karamitrou-Mentessidi G. (2009): Analytical study of ancient pottery from the archaeological site of Ariani, northern Greece. *Materials Characterization*, **60**, 292-302.
- Jordan M.M., Boix A., Sanfeliu T., De La Fuente C. (1999): Firing transformations of Cretaceous clays used in the manufacturing of ceramic tiles. *Applied Clay Science*, **14**, 225-234.
- Kingery W. D. (1997): Operational principles of ceramic kilns. *The American Ceramic Society*, **7**, 11-9.
- Komadel P. (2003): Chemically modified smectites. *Clay Minerals*, **38**, 127-138.
- Kreimeyer R. (1987): Some notes on the firing color of clay bricks. *Applied Clay Science*, **2**, 175-183.
- Legodi M. A., De Waal D. (2007): Raman spectroscopic study of ancient South African domestic clay pottery. *Spectrochimica Acta*, **66**, 135-142.
- Letsch J., Noll W. (1983): Phase formation in several ceramics subsystems at 600 jC-1000 jC as a function of oxygen fugacity. *cfi/Ber. DKG*, **7**, 259-267.
- Liou Y. S., Chang Liu Y., Huang H. Y. (2011): Micro-Raman spectroscopic study of cord-marked pottery decorated with red coatings from Taiwan, ca 2600–1700 BC. *Journal of Raman Spectroscopy*, **42**, 1062-1068.
- Lofrumento C., Zoppi A., Castellucci E.M. (2004): Micro-Raman spectroscopy of ancient ceramics: a study of French sigillata wares. *Journal of Raman Spectroscopy*, **35**, 650-655.
- Madejova J. (2003): FTIR techniques in clay mineral studies. *Vibrational Spectroscopy*, **31**, 1-10.
- Maggetti M. (1982): Phase analysis and its significance for technology and origin. In "Archaeological ceramics", J.S. Olin and A.D. Franklin, ed., Smithsonian Institution Press, Washington, 121-133.
- Maggetti M., Küpfer T. (1978): Composition of the terra sigillata from La Péniche (Vidy/Lausanne, Switzerland). *Archaeometry*, **20**, 183-188.
- Maggetti M., Neururer C., Ramseyer D. (2011): Temperature evolution inside a pot during experimental surface (bonfire) firing. *Applied Clay Science*, **53**, 500-508.
- Majzlan J., Lang B.E., Stevens R., Navrotsky A., Woodfield B.F., Boerio-Goates J. (2003): Thermodynamics of Fe oxides: Part I. Entropy at standard temperature and pressure and heat capacity of goethite (α -FeOOH), lepidocrocite (γ -FeOOH), and maghemite (γ -Fe₂O₃). *American Mineralogist*, **88**, 846-854.
- Maniatis Y., Tite M. S. (1981): Technological examination of Neolithic-Bronze Age pottery from central and southeast Europe and from the Near East. *Journal of Archaeological Science*, **8**, 59-76.
- Manoharan C., Venkatchalapathy R., Dhanapandian S., Deenadayalan K. (2007): FTIR and Mössbauer spectroscopy applied to study of archaeological artefacts from Maligaimedu, Tamilnadu, India. *Indian Journal of Pure and Applied Physics*, **45**, 860-865.
- Maritan L. (2002): Studio archeometrico di ceramiche di tipo Etrusco Padano dell'area veneta: indagini petrografiche, mineralogiche, chimico-fisiche e confronto con i risultati ottenuti da prove sperimentali di cottura di materiali argillosi, Unpublished Ph.D. thesis on earth sciences, University of Padova, Italy.
- Maritan L. (2004): Archaeometric study of Etruscan-Padan type pottery from the Veneto region petrographic, mineralogical and geochemical-physical characterisation. *European Journal of Mineralogy*, **16**, 297-307.
- Maritan L., Mazzoli C. (2004): Phosphates in archaeological finds: implications for environmental conditions of burial. *Archaeometry*, **46**, 673-683.

- Maritan L., Mazzoli C., Freestone I. (2007): Modelling changes in mollusc shell internal microstructure during firing: implications for temperature estimation in shell-bearing pottery. *Archeometry*, 49, 529-541.
- Maritan L., Mazzoli C., Nodari L., Russo U. (2005): Second Iron Age grey pottery from Este (northeastern Italy): study of provenance and technology. *Applied Clay Science*, 29, 31-44.
- Maritan L., Nodari L., Mazzoli C., Milano A., Russo U. (2006): Influence of firing conditions on ceramic products: experimental study on clay rich in organic matter. *Applied Clay Science*, 31, 1-15.
- McConville C.J., Lee W.E., Sharp J.H. (2000): Microstructural Evolution in Dense Kaolinite, Illite and Smectite Clay Bodies. In: Crathy, W. M., Sinton, C.W. (Eds.). *Science of White-ware II*. The American Ceramic Society, Ohio.
- Mendelovici E., Yariv S.H., Villalba R. (1979): Iron-bearing kaolinite in Venezuelan laterites: I. Infrared spectroscopy and chemical dissolution evidence. *Clay Minerals*, 14, 323-331.
- Mirwald P.V. (2008): Experimental study of dehydration reactions gypsum-bassanite and bassanite-anhydrite at high pressure: indication of anomalous behavior of H₂O at high pressure in the temperature range of 50-300 °C. *Journal of Chemical Physics*, 128, 0745021-0745027.
- Molera J., Pradell T., Vendrell-Saz M. (1998): The colors of Carich ceramic pastes: origin and characterisation. *Applied Clay Science*, 13, 187-202.
- Murad E., Wagner U. (1998): Clay and Clay minerals: the firing process. *Hyperfine Interactions*, 117, 337-356.
- Peters T., Iberg R. (1978): Mineralogical changes during firing of calcium-rich brick clays. *Ceramic Bulletin*, 57, 503-509.
- Nodari L., Marcuz E., Maritan L., Mazzoli C., Russo U. (2007): Hematite nucleation and growth in the firing of carbonate-rich clay for pottery production. *Journal of the European Ceramic Society*, 27, 4665-4673.
- Nodari L., Maritan L., Mazzoli C., Russo U. (2004): Sandwich structures in the Etruscan-Padan type pottery. *Applied Clay Science*, 27, 119-128.
- O'Gorman J. V., Walker J.P. L. (1973): Thermal behavior of mineral fractions separated from selected American coals. *Fuel*, 52, 71-79.
- Papachristodoulou C., Oikonomou A., Ioannides K., Gravani K. (2006): A study of ancient pottery by means of X-ray fluorescence spectroscopy, multivariate statistics and mineralogical analysis. *Analytica chimica acta*, 573, 347-353.
- Perez-Monserrat E.M., Fort R., Lopez-Arce P., Alvarez M., Varas-Muriel M.J (2012): Contribution of analytical techniques to determine the technologies used in the ceramic materials from the Former Workers Hospital of Maudes, Madrid (Spain). *Journal European Ceramic Society*, 2012; xxx:xxx-xxx.
- Peters T., Iberg R. (1978): Mineralogical changes during firing of calcium-rich brick clays. *Ceramic Bulletin*, 57, 503-509.
- Picon M. (1973): Introduction à l'étude technique des céramiques sigillées de Lezoux. Université de Dijon, Centre de recherches sur les techniques greco-romaines, Dijon.
- Quinn P.S. (2013): *Ceramic Petrography: The Interpretation of Archaeological Pottery & Related Artefacts in Thin Section*. Archaeopress, Oxford, pp.250.
- Ramasamy K., Kamalakkannan M. (1987): Infrared study of some South Indian clays. *Indian Journal of Pure and Applied Physics*, 25, 284-286.
- Raškovska A., Minčeva-Šukarova B., Grupče O., Colombari P. (2010): Characterization of pottery from Republic of Macedonia II. Raman and infrared analyses of glazed pottery finds from Skopsko Kale. *Journal of Raman Spectroscopy*, 41, 431-439.

- Rathossi C., Pontikes Y. (2010): Effect of firing temperature and atmosphere on ceramics made of NW Peloponnese clay sediments. Part I: Reaction paths, crystalline phases, microstructure and colour. *Journal of European Ceramic Society*, **30**, 1841-1851.
- Rathossi C., Tsolis-Katagas P., Katagas C. (2004): Technology and composition of Roman pottery in northwestern Peloponnese, Greece. *Applied clay science*, **24**, 313-326.
- Riccardi M.P., Messiga B., Duminuco P. (1999): An approach to the dynamics of clay firing. *Applied Clay Science*, **15**, 393-409.
- Russell J.D. (1987): A hand book of determinative methods in clay mineralogy, ed. M.J. Wilson, Blackie and Son Ltd., pp. 133-173.
- Rye O. (1981): Pottery Technology: Principles and Reconstruction. Taraxacum, Washington, pp. 147.
- Schwedt A., Mommsen H., Zacharias N. (2004): Post-depositional elemental alterations in pottery: neutron activation analyses of surface and core samples. *Archaeometry*, **46**, 85-101.
- Schwedt A., Mommsen H., Zacharias N., Buxeda i Garrigós J. (2006): Analcime crystallization and compositional profile-comparing approaches to detect post-depositional alteration in archaeological pottery. *Archaeometry*, **48**, 237-51.
- Secco M., Maritan L., Mazzoli C., Lampronti G.I., Zorzi F., Nodari L., Russo U., Mattioli S.P. (2011): Alteration processes of pottery in lagoon-like environments. *Archaeometry*, **53** (4), 809-829.
- Sendova M., Zhelyaskov V., Scalera M., Ramsey, M. (2005): Micro-Raman spectroscopic study of pottery fragments from the Lapatsa tomb, Cyprus, ca 2500 BC. *Journal of Raman Spectroscopy*, **36**, 829-833.
- Sherriff B.L., Court P., Johnston S., Striling L. (2002): The source of raw materials for Roman pottery from Leptiminus, Tunisia. *Geoarchaeology: An International Journal*, **17**, 835-861.
- Shoval S. (1994): The firing temperature of a Persian-period pottery kiln at Tel Mihal, Israel, estimated from the composition of its pottery. *Journal of Thermal Analysis*, **42**, 175-185.
- Shoval S. (2003): Using FT-IR spectroscopy for study of calcareous ancient ceramics. *Optical materials*, **24**, 117-122.
- Shoval S., Nathan Y. (2011). Analyzing the calcination of sulfur-rich calcareous oil shales using FT-IR spectroscopy and applying curve-fitting technique. *Journal of thermal analysis and calorimetry*, **105**, 883-896.
- Tite, M. S. (1995): Firing temperature determination--how and why?. in "The aim of laboratory analyses of ceramics in archaeology", April 7-9, 1995 in Lund, Sweden (pp. 37-42). Kungliga vitterhets-, historie-och antikvitets akademien, Stockholm, Sweden.
- Tite M. S., Kilikoglou V., Vekinis G. (2001): Review article: strength, toughness and thermal shock resistance of ancient ceramics, and their influence on technological choice. *Archaeometry*, **43**, 301-324.
- Tochilin C., Dickinson W.R., Felgate M.W., Pecha M., Sheppard P., Damon F.H., Bickler F., Gehrels G.E. (2012): Sourcing temper sands in ancient ceramics with U-Pb ages of detrital zircons: a southwest Pacific test case. *Journal of Archeological Science*, **39**, 2583-2591.
- Traoré K., Siméon Kabré T., Blanchart P. (2000): Low temperature sintering of a pottery clay from Burkina Faso. *Applied Clay Science*, **17**, 279-292.
- Trindade M.J., Dias M.I., Coroado J., Rocha F. (2009): Mineralogical transformations of calcareous rich clays with firing: a comparative study between calcite and dolomite rich clays from Algarve, Portugal. *Applied Clay Science*, **42**, 345-355.
- Tschegg C. (2009): Post-depositional surface whitening of ceramic artifacts: alteration mechanisms and consequences. *Journal of Archaeological Science*, **36**, 2155-2161.

- Van der Weerd J., Smith G. D., Firth S., Clark R. J. (2004): Identification of black pigments on prehistoric Southwest American potsherds by infrared and Raman microscopy. *Journal of archaeological science*, **31**, 1429-1437.
- Velraj G., Janaki K., Musthafa A.M., Palanivel R. (2009): Spectroscopic and porosimetry studies to estimate the firing temperature of some archaeological pottery sherds from India. *Applied Clay Science*, **43**, 303-307.
- Veniale F. (1990): Modern techniques of analysis applied to ancient ceramics. Proc. Workshop Analytical methodologies for the investigation of damaged stones, pp. 1–45.
- Venkatachalapathy R., Loganathan A., Manoharan C., Veeramuthu K. (2010): Physical sciences FTIR and XRD studies on some archaeological artifacts from Bohn, India. *Recent Research in Science and Technology*, **2**, 51-55.
- Venkatachalapathy R., Sridharan T., Dhanapandian S., Manoharan C. (2002): Determination of Firing temperature of Ancient Potteries by means of Infrared and Mössbauer studies. *Spectroscopy Letters*, **35**, 769-779.
- Wieder M., Adan-Bayewitz D. (1999): Pottery manufacture in early Roman Galilee: a micro-morphological study. *Catena*, **35**, 327-341.

6. ADVANTAGES AND DRAWBACKS OF ANALYTICAL METHODOLOGIES USED: THE CASE OF KHIRBET AL-BATRAWY

The results of this PhD thesis permit an evaluation of the advantages and drawbacks of the different methodologies here applied and currently used to study archaeological pottery.

Discussions and considerations drawn in this chapter have been obtained considering the nature of the Jordan pottery analyzed (not purified, with coarse-grain sized), whereas different conclusions could be reached in the case of pottery with fine-grain sized.

6.1 Technological level of production

6.1.1 Mineralogical composition

Raman and Infrared spectroscopies, optical microscopy, X-ray diffraction and Scanning Electron microscopy coupled with Energy Dispersive Spectroscopy are the methodologies that mainly contribute to the identification of the mineralogical composition of the ancient ceramic materials.

The results obtained for each samples are listed in Appendix C and a visual representation to clearly show the contribution of each analysis has been reported in Fig. 1.

Raman spectroscopy is the methodology that detected the major number of mineralogical phases. The application of μ -Raman spectroscopy shows great potential for disclosing the mineral composition and exploring technological aspects of pottery production. It is a non-destructive technique that does not require sample preparation and does not generally cause damage, alteration or consumption of the sample, allowing to perform further investigations with other techniques. This is a fundamental aspect in the field of cultural heritage, where usually the samples are microscopic and where the sampling is often unique. Indeed, the possibility to select a well-defined spot in a micrometric range can minimize mistakes and allows identifying single crystals without the interference of the signal of the matrix allowing a complete picture of the mineralogical composition. Moreover, μ -Raman technique allows repeating the measure several times in the same spot or in different points of the same sample in a very short time.

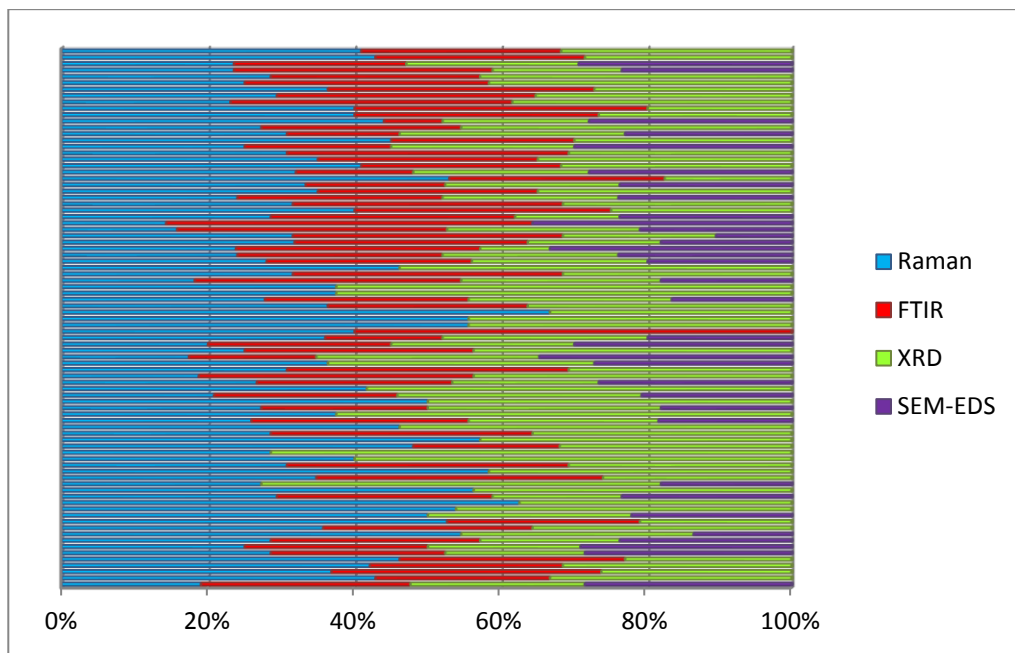


Figure 20: Diagram showing the contribution of each analytical technique in the identification of the mineralogical composition of potsherds from Khirbet al-Batrawy.

However, despite the amount of information obtained and the mineral phases identified, no quantitative information can be obtained by Raman results; therefore, the principal mineral components and accessories have been identified. The numerous mineralogical phases identified by this technique are the result of a very detailed and accurate Raman study that collected a minimum of thirty spectra for each sample. However, this kind of study, based on data acquisition point by point with the support of a microscope, requires long time of acquisition and several month of analysis every day. The low Raman scattering efficiency of clay components and the fluorescence commonly associated with pottery samples prevent the possibility to use the Raman mapping. Numerous Raman mapping texts on thin section have been carried out with the purpose to obtain visual maps representing the distribution of different mineral inclusions. Unfortunately, the high fluorescence of the matrix not allowed to produce these maps.

Infrared spectroscopy also contributes in mineralogical characterization, although the interpretation of FTIR spectra, based on the attribution of all the spectra transitions, is not straightforward. Vibrational bands are represented in the spectra as sum of different mineralogical contributions. The identification of the single contribute is difficult due to the interferences and split of vibrational bands connected to the surrounding. Moreover, the wavelength range in which mineral phases can be identified is narrow

and this further contributes to create a much more overlapping among the vibrational bands preventing the possibility to clearly identify different mineral phases. Samples preparation for FTIR analysis consists in grinding together inclusions and matrix; therefore, the information obtained refers to the whole mineralogical composition of the sherds. For this reason FTIR analysis reveals the occurrence of illite, while Raman spectroscopy did not identify this mineral phase.

X-ray powder diffraction analysis usually provides a general characterization of the mineralogical composition of the samples. Also in this case, sample preparation is a micro-destructive action that produces a powder containing both inclusions and matrix. XRD analysis allows the identification of clay minerals (illite in our case), which is fundamental to reconstruct the nature of the original raw materials used for ceramic production. The reduced amount of sample required, the speed of analysis and the completeness of information obtained including both qualitative and semi-quantitative results, make XRD the most applied methodology in the mineralogical characterization of ancient potteries.

In the study of heterogeneous and complex materials such as pottery, SEM results are complicated to be discussed. The results provide the chemical composition of the different inclusions and matrix analyzed. In this view, a simple chemical composition including a few chemical elements (e.g., calcite, apatite, quartz etc.) generally allows to clearly identify a mineral phase, whereas when the chemical elements are numerous the identification became more complex. SEM images allow to easily discriminate mineralogical phases containing chemical elements with high atomic weight as they appear much more brilliant than the rest of the sample. In this way, accessory minerals (for example, barite and apatite), whose identification is generally difficult by means of other methodologies, can be easily detected by SEM.

Optical microscopy in thin section allows the identification not only of mineral phases but also of the all aplastic inclusions present and to analyze the distribution of these inclusions in the pottery.

The identification of aplastic inclusions allow to speculate about the production process of pottery: choice of the raw materials used, its purification and preparation and tempers added by the potter. Moreover, the analysis of porosity the shape and distributions of pores in thin section further contributes in the definition of the ancient way of modeling the ceramic paste. Finally, microscopic investigations, and in particular the “grouping analyses”, allow to group samples on the basis of textural features distinguishing among the different type of pottery and to separate local pottery from that imported.

6.1.2 Firing

The definition of firing conditions is strictly related to the mineral assemblage identified in the samples. The discussion about the role of different methodologies in this task has been presented here divided into two sections: “Temperature” and “Atmosphere”.

6.1.2.1 Maximum firing temperatures

The presence or absence of primary calcite, illite, diopside and gehlenite has been used as indicator to define the maximum firing temperatures. The identification of these minerals by the different methodologies in each samples has been listed in Appendix C and represented in Fig. 2.

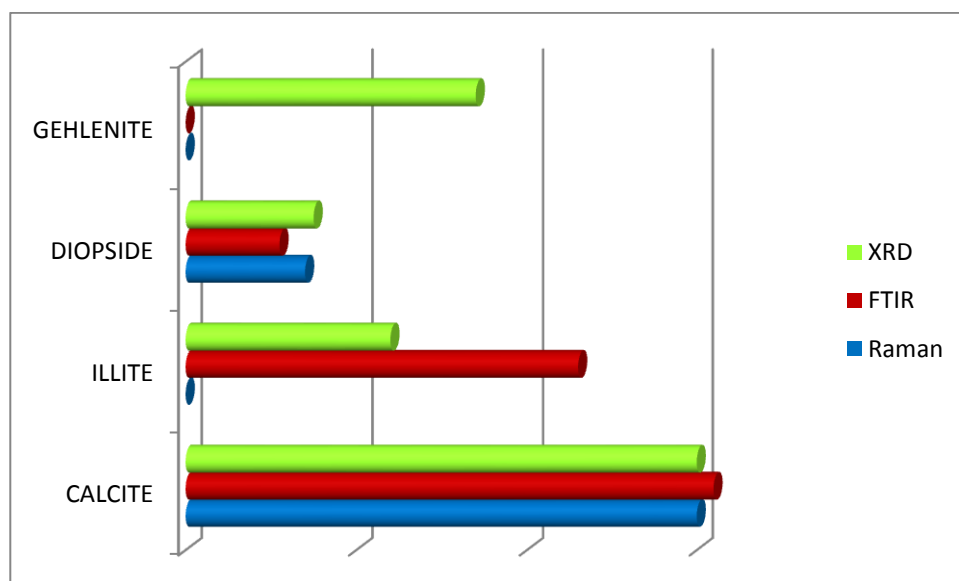


Figure 21: Diagram showing the contribution of each analytical technique in the identification of the mineralogical phases used as indicator to define the maximum firing temperature.

The diagrams clearly shows that XRD is the methodology that provides the more resolved results in the identification of the “firing indicators”.

In this field, Raman spectroscopy shows its limits in the identification of clay minerals; also gehlenite, which is diffuse in samples, was not detected by any spectroscopic methodology.

The inability of XRD analysis to discriminate between primary and secondary calcite is the only weak point of this analytical technique in the definition of the maximum firing temperature. In this view, optical microscopy and SEM analysis can significantly contribute in distinguishing different calcite generations.

6.1.2.2 Firing atmosphere

Information about the redox state of firing atmosphere is generally provided by the color of the ceramic body and the occurrence of the different forms of iron oxides. Indeed, the total amount of iron in the raw material and the redox conditions are the principal factors that determine the color in ceramic fragments. The analysis of color of pottery can be conducted by macroscopic and microscopic analysis.

Macroscopic analysis of ceramic samples is the first step of pottery characterization. It is an important instrument to direct and choose the subsequent investigations on pottery fragments.

Macroscopic analysis does not require sophisticated technologies as it is performed by comparing and describing the color of the matrix with respect those reported in the Munsell chart. It provides information about homogeneity and inhomogeneity of the color in artifacts and color differences between the inner and outer parts of the ceramic. These results are useful to make hypothesis about different redox conditions developed during firing. In this view, the great variability in the color matrix of the Khirbet al-Batrawy ceramic along with the variation in color and intensity observed along the cross-section of numerous sherds allowed to obtain preliminary information about low firing temperature and uncontrolled redox conditions during firing.

The identification of iron oxides has been obtained by Raman, FTIR, XRD and SEM-EDS analysis. However, the limited amounts of iron oxides in the studied pottery affected their detection by the different analytical methodologies used. Indeed, as reported in Appendix C, Raman shows the most diffuse capability in the differentiation of iron oxides. Indeed, magnetite was mainly identified by this technique. XRD and FTIR analysis in this context show their limits in the detection of mineralogical phases occurring in lower amounts. Moreover, SEM-EDS allows the identification of iron oxides, although it does not distinguish the different forms. However, SEM-EDS analysis allowed the analysis of the “black core” fragments, confirming the hypothesis that the different color was not related to the chemical composition, but to the firing process.

In this view, the application of Raman spectroscopy in conjunction with macroscopic analysis was helpful and decisive to infer the redox state of firing atmosphere.

6.1.3 Decorations and superficial treatments

In the analysis of archaeological pottery from Khirbet al-Batrawy particular attention has been given to the decoration and superficial treatments.

Macroscopic analysis was the first tool to separate different types of superficial treatments, allowing the identification of the decorations to be further analyzed. Generally,

decorated ceramics are not easily analyzed because of the difficulty to isolate the pictorial layer from the bulk paste. In this study, decorations and superficial treatments have been easily analyzed by Raman spectroscopy as this technique gives the possibility to focus the laser beam to a micrometric-spot and to choose with extreme precision the inclusion to be analyzed. The attempts to analyze superficial decorations by other methodologies proved to be useless. The thin thickness of coating and the small quantities found in the potsherds generally affected in a negative way the analytical characterization of the materials used in surface decorations by means of FTIR and XRD analysis. In particular, in the case of XRD, although only the powder of the decoration scrapped by the surface of the samples was analyzed in order to minimize the matrix interference, the mineralogical identification of the pigments failed due to the high background of XRD patterns. Only micro-Raman analysis was able to identify the different pigments and showed that hematite has been used in red bands of pottery of EB IIIA group. On the contrary, the black pigment used on the surface of the sherds was identified as amorphous carbon. Generally, other common methodologies extensively applied in cultural heritage, such as for example XRD, do not allow the recognition of this amorphous phase.

6.2 Provenance

The identification of the origin of ceramic objects and the sites of supply of raw materials is fundamental in the study of archaeological pottery. These goals can be achieved by characterizing the mineralogical and chemical compositions of the samples and by comparison with those of known pottery or raw materials.

In this view, Raman and FTIR spectroscopy, optical microscopy in thin section, XRD and SEM-EDS provide essential information to infer the provenance of the raw materials used in the pottery production.

In the case of coarse-grain sized low fired ceramic such as that of Khirbet al-Batrawy, the components of pottery that mainly contribute to the identification of the provenance were identified by microscopic analysis in thin section. Fragments of rocks (in our case basaltic rocks) and fragments of fossils can be considered the indicator markers to define local or foreign production of ceramic materials by comparison to the geological setting of the area. However, only the combination of results obtained by different methodologies can support and prove the provenance of the sherds. In this view, the detailed analysis of fragments of basaltic rocks obtained by SEM-EDS allow to relate these fragments to the Jordan Plateau Basalt, that extensively outcrops around the archaeological site, further supporting the hypothesis of a local provenance of the studied ceramic fragments.

The results of chemical analysis also contribute in the definition of the provenance, providing chemical markers of pottery that can be related to the mineralogical-petrographical characteristics of the rocks outcropping in the area of production. However, without a significant number of representative samples of the local clays or chemical data of other potteries from the same area, the results of chemical analysis can only provide information about similarity and differences among samples. Furthermore, the analysis should involve a large number of representative samples and results should be analyzed by statistical methods to obtain a more plausible interpretation. In these conditions, chemical methodologies could provide data that can be useful for the differentiation between local or imported potteries.

Conclusions

The different methodologies applied in this study proved to have a specific role in the different aspects of ceramic characterization. However, in the analysis of coarse-grain size archaeological pottery, the combination of XRD, microscopic analysis and Raman spectroscopy could be considered the best solution in terms of costs and benefits.

7. CONCLUSIONS

The results of this study allow characterizing the pottery from Khirbet al-Batrawy by means of a multi-analytical approach. The application of such approach to archaeological ceramic demonstrates to have a great potentiality to disclose secrets of technological aspects of the production and provenance of the raw material.

The ceramic sherds have been produced using a calcareous clay with quartz, feldspars, and minor amounts of oxides and hydroxides.

The potsherds have almost the same mineralogical and composition, however, on the basis of the prevalence of particular inclusions, twelve *fabrics* have been distinguished as reported in chapter 4.2.

The abundance of tempers, having coarse-sized dimensions and distributed in an unimodal grain size, suggests that the raw material has not been subjected to a purification process; moreover, the presence of clay pallets, resulting from an inadequate mixing of the clays during the preparation, highlights the “a low quality” and “a poor-advanced technology” of manufacturing of Jordan pottery during Bronze Age. However, the occurrence of grog, voluntarily added as tempers, and the aware choice of raw material, different from those used in the production of building material, suggest an awareness that considered the features of material in the workability and particularly in the pottery production. Furthermore, the variability in size of the tempers, which is directly related to the different shape and use of the vessels, allows to hypothesize an initial differentiation of the material used in the various typologies and functions of the pottery.

In addition, the co-occurrence of *vughs* and vesicles in the external and internal part of the section respectively, supports the archaeological hypothesis that a mixed technique of hand and potter’s wheel was applied during the manufacturing of the ceramic. In particular, the absence of evident orientation of the mineral grains in thin section confirms that the intensity of shaping the pot on the potters’ wheel was low.

The technological evolution of the production in the Jordan pottery is marked by an initial research and study of the raw materials and shape in the EB II phase, continuing through a major and diffuse experimentation in the use of materials and procedures of modeling observed in EB IIIA phase, to finish with a sort of standardization and selection characterized by a minor number of fabrics with specific features to satisfy the request and necessity of a particular production in the EB IIIB and EB IV phases.

The results of the study allowed to estimate low firing temperatures, generally below 950 °C. A limited increase of firing temperature from EB II pottery to EB IV phases can be inferred, along with a narrowing of the range of the firing temperature between

850-950 °C that suggests a major control of temperature conditions during firing. The redox state of the atmosphere of firing was variable from oxidizing to reducing, frequently alternated in the same pottery production. No relationship has been observed between the redox state of the atmosphere and the phases of Batrawy urbanization or between the different types of pottery. In this view, the high variability in atmosphere conditions of the pottery suggests uncontrolled firing conditions that are common in open kiln, where the control of temperature and the diffusion of oxygen were difficult to monitor and to keep constant.

Decorations and superficial treatments show an evolution during the long history of Batrawy. From initial burnishing and polishing in EB II, passing through decoration in EB IIIA to finish with combed, applied and punctuate decoration in the later phases. The red color is due to hematite, whereas the dark pigment to amorphous carbon. The lustrous slip that characterizes some samples was not obtained by the vitrification of the thin superficial layer due to high firing temperatures, but it is connected to mechanic hand-burnishing that allows the alignment of particles parallel to the surface giving a lustrous aspect, as in the KKW pottery.

The occurrence of mineral phases such as ilmenite, anatase, zircon, apatite and fragments of basaltic rocks suggest the local supply of raw material.

The mineralogical composition of the pottery does not change over time, suggesting that the supply of raw material had the same provenance during the long history of Khirbet al-Batrawy. This hypothesis is further supported by the results of chemical analysis that show the same chemical composition among all the sherds.

Even if no evident changes in the supply of raw material and technology have been observed, the variability of fabrics suggests that the raw materials, in particular the type and proportion between clay and inclusions, were selected on the basis of the pottery function. The general similarity in the chemical and mineralogical composition of pottery supports the hypothesis that during the long history of the city, the technological background did not apparently evolve. However, a major selection in the material and a major control of firing condition depict a limited evolution in the pottery production technology.






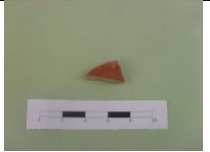


The methodologies applied in this study proved to have a specific role in the definition of the different aspects of ceramic characterization. However, the results further prove the necessity to apply a multi-analytical approach to have an overall characterization of ancient ceramic material. According to the analytical results here reported, it is also possible to conclude that, in the analysis of coarse-grain size archaeological pottery, the combination of XRD, microscopic analysis and Raman spectroscopy could be considered the best solution in terms of costs and benefits.

APPENDIX A

2. MATERIALS AND ANALYTICAL METHODS

List of pottery sherds with photographs divided in the four periods of urbanization with the indication of class, pottery type, and the place of findings.

SAMPLES	Class	Pottery Type	
EB II 3000-2700 B.C.			
AREA B near the main Early Bronze II-III city-wall and the city gate			
KB.06.B.392/8	Storage ware	jar	
AREA E southern fortification line with the secondary entrance			
KB.06.E.702/10	Red Polished ware	jug	
KB.06.E.703/5	Simple ware	jar	
KB.06.E.703/6	Storage ware	jar	
KB.06.E.704/1	Red burnished ware	platter	
KB.06.E.704/6	Red burnished ware	bowl	
KB.06.E.706/2	Red burnished ware	platter	



SAMPLES	Class	Pottery Type	
KB.06.E.706/1	Red burnished ware	platter	
EB IIIA 2700-2500 B.C.			
AREA A Acropolis			
KB.05.A.52/8	Storage Ware	hole-mouth jar	
KB.05.A.58/1	Red polished ware	jug	
KB.05.A.64/1	Red burnished ware	platter	
KB.05.A.64/13	Storage ware	jar	
AREA B near the main Early Bronze II-III city-wall and the city gate			
KB.05.B.110/15	Red Polished Ware	jug	
KB.05.B.126/1	Red polished ware	jug	
KB.05.B.126/3	Red burnished ware	platter	







SAMPLES	Class	Pottery Type	
KB.05.B.126/4	Simple painted ware	bowl	
KB.05.B.136/1	Simple painted ware	jar	
KB.05.B.136/3	Simple ware	jar	
KB.05.B.136/5	Storage ware	phitos	
KB.05.B.146/1	Red burnished ware	platter	
KB.05.B.146/3	Simple painted ware	jar	
KB.05.B.146/4	Simple ware	jar	
KB.05.B.146/5	Simple ware	juglet	
KB.05.B.146/6	Simple ware	juglet	



SAMPLES	Class	Pottery Type	
KB.05.B.146/7	Red polished ware	jug	
KB.05.B.146/8	Red burnish ware	platter	
KB.05.B.146/15	Simple painted ware	bowl	
KB.05.B.146/20	Kitchen Ware	hole-mouth pot	
KB.05.B.146/24	Simple ware	juglet	
KB.05.B.146/30	Red polished ware	jug	
KB.06.B.167/4	Storage (grain wash)	jar	
KB.06.B.376/4	Red polished ware	jug	

KB.06.B.413/2	Kitchen Ware	hole-mouth pot	
----------------------	--------------	----------------	--




SAMPLES	Class	Pottery Type	
KB.06.B.427/1	Khirbet Kerak Ware	jug	
KB.08.B.805/6	Khirbet Kerak Ware	jug	
KB.09.B.820.10	Khirbet Kerak Ware	bowl	
KB.09.B.820.12	Khirbet Kerak Ware	bowl	
KB.09.B.820/13	Khirbet Kerak Ware	jug	
KB.08.B.805/32	Khirbet Kerak Ware	jug	
KB.08.B.805/33	Khirbet Kerak Ware	jug	






KB.08.B.805/34	Khirbet Kerak Ware	jug	
AREA E southern fortification line with the secondary entrance			
KB.06.E.701/2	Simple painted ware	jar	





SAMPLES	Class	Pottery Type	
KB.06.E.703/3	Simple ware	juglet	
EB IIIB 2500-2300 B.C.			
AREA A Acropolis			
KB.05.A.46/2	Storage Ware	jar	
KB.05.A.46/8	Storage Ware	pithos	
KB.05.A.216/4	Storage Ware	jar	
KB.05.A.204/2	Storage Ware	hole-mouth jar	
KB.05.A.204/3	Kitchen Ware	hole-mouth pot.	





KB.05.A.220/5	Storage ware	pithos	
KB.05.A.224/2	Storage Ware	pithos	

SAMPLES	Class	Pottery Type	
KB.06.A.120/6	Red Polished Ware	jug	
AREA B near the main Early Bronze II-III city-wall and the city gate			
KB.05.B.111/3	Simple Ware	jar.	
KB.10.B.1040/8	Storage Ware	pithos	
KB.11.B.1054/2	-	pithos	
KB.10.B.1054/6	Simple Ware	vat	
KB.11.B.1054/12	Simple Ware	jar	




KB.11.B.1054/13	Red burnished Ware	jar	
KB.11.B.1054/21	Metallic Ware	pattern combed jar	
KB.10.B.1054/22	Red burnished Ware	jar	

SAMPLES	Class	Pottery Type	
KB.10.B.1054/24	Storage Ware	pithos	
KB.10.B.1054/62	Simple Ware	jar	
KB.11.B.1124/1	-	hole mouth jar	
KB.11.B.1124/3	Storage Ware	hole mouth jar	
KB.11.B.1124/8	Storage Ware	jar	






KB.11.B.1124/10	Storage Ware	pithos	
KB.11.B.1124/15	Storage Ware	hole mouth jar	
KB.11.B.1124/19	-	spouted vat	
KB.11.B.1124/22	Simple Ware	jar	



SAMPLES	Class	Pottery Type	
KB.11.B.1124/24	Storage Ware	jar	
KB.11.B.1124/28	-	pithos	
KB.11.B.1124/29	Storage Ware	jar	
KB.11.B.1124/33	Red burnished Ware	juglet	




KB.11.B.1128/1	Storage Ware	jar	
KB.11.B.1128/50	Storage Ware	pithos	
KB.11.B.1128/51	Storage Ware	pithos	
KB.11.B.1128/52	Storage Ware	hole-mouth jar	
KB.11.B.1128/65	Red burnished ware	juglet	

SAMPLES	Class	Pottery Type	
EB IV 2300-2000 B.C.			
AREA A Acropolis			
KB.05.5/D200	Simple Ware	jar	
KB.05.A.6b/1	Kitchen Ware	hole-mouth pot	
KB.05.A.18/5	Simple Ware	jar	

KB.05.A.21/27	Storage Ware	jar	
KB.05.A.34/2	Simple Ware	jar	
KB.05.A.62/1	Simple Ware	jar	
KB.05.A.62/2	Simple Ware	jar	
KB.05.A.68/2	Storage Ware	jar	
KB.05.A.82/4	Simple Ware	jar	
SAMPLES	Class	Pottery Type	
KB.05.A.84/3	Simple Ware	jar	
KB.05.A.8b/3b	Kitchen Ware	hole-mouth pot	
KB.05.A.88/1	Storage Ware.	hole-mouth jar.	

KB.05.A.96/1	Simple Ware	jar	
KB.05.A.98/1	Kitchen Ware.	hole-mouth pot	
KB.05.A.210/2	Simple Ware	jar	
KB.05.A.210/4	Simple Ware	jar	
KB.05.A.212/6	Simple Ware	jar	
KB.05.A.216/12	Storage Ware	jar	

SAMPLES	Class	Pottery Type	
KB.06.A.248/2	Storage Ware	jar	
KB.06.A.256/1	Storage Ware	jar	

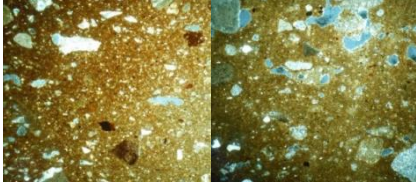
KB.06.A.9/18	Storage Ware	jar	
AREA B near the main Early Bronze II-III city-wall and the city gate			
KB.05.B.128/3	Kitchen Ware.	hole-mouth pot	
KB.06.B.383/7	Storage Ware	jar	

APPENDIX B

4.2 OPTICAL MICROSCOPY ANALYSIS IN THIN SECTION (OM)

Thin section photomicrographs of samples, divided into *fabrics* (mag 2.5 x and crossed polarizers). The four historical periods are indicated by different colors: EB II samples blue, EB IIIA pink, EB IIIB green and EB IV violet.

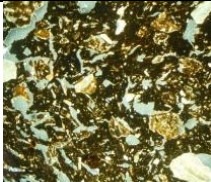
FABRIC A *calcite, micritic and sparry calcite with vesicles*



KB.06.E.706/1 KB.06.E.706/2

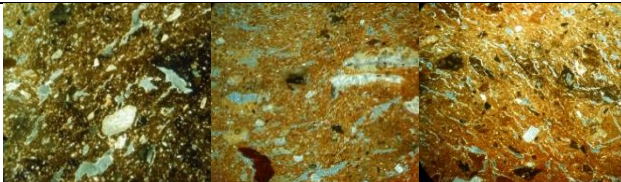
FABRIC B *clay pallets and fragments of grog*

FABRIC B1



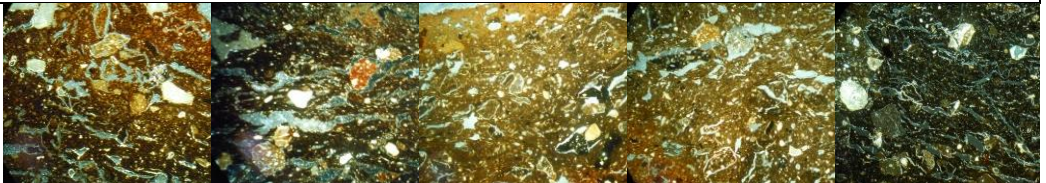
KB.06.B.703/6

FABRIC B2

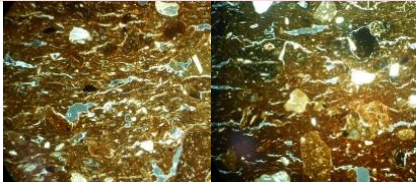


KB.06.B.392/8 KB.06.E.703/5 KB.05.B.146/4

FABRIC B3



KB.05.B.136/5 KB.05.A.64/13 KB.05.B.111/3 KB.05.A.204/3 KB.10.B.1040.8



KB.11.B.1124/24 KB.11.B.1128/76

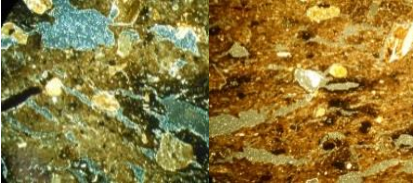
FABRIC C calcite and clay pallets

FABRIC C1



KB.06.E.702/10

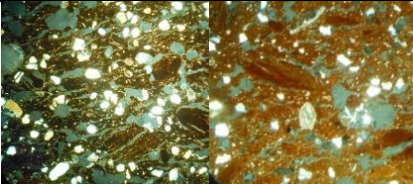
FABRIC C2



KB.05.B.146/7 KB.05.B.146/8

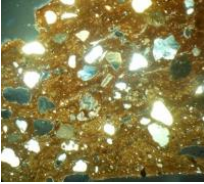
FABRIC D crystals of calcite

FABRIC D1



KB.06.E.704/1 KB.06.E.704/6

FABRIC D2

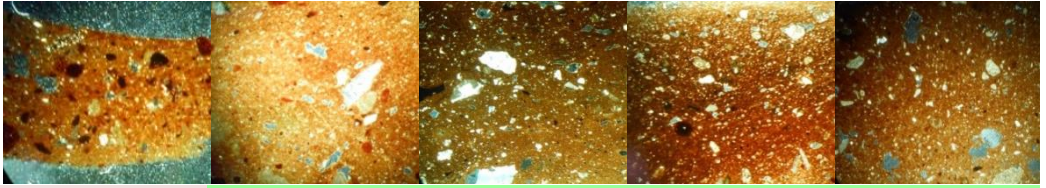


KB.11.B.1054/13

FABRIC E fine calcite



KB.05.B.146/6 KB.05.A.58/1 KB.05.B.146/24 KB.05.B.126/1 KB.05.B.136/1



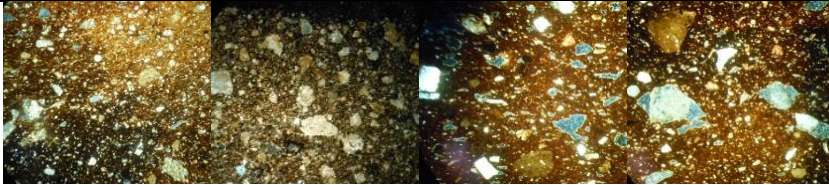
KB.06.E.703/3

KB.10.B.1054/21

KB.10.B.1054/22

KB.11.B.1124/33

KB.11.B.1126/65

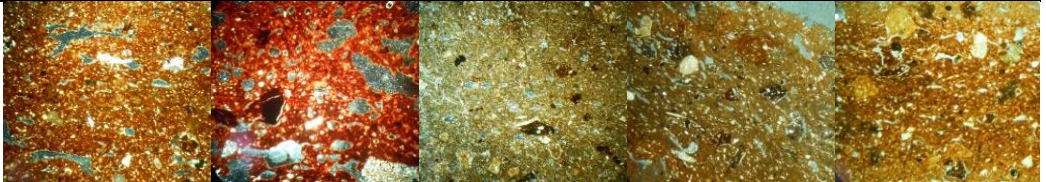
FABRIC F *fossils and sedimentary rocks***FABRIC F1**

KB.05.B.146/30

KB.06.B.427/1

KB.05.B.146/1

KB.05.B.126/3

FABRIC F2

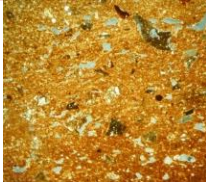
KB.05.A.64/1

KB.06.B.376/4

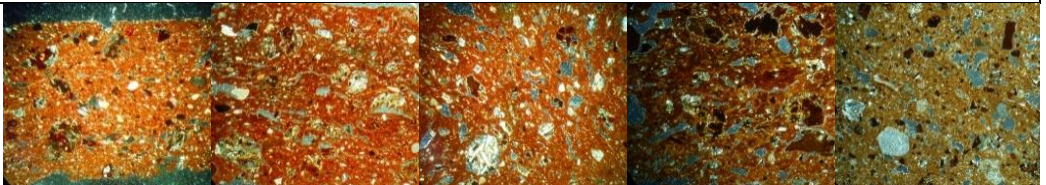
KB.09.B.820/12

KB.05.A.82/4

KB.05.5/D200



KB.05.A.96/1

FABRIC G *basaltic rocks and fragments of fossils***FABRIC G1**

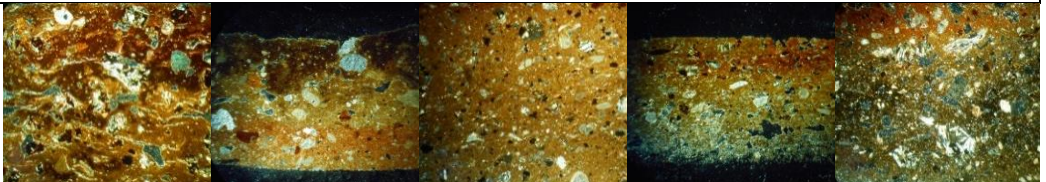
KB.06.E.701/2

KB.05.B.146/3

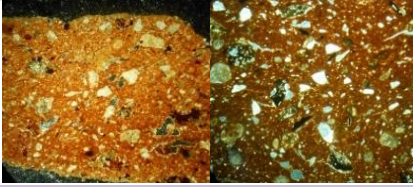
KB.05.B.146/5a

KB.05.B.146/15

KB.05.B.126/4

FABRIC G2

KB.09.B.820/13 KB.08.B.805/6 KB.05.B.110/15 KB.09.B.820/10 KB.05.B.136/3

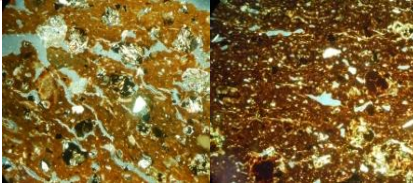


KB.05.A.34/2 KB.05.A.18/5

FABRIC H *clay pallets, calcite and iron oxides*

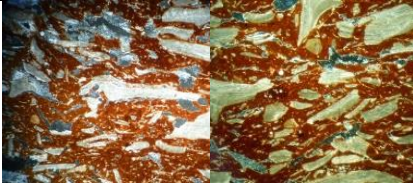


KB.06.B.167/4 KB.05.A.52/8 KB.10.B.1054/24 KB.11.B.1124/8 KB.11.B.1124/10



KB.05.A.62/1 KB.05.B.128/3

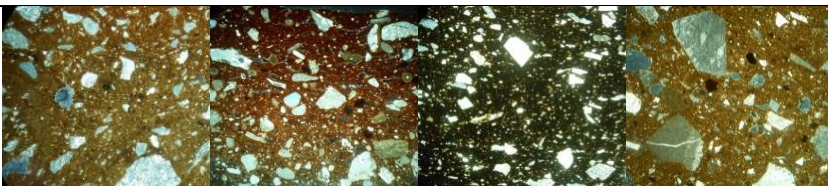
FABRIC I *fragments of shells*



KB.06.B.413/2a KB.06.B.146/20

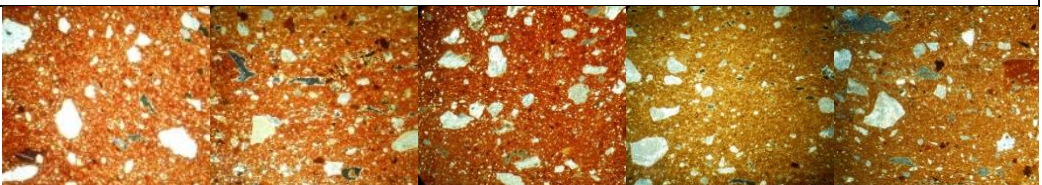
FABRIC L *crystals of calcite and micritic calcite*

FABRIC L1

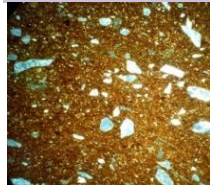


KB.05.A.204/2 KB.11.B.1054/12 KB.05.A.68/2 KB.06.A.248/2

FABRIC L2



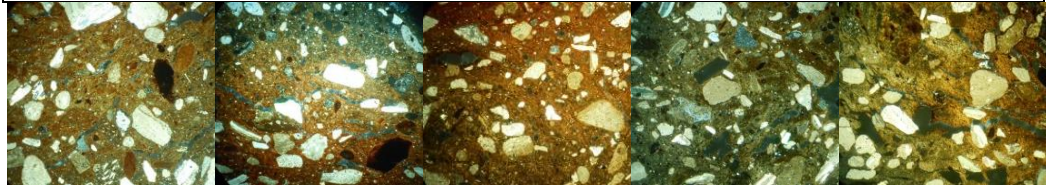
KB.05.A.6b/1 KB.05.A.21/27 KB.05.A.8b/3b KB.05.A.88/1 KB.05.A.98/1



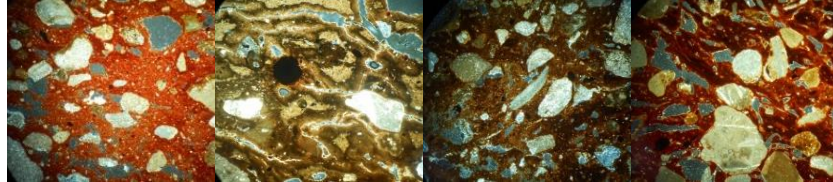
KB.06.ø/18

FABRIC M *micritic, calcite and fragments of sedimentary rocks*

FABRIC M1

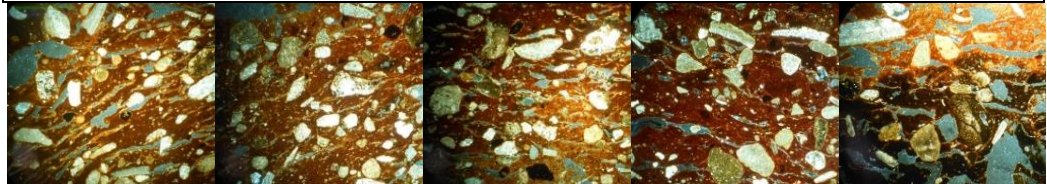


KB.05.A.46/8 KB.05.A.216 KB.06.A.220/5 KB.05.A.224/2 KB.10.B.1054/6



KB.10.B.1054/62 KB.11.B.1128/1 KB.11.B.1124/29 KB.11.B.1128/50

FABRIC M2



KB.11.B.1124/15 KB.06.A.120/6 KB.11.B.1124/3 KB.11.B.1128/52 KB.11.B.1128/51



KB.11.B.1224/22

FABRIC N *clay pallets and rare calcite*

FABRIC N1



KB.05.A.210/2

KB.05.A.210/4

KB.06.B.383/7

KB.06.A.256/1

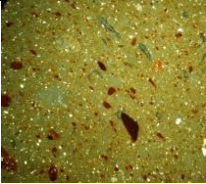
KB.05.A.84/3

FABRIC N2



KB.05.A.216/12

LONER



KB.05.A.212/6

APPENDIX C

5. DISCUSSION

The mineralogical composition of each samples obtained by Raman and FTIR spectroscopy, XRD and SEM-EDS analysis.

	RAMAN	FTIR	XRD	SEM	TOT
KB.06.B.392/8	Calcite Hematite Apatite Carbon	Calcite +++ Hematite tr Magnetite tr Quartz ++ K-feldspar tr Illite tr	Calcite +++ Quartz ++ K-feldspar tr Plagioclase tr Illite tr	Calcite Iron oxides Ilmenite Apatite Quartz Feldspars	Calcite Hematite Magnetite Ilmenite Apatite Quartz K-feldspar Plagioclase Illite Carbon
KB.06.E.702/10	Calcite Hematite Magnetite Ilmenite Anatase Gypsum Apatite Quartz Carbon	Calcite + Magnetite tr Quartz +++ K-feldspar tr Illite tr	Calcite tr Hematite tr Gypsum + Quartz +++ K-feldspar tr Plagioclase tr Illite tr		Calcite Hematite Magnetite Ilmenite Anatase Gypsum Apatite Quartz K-feldspar Plagioclase Illite Carbon
KB.06.E.703/6	Calcite Hematite Anatase Gypsum Barite Quartz Carbon	Calcite +++ Magnetite tr Gypsum ++ Quartz ++ K-feldspar tr Albite tr Illite tr	Calcite +++ Gypsum + Quartz + Plagioclase tr Gehlenite +		Calcite Hematite Magnetite tr Anatase Gypsum Barite Quartz K-feldspar Albite Gehlenite Illite Carbon
KB.06.E.703/5	Calcite Hematite Ilmenite Anatase Apatite Quartz K-feldspar Carbon	Calcite ++ Magnetite tr Quartz +++ Albite tr Illite tr	Calcite +++ Hematite tr Gypsum tr Quartz ++ K-feldspar tr Illite +		Calcite Hematite Magnetite Ilmenite Anatase Gypsum Apatite Quartz K-feldspar Albite Illite Carbon

KB.06.E.704/1	Calcite Hematite Magnetite Bassanite Quartz Carbon	Calcite + Quartz +++ K-feldspar tr Illite tr	Calcite + Quartz +++ K-feldspar tr		Calcite Hematite Magnetite Bassanite Quartz K-feldspar Illite Carbon
KB.06.E.704/6	Calcite Hematite Magnetite Apatite Quartz Carbon	Calcite ++ Magnetite tr Quartz +++ K-feldspar tr Illite tr	Calcite + Quartz +++ K-feldspar tr Plagioclase tr	Calcite Iron oxides Mn oxides Ti oxides Barite Quartz	Calcite Hematite Magnetite Mn oxides Ti oxides Barite Apatite Quartz K-feldspar Plagioclase Illite Carbon
KB.06.E.706/2	Calcite Hematite Gypsum Bassanite Quartz Carbon	Calcite +++ Hematite tr Magnetite tr Gypsum + Quartz ++ Illite tr	Calcite +++ Hematite tr Gypsum + Quartz + Gehlenite tr	Calcite Iron oxides Ilmenite Barite Apatite Quartz Zircon	Calcite Hematite Magnetite Ilmenite Gypsum Bassanite Barite Apatite Quartz Gehlenite Zircon Illite Carbon
KB.06.E.706/1	Calcite Hematite Rutile Barite Quartz Carbon	Calcite +++ Magnetite tr Gypsum tr Quartz ++ K-feldspar tr Illite tr	Calcite +++ Hematite tr Quartz ++ Gehlenite tr	Calcite Iron oxides Barite Apatite Quartz	Calcite Hematite Magnetite Rutile Gypsum Barite Apatite Quartz K-feldspar Gehlenite Illite Carbon
KB.05.A.52/8	Calcite Hematite Magnetite Ilmenite Gypsum Apatite Quartz Diopside Forsterite Albite Anorthite K-feldspar		Calcite +++ Hematite tr Quartz ++ Diopside + Plagioclase ++ K-feldspar ++ Illite tr	Calcite Ilmenite Quartz	Calcite Hematite Magnetite Ilmenite Gypsum Apatite Quartz Diopside Forsterite Albite Anorthite K-feldspar Illite

KB.05.A.58/1	Calcite Hematite Magnetite Anatase Quartz	Calcite + Quartz +++ Anorthite + Diopside +	Calcite ++ Hematite tr Quartz +++ Plagioclase tr K-feldspar tr		Calcite Hematite Magnetite Anatase Quartz Anorthite Diopside K-feldspar
KB.05.A.64/1	Calcite Hematite Ilmenite Rutile Apatite Quartz Diopside Forsterite Albite K-feldspar	Calcite ++ Hematite tr Quartz +++ Anorthite tr Illite +	Calcite + Quartz +++ Plagioclase + K-feldspar +		Calcite Hematite Ilmenite Rutile Apatite Quartz Diopside Forsterite Albite Anorthite K-feldspar Illite
KB.05.A.64/13	Calcite Hematite Magnetite Anatase Gypsum Apatite Quartz Albite Carbon		Calcite ++ Hematite tr Quartz +++ Plagioclase ++ Gehlenite tr	Calcite Iron oxides Ilmenite Feldspars	Calcite Hematite Magnetite Ilmenite Anatase Gypsum Apatite Quartz Albite Plagioclase Gehlenite Carbon
KB.05.B.110/15	Calcite Hematite Magnetite Ilmenite Quartz Diopside K-feldspar		Calcite +++ Quartz + Diopside + Plagioclase ++ K-feldspar tr Gehlenite tr		Calcite Hematite Magnetite Ilmenite Quartz Diopside Plagioclase K-feldspar Gehlenite
KB.05.B.126/1	Calcite Hematite Magnetite Quartz Carbon		Calcite +++ Quartz + Gehlenite tr		Calcite Hematite Magnetite Quartz Gehlenite Carbon
KB.05.B.126/3	Calcite Hematite Apatite Quartz Carbon	Calcite +++ Gypsum tr Quartz ++ K-feldspar tr Illite tr	Calcite +++ Hematite tr Quartz ++	Calcite Iron oxides Apatite Pyroxene	Calcite Hematite Apatite Gypsum Quartz Pyroxene K-feldspar Illite Carbon

KB.05.B.126/4	Calcite Hematite Magnetite Apatite Quartz Diopside Albite Anorthite Carbon		Calcite +++ Hematite tr Quartz ++ Diopside ++ Plagioclase ++ K-feldspar ++ Illite tr	Calcite Hematite Magnetite Apatite Quartz Diopside Albite Anorthite K-feldspar Illite Carbon
KB.05.B.136/1	Calcite Hematite Quartz		Calcite ++ Hematite tr Quartz +++ Plagioclase tr K-feldspar tr Illite tr	Iron oxides Quartz Calcite Hematite Quartz Plagioclase K-feldspar Illite
KB.05.B.136/3	Calcite Hematite Magnetite Ilmenite Diopside Albite K-feldspar Carbon	Calcite ++ Hematite tr Magnetite tr Gypsum + Quartz +++ Diopside tr Anorthite tr K-feldspar tr Illite tr	Calcite +++ Quartz ++ Diopside + Plagioclase ++ K-feldspar ++ Illite tr	Calcite Hematite Magnetite Ilmenite Gypsum Quartz Diopside Anorthite K-feldspar Illite Carbon
KB.05.B.136/5	Calcite Hematite Gypsum Barite Quartz K-feldspar Carbon		Calcite +++ Quartz + Plagioclase + K-feldspar + Gehlenite tr	Calcite Hematite Gypsum Barite Quartz Plagioclase K-feldspar Gehlenite Carbon
KB.05.B.146/1	Calcite Hematite Quartz Carbon	Calcite +++ Gypsum tr Quartz ++ K-feldspar tr Illite tr	Calcite +++ Hematite tr Quartz + Gehlenite tr	Calcite Hematite Gypsum Quartz K-feldspar Gehlenite Illite Carbon
KB.05.B.146/3	Calcite Hematite Magnetite Quartz		Calcite ++ Hematite tr Quartz +++ Diopside + Plagioclase +++ K-feldspar ++	Calcite Hematite Magnetite Quartz Diopside Plagioclase K-feldspar
KB.05.B.146/4	Calcite Hematite		Calcite ++ Quartz +++ Plagioclase tr K-feldspar tr Illite tr	Calcite Hematite Quartz Plagioclase K-feldspar Illite

KB.05.B.146/5	Calcite Hematite Magnetite Ilmenite Rutile Gypsum Barite Quartz Diopside Albite Lazurite Carbon	Calcite + Gypsum +++ Quartz + Diopside + Al- bite +	Calcite +++ Hematite tr Quartz ++ Diopside + Plagioclase + K-feldspar + Gehlenite tr Illite tr	Calcite Hematite Magnetite Ilmenite Rutile Gypsum Barite Quartz Diopside Albite K-feldspar Gehlenite Illite Lazurite Carbon
KB.05.B.146/6	Calcite Anatase Quartz Lazurite		Calcite + Quartz +++ Illite tr	Calcite Anatase Quartz Lazurite Illite
KB.05.B.146/7	Calcite Hematite Magnetite Carbon	Calcite +++ Quartz ++ Diopside + Albite + Anorthite +	Calcite + Quartz +++ Plagioclase + K-feldspar + Gehlenite tr	Calcite Hematite Magnetite Quartz Diopside Albite Anorthite K-feldspar Gehlenite Carbon
KB.05.B.146/8	Calcite Hematite Anatase Corundum Quartz Carbon		Calcite Iron oxides Ilmenite Apatite Quartz Olivine Feldspars	Calcite Iron oxides Ilmenite Anatase Corundum Apatite Quartz Olivine Feldspars Carbon
KB.05.B.146/15	Calcite Hematite Magnetite Gypsum Apatite Diopside K-feldspar	Calcite ++ Gypsum tr Quartz ++ Diopside ++ Albite +++ Anorthite +++ K-feldspar + Illite tr	Calcite ++ Quartz ++ Diopside + Plagioclase +++ K-feldspar +++ Epidote + Illite tr	Calcite Ilmenite Barite Pyroxene Feldspars
			Calcite	Calcite Hematite Magnetite Ilmenite Gypsum Barite Apatite Quartz Diopside Albite Anorthite K-feldspar Epidote Illite

KB.05.B.146/20	Calcite Hematite		Calcite +++		Calcite Hematite Quartz K-feldspar Epidote Illite Carbon
	Carbon		Quartz + K-feldspar tr Epidote + Illite tr		
KB.05.B.146/24	Calcite Hematite Corundum Gypsum	Calcite ++	Calcite + Hematite tr	Calcite Iron oxides	Calcite Hematite Corundum Gypsum Quartz Diopside Albite Anorthite K-feldspar Zircon Gehlenite
	K-feldspar Zircon	Quartz + Diopside + Albite + Anorthite +	Quartz +++ Diopside tr Plagioclase + K-feldspar + Gehlenite +	Quartz Pyroxenes	
KB.05.B.146/30	Calcite Hematite Magnetite Ilmenite Quartz		Calcite +		Calcite Hematite Magnetite Ilmenite Quartz Plagioclase K-feldspar Gehlenite Illite Carbon
	Carbon		Quartz +++ Plagioclase + K-feldspar + Gehlenite tr Illite tr		
KB.06.B.167/4	Hematite Magnetite	Calcite +	Calcite +++	Calcite Iron oxides Ilmenite	Calcite Hematite Magnetite Quartz Diopside Albite Anorthite K-feldspar Gehlenite Epidote Illite
	Diopside Albite K-feldspar	Quartz +++ Diopside + Albite + Anorthite tr Illite tr	Quartz ++ Diopside ++ Plagioclase ++ K-feldspar ++ Gehlenite tr Epidote + Illite tr	Pyroxenes Feldspars	
KB.06.B.376/4	Hematite Magnetite Gypsum Apatite Quartz		Hematite +		Hematite Magnetite Gypsum Apatite Quartz Diopside Plagioclase K-feldspar Gehlenite
			Gypsum + Quartz +++ Diopside + Plagioclase + K-feldspar + Gehlenite tr		
KB.06.B.413/2	Calcite Hematite Gypsum	Calcite +++	Calcite +++	Calcite Iron oxides	Calcite Hematite Gypsum Quartz Feldspars Gehlenite Illite Carbon
	Carbon	Gypsum tr Quartz ++ Illite tr	Quartz + Gehlenite +	Quartz Feldspars	

KB.06.E.701/2	Calcite Hematite Quartz	Calcite + Quartz +++ Diopside tr Albite tr Anorthite tr Illite tr	Calcite + Hematite + Quartz +++ Diopside + Plagioclase + K-feldspar + Illite tr		Calcite Hematite Quartz Diopside Albite Anorthite K-feldspar Illite
KB.06.E.703/3	Hematite Magnetite Corundum Quartz	Calcite + Gypsum tr Quartz +++ K-feldspar tr Illite tr	Hematite tr Quartz +++ K-feldspar tr Gehlenite tr		Calcite Hematite Magnetite Corundum Gypsum Quartz K-feldspar Gehlenite Illite
KB.06.B.427/1	Calcite Gypsum Quartz Carbon		Calcite +++ Quartz ++ Diopside tr Gehlenite tr	Calcite Quartz Py- roxenes	Calcite Gypsum Quartz Diopside Gehlenite Carbon
KB.08.B.805/6	Calcite Hematite Barite Quartz ++ Carbon	Calcite +++ Hematite tr Gypsum tr Quartz ++	Calcite +++ Hematite tr Quartz + Plagioclase tr K-feldspar tr Gehlenite tr Illite tr	Calcite Iron oxides Ilmenite Barite Apatite Quartz Pyroxenes Feldspars	Calcite Hematite Ilmenite Gypsum Barite Apatite Quartz Pyroxenes Plagioclase K-feldspar Gehlenite Illite Carbon
KB.09.B.820.10	Calcite Hematite Diopside Carbon	Calcite +++ Quartz ++ Diopside tr K-feldspar tr Illite tr	Calcite +++ Quartz + Diopside + Plagioclase + K-feldspar + Gehlenite tr Epidote tr		Calcite Hematite Quartz Diopside Plagioclase K-feldspar Gehlenite Epidote Illite Carbon
KB.09.B.820.12	Calcite Goethite Quartz Carbon	Calcite +++ Quartz ++ Albite tr K-feldspar tr Illite tr	Calcite +++ Quartz + K-feldspar tr Epidote ++ Illite tr	Calcite Iron oxides Ilmenite Apatite Pyroxenes Feldspars	Calcite Goethite Ilmenite Apatite Quartz Pyroxenes Albite K-feldspar Epidote Illite Carbon

KB.09.B.820/13A+13B	Calcite Hematite Magnetite Ilmenite Gypsum	Calcite ++	Calcite +++ Hematite tr	Calcite Ilmenite Apatite	Calcite Hematite Magnetite Ilmenite Gypsum Apatite Quartz Diopside
	Diopside Albite K-feldspar Carbon	Quartz ++ K-feldspar + Illite tr	Quartz + Plagioclase + K-feldspar + Gehlenite tr Illite tr	Feldspars Olivine	Albite K-feldspar Olivine Gehlenite Illite Carbon
KB.08.B.805/32	Calcite Carbon				Calcite Carbon
KB.08.B.805/34	Calcite Carbon	Calcite +++ Quartz ++ Illite tr			Calcite Quartz Illite Carbon
KB.05.A.46/2	Calcite Hematite Magnetite Olivine Carbon		Calcite ++ Quartz +++ Plagioclase tr K-feldspar tr		Calcite Hematite Magnetite Quartz Olivine Plagioclase K-feldspar Carbon
KB.05.A.46/8	Calcite Hematite Magnetite Apatite Quartz		Calcite +++ Quartz ++ Plagioclase tr K-feldspar tr		Calcite Hematite Magnetite Apatite Quartz Plagioclase K-feldspar
KB.05.A.216/4	Calcite Hematite Gypsum Barite Quartz Carbon		Calcite +++ Quartz ++ Illite tr		Calcite Hematite Gypsum Barite Quartz Illite Carbon
KB.05.A.204/2	Calcite Magnetite Quartz Carbon	Calcite ++ Quartz +++ Anorthite ++	Calcite +++ Hematite tr Quartz ++ Gehlenite tr		Calcite Magnetite Quartz Anorthite Gehlenite Carbon
KB.05.A.204/3	Calcite Rutile Quartz Olivine Carbon	Calcite +++ Hematite + Quartz +++ Albite ++ Anorthite ++	Calcite +++ Quartz + Plagioclase tr K-feldspar tr Gehlenite tr	Calcite Iron oxides Quartz	Calcite Hematite Rutile Quartz Olivine Albite Anorthite K-feldspar Gehlenite Carbon

KB.05.A.220/5	Calcite Hematite		Calcite +++ Hematite + Quartz ++ Gehlenite tr Illite tr		Calcite Hematite Quartz Gehlenite Illite Carbon
	Carbon				
KB.05.A.224/2	Calcite Hematite		Calcite +++ Quartz ++ Plagioclase tr K-feldspar tr Illite tr		Calcite Hematite Quartz Plagioclase K-feldspar Illite Carbon
	Carbon				
KB.06.A.120/6	Calcite Hematite	Calcite ++ Hematite + Gypsum tr	Calcite +++ Hematite tr	Calcite Iron oxides	Calcite Hematite Gypsum Apatite Quartz Albite Anorthite K-feldspar Gehlenite Illite Carbon
	Quartz	Quartz +++ Albite + Anorthite + K-feldspar + Illite +	Quartz ++ K-feldspar tr Gehlenite tr Illite tr	Apatite Feldspars	
	Carbon				
KB.05.B.111/3	Calcite Hematite Magnetite Ilmenite Corundum	Calcite +++ Hematite + Gypsum tr Quartz +++ Albite ++ Anorthite ++ Illite +	Calcite ++ Hematite tr Quartz +++ Diopside tr Plagioclase ++ Gehlenite ++		Calcite Hematite Magnetite Ilmenite Corundum Gypsum Quartz Diopside Albite Anorthite Gehlenite Illite Carbon
	Carbon				
KB.10.B.1040/8	Calcite Hematite Magnetite Quartz		Calcite +++ Hematite tr Quartz ++ Diopside + Plagioclase ++ K-feldspar ++ Gehlenite +		Calcite Hematite Magnetite Quartz Diopside Plagioclase K-feldspar Gehlenite Zircon Carbon
	Zircon Carbon				
KB.11.B.1054/2	Calcite Hematite Magnetite Gypsum Barite Diopside Carbon				Calcite Hematite Magnetite Gypsum Barite Diopside Carbon
KB.10.B.1054/6	Calcite Hematite Magnetite Quartz Carbon				Calcite Hematite Magnetite Quartz Carbon

KB.11.B.1054/12	Calcite Hematite Magnetite Gypsum Barite Quartz Carbon				Calcite Hematite Magnetite Gypsum Barite Quartz Carbon
KB.11.B.1054/13	Calcite Hematite Quartz Olivine Carbon				Calcite Hematite Quartz Olivine Carbon
KB.11.B.1054/21	Calcite Hematite Magnetite Anatase Quartz K-feldspar Carbon	Calcite +++ Hematite + Quartz ++ Albite + Anorthite + K-feldspar + Illite +	Calcite +++ Hematite tr Quartz ++ Plagioclase tr K-feldspar tr Gehlenite tr	Calcite Iron oxides Ilmenite Apatite Quartz	Calcite Hematite Magnetite Ilmenite Anatase Apatite Quartz Albite Anorthite K-feldspar Gehlenite Illite Carbon
KB.10.B.1054/22	Calcite Hematite Magnetite Carbon				Calcite Hematite Magnetite Carbon
KB.10.B.1054/24	Calcite Hematite Magnetite Ilmenite Quartz Carbon	Calcite ++ Hematite + Quartz +++ Albite + Anorthite + K-feldspar + Illite +	Calcite tr Hematite tr Quartz +++ Plagioclase + K-feldspar + Gehlenite tr	Calcite Iron oxides Ilmenite Apatite Pyroxenes Feldspars	Calcite Hematite Magnetite Ilmenite Apatite Quartz Pyroxenes Albite Anorthite K-feldspar Gehlenite Illite Carbon
KB.10.B.1054/62	Calcite Hematite Magnetite Gypsum Quartz	Calcite ++ Hematite ++ Quartz +++ Albite + Anorthite + K-feldspar + Illite +	Calcite +++ Quartz +	Calcite Iron oxides Ilmenite Barite Apatite Pyroxenes Feldspars	Calcite Hematite Magnetite Gypsum Barite Apatite Quartz Pyroxenes Albite Anorthite K-feldspar Illite

KB.11.B.1124/1	Calcite Hematite Magnetite Corundum Quartz Diopside Carbon				Calcite Hematite Magnetite Corundum Quartz Diopside Carbon
KB.11.B.1124/3	Calcite Hematite Magnetite Ilmenite Anatase Quartz Carbon	Calcite +++ Hematite + Quartz ++ Albite + Anorthite ++ K-feldspar + Illite +	Calcite +++ Quartz ++ K-feldspar tr Gehlenite tr	Calcite Iron oxides Apatite Quartz	Calcite Hematite Magnetite Ilmenite Anatase Apatite Quartz Albite Anorthite K-feldspa Gehlenite Illite Carbon
KB.11.B.1124/10	Calcite Hematite Magnetite Rutile Gypsum Diopside Olivine Carbon				Calcite Hematite Magnetite Rutile Gypsum Diopside Olivine Carbon
KB.11.B.1124/15	Calcite Hematite Rutile Quartz Diopside Carbon	Calcite +++ Hematite + Quartz +++ Albite + Anorthite + K-feldspar + Illite +	Calcite +++ Quartz ++ K-feldspar tr Illite tr	Calcite Apatite	Calcite Hematite Rutile Apatite Quartz Diopside Albite Anorthite K-feldspar Illite Carbon
KB.11.B.1124/19	Calcite Hematite Carbon				Calcite Hematite Carbon
KB.11.B.1124/22	Calcite Carbon				Calcite Carbon
KB.11.B.1124/24	Calcite Hematite Quartz Carbon				Calcite Hematite Quartz Carbon
KB.11.B.1124/28	Calcite Hematite Magnetite Anatase Gypsum Barite Quartz Carbon				Calcite Hematite Magnetite Anatase Gypsum Barite Quartz Carbon

KB.11.B.1124/29	Calcite Hematite	Calcite ++ Hematite + Quartz +++ Albite ++ Anorthite + K-feldspar + Illite +	Calcite ++ Hematite tr Quartz +++ Plagioclase + Illite tr	Calcite Iron oxides Apatite Quartz	Calcite Hematite Apatite Quartz Albite Anorthite K-feldspar Illite Carbon
	Carbon				
KB.11.B.1124/33	Calcite	Calcite ++ Hematite + Quartz +++ K-feldspar + Albite + Anorthite + Illite +		Calcite Iron oxides Barite Apatite Quartz	Calcite Hematite Barite Apatite Quartz K-feldspar Albite Anorthite Illite Carbon
	Carbon				
KB.11.B.1124/8	Calcite Hematite Magnetite Ilmenite Anatase	Calcite +++ Hematite + Quartz +++ Albite + Anorthite + K-feldspar + Illite +	Calcite +++ Quartz ++ Gehlenite +	Calcite Iron oxides Ilmenite Pyroxenes Feldspars	Calcite Hematite Magnetite Ilmenite Anatase Quartz Pyroxenes Albite Anorthite K-feldspar Gehlenite Illite Carbon
	Carbon				
KB.11.B.1128/76	Calcite Hematite Quartz Carbon				Calcite Hematite Quartz Carbon
KB.11.B.1128/1	Calcite Hematite Magnetite Rutile Gypsum Barite Quartz Carbon				Calcite Hematite Magnetite Rutile Gypsum Barite Quartz Carbon
KB.11.B.1128/50	Calcite Hematite Ilmenite Anatase Gypsum Barite Quartz	Calcite ++ Hematite + Quartz +++ Albite + Anorthite + K-feldspar + Illite +	Calcite +++ Quartz + Plagioclase tr K-feldspar tr Gehlenite tr		Calcite Hematite Ilmenite Anatase Gypsum Barite Quartz Albite Anorthite K-feldspar Gehlenite Illite Carbon
	Carbon				

<p>KB.11.B.1128/51</p>	<p>Calcite Hematite Gypsum Barite Quartz Carbon</p>	<p>Calcite ++ Hematite + Quartz +++ Albite + Anorthite ++ K-feldspar + Illite +</p>	<p>Calcite +++ Quartz + Plagioclase tr K-feldspar tr Gehlenite tr Illite tr</p>	<p>Calcite Hematite Gypsum Barite Quartz Albite Anorthite K-feldspar Gehlenite Illite Carbon</p>
<p>KB.11.B.1128/52</p>	<p>Calcite Hematite Magnetite Gypsum Barite Apatite Quartz Carbon</p>			<p>Calcite Hematite Magnetite Gypsum Barite Apatite Quartz Carbon</p>
<p>KB.11.B.1128/65</p>	<p>Calcite Hematite Anatase Rutile Gypsum Quartz</p>	<p>Calcite +++ Hematite + Quartz +++ Albite + Anorthite + K-feldspar + Illite +</p>	<p>Calcite ++ Hematite tr Gypsum + Quartz +++ Plagioclase tr Gehlenite tr</p>	<p>Calcite Iron oxides Ilmenite Quartz Feldspars Zircon Calcite Hematite Ilmenite Anatase Rutile Gypsum Quartz Albite Anorthite K-feldspar Gehlenite Zircon Illite</p>
<p>KB.05.5/D200</p>	<p>Calcite Hematite Magnetite Ilmenite Gypsum Quartz Carbon</p>	<p>Calcite ++ Hematite + Quartz +++ Albite ++ Anorthite ++ Illite +</p>	<p>Calcite ++ Hematite tr Quartz +++ Plagioclase + K-feldspar + Gehlenite + Epidote tr</p>	<p>Calcite Hematite Magnetite Ilmenite Gypsum Quartz Albite Anorthite K-feldspar Gehlenite Epidote Illite Carbon</p>
<p>KB.05.A.6b/1</p>	<p>Calcite Hematite Magnetite Ilmenite Quartz K-feldspar Carbon</p>	<p>Calcite +++ Quartz +++ Albite ++ Illite +</p>	<p>Calcite +++ Quartz ++ Plagioclase + K-feldspar + Illite +</p>	<p>Calcite Iron oxides Ilmenite Quartz Feldspars Calcite Hematite Magnetite Ilmenite Quartz Albite K-feldspar Illite Carbon</p>

KB.05.A.18/5	Calcite Hematite Magnetite Ilmenite Anatase Quartz Aegirine Zircon Carbon	Calcite ++ Hematite + Quartz +++ Diopside + K-feldspar ++	Calcite +++ Quartz ++ K-feldspar tr		Calcite Hematite Magnetite Ilmenite Anatase Quartz Diopside K-feldspar Aegirine Zircon Carbon
KB.05.A.21/27	Calcite Hematite Apatite Quartz Diopside K-feldspar Aegirine Carbon	Calcite +++ Quartz ++ Albite ++ Anorthite +	Calcite +++ Hematite tr Quartz ++ Diopside + Plagioclase + K-feldspar +	Calcite Iron oxides Ilmenite Apatite Barite Quartz Feldspars	Calcite Hematite Ilmenite Apatite Barite Quartz Diopside Albite Anorthite K-feldspar Aegirine Carbon
KB.05.A.34/2	Calcite Hematite Magnetite Ilmenite Apatite Quartz Diopside Olivine Carbon	Calcite +++ Hematite + Quartz ++ Albite ++ Anorthite ++ Illite +	Calcite +++ Hematite tr Quartz ++ Diopside tr Plagioclase + K-feldspar + Gehlenite tr		Calcite Hematite Magnetite Ilmenite Apatite Quartz Diopside Olivine Albite Anorthite K-feldspar Gehlenite Illite Carbon
KB.05.A.62/1	Calcite Hematite Magnetite Ilmenite Gypsum Diopside Carbon	Calcite +++ Hematite + Quartz +++ Albite ++ Anorthite ++ Illite +	Calcite +++ Hematite tr Quartz + Diopside tr Plagioclase + K-feldspar + Epidote tr		Calcite Hematite Magnetite Ilmenite Gypsum Quartz Diopside Albite Anorthite K-feldspar Epidote Illite Carbon
KB.05.A.62/2	Calcite Magnetite Lepidocrocite Quartz	Calcite +++ Quartz +++ Albite ++ Anorthite ++ K-feldspar ++	Calcite +++ Hematite + Quartz +++ Plagioclase +		Calcite Magnetite Lepidocrocite Quartz Albite Anorthite K-feldspar

<p>KB.05.A.68/2</p>	<p>Calcite Hematite Magnetite</p> <p>Quartz</p> <p>Carbon</p>	<p>Calcite +++</p> <p>Quartz +++ Albite ++</p> <p>Illite +</p>	<p>Calcite +++</p> <p>Quartz ++ Plagioclase + K-feldspar + Epidote tr</p>	<p>Calcite Iron oxides</p> <p>Ilmenite Apatite Barite Quartz</p> <p>Calcite Hematite Magnetite Ilmenite Apatite Barite Quartz Albite K-feldspar Epidote Illite Carbon</p>
<p>KB.05.A.82/4</p>	<p>Calcite Hematite Magnetite Ilmenite Corundum Apatite Quartz</p> <p>Aegirina</p> <p>Carbon</p>	<p>Calcite +++</p> <p>Quartz +++</p> <p>Albite ++ Anorthite ++</p> <p>Illite +</p>	<p>Calcite +++</p> <p>Quartz ++ Diopside tr Plagioclase +</p> <p>K-feldspar + Gehlenite +</p>	<p>Calcite Hematite Magnetite Ilmenite Corundum Apatite Quartz Diopside Albite Anorthite K-feldspar Gehlenite Aegirina Illite Carbon</p>
<p>KB.05.A.84/3</p>	<p>Calcite Hematite Magnetite Ilmenite Gypsum</p> <p>Apatite Quartz</p> <p>Carbon</p>	<p>Calcite +++</p> <p>Quartz +++ Albite ++ Anorthite ++</p>	<p>Calcite ++ Hematite tr</p> <p>Quartz +++ Plagioclase +</p> <p>K-feldspar + Gehlenite + Epidote tr Illite tr</p>	<p>Calcite Iron oxides</p> <p>Ilmenite</p> <p>Barite Apatite</p> <p>Feldspars</p> <p>Calcite Hematite Magnetite Ilmenite Gypsum Barite Apatite Quartz Albite Anorthite K-feldspar Gehlenite Epidote Illite Carbon</p>
<p>KB.05.A.8b/3b</p>	<p>Calcite Hematite Quartz</p>	<p>Calcite +++</p> <p>Quartz +++</p> <p>K-feldspar ++</p>	<p>Calcite +++</p> <p>Quartz ++ Diopside tr K-feldspar + Illite tr</p>	<p>Calcite Hematite</p> <p>Quartz Diopside K-feldspar Illite tr</p>

KB.05.A.88/1	Calcite Hematite Magnetite Ilmenite Anatase Gypsum	Calcite +++	Calcite +++	Calcite Iron oxides Ilmenite Apatite Quartz Olivine Feldspars	Calcite Hematite Magnetite Ilmenite Anatase Gypsum Apatite Quartz Diopside Olivine Plagioclase K-feldspar Illite Carbon
	Quartz Diopside Olivine K-feldspar Carbon	Quartz +++	Quartz ++ Plagioclase + K-feldspar + Illite tr		
KB.05.A.96/1	Calcite Hematite Rutile Corundum	Calcite +++	Calcite +++		Calcite Hematite Rutile Corundum Quartz Albite Anorthite K-feldspar Gehlenite Illite Carbon
	Quartz Albite ++ Anorthite ++ K-feldspar Illite + Carbon	Quartz +++ Albite ++ Anorthite ++	Quartz ++ Gehlenite tr Illite tr		
KB.05.A.98/1	Calcite Hematite Magnetite Ilmenite Quartz	Calcite ++	Calcite +++		Calcite Hematite Magnetite Ilmenite Quartz Diopside Albite Anorthite Illite Carbon
	Quartz Diopside + Albite ++ Anorthite ++ Illite + Carbon	Quartz +++ Diopside + Albite ++ Anorthite ++ Illite +	Quartz ++ Illite tr		
KB.05.A.210/2	Calcite Hematite	Calcite +++	Calcite +		Calcite Hematite Quartz Diopside Albite Anorthite Illite Carbon
	Quartz Albite ++ Anorthite ++ Illite + Carbon	Quartz +++ Albite ++ Anorthite ++ Illite +	Quartz +++ Diopside + Plagioclase ++ Illite +		
KB.05.A.210/4	Calcite Hematite Magnetite Ilmenite Corundum	Calcite +++	Calcite +++		Calcite Hematite Magnetite Ilmenite Corundum Quartz Diopside Albite Anorthite K-feldspar Gehlenite Illite
	Quartz Albite ++ Anorthite ++ K-feldspar ++ Illite +	Quartz +++ Albite ++ Anorthite ++ K-feldspar ++ Illite +	Quartz ++ Diopside tr Plagioclase + K-feldspar + Gehlenite tr		

KB.05.A.212/6	Calcite Hematite Corundum	Calcite ++ Quartz +++ Albite ++ Anorthite ++	Calcite +++ Quartz ++ Gehlenite tr		Calcite Hematite Corundum Quartz Albite Anorthite Gehlenite Carbon
	Carbon				
KB.05.A.216/12	Calcite Hematite Magnetite	Calcite +++ Quartz +++ Albite ++ Anorthite ++	Calcite +++ Quartz ++ K-feldspar + Gehlenite tr Epidote tr		Calcite Hematite Magnetite Quartz Albite Anorthite K-feldspar Gehlenite Epidote
	Carbon				
KB.05.B.128/3	Calcite Hematite	Calcite +++ Quartz +++	Calcite ++ Hematite tr Quartz +++		Calcite Hematite Quartz Diopside Albite K-feldspar
	Diopside	Albite ++ K-feldspar ++	Plagioclase ++ K-feldspar ++ Illite tr		Illite Carbon
KB.06.A.248/2	Calcite Hematite	Calcite +++ Hematite +	Calcite ++ Hematite +	Calcite Iron oxides Ilmenite	Calcite Hematite Ilmenite
	Quartz	Quartz +++ K-feldspar ++ Albite ++ Illite +	Quartz +++	Quartz	Quartz K-feldspar Albite Illite Carbon
KB.06.A.256/1	Calcite Hematite	Calcite +++	Calcite ++	Calcite Iron oxides Ilmenite	Calcite Hematite Ilmenite
	Quartz	Quartz +++ K-feldspar ++ Illite +	Quartz +++ K-feldspar tr Illite tr	Quartz Feldspars	Quartz K-feldspar Illite Carbon
KB.06.A.ø/18	Calcite Hematite Magnetite Ilmenite Quartz	Calcite +++ Quartz ++ Albite ++	Calcite +++ Quartz + Gehlenite tr Epidote ++		Calcite Hematite Magnetite Ilmenite Quartz Albite Gehlenite Epidote Illite Carbon
	Carbon	Illite +			

KB.06.B.383/7	Calcite	Calcite +++		Calcite
	Hematite	Hematite +	Hematite tr	Hematite
	Magnetite			Magnetite
	Ilmenite			Ilmenite
	Gypsum		Gypsum ++	Gypsum
	Quartz	Quartz +++	Quartz +++	Quartz
	Olivina			Olivina
	Diopside			Diopside
		Albite ++	Plagioclase ++	Albite
		Anorthite ++		Anorthite
			K-feldspar ++	K-feldspar
		Gehlenite ++	Gehlenite	
		Epidote +	Epidote	
	Illite +		Illite	
Carbon			Carbon	

APPENDIX D

KHIRBET KERAK WARE FROM KHIRBET AL-BATRAWY (JORDAN)

1. Introduction

In this appendix, is reported a study on a specialized group of ceramic, called Khirbet Kerak Ware (KKW), of the Early Bronze Age from Khirbet al-Batrawy site with the aim to prove its local or imported origin. To achieve this purpose, both micro-Raman and infrared spectroscopy, together with petrographic analysis, Scanning Electron Microscopy and X-ray powder Diffraction, have been applied for mineralogical characterization. The results provide information useful in reconstructing the provenance of raw materials.

In addition, the technological aspects and the firing conditions, i.e. temperatures and redox state of atmosphere (Cultrone *et al.*, 2001; Barone *et al.*, 2002; Maritan, 2004; Rathossi *et al.*, 2004; Iordanidis *et al.*, 2009; Tschegg *et al.*, 2009; Velraj *et al.*, 2009; Belfiore *et al.*, 2010) have also been explored. These results are then compared with those from other coeval ceramic fragments from the same archaeological site, thus clarifying the attribution of the Khirbet Kerak Ware vessels.

Khirbet Kerak Ware (KKW) is a Levantine specialized pottery production, identified for the first time by Albright (1926) at the homonymous site of Khirbet Kerak in northern Palestine. This pottery production is dated approximately to 2750-2500 B.C., the Early Bronze III (EB III) of local chronology, and had a distribution which stretched from Palestine (as far south as Tell el-Hesi and Har Hemar) through the Orontes Valley as far north as the 'Amuq region (De Miroschedji, 2000).

The KKW ceramic consists of distinctive pottery shapes with a characteristic black and/or red lustrous slip, resulting from a manufacturing technique alien to the other EB III Syro-Palestinian ceramic industries (Sukernik, 1947). This immediately gave rise to the debate about its origin and the trade routes which it followed.

At the time of its identification, KKW was considered a foreign production, more specifically associated to Early Bronze Age eastern Anatolian and Transcaucasian/Kura-Araxes ceramic traditions (Amiran, 1952; Burney, 1989). Firstly, the presence of the foreign KKW production, among the EB III standard local ceramics, was explained with possible invasion and/or migration of people coming from the northern regions (Woolley, 1953).

Nevertheless, in the last decades, systematic petrographic studies made on KKW samples from different sites of the Levant proved consistently that Levantine KKW was locally produced, and supported the hypothesis that itinerant potters from Anatolia es-

tablished in the Levant, serving the local population and introducing such pottery production in the local ceramic industry (Chazan and McGovern, 1984; Esse and Hopke, 1986).

The origin of KKW pottery, linked to the arrival of new people in the Levantine lowlands, has never been questioned (Paz, 2009). However, the latest typological and chronological studies, i.e., the re-examination of ceramic materials from Tell es-Sultan/ancient Jericho and other south-central Palestinian sites (like et-Tell, Tell ed-Duweir, Tell el-Hesi and Har Hemar), have highlighted also the existence of local imitations (and local workshops) of proper KKW vessels, away from the centres of intensive KKW production and consumption located in northern Palestine (Sala, 2008). Thus, these studies underline the local nature of what was essentially a cultural phenomenon in the EB III Levantine society (Greenberg, 2007).

2. Materials

A total number of eighteen pottery samples of the EB IIIA phase have been investigated. The potsherds consist of bowl fragments (SPW), platter fragments (RBW), jug and juglet fragments (RPW, SW), small and medium size jar fragments (SW, SPW, StW). Among them, six samples exhibit a surface decoration consisting of simple red or dark strips. A sub-group of five pottery sherds, referred to as KKW, dated back in the same traditional chronological framework, have been unearthed from the layers associated to the destruction of the EB IIIA city.

The analyzed pottery sherds consist of bowls and jugs fragments characterized by a red/brown and black highly polished surface (Sala, 2012). In particular,

KB.08.B.805/6 is a fragments of jug with an outer red lustrous slip; KB.09.B.820/10 is a fragment of hemispherical bowl with plain rim and flat base, black polished inside and outside over the rim, red-polished outside, with an unusual inversion in the in-

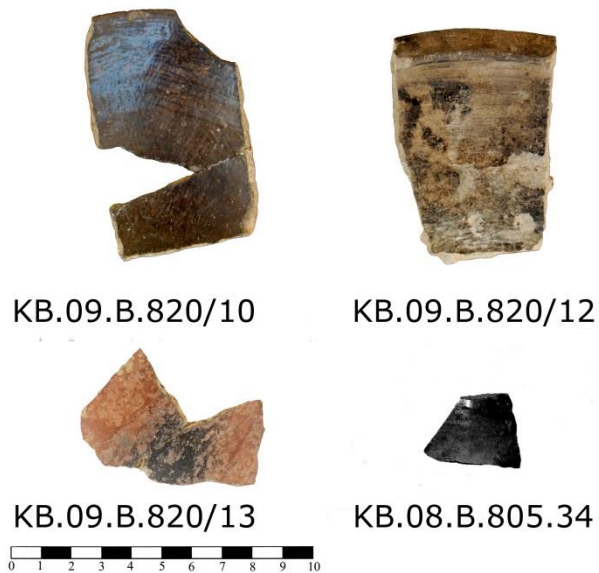


Figure 1: Representative KKW pottery fragments from the archaeological site of Khirbet al-Batrawy.

ner/outer colour of the surface; KB.09.B.820/12 is a fragment of inturned-rim bowl, black polished inside and outside on the upper half, brown-polished outside on the lower half; KB.09.B.820/13 is a fragment of jug with a red to black colour change of the outer slip; and finally KB.08.B.805.34 is a fragment of jug with an outer black lustrous slip (Fig. 1).

3. Results

3.1 Micro-Raman analysis

Micro-Raman results of KKW fragments revealed a simple mineralogical composition. Calcite [CaCO_3], identified by a strong band at 1086 cm^{-1} and other two bands at 712 and 281 cm^{-1} , and quartz [$\alpha\text{-SiO}_2$], with the strong band at 465 cm^{-1} , a medium intensity band at 207 cm^{-1} and a weak band at 356 cm^{-1} , are the main components of the inclusions in the sherds. In the internal body, the bands at 224 , 245 , 299 , 411 , 498 and 611 cm^{-1} are attributed to hematite [$\alpha\text{-Fe}_2\text{O}_3$], whereas amorphous carbon has been clearly identified by the two typical broad bands at 1372 and 1590 cm^{-1} .

Gypsum [$\text{CaSO}_4\cdot 2\text{H}_2\text{O}$], with the strong band at 1008 cm^{-1} , barite, pyroxene [diopside [$\text{Ca}(\text{Mg},\text{Al})(\text{Si},\text{Al})_2\text{O}_6$]] and feldspars [K-feldspar (KAlSi_3O_8), plagioclase [$(\text{Na},\text{Ca})\text{AlSi}_3\text{O}_8$]], with the typical two-peaked feature $\sim 500\text{ cm}^{-1}$ have been also identified in the cross cuts of the sherds.

Particular attention has been given to the polished layers, representing the most distinctive feature of KKW samples. A significant number of spectra collected on this surface revealed the presence of amorphous carbon in the dark zones and hematite in the red ones (Fig. 2).

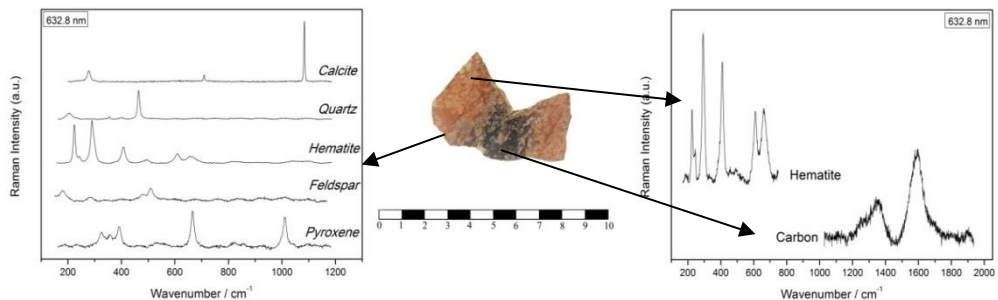


Figure 2: Micro-Raman spectra of a KKW sample KB.09.B.820/13. Raman spectra of the mineralogical components found in the ceramic body (left); Raman spectra collected from the two different coloured surfaces (right), a.u. = arbitrary units.

Table 1: The mineral phases and their relative abundances (+++=abundant; ++=present; +=scarce; tr=traces) occurring in the internal body, decoration and surface, identified by FTIR and by micro-Raman spectroscopies. The symbol (•) identifies the mineralogical phases detected by micro-Raman spectroscopy. Cal: calcite; Hem: hematite; Mag: magnetite; Ant: anatase; Rt: rutile; Gp: gypsum; Brt: barite; Ap:apatite; Qtz:quartz; Di: diopside; Ol: olivine; Kfs: K-feldspar; Pl: plagioclase; Ill: illite; Car: carbon.

Samples	Pot-tery Type	Internal body														Decoration		Surface			
		Cal	Hem	Mag	Ant	Rt	Gp	Brt	Ap	Qtz	Di	Ol	Kfs	Pl	Ill	Car	Hem	Car	Gp	Car	
KB.05.B.136/3	Jar, SW	+++	•	•						+++	tr•		tr•	tr•	tr					•	
KB.05.B.146/5	Juglet, SW	+•	•	•		•	+++•	•		+•	+•			+•						•	•
KB.06.E.703/3	Juglet, SW	+	•	•			tr			+++•			tr		tr						
KB.05.B.146/15	Bowl, SPW	+++	•	•			•		•	++	+++		++	+++	tr		•			•	
KB.06.E.701/2	Jar, SPW	+•	•	•	•					+++•	tr			tr	tr		•				
KB.06.B.167/4	Jar, StW	+	•	•						+++	+•		•	++	tr		•				
KB.06.B.413/2	Hole-mouth jar, StW	+++•	•				tr•			++					tr						•
KB.05.A.58/1	Jug, RPW	+•	•	•	++					+++•	+						•				
KB.05.B.126/1	Jug, RPW	+++•	•	•			tr		•	+++			tr		tr		•				•
KB.05.B.146/7	Jug, RPW	+++•	•	•						++	+			+			•	•			•
KB.05.A.64/1	Platter, RBW	+++	tr•	•		•			•	+++•	•	•	•	tr•	+		•				
KB.05.B.126/3	Platter, RBW	+++•	•				tr		•	+++			tr		tr		•	•			•
KB.05.B.146/1	Platter, RBW	+++•	•				tr			+++			tr		tr		•	•			•
KB.08.B.805/6	Jug, KKW	+++•	tr•				tr•	•		++						•	•				•
KB.09.B.820/10	Bowl, KKW	+++•	•							+++	tr•		tr	tr	tr	•				•	
KB.09.B.820/12	Bowl, KKW	+++•								+++			tr		tr	•				•	
KB.09.B.820/13	Jug, KKW	+++•	•				•			++	•		tr•	•	tr	•				•	
KB.08.B.805.34	Jug, KKW	+++•								++					tr	•				•	

Raman spectra of other EB IIIA fragments suggest a mineralogical composition of the matrix and inclusions similar to that of KKW: the main minerals being calcite, quartz, hematite and magnetite, a mineral of the spinel group, having a strong band at $\sim 660 \text{ cm}^{-1}$.

Minor amounts of gypsum, apatite $[\text{Ca}_5(\text{PO}_4)_3(\text{F}, \text{OH}, \text{Cl})]$ with the band at 961 cm^{-1} and feldspars have also been identified in the cross cuts of the fragments. In addition, the two different polymorphs of titanium dioxide TiO_2 (anatase and rutile), pyroxene (diopside), barite $[\text{BaSO}_4]$, and olivine $[(\text{Mg}, \text{Fe}^{2+})_2\text{SiO}_4]$ are also detected as rare

phases.

Micro-Raman spectroscopy has been also useful in the identifications of pigments used in the surface decoration of EB IIIA group fragments. Spectra collected in different surface points of the decorations revealed the occurrence of hematite in red areas, whereas carbon has been found in the black ones. Moreover, carbon has been also identified in the surface of EB IIIA samples in not-decorated areas.

3.2 FTIR analysis

Infrared spectroscopy has been also applied on KKW samples to complete the results obtain by micro-Raman spectroscopy.

The absorption bands of quartz, i.e. the SiO_2 stretching band at about 1080 cm^{-1} , the shoulders at 1165 and 512 cm^{-1} and the distinctive doublet at 778 and 797 cm^{-1} were detected in all samples. The presence of calcite is testified by the bands at 1420 , 870 , and 714 cm^{-1} in all samples. Illite $[(\text{K},\text{H}_3\text{O})(\text{Al},\text{Mg},\text{Fe})_2(\text{Si},\text{Al})_4\text{O}_{10}(\text{OH})_2(\text{H}_2\text{O})]$ was identified by the characteristic main modes at 460 and 430 cm^{-1} that discriminate it from muscovite. The absorption peaks at 965 , 920 , 865 and 630 cm^{-1} have been attributed to diopside. In addition, minor amounts of plagioclase and K-feldspar have been identified.

The EB IIIA pottery samples mainly contain calcite, quartz and illite, together with rare plagioclase, K-feldspar, gypsum and hematite. A summary of the mineral phases, identified using micro-Raman and FTIR spectroscopies, is shown in Table 1. The relative abundances of each phases, estimated on the basis of the intensity of peaks in the FTIR patterns, are also given. FTIR data, after the manipulation previously described, were investigated using PCA.

The loading plot provides information about the bands that mainly contribute in the differentiation among the spectra. The first 5 PCs together explain 65,17% of the total spatial variance (Table 2), where PC1 and PC2 represent 18,31% and 15,85% of the total variance, respectively. The scores plot (Fig. 3), with the exception of three outliers, shows that the majority of samples, both KKW and EB IIIA, are grouped into an

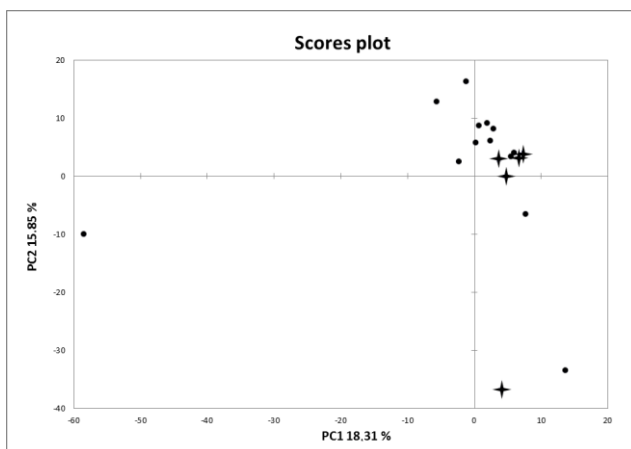


Figure 3: Scores plot of PCA model obtained using the spectral region $400\text{-}1600\text{ cm}^{-1}$. The circles and the crosses identify EB IIIA and KKW pottery, respectively.

unique cluster.

Table 2: Results of PCA performed on dataset.

	PC1	PC2	PC3	PC4	PC5
Value	218.82	189.42	147.15	127.61	95.81
Variability (%)	18.31	15.85	12.31	10.68	8.02
Cumulative variance (%)	18.31	34.16	46.48	57.15	65.17

3.3 Optical microscopy analysis

The analysis in thin sections showed that all samples have similar mineralogical and petrographic characteristics. The shares show also similar textural features: the porosity ranges from 10 to 40%, with vesicles and *vughs*, variable in size between 0.05 and 2 mm. The spatial distribution of the non-plastic inclusions is from single to double spaced without a preferential orientation. The groundmass is generally heterogeneous with an optically active micromass. The ceramics are characterized by abundant non-plastic inclusions amount ranging from 20 to 40%, represented mainly by calcite (micritic or sparry), grog, fragments of sedimentary rock and fossils; less abundant are small-sized crystals of quartz.

The composition of the non-plastic inclusions, the packing and the mean size allow to distinguish three groups having different petrographic fabrics for EB IIIA Khirbet al-Batrawy potteries.

These groups have almost the same mineralogical composition. However, the petrographic group (E), i.e. KB.05.B.126/1, KB.05.A.58/1 and KB.06.E.703/3, can be discriminated on the basis of fine grained inclusions of quartz and calcite in a calcareous brown fine clay matrix containing mainly vesicles. The petrographic group (F), i.e. KB.09.B.820/12, KB.05.A.64/1, KB.05.B.126/3 and KB.05.B.146/1, is characterized by the presence of fragments of fossils and sedimentary rocks as inclusions

Finally, the petrographic group (G), having a calcareous matrix with inclusions of basaltic rocks and fragments of fossils, is divided into two sub-groups. Samples KB.05.B.136/3, KB.08.B.805/6, KB.09.B.820/10 and KB.09.B.820/13 show a matrix brown in colour, whereas samples KB.05.B.146/5, KB.05.B.146/15 and KB.06.E.701/2 present a red matrix. Furthermore, other three samples (KB.05.B.146/7, KB.06.B.167/4, and KB.06.B.413/2) can be considered as petrographic ‘loners’, having different compositional and textural features. The first sample

is characterized by mega-vughs, diffuse clay pallets and fragments of calcite; the second sample by calcite crystals and fragment of basaltic rocks; whereas in the third fragments of shells as inclusions have been identified.

The results of grouping analysis highlight that KKW sherds (Table 3) have fabrics comparable to the EB IIIA petrographic groups.

Table 3: Detailed results of optical microscopy analysis in thin section. In the last column the petrographic fabric groups are indicated.

EB IIIA	PORES	C:f	INCLUSIONS>0.125mm	INCLUSIONS<0.125mm	
KB.05.B.136.3	20-30% vesicles/vughs not aligned 0.05-2mm	20-30%	calcite (sa-sr 0.7-1.5 mm), fossils fragments oolites (r-wr 0.6-0.8 mm), fragments of rocks (va 1.0-2.0 mm), iron oxides nodules (wr 0.8-4.0 mm)		G
KB.05.B.146.5	30% vughs not aligned 0.05-2mm	20%	fragments of rocks (va 0.5-2.1 mm), iron oxides nodules (a-wr 0.2-0.7 mm) fossils fragments (va-wr 0.2-0.7 mm)		G
KB.06.E.703.3	10% vughs not aligned 0.05-2mm	20%	iron oxides nodules (r 0.15-2.1 mm)		E
KB.05.B.146.15	20% vughs not aligned 0.05->2mm	20%	calcite (va-a 0.6-1.2 mm), iron oxides nodules (sa-r 0.5-1.9 mm), fragments of rocks (va 0.8-2.0 mm), sedimentary rocks (sa-r 0.5-1.3 mm)		G
KB.06.E.701.2	30% vughs/vesicles not aligned 0.05-2 mm	30%	fragments of rocks (va 0.2-1.2 mm), iron oxides nodules (r 0.2-0.5 mm) micritic calcite (wr 0.2-1.2 mm), calcite (wr 0.2-1.0 mm), olivine (wr 0.2-0.5 mm)		G
KB.06.B.167.4	20% vesicles/vughs not aligned 0.05->2mm	20%	fragments of rocks (a-sa 1.0-2.0 mm), sedimentary rocks (a 0.9-2.0 mm) iron oxides nodules (sr 0.2-1.0 mm), quartz (sr-sa 0.1)		Loner (H)
KB.06.B.413/2	10% vughs Not aligned 0.05-0.5mm	40%	fossils (el va 0.25-3.0 mm), micritic calcite (sa 0.2-0.7 mm)		Loner (I)
KB.05.A.58.1	30% vesicles/vughs not aligned 0.05-0.5mm	30%	quartz (sa-sr 0.25-0.5 mm), calcite (sa-sr 0.25-3 mm), iron oxides nodules (r 0.5 mm)		E
KB.05.B.126.1	20% vesicles/vughs not aligned 0.05->2mm	10% 5:95	micritic calcite (va-sr 0.5-1.0 mm), iron oxides nodules (r 0.15-2.1 mm)	quartz (sa-a 0.1 mm)	E
KB.05.B.146.7	40% vughs not aligned 0.5->2mm	20% 85:15	sparry calcite (sa-a 0.8-1.5 mm), micritic calcite (sa-sr 0.5-1.8 mm) iron oxides nodules (r 0.8 mm), grog (sa 1.0-1.9 mm), olivine (1 0.5 mm)	quartz (sr 0.1 mm)	Loner (C)
KB.05.A.64.1	10% vughs/vesicles not aligned 0.05- >2mm	20% 20:80	sedimentary rocks (a-sr 0.6-1.3 mm), sparry calcite (sa-a 0.8-1.5 mm), iron oxides nodules (sa 0.9-2.0 mm)	quartz (sa-a 0.1 mm)	F
KB.05.B.126.3	10% vesicles/vughs not aligned 0.05-0.5 mm	20% 20:80	sedimentary rocks (sr-r 0.3-1.3 mm), fossils fragments (va-wr 0.2-0.6 mm)	calcite (wr-r 0.05-0.1 mm)	F
KB.05.B.146.1	10% vesicles/vughs subparallel 0.05-0.5mm	20% 40:60	micritic calcite (va-sr 0.3-0.8 mm), calcite (va-sr 0.3-1.0 mm), sedimentary rocks (a-sr 0.6-1.0 mm), olivine (1	calcite (wr-r 0.05-0.1 mm)	F

				0.5 mm)		
KB.08.B.805.6	20%	vughs 0.05-0.5mm	not aligned	30%	calcite (va 0.3-1.2 mm)	G
KB.09.B.820.10	10%	vesicles/vughs 0.05-2mm	not aligned	30%	calcite (a-sr 0.6-0.9 mm), fragments of rocks (sa 0.8-0.9 mm), fragments of fossils (sr-a 0.5-0.7 mm), iron oxides nodules (sa-sr 0.5-0.6 mm), quartz (sa-a 0.1 mm)	G
KB.09.B.820.12	10%	vughs 0.05-2.0mm	not aligned	20%	fossils oosparite (wr 1.0-2.0 mm), micritic calcite (sa 0.2-0.7 mm), sparry calcite (sa 0.2-0.7 mm), iron oxides nodules (r 0.15-2.1 mm)	F
KB.09.B.820.13	10%	vughs/vesicles 0.05-2mm	not aligned	30%	fragments of rocks (a 0.8-2.0 mm), calcite (va 0.2-1.0 mm), iron oxides nodules (wr 0.2-0.7 mm)	G

3.4 XRD and SEM analysis

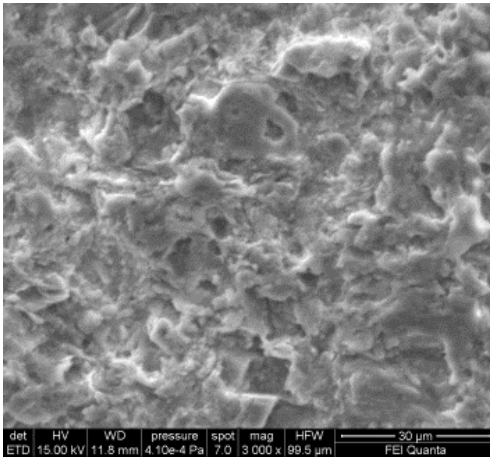


Figure 4: SEM image, matrix in the sample KB.05.B.146/15 Example of “first stage of vitrification”.

XRD results highlighted the presence of quartz, calcite and less abundant illite.

SEM images permit to define the degree of vitrification of the pottery samples to give preliminary information about the maximum firing temperature. Images clearly show that the glass phase did not develop in the studied samples, whereas only isolated smooth-surfaced areas or filaments of glass appeared (Fig. 4). Chemical analysis showed that the composition of the groundmass is characterized by high contents of Si, Al, Mg, K, Na, Ca, Fe and that it is very similar in all the fragments.

4. Discussion

Despite the different macroscopic features, the results of micro-Raman and FTIR spectroscopies, thin section analysis, SEM-EDS and XRD analysis showed that groundmass and inclusions are the same in all analyzed fragments.

The analysed samples contain mainly quartz and calcite as inclusions. K-feldspar and plagioclase have been also identified as inclusions in the matrix, probably deriving from igneous and/or metamorphic rocks outcropping in the area.

Petrographic analysis, showing an homogeneous distribution of the different granulometric classes of inclusions, indicates the use of poorly purified materials. This observation seems to support the hypothesis that the minerals present in the matrix could be natural inclusions of the clay and not intentionally added tempers.

The mineralogical composition is an important tool in the analysis of ceramic materials to identify the newly formed minerals during firing process, and to establish the maximum firing temperature and the redox conditions of atmosphere, (Maggetti, 1982; Cultrone *et al.*, 2001; Maritan *et al.* 2005, 2006) giving information about the technological level reached at that time.

Calcite is considered an important tracing of firing temperature as its thermal decomposition into CaO and CO₂, starting at around 650 °C, is completed at about 900 °C. In our samples, the diffuse presence of primary calcite marks a low firing temperature of the sherds. This hypothesis is supported by thin section analysis that allows to identify calcite as a primary phase, having typical features of an initial stage of breakdown.

The presence of diopside in the ceramic samples further contributes to estimate the firing temperature: its crystallization starts at temperatures higher than 850 °C as a product of the reaction between clay minerals and calcium carbonate.

Illite, identified by FTIR and XRD analysis, breaks down in the temperature range 800-900 °C (Duminuco *et al.*, 1998; Riccardi *et al.*, 1999; Aras, 2004).

Moreover, the occurrence of titanium dioxide polymorphs in four samples give further information on firing temperature; indeed, anatase remains stable in the range 600-900 °C, and above this temperature range it converts into rutile.⁴⁰ The presence of anatase may indicate a firing temperature lower than 900 °C (Gennari and Pasquevich, 1999).

The presence of diopside, illite and calcite suggests a firing temperature ranging from 850 °C to 900 °C, where these phases coexist and confirmed by morphological analysis that allow to identify the “first stage of vitrification” (Tite and Maniatis, 1975; Tite *et al.*, 1982).

Hematite and magnetite play a significant role in defining the atmosphere conditions during firing. The samples containing hematite show a red matrix related to an oxidizing atmosphere.

On the contrary, the Raman spectra of ten samples with grey colour matrix reveal the only presence of magnetite suggesting reducing firing conditions. Furthermore, the majority of samples having a heterogeneous colour of the matrix, along the cross section, suggests uncontrolled redox conditions during firing.

Finally, apatite, barite and olivine occasionally occur in the samples and may be considered naturally present as non-plastic inclusions into the clays derived from geological formations occurring in the area of Khirbet al-Batrawy. In particular, the presence of rare crystals of olivine is due to the presence of basaltic (olivine-bearing) rocks occurring in the area and confirmed by microscopic analysis, whereas the presence of apatite suggests a contribution of granitic-metamorphic rocks.

Gypsum has been identified in the ceramic matrix of the sherds, as scattered crystals and on the surface as grey incrustations. Its presence in the ceramic matrix could be

related to the occurrence of sulphate minerals in the calcareous and evaporitic rocks of Batrawy region used as raw materials (Freyer and Voigt, 2003). According to experimental data, as the gypsum-bassanite transition starts at 393 K (isothermal condition), and the transition bassanite-anhydrite is completed at 408 K we can make two assumptions (Ballirano and Melis, 2009a, 2009b). The first hypothesis is that the raw materials contained gypsum which during the heating cycle was transformed via dehydration into anhydrite, which remained stable up to 1000 °C. The second one is that the raw material contained anhydrite which remained unaffected during the heating process. In post-heating processes both anhydrite or bassanite were rehydrated into gypsum.

The occurrence of gypsum as crusts on the surface may be related to the interaction of sherds with sulphate-rich fluids in burial environment.

Micro-Raman analysis was the only procedure available in the characterization of pigments used for the surface decoration of the samples. Hematite has been used in red bands of sherds, whereas the black pigment was identified as amorphous carbon. In some EB IIIA samples carbon has been identified in the surfaces of undecorated areas. In this case, the occurrence of carbon on the surface can be explained as due to the use of the vessels or to the fire that destroyed Batrawy at the end of EB IIIB.

Despite the macroscopic differences observed among samples, the results of both micro-Raman spectroscopy and FTIR analysis support the hypothesis that KKW samples can be assigned to the same pottery production to which the other EB IIIA local potteries belong. In particular, from the elaboration of FTIR spectra by PCA we can attribute the KKW to the same local production of the Khirbet al-Batrawy ceramic industry.

The *fabric* analysis, performed using polarized microscope, supports the local origin of KKW, previously quoted by spectroscopic analysis. The presence of apatite, olivine and basalt rocks fragments allows to hypothesize a local supply of raw material, probably from sources in the vicinity of the archaeological site.

Information about the main feature of KKW sherds, i.e. the polished surface, have been also obtained. The Raman spectra of the only sherd with a red polished surface (KB.08.B.805/6) show the presence of hematite. The red colour of the matrix and the identification of hematite also in the matrix suggests a firing process characterized by oxidizing atmosphere. In the other dark polished surface fragments only amorphous carbon has been identified: in these samples Fe-spinel does not occur. This amorphous phase might have a more significant role in the production process than ferrous compounds allowing the hypothesis of a reducing atmosphere produced by surrounding pottery with organic packing. High carbon content can be related to the use of organic matter-rich clay, probably used to make the thick slip of the surface. This hy-

pothesis can be supported for the samples KB.09.B.820/10 and KB.09.B.820/13 which have an oxidized body, which is not supported by the presence of ferrous spinels (Tite *et al.*, 1982). On the other hand, samples KB.09.B.820/12 and KB.08.B.805.34 show a dark colour of the matrix. No evidence of magnetite has been found. The hypothesis is that the high concentration of organic matter creates a reducing atmosphere that prevents the re-oxidation of the body.

This variability in the resulting products indicates a not complete knowledge of the technological aspects of production of the original KKW, further supporting the local attribution of the samples analysed. It is also important to highlight that the shining slip of KKW was not due to a selected fine clay added on the surface or to particular firing process, but it is related to a mechanic hand-burnishing that allows the alignment of particles parallel to the surface, giving the lustrous aspect.

5. Conclusions

Archaeometric analysis allows to characterize pottery fragments and to contribute at the archaeological problem in the attribution of the origin of KKW pottery from Khirbet al-Batrawy. Indeed, the mineral composition of pottery allows identifying and defining technological aspects of pottery production.

The results suggest that the ceramic body of KKW was composed by quartz, calcite, hematite and minor amounts of feldspars and diopside, whereas the color of pigments of the surface are attributed to hematite and amorphous carbon for red and dark areas, respectively.

Micro-Raman spectroscopy permits also the identification of the pigments of the surface: the red areas are attributed to hematite, whereas the dark ones to amorphous carbon.

The mineralogical assemblage indicates that the potteries were fired in the range of temperature between 850-900 °C in an uncontrolled atmosphere.

The same conclusions are drawn for others EB IIIA potteries. The mineralogical compositions of the body and the petrographic fabrics identified further support the attribution of KKW to the Khirbet al-Batrawy ceramic production. Moreover, the presence of apatite and olivine as well as fragments of basalt rocks allow to hypothesize a local provenance for the raw material.

The results of this section are reported in the article:

Medeghini L., Mignardi S., De Vito C., Bersani D., Lottici P.P., Turetta M., Sala M. and Nigro L. (2013): Is Khirbet Kerak Ware from Khirbet al-Batrawy (Jordan) local or imported pottery? Analytical Methods, Accepted manuscript, DOI: 10.1039/C3AY41304G.

References

- Albright W.F. (1926): The Jordan Valley in the Bronze Age. *Annual of the American Schools of Oriental Research*, **6**, 13-16.
- Amiran R. (1952): Connections between Anatolia and Palestine in the Early Bronze Age. *IEJ*, **2**, 89-103.
- Aras A. (2004): The change of phase composition in kaolinite and illite-rich clay-based ceramic bodies. *Applied Clay Science*, **24**, 257-269.
- Ballirano P., Melis E. (2009): Thermal behaviour and kinetics of dehydration in air of bassanite, calcium sulphate hemihydrate ($\text{CaSO}_4 \cdot 0.5 \text{H}_2\text{O}$), from X-ray powder diffraction. *European Journal of Mineralogy*, **21**, 985-993.
- Ballirano P., Melis E. (2009): Thermal behaviour and kinetics of dehydration of gypsum in air from in situ real-time laboratory parallel-beam X-ray powder diffraction. *Physics and Chemistry of Minerals*, **36**, 391-402.
- Barone G., Ioppolo S., Majolino D., Migliardo P., Tigano G. (2002): A multidisciplinary investigation on archaeological excavation in Messina (Sicily). Part I: a comparison of pottery findings in “the Strait of Messina area”. *Journal of Cultural Heritage*, **3**, 145-153.
- Belfiore C. M., Di Bella M., Triscari M., Viccaro M. (2010): Production technology and provenance study of archaeological ceramics from relevant sites in the Alcantara River Valley (North-eastern Sicily, Italy). *Materials Characterization*, **61**, 440-451.
- Burney C.A. (1989): The Khirbet Kerak Question and the Early Transcaucasian Background. in “L’urbanisation de la Palestine à l’âge du Bronze Ancien”, de Miroschedji P. ed., Oxford, 331-339.
- Chazan M., McGovern P.E. (1984): The Khirbet Kerak Pottery from Beth Shan: Technological evidence for local manufacture? *Museum Applied Science Center for Archaeology Journal*, **3**, 20-24.
- Cultrone G., Rodriguez-Navarro C., Sebastian E., Cazalla O., De La Torre M. J. (2001): Carbonate and silicate phase reactions during ceramic firing. *European Journal of Mineralogy*, **13**, 621-634.
- Duminuco P., Messiga B., Riccardi M.P. (1998): Firing process of natural clays. Some microtextures and related phase composition. *Thermochimica Acta*, **321**, 185-190.
- Esse D.L., Hopke P. (1986): Levantine Trade in the Early Bronze Age: From Pots to People. in: “Proceeding of the 24th International Archaeometry Symposium” Olin J. and Blackman M.J. eds., Washington, 327-329.
- Freyer D., Voigt W. (2003): Crystallization and Phase Stability of CaSO_4 and CaSO_4 -based salts. *Monatshefte für Chemie/Chemical Monthly*, **134**, 693-719.
- Gennari F. C., Pasquevich D. M. (1999): Enhancing effect of iron chlorides on the anatase-rutile transition in titanium dioxide. *Journal of the American Ceramic Society*, **82**, 1915-1921.
- Greenberg R. (2007): Transcaucasian Colors: Khirbet Kerak Ware at Khirbet Kerak (Tel Bet Yerah). in “Les cultures du Caucase (VIe–IIIe millénaires avant notre ère), Lyonnet B. ed., Paris, 257-268.
- Iordanidis A., Garcia-Guinea J., Karamitrou-Mentessidi G. (2009): Analytical study of ancient pottery from the archaeological site of Aiani, northern Greece. *Materials Characterization*, **60**, 292-302.
- Maritan L. (2004): Archaeometric study of Etruscan-Padan type pottery from the Veneto region petrographic, mineralogical and geochemical-physical characterisation. *European Journal of Mineralogy*, **16**, 297-307.

- Maritan L., Mazzoli C., Nodari L., Russo U. (2005): Second Iron Age grey pottery from Este (northeastern Italy): study of provenance and technology. *Applied Clay Science*, **29**, 31-44.
- Maritan L., Nodari L., Mazzoli C., Milano A., Russo U. (2006): Influence of firing conditions on ceramic products: experimental study on clay rich in organic matter. *Applied Clay Science*, **31**, 1-15.
- Maggetti M. (1982): Phase analysis and its significance for technology and origin. In "Archaeological ceramics", J.S. Olin and A.D. Franklin, ed., Smithsonian Institution Press, Washington, 121-133.
- Miroschedji P.de (2000): La céramique de Khirbet Kerak en Syro-Palestine: état de la question. in "Chronologie des pays du Caucase et de l'Euphrate aux IVe-IIIe millénaires" Marro C. and Hauptmann H. eds., Paris, 255-278.
- Paz S. (2009): A Home Away from Home? The Settlement of Early Transcaucasian Migrants at Tel Bet Yeor. *Tel Aviv*, **36**, 196-216.
- Rathossi C., Tsolis-Katagas P., Katagas C. (2004): Technology and composition of Roman pottery in northwestern Peloponnese, Greece. *Applied clay science*, **24**, 313-326.
- Riccardi M.P., Messiga B., Duminuco P. (1999): An approach to the dynamics of clay firing. *Applied Clay Science*, **15**, 393-409.
- Sala M. (2008): Khirbet Kerak Ware from Tell es-Sultan/ancient Jericho: a Reassessment in the Light of the Finds of the Italian-Palestinian Expedition (1997-2000). Proceedings of the 5th International Congress on the Archaeology of the Ancient Near East, Madrid, 2008.
- Sala M. (2012): Appendix C. Khirbet Kerak Ware from Khirbet al-Batrawy. in "Khirbet al-Batrawy III. The EB II-III triple fortification line and the EB IIIB quarter inside the city-wall. Preliminary report of the fourth (2008) and fifth (2009) seasons of excavations" ed. L. Nigro, Rome «La Sapienza» Studies on the Archaeology of Palestine & Transjordan, Rome, vol. 8, pp. 371-380,
- Sukenik Y. (1947): On the Technique of Khirbet Kerak Ware. *Bulletin of the American Schools of Oriental Research*, **106**, 9-17.
- Tite M.S., Freestone I.C., Meeks N.D., Bimson M. (1982): The use of scanning electron microscopy in the technological examination of ancient ceramics. In "Archaeological Ceramics", ed. Olin J.S., Franklin A.D., Smithsonian Institution Press, Washington DC, 109-120.
- Tite M.S., Maniatis Y. (1975): Examination of ancient pottery using the scanning electron microscope. *Nature*, **257**, 122-123.
- Woolley L. (1953): A forgotten kingdom. Baltimore, pp. 191.
- Tschegg C., Ntaflos T., Hein I. (2009): Thermally triggered two-stage reaction of carbonates and clay during ceramic firing—A case study on Bronze Age Cypriot ceramics. *Applied Clay Science*, **43**, 69-78.
- Velraj G., Janaki K., Musthafa A. M., Palanivel R. (2009): Spectroscopic and porosimetry studies to estimate the firing temperature of some archaeological pottery shreds from India. *Applied clay science*, **43**, 303-307.

